Biological and Medical Physics, Biomedical Engineering

Stephen J. Hagen *Editor*

The Physical Basis of Bacterial Quorum Communication

Springer

The Physical Basis of Bacterial Quorum Communication

BIOLOGICAL AND MEDICAL PHYSICS, BIOMEDICAL ENGINEERING

The fields of biological and medical physics and biomedical engineering are broad, multidisciplinary and dynamic. They lie at the crossroads of frontier research in physics, biology, chemistry, and medicine. The Biological and Medical Physics, Biomedical Engineering Series is intended to be comprehensive, covering a broad range of topics important to the study of the physical, chemical and biological sciences. Its goal is to provide scientists and engineers with textbooks, monographs, and reference works to address the growing need for information.

Books in the series emphasize established and emergent areas of science including molecular, membrane, and mathematical biophysics; photosynthetic energy harvesting and conversion; information processing; physical principles of genetics; sensory communications; automata networks, neural networks, and cellular automata. Equally important will be coverage of applied aspects of biological and medical physics and biomedical engineering such as molecular electronic components and devices, biosensors, medicine, imaging, physical principles of renewable energy production, advanced prostheses, and environmental control and engineering.

For further volumes:
http://www.springer.com/series/3740

Stephen J. Hagen
Editor

The Physical Basis of Bacterial Quorum Communication

Springer

Editor
Stephen J. Hagen
Department of Physics
University of Florida
Gainesville, FL, USA

ISSN 1618-7210 ISSN 2197-5647 (electronic)
ISBN 978-1-4939-1401-2 ISBN 978-1-4939-1402-9 (eBook)
DOI 10.1007/978-1-4939-1402-9
Springer New York Heidelberg Dordrecht London

Library of Congress Control Number: 2014949378

Printed on acid-free paper

Springer is part of Springer Science+Business Media (www.springer.com)

Contents

Contributors

Gil Ariel Department of Mathematics, Bar-Ilan University, Ramat Gan, Israel

Arnab Bandyopadhyay Department of Chemistry, Bose Institute, Kolkata, India

Suman K. Banik Department of Chemistry, Bose Institute, Kolkata, India

Avraham Be'er Zuckerberg Institute for Water Research, The Jacob Blaustein Institutes for Desert Research, Ben-Gurion University of the Negev, Midreshet Ben-Gurion, Israel

Sivan Benisty Zuckerberg Institute for Water Research, The Jacob Blaustein Institutes for Desert Research, Ben-Gurion University of the Negev, Midreshet Ben-Gurion, Israel

Eshel Ben-Jacob School of Physics and Astronomy, Raymond and Beverly Sackler Faculty of Exact Sciences, Tel Aviv University, Tel Aviv, Israel

Center for Theoretical Biological Physics, Rice University, Houston, TX, USA

James Q. Boedicker Department of Physics and Astronomy, Seaver Science Center (SSC) 223, University of Southern California, Los Angeles, CA, USA

Lauren Boudreau Division of Math, Science and Technology, Nova Southeastern University, Fort Lauderdale, FL, USA

Katie Brenner Department of Biochemistry, University of Wisconsin-Madison, Madison, WI, USA

Javier Buceta Department of Chemical and Biomolecular Engineering, Lehigh University, Bethlehem, PA, USA

Raf De Dier Soft Matter, Rheology and Technology, KU Leuven – University of Leuven, Heverlee, Belgium

The laboratory of Soft Materials, Department of Materials at ETH Zürich, Zürich, Switzerland

Alan W. Decho Microbial Interactions Laboratory, Department of Environmental Health Sciences, Arnold School of Public Health, University of South Carolina, Columbia, SC, USA

Maarten Fauvart Centre of Microbial and Plant Genetics, KU Leuven – University of Leuven, Heverlee, Belgium

Andrew T. Fenley Skaggs School of Pharmacy and Pharmaceutical Sciences, University of California at San Diego, La Jolla, CA, USA

Stephen J. Hagen Physics Department, University of Florida, Gainesville, FL, USA

B.A. Hense Helmholtz Zentrum München, Institute of Computational Biology, Neuherberg/Munich, Germany

Sara Jabbari School of Mathematics and Institute of Microbiology and Infection, University of Birmingham, Birmingham, UK

John R. King School of Mathematical Sciences, University of Nottingham, Nottingham, UK

Rahul V. Kulkarni Department of Physics, University of Massachusetts, Boston, MA, USA

Volker Kurz Electrical Engineering, University of Notre Dame, Notre Dame, IN, USA

C. Kuttler Technical University München, Centre for Mathematical Sciences, Garching, Germany

Jan Michiels Centre of Microbial and Plant Genetics, KU Leuven – University of Leuven, Heverlee, Belgium

Utkur Mirsaidov Department of Physics, National University of Singapore, Singapore, Singapore

J. Müller Helmholtz Zentrum München, Institute of Computational Biology, Neuherberg/Munich, Germany

Technical University München, Centre for Mathematical Sciences, Garching, Germany

Edward M. Nelson Electrical Engineering, University of Notre Dame, Notre Dame, IN, USA

Nicolas Perry Electrical Engineering, University of Notre Dame, Notre Dame, IN, USA

Koshala Sarveswaran Electrical Engineering, University of Notre Dame, Notre Dame, IN, USA

Robert Phillip Smith Division of Math, Science and Technology, Nova Southeastern University, Fort Lauderdale, FL, USA

Gregory Timp Electrical Engineering and Biological Sciences Departments, University of Notre Dame, Notre Dame, IN, USA

Winston Timp Department of Biomedical Engineering, Johns Hopkins University, Baltimore, MD, USA

Jan Vermant Soft Matter, Rheology and Technology, KU Leuven – University of Leuven, Heverlee, Belgium

The laboratory of Soft Materials, Department of Materials at ETH Zürich, Zürich, Switzerland

Marc Weber Co.S.Mo. Lab (Computer Simulation and Modeling), Parc Cientific de Barcelona, Barcelona, Spain

Douglas B. Weibel Department of Biochemistry, University of Wisconsin-Madison, Madison, WI, USA

Department of Biomedical Engineering, University of Wisconsin-Madison, Madison, WI, USA

Department of Chemistry, University of Wisconsin-Madison, Madison, WI, USA

Lingchong You Department of Biomedical Engineering, Duke University, Durham, NC, USA

Center for Systems Biology, Duke University, Durham, NC, USA

Chapter 1
Introduction

Stephen J. Hagen

Many bacterial species engage in the behavior known as quorum sensing (QS), which can be described as the regulation of gene expression in response to changes in the bacterial population density [1]. The bacteria synthesize and release diffusible small molecules known as autoinducers, which accumulate in the environment. When the concentration of autoinducer (AI) reaches a threshold level, indicating the presence of a "quorum" of cells, the population responds as a whole by activating certain gene regulatory networks, leading to colony-wide changes in phenotype. A wide range of bacterial behaviors are now known to be regulated through QS. These include biofilm production, genetic competence, bioluminescence, various types of motility, and the production of exoenzymes, toxins, bacteriocins, and other types of virulence factors and secreted products. As the collective production and detection of the autoinducer signal allows the entire population to synchronize gene regulation, quorum sensing (QS) is a form of chemical communication and a social behavior. Accordingly it has attracted tremendous interest from researchers in many fields.

QS gene regulatory networks respond not only to bacterial population as indicated by autoinducer signals but also to a range of physiological and environmental inputs [2, 3]. While a host of individual QS systems have been characterized in great molecular and chemical detail, quorum communication raises many fundamental quantitative problems. These problems are attracting the attention of physical scientists and mathematicians: How does QS function in complex, spatially structured environments such as biofilms? What kinds of information can a bacterium gather about its environment through QS? What physical principles ultimately constrain the efficacy of diffusion-based communication? How do QS regulatory networks maximize information throughput while minimizing undesirable noise

S.J. Hagen (✉)
Physics Department, University of Florida, Gainesville, FL 32611-8440, USA
e-mail: sjhagen@ufl.edu

S.J. Hagen (ed.), *The Physical Basis of Bacterial Quorum Communication*, Biological and Medical Physics, Biomedical Engineering, DOI 10.1007/978-1-4939-1402-9_1

and crosstalk? What can we learn from computation and modeling of QS systems? The chapters in this volume address these physical, quantitative questions. With contributions by leading scientists working in the field of physical biology, it examines the interplay of diffusion and signaling, collective and coupled dynamics of gene regulation, environmental manipulations, and spatiotemporal QS phenomena.

The chapter by Arnab Bandyopadhyay and coworkers introduces the topic with a broad overview of QS regulation. It then presents a detailed case study of a classic QS system, the *lux* genes that regulate the natural bioluminescence of the marine bacterium *Vibrio harveyi*. As one of the best known and best studied QS systems, the *lux* system of *V. harvei* has been the target of a wide array of sophisticated experimental techniques as well as detailed theory and modeling aimed at understanding the role of feedback, noise, robustness, kinetics, and other phenomena in its signal transduction. The chapter summarizes some key approaches in the modeling of QS at the population level as well as at the single-cell level. It compares the *V. harveyi* system to the closely related QS system in *Vibrio cholerae*. It also describes what can be learned by studying QS regulation at the single-cell and single-molecule levels.

The dynamics of QS circuits have been a subject of particular interest for theorists. The chapter by Marc Weber and Javier Buceta investigates the relationship between diffusion, stochasticity, and switching in QS, with a focus on the LuxI/LuxR system. Using a simplified model of a noisy LuxI/LuxR circuit, the authors examine how the rate of diffusive or active transport into and out of the cell affects fluctuations in the intracellular autoinducer concentration. They find evidence that tuning the rate of diffusive transport could be one way for the cell to optimize noise performance. They also introduce the concept of "precision" in QS response in order to analyze the effect of bursting transcription on the range or window of environmental conditions that permit a bistable response. Finally they show how stochasticity in gene expression can either accelerate, or delay the transition between the activated (on) and inactivated (off) states of the QS circuit.

It is important of course to consider the environmental context in which QS circuits operate. The chapter by James Boedicker and coworkers examines the structured microbial communities and the physical factors influencing communication and cooperation in these communities. The authors summarize the types of spatial structures and environments in which bacterial communities are found, including soils, aggregates, and surfaces in fresh and salt water, and in the human body. They summarize the biophysical problem of signaling by diffusion, its length and time scales as they apply to microbiology, and the activation time scales of the gene regulatory systems that respond to diffusing signals. The authors then survey the growing research interest in artificially engineering cell organization and spatial arrangements, including microfabrication methods as well as schemes for single-cell manipulation. Such approaches hold potential for greater understanding of complicated microbial systems such as "unculturable" bacteria. The authors close by considering future research directions in the investigation of how the structure of microbial communities affects their composition and function.

The chapter by Burkhard Hense goes into greater detail on such issues by reviewing the interpretation of QS behavior and its physical function and capability. It discusses the ecological function of autoinducer production and the ways that it can permit the sensing of population as well as environment, efficiency sensing, and how bacteria use QS to control not just specific targeted genes but larger lifestyle transformations (activation of virulence factors, etc.). In a case study of QS regulation of bioluminescence, Hense considers the hypothesis that QS regulated bioluminescence may have first emerged as a mechanism for relieving oxidative stress by removal of molecular oxygen from the environment. That is, QS does not so much produce a public good but remove a negative from the environment. The chapter also explores the role of nutrient in QS regulation. It presents an argument that QS signals may provide useful means for cells to communicate about nutrient deficiency in spatially structured environments. It then describes a model in which AI production that is sensitive to nutrient concentration leads to spatially nonuniform AI production in a bacterial colony. The chapter also discusses the concept of "push" and "pull" modes of regulation in quorum sensing, through which QS seems to permit a complex or contextual response of a cell not only to its own local conditions but also to conditions faced by neighboring cells. Finally the chapter discusses the possibility that AIs are not necessarily intended to signal population-wide but may often be aimed at signaling only at the level of cell clusters.

In any communication system it is important to understand how the signal interacts with the medium through which it travels. Very often autoinducer signals must diffuse through a biofilm composed of extracellular polymeric substances (EPS) secreted by the microorganisms. Quorum sensing signals encounter many types of physical and chemical interactions and obstacles as they diffuse through this matrix, with consequences for the physical range and time scales of bacterial signaling. The chapter by Alan Decho reviews the complex physical and chemical properties of AHL signals as well as those of the EPS matrix. It describes the chemical and spatial composition, microstructure, and physical flexibility of the matrix, as well as the ways that it interacts with the diffusion of signals and other small molecules. The chapter also describes how experimental techniques such as Raman spectroscopy and cryo-TEM tomography can be used to study biofilm composition and structure at high spatial resolution.

The physical process of signal diffusion is clearly central to autoinducer signaling in heterogeneous, structured environments such as biofilms. Many authors have suggested that cells in such environments can use QS individually to gather information about their surroundings [4, 5]. The chapter by Steve Hagen examines quorum sensing from the perspective of a single cell. It asks what kinds of information a cell can gather about its physical environment by producing and detecting a diffusing signal, and what are some of the limitations on information gathering. The chapter also describes how information theory can shed some light on the evolutionary optimization of quorum sensing circuits.

The chapter by Avraham Be'er and coauthors steps away from the single-cell level and investigates the social uses of bacterial signaling. It addresses the question of how a colony of bacteria can detect—or inhibit the growth of—another

nearby colony of the same species. The authors study an inhibitory behavior in the bacterium *Paenibacillus dendritiformis*, where the close proximity of neighboring sibling colonies induces the transition from a rod-shaped phenotype to a slower-growing cocci phenotype. The authors show that the organism produces a species specific bacteriocin protein (Slf) that promotes the transition to the cocci form. Interestingly, the rods also produce a signal, designated Ris, that promotes the transition from the cocci back to the rod phenotype. They performed mathematical modeling that shows that autoregulation of the concentration of growth-promoting subtilisin in the colony is the key. Diffusion of subtilisin from a neighboring colony disturbs the carefully regulated subtilisin concentration, leading to production of Slf and driving the transition to the cocci form with hindered growth.

One of the salient features of the architecture of many quorum sensing regulatory circuits is the presence of feedback and nonlinearity. These can often give rise to complex and important properties such as switching, bistability, or even multistability. In their chapter, Sara Jabbari and John King provide a review of some of the most important quorum sensing circuit architectures and the role of feedback in those systems. They construct simple, deterministic models for several classic quorum sensing systems and use these models to analyze the role and consequences of feedback in those systems. They show how positive and negative feedback can shape the overall character of the regulatory behavior (e.g., bistability) as well as the tuning of signal and regulatory levels and the suppression of noise in the system.

Motility is one behavior in bacterial colonies that is often regulated through QS. There are many mechanisms of bacterial motility in addition to planktonic swimming; swarming behavior is a particularly interesting form of spreading on a moist surface. It is quorum-regulated and is facilitated through the physical-chemical properties of the colony biofilm. The chapter by Raf De Dier and coworkers discusses how the production of surfactants and their concentration gradients give rise to a Marangoni effect that aids in the physical spreading of the biofilm. They present comparisons of simulations and experiments that show how depth profiles, spreading patterns, and swarming speed in biofilms can be understood in physical terms through modeling of such forces.

One innovative approach to studying the role of spatial organization in bacterial signaling is to create synthetic assemblies of cells using micromanipulation and tissue-engineering methods. The chapter by Edward Nelson and coauthors describes how optical tweezers and photopolymerizable gels can be used to assemble and immobilize engineered cells into synthetic, biofilm-like arrays. When such arrays are constructed in a microfluidic environment, the overall physical geometry as well as the chemical environment for the synthesis and diffusion of quorum sensing signals can be kept under tight experimental control. The authors placed autoinducer-synthesizing cells in fixed locations and positions with respect to AHL receiving cells and studied the kinetics of the signaling and response via fluorescent reporter proteins. Interestingly, they found that the amplitude of the response is much more sensitive to physical location in the array than is the timing of that response—an issue addressed also in the chapter by Hagen. They also measured an interesting ‘blinking’ phenomenon in the output of the quorum sensing circuit at

the level of individual cells. This phenomenon can be linked to a sort of epigenetic memory in the regulation of the intracellular receptor of autoinducer; this memory appears to permit some heritable training of the cells in a population, minimizing the population-wide variability in the response to a given environmental condition.

Finally, one can also use QS as a tool for studying problems in evolution and ecology. The article by Robert Smith and coworkers takes a synthetic biology approach toward understanding how social behaviors of communication, cooperation, and competition lead to costs and benefits in mixed-strain cultures. The authors have engineered a variety of mixed-strain systems in which QS signals manipulate and interact with predator–prey relationships, the costs and benefits of cheating versus cooperation, antibiotic resistance, the production of public goods, and even altruistic cell death. The article shows how designed synthetic systems can help us to test and advance our ideas about the relationship between cell-to-cell communication and important ecological and evolutionary phenomena.

The goal of this volume is to educate interested scientists in a range of fields on the application of physical and mathematical ideas, together with appropriate modeling and experimentation, toward the understanding and interpretation of microbial quorum communication. It is hoped that the volume succeeds in conveying the importance of microbial signaling and communication as well as the richness of the signaling behaviors and systems that exist in nature. This author gratefully acknowledges the efforts of the many contributors to this volume.

References

1. Waters CM, Bassler BL (2005) Quorum sensing: cell-to-cell communication in bacteria. Annu Rev Cell Dev Biol 21:319–346
2. Dunn AK, Stabb EV (2007) Beyond quorum sensing: the complexities of prokaryotic parliamentary procedures. Anal Bioanal Chem 387:391–398
3. Boyer M, Wisniewski-Dye F (2009) Cell–cell signalling in bacteria: not simply a matter of quorum. FEMS Microbiol Ecol 70:1–19
4. Redfield RJ (2002) Is quorum sensing a side effect of diffusion sensing? Trends Microbiol 10:365–370
5. Hense BA, Kuttler C, Mueller J, Rothballer M, Hartmann A, Kreft J (2007) Opinion - does efficiency sensing unify diffusion and quorum sensing? Nat Rev Microbiol 5:230–239

Chapter 2
Modeling of Signal Transduction by the Quorum-Sensing Pathway in the Vibrios

Arnab Bandyopadhyay[$], Andrew T. Fenley[$], Suman K. Banik, and Rahul V. Kulkarni

2.1 Introduction

Bacterial survival under changing conditions is critically dependent on regulatory networks that sense and respond to environmental fluctuations. A prominent example is the global regulatory network responsible for quorum sensing, commonly defined as the regulation of gene expression in response to cell density [1]

During the process of quorum sensing, each bacterium generates, secretes, detects and responds to extracellular signaling molecules called autoinducers. Changes in the concentration of autoinducers at any given time are directly related to changes in the local cell density, and differential expression of quorum sensing regulated genes occurs when the autoinducer concentration exceeds a critical threshold. This observation suggests that bacteria undertake certain cellular activities once a "quorum" is present, hence the name quorum sensing. Consistent with this interpretation, it is observed that quorum sensing often leads to the regulation of cooperative processes such as bioluminescence, secretion of virulence factors, and biofilm formation [1–3].

[$]Authors contributed equally.

A. Bandyopadhyay • S.K. Banik
Department of Chemistry, Bose Institute, 93/1 A P C Road, Kolkata 700 009, India

A.T. Fenley
Skaggs School of Pharmacy and Pharmaceutical Sciences, University of California at San Diego, La Jolla, CA 92093-0736, USA

R.V. Kulkarni (✉)
Department of Physics, University of Massachusetts, Boston, MA 02125, USA
e-mail: rahul.kulkarni@umb.edu

S.J. Hagen (ed.), *The Physical Basis of Bacterial Quorum Communication*, Biological and Medical Physics, Biomedical Engineering, DOI 10.1007/978-1-4939-1402-9_2

In a given bacterial species, autoinducer molecules are produced and recognized by specific synthases and sensors, respectively. Binding of a particular autoinducer by its cognate sensor leads to changes in signal transduction via downstream phosphorelay networks. These networks are typically composed of orthodox two component systems (TCS) including a histidine based sensor kinase and an aspartate based response regulator [4, 5] or more complex phosphorelay networks. The combination of kinase/phosphatase activities of different sensors determines the phosphorylation state of the regulator which, in turn, affects its activity as a transcription factor and can lead to global changes in downstream gene expression.

While there are many bacteria capable of QS, this chapter will primarily focus on theoretical modeling efforts aimed at understanding signal transduction within one of most studied model organisms, *Vibrio harveyi*. *V. harveyi* is a gram-negative, bioluminescent, free-living marine bacterium, which is also an important pathogen for marine organisms. Experimental studies have led to a detailed characterization of regulatory elements in the pathway [6–9]. The signal transduction network in *V. harveyi* (shown in Fig. 2.1) includes multiple autoinducers and their cognate sensor proteins acting together to control the phosphorylation of the response regulator protein, LuxO. The phosphorylated form of LuxO then activates the production of multiple small RNAs (sRNAs) that in turn post-transcriptionally repress the QS master regulatory protein, LuxR. At low cell density, the sRNAs are activated and act to effectively repress LuxR expression. In contrast, sRNA production is significantly reduced at high cell density, thereby giving rise to increased levels of LuxR which leads to the activation of luminescence genes. The corresponding luminescence output per cell profile (i.e., colony luminescence/cell output as a function of cell density) is frequently used as a reporter to characterize the state of the QS pathway.

Although there has been considerable effort focused on experimentally characterizing the *V. harveyi* QS signal transduction network (see [10]), the corresponding theoretical efforts for modeling the QS network have been relatively limited [11–15]. A detailed theoretical model of the QS network that agrees with known experimental results can lead to a framework for making testable predictions and provide fundamental quantitative insights into the process of quorum sensing. In what follows, we describe key elements towards building such theoretical models and discuss the current progress in the literature.

2.2 Signal Transduction Network

The key components of the QS network pathway in *V. harveyi* are shown in Fig. 2.1. At the top of the pathway are the three sensors, LuxN, LuxPQ, and $CqsS_{Vh}$. Their corresponding autoinducer synthases, LuxM, LuxS, and $CqsA_{Vh}$ are responsible for producing the three autoinducers: H-AI1, AI-2, and CAI-1, respectively. Biochemically, H-AI1 belongs to acyl homoserine lactones, whereas AI-2 is a

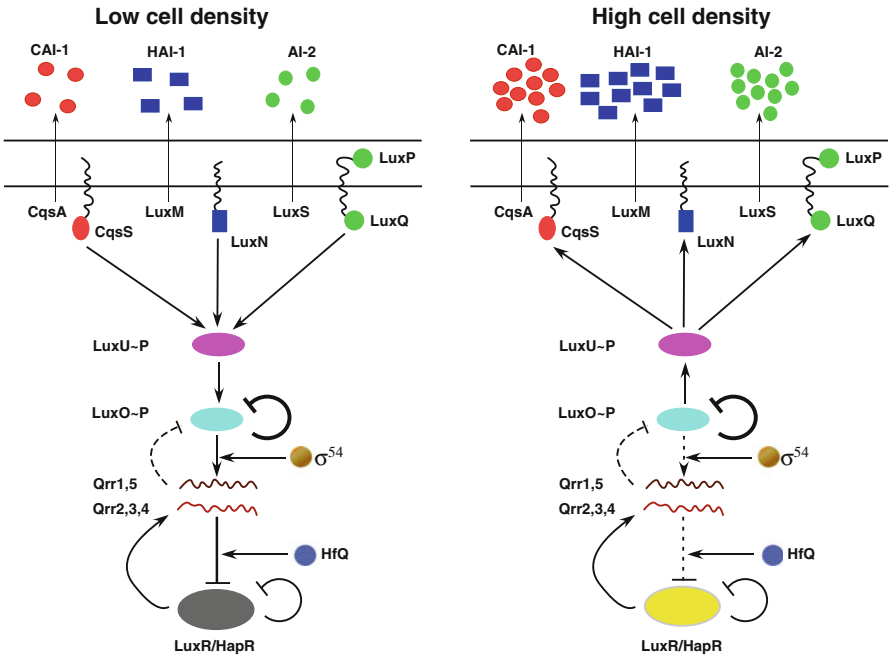

Fig. 2.1 The *V. harveyi* quorum sensing gene network. (*Left*) Low cell density state and (*Right*) high cell density state. *V. harveyi* secretes and detects the concentrations of three different autoinducers (CAI-1, HAI-1, and AI-2). At low cell density, phosphorelay networks transfer phosphate groups to the protein LuxU. LuxU then transfers the phosphate groups to the protein LuxO which, when phosphorylated, is responsible for promoting the production of sRNAs (Qrrs). The sRNAs are responsible for post-transcriptional repression of LuxR. At high cell density, the net flow of phosphate groups reverses direction which reduces the production of the sRNAs resulting in higher LuxR concentrations and activation of bioluminescence

set of inter-converting molecules derived from the shared precursor 4,5-dihidroxy-2,3-pentanedione, with its active form containing boron. Although originally, CAI-1 has been purified from a related bacteria, *Vibrio cholerae*, its presence and role in the QS network of *V. harveyi* has been detected and identified as (S)-3-hydroxytridecan-4-one [6].

The membrane bound histidine kinases are highly specific to the autoinducer they bind. HAI-1 binds only to LuxN histidine kinase. AI-2 is detected by the periplasmic protein LuxP which is in a complex with the LuxQ histidine kinase. And CAI-1 binds specifically to CqsSVh histidine kinase. All the three sensors, LuxN, LuxQ, and $CqsS_{Vh}$ are two-component enzymes of dual functionality, i.e., they can act as kinases as well as phosphatases.

2.2.1 Core Motifs

The signal transduction network in *V. harveyi* can be conveniently described in terms of functional modules [11, 13]. The first (or input) module includes interactions between autoinducers and the corresponding sensor proteins which, through a phosphorelay mechanism, determines the overall phosphorylation state of the response regulator LuxO. At low cell density, the sensors are primarily in kinase mode leading to ATP driven autophosphorylation at the conserved histidine kinase domain of the sensors. The phosphate group is next transferred to the conserved aspartate receiver domain present at the C-terminus of each receptor. All the sensors can then transfer their phosphate group to the intermediary phospho-transfer protein, LuxU, which subsequently transfers the phosphate to the response regulator protein, LuxO. LuxO, when phosphorylated, acts as transcriptional activator.

The second module focuses on the regulated production of quorum sensing small RNAs (sRNAs) (depending on the phosphorylation state of LuxO) and the interaction between the sRNAs and the master regulator protein, LuxR. Phosphorylated LuxO in conjugation with σ^{54}-loaded RNA polymerase activates transcription of the five sRNAs, known as Qrr1-5. At LCD, the transcribed Qrr sRNAs, with the help of the RNA chaperone Hfq, destabilize LuxR by base pairing with luxR mRNA. The sRNA-mRNA complex is then degraded by the system which effectively leads to post-transcriptional repression of LuxR protein [9, 16].

At high cell density, the amount of autoinducers in the extracellular matrix exceeds the critical autoinducer concentration. Consequently, the sensors function primarily as phosphatases which reverses the direction of the phosphate group flow in the network. The corresponding lowering of LuxO-P levels leads to reduced transcription of the Qrr sRNAs. This, in turn, relieves sRNA-based repression of LuxR leading to large-scale changes in gene expression.

The interaction between sRNAs and LuxR has been the focus of several attempts to model the behavior of the QS transduction network [13, 16–21]. In these studies, the luxR/LuxR concentration is determined as a function of the expression rate of the sRNAs. The concentration of LuxR determines the level of activation or repression of a multitude of genes including the genes involved in bioluminescence [8]. In particular, the phenotypic response of luminescence in *V. harveyi* is triggered by the binding of LuxR to the promoter region of the luxCDABE operon. The corresponding change in the luminescence per cell is frequently used to infer network characteristics such as the relative rates of kinase/phosphatase activities by the sensor proteins [6].

2.2.2 Feedback Loops

In *V. harveyi*, different feedback loops have been identified experimentally that control the timing of QS transitions. For example, LuxR synthesis is controlled by an auto-repression loop [22]. In the sRNA-luxR interaction, a different feedback

loop is in operation. LuxR has been shown to activate Qrr production which in turn leads to downregulation of luxR mRNA [9]. If the colony switches rapidly from low cell density to high cell density, this feedback loop can extend the production of Qrr sRNAs and thus delay entry into the high cell density mode. In the reverse transition, i.e. rapidly changing from high cell density to low cell density, the same feedback loop increases the production of Qrr sRNAs and enables cells to rapidly switch to the low cell density state. Note that, of the five Qrr sRNAs, only *qrr2*, *qrr3*, and *qrr4* are known to participate in this feedback loop [9].

Another feedback loop arises from the location of the *qrr1* and *luxO* genes in the *V. harveyi* genome. The genes for *qrr1* and *luxO* lie adjacent to one another and are transcribed divergently. The LuxO binding site in the *qrr1* promoter overlaps with the −35 site of the *luxO* promoter. Therefore, whenever LuxO promotes *qrr1* expression, it simultaneously represses transcription of its own mRNA via blocking access to RNA polymerase [3]. Furthermore, LuxO does not need to be phosphorylated to repress the transcription of luxO. The Qrr sRNAs can also accelerate the degradation of the luxO mRNA transcript. Finally, recent work has also demonstrated that the expression of the *luxMN* operon, encoding the HAI-1 synthase and receptor, is repressed by the Qrr sRNAs [23]. The combination of these various elements of feedback regulation allows for precise control over LuxO concentration such that the production of QS sRNAs can be fine-tuned.

2.3 Modeling Approaches

From a modeling perspective, the QS signal transduction network has been explored using two different approaches: population level models [11, 13–15] and single-cell analysis [12, 19, 23–25].

2.3.1 Population Level Models

The response of the QS network critically depends on the autoinducers and their interaction with the cognate sensors. The presence of bound autoinducer to the sensors biases the transition to phosphatase mode for the sensor. Thus, removal of autoinducers or deletion of the sensors can dramatically alter phosphorelay kinetics. Figure 2.2 shows the luminescence response of several mutant variants of *V. harveyi* [6]. The difference in the luminescence profiles for different mutants can be used to infer the relative kinase/phosphatase strengths of the different sensors. These experimental results motivated the development of a minimal theoretical model based on the input module of the QS network of *V. harveyi* [11]. The theoretical formalism uses dimensionless parameters to model the phosphorelay kinetics from the sensors to the response regulator (LuxO) and is able to explain

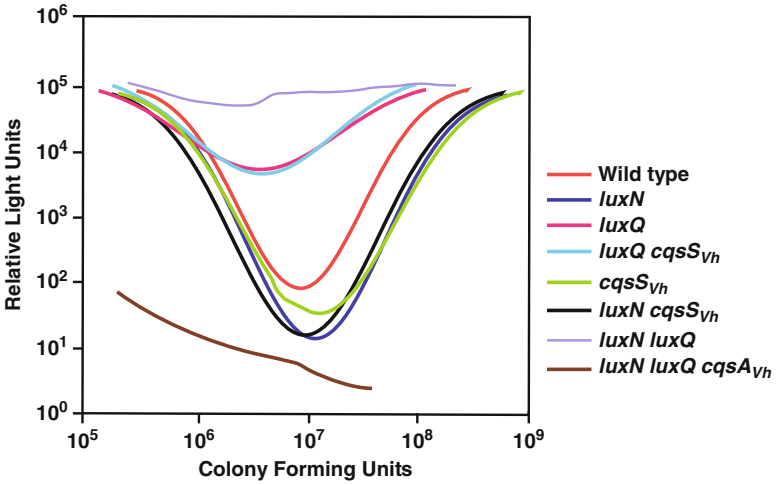

Fig. 2.2 Luminescence profiles for a variety of sensor mutants of *V. harveyi* as a function of colony forming units (cell density). Many of the mutants ($cqsS_{\mathrm{Vh}}$, $luxN\ cqsS_{\mathrm{Vh}}$, and $luxN$) show a canonical luminescence profile similar to wild-type. However, the $luxQ$ and $luxQ\ cqsS_{\mathrm{Vh}}$ mutants show a significantly degraded response. The $luxN\ luxQ$ double mutant shows almost no dependence on the size of the colony and remains at maximum light production. The triple mutant $luxN\ luxQ\ cqsA_{\mathrm{Vh}}$ shows a decay in light production as the colony grows in size

the behavior of different luminescence phenotypes for the WT strain and the mutant strains.

Important insights into the QS network of *V. harveyi* have been obtained by modeling efforts that compare the responses of QS networks of *V. harveyi* and *V. cholerae*. The regulatory networks of these two *Vibrios* are nearly topologically equivalent and homologous. However the master regulator of *V. cholerae*, HapR, is experimentally characterized as being more robust than LuxR to changes in Qrr concentrations. A detailed quantitative data driven modeling of the sRNA circuit related to the QS network of *V. harveyi* and *V. cholerae* has recently been proposed by Hunter et al [14, 15]. In their work, the authors explore the details and origin of dosage compensation, a phenomenon seen in experiments [26], between the two *Vibrios*. Their analysis also includes the proposal of new experiments, the results of which would provide a better understanding of the QS regulatory networks in the two *Vibrios*.

A study by Fenley et al. [13] also explored the different behaviors of the QS regulatory network between *V. harveyi* and *V. cholerae*. They primarily focused on the equations governing the interactions between the Qrr sRNA and LuxR/HapR mRNA using a minimal model with parameters based on experimental results. Furthermore, they investigated how the distribution of the LuxR/HapR protein concentration within the bacteria changes depending on whether the cells are at low cell density, high cell density, or at stationary phase. The LuxR/HapR protein distribution across the population of cells was modeled as a gamma distribution [27, 28] and their

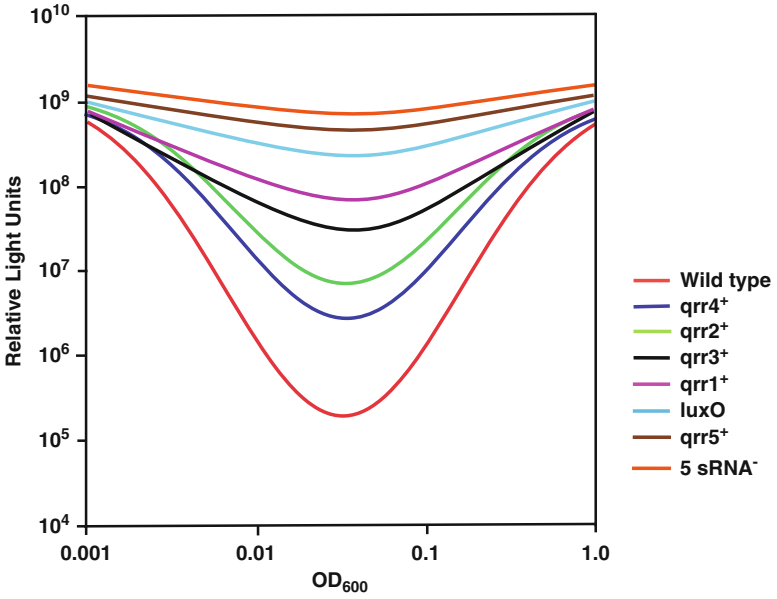

Fig. 2.3 Modeled luminescence profiles for a variety of sRNA mutants of *V. harveyi* as a function of optical density at 600 nm

approach was able to reproduce phenotypic differences between the two *Vibrios* for a variety of mutant phenotypes. Experiments have shown that the threshold of light activation requires a larger cell density for *V. cholerae* than *V. harveyi*. The theoretical model offered an explanation for this experimental observation. It was postulated that luminescence activation within *V. harveyi* is entirely governed by the QS regulatory network, whereas for *V. cholerae*, luminescence activation occurs from the combination of the QS regulatory network and additional changes in the HapR levels associated with entry into the stationary phase.

Fenley et al [13] also calculated the distribution of protein concentrations for different mutants containing only one of the active four Qrrs. The modeled phenotypic responses of the various Qrr mutants are shown in Fig. 2.3. At low cell density, all the distributions have regions extending past the threshold for light activation in *V. harveyi* resulting in some light production. However, for *V. cholerae* all the distributions are below the threshold for luminescence even at high cell density. The transition into stationary phase moves the mean of the distributions past the threshold and hence luminescence occurs *V. cholerae*. The authors are thus able to predict the additive sRNA phenotype in *V. harveyi* and the redundant behavior in *V. cholerae* by assigning different threshold values for light activation between the two *Vibrios*.

Recent work by Hunter and Keener took a different approach to modeling the *V. harveyi* and *V. cholerae* QS networks in an effort to first explain dosage compensation [15], a phenomenon originally proposed and demonstrated by Svenningsen et al [26] which provides a way to explain the differences in sRNA behavior between

the two *Vibrios*. Dosage compensation occurs when a given Qrr is absent from the system. The absence of any of the Qrrs should result in the target mRNA rising in concentration. However, due to a feedback loop, the increase in concentration of the target mRNA leads to an increase in the production of the rest of the available Qrrs and thus lowers the concentration of target mRNA to wild-type like levels. The model proposed by Hunter and Keener [15] shows that Qrr feedback is unnecessary and insufficient for Qrr redundancy in *V. cholerae*. They argue that dosage compensation is not the required mechanism as proposed by Svenningsen et al [26] behind the Qrr redundancy. Instead, they argue that sRNA additivity seen in *V. harveyi* and sRNA redundancy seen in *V. cholerae* is the result of different available concentrations of Hfq-Qrr complex needed to bind and degrade the mRNA transcript of LuxR/HapR.

Hunter and Keener [15] investigate the sensitivity of LuxR/HapR with respect to Qrr concentrations and find the sensitivity needs to be very small for Qrr redundancy to occur. Their analysis of the QS network indicates that the network architecture allows different approaches for maintaining such a low sensitivity. The first approach involves limiting the available concentration of the Hfq-Qrr complex which would lower the repression rate of LuxR/HapR by Qrr. This sets up a scenario where the concentration of LuxR/HapR is high relative to the Hfq-Qrr complex. The authors show that limitation of the concentration of the Hfq-Qrr complex can be achieved via a few different network mechanisms: a strong LuxO-Qrr feedback loop, a weak LuxR/HapR-Qrr feedback loop, a weak affinity of phosphorylated LuxO to Qrr, a high expression of LuxO relative to LuxR/HapR, and/or by a high expression of LuxR/HapR relative to Qrr. The other approach to maintaining low sensitivity results in an opposite situation as the first approach. In this case redundancy is achieved by saturating all available Hfq with Qrr and thus maximizing the Hfq-Qrr complex concentration. The authors show that in this second scenario, the repression of LuxR/HapR then becomes independent of the stoichiometry of Qrr and occurs when there is: weak LuxO-Qrr feedback, strong LuxR/HapR-Qrr feedback, low expression of LuxO relative to LuxR/HapR, and/or low expression of LuxR/HapR relative to Qrr. Based on these results, the authors thus claim that differences in Qrr feedback are neither necessary nor sufficient to explain Qrr redundancy [15].

2.3.2 Single Cell Analysis

In the QS regulatory network, multiple signals are integrated and funneled through a single channel to produce the desired network output. To understand the process of signal integration at the single cell level, Long et al [12] used single-cell fluorescence microscopy to measure the level of Qrr4-GFP for different sensor mutants. Their study revealed that in *V. harveyi*, the QS circuit allows for the synchronized response of each of the colony forming units towards the change in the level of the autoinducers. Furthermore, the results give insight into the additive nature of signal integration in the circuit.

Accurate measurement of the master regulatory protein within a QS regulatory network provides valuable information for the determination of model parameters. To determine the in vivo copy number of LuxR in *V. harveyi*, Teng et al [25] employed time lapse fluorescence microscopy [29, 30] and a static snapshot approach to measure the copy number of LuxR-*m*Cherry. The static distribution of LuxR over a large population (∼3,000 cells) gives an estimate of the Fano factor (ratio of the variance and the mean) of the protein distribution and the burst size when LuxR is highly expressed. From the single cell experimental data, the burst size was found to be ∼50 dimers when LuxR is highly expressed, i.e., in the high cell density limit. This in turn gives a measure of the average number of mRNAs (∼11) during a cell cycle. The methodology employed by Teng et al [25] is a general in vivo technique for measuring the protein copy number and burst size. In addition, this is the first report of a quantitative measurement of LuxR transcription and translation related to QS network in the high cell density limit.

In a subsequent study, Teng et al [23] further identified a negative feedback loop from Qrr sRNA to LuxMN mRNA by employing single-cell fluorescence microscopy. In addition, they created different mutants to study the input–output relation in the QS regulatory network of *V. harveyi*. They were able to determine the role of different feedback loops by varying the concentration of autoinducers and measuring the LuxR output at the single cell level using the technique developed earlier [25]. They also measured noise in LuxR protein levels for different mutants with specific feedback loops in the network disrupted as a means to investigate the role of noise in the behavior of the QS regulatory network.

Mehta et al [24] proposed a theoretical formalism for signal integration in the QS regulatory network based on information theory. Signal transduction within the QS regulatory network involves funneling multiple inputs into a single output. This type of network architecture renders unclear the extent to which bacteria are processing information from the individual inputs. Mehta et al [24] investigated why bacteria use such a mechanism for signal transduction by calculating the corresponding mutual information between the individual inputs and output. They then discuss possibly strategies the bacteria can adopt to increase information transmission from individual inputs.

In their work, receptor kinetics is modeled by a two state (on → high kinase and off → low kinase) system. Experimental results of Long et al [12] suggest that: (1) kinase activity of HAI-1 and AI-2 are nearly equal; (2) standard deviation due to cell-to-cell variations can be measured by single cell fluorescence microscopy; (3) fluctuations can be well approximated by a Gaussian function and are much smaller than mean signal. With the help of previous experimental results and assuming three types of priors [(a) a flat prior where all inputs are equally likely, (b) a bimodal prior which is symmetric for the two input signal and (c) a nonsymmetric bimodal prior] they calculated the mutual information, between the inputs (the probabilities that the LuxN and LuxPQ sensors are in their kinase mode) and the outputs (the fraction of phospho-LuxO).

Next they investigated how the kinase rate of the two pathways, k_X (HAI-1) and k_Y (AI-2) and total phosphatase rate (p) affects information transmission by

the pathway. The results show that information varies dramatically with the kinase rates. However, when phosphatase activity is large compared to kinase activity and the noise is small, the net phosphatase activity p affects information modestly. If the kinase activity of one path is much larger than the other, the cell can only learn about the stronger pathway. The cell can learn about both pathways only when both pathways are roughly equal in activity. The authors argued that this might be the reason why bacteria have almost equal kinase activity for HAI-1 and AI-2 as shown experimentally by Long et al [12].

Interestingly, setting $k_X \approx k_Y$ poses a problem to the bacteria as they can no longer distinguish the input (X, Y) from (Y, X). For example, the bacteria would not be able to distinguish the two situations: saturating HAI-1 and no AI-2 from saturating AI-2 and no HAI-1. For $k_X \approx k_Y$, the mutual information is around 0.6–0.8, which is very low. Bacteria need to learn at least 1 bit of information to differentiate the two concentration states of the autoinducers. So what are the possible mechanisms by which bacteria can learn more about the inputs? To answer this question, Mehta et al [24] discussed two possibilities: manipulation of individual input signals and feedback on receptors. Bacteria can increase the information gained by manipulating the relative autoinducer production rate. The bacterial environment contains more AI-2 than HAI-1 because AI-2 is produced by almost all bacteria whereas HAI-1 is produced only by *V. harveyi*. In this scenario where $k_X \approx k_Y$ and $x \geqslant y$, bacteria could learn about 1.5 bits of information, almost double of the previous scenario. The additional information gained by the cells is due to loss of degeneracy between HAI-1 and AI-2.

2.4 Conclusion

While QS has been extensively studied in the Vibrios, there are still multiple open questions that need to be addressed. For example, there continues to be considerable focus on understanding the specific roles of each individual AIs during QS [12,25,31,32]. Future studies along these lines will provide greater insights into the advantages and constraints relating to the QS network architecture which integrates multiple inputs signals through a single channel.

The QS pathway contains multiple feedback loops whose precise roles are still being elucidated [23]. The majority of feedback loops in the QS network are negative feedback loops. The negative feedback loop is a common network motif of gene regulatory networks, and is known to play important roles such as reducing noise in the expression of key network proteins and decreasing response times. However the precise functional roles of negative feedback loops in the QS pathway have not yet been elucidated. For example, Tu et al. [33] focused on the LuxO autorepression feedback loop and sRNA to LuxO negative feedback loop. Surprisingly they found no apparent difference in relative noise ($= \frac{\text{S.D.}}{\text{mean}}$, 20% at HCD) between the wild-type and mutant strains. They obtained similar results for qrr response times during HCD to LCD transition: the presence or absence

of feedback loops apparently made no difference in the response times. They also showed that the slope of LuxR dose response curves is very similar for wild-type and engineered mutant strains. Thus these negative feedback loops are not involved in making the dose response curve more graded in response to AI concentration. These results directed them to conclude that the role played by the different feedback loops are beyond those that had already been recognized.

Finally, while the impact of other network components (not included in the models discussed above) is currently being characterized experimentally, e.g. AphaA [34, 35], their role has yet to be explored using theoretical models. As time progresses, we anticipate that additional network components will be incorporated into the theoretical models with the aim of further increasing agreement with experiment and prediction power. Clearly there are several open questions that need to be analyzed further using a combination of experiments and modeling approaches for increased quantitative understanding of bacterial quorum sensing.

Acknowledgements AB is thankful to CSIR (09/015(0375)/2009-EMR-I) for research fellowship. SKB acknowledges support from Bose Institute through Institutional Programme VI—Development of Systems Biology. RVK would like to acknowledge funding support from the NSF through award PHY-0957430.

References

1. Miller MB, Bassler BL (2001) Quorum sensing in bacteria. Annu Rev Microbiol 55:165–199
2. Waters CM, Bassler BL (2005) Quorum sensing: cell-to-cell communication in bacteria. Annu Rev Cell Dev Biol 21:319–346
3. Ng WL, Bassler BL (2009) Bacterial quorum-sensing network architectures. Annu Rev Genet 43:197–222
4. Appleby JL, Parkinson JS, Bourret RB (1996) Signal transduction via the multi-step phosphorelay: not necessarily a road less traveled. Cell 86:845–848
5. Laub MT, Goulian M (2007) Specificity in two-component signal transduction pathways. Annu Rev Genet 41:121–145
6. Henke JM, Bassler BL (2004) Three parallel quorum-sensing systems regulate gene expression in Vibrio harveyi. J Bacteriol 186:6902–6914
7. Mok KC, Wingreen NS, Bassler BL (2003) Vibrio harveyi quorum sensing: a coincidence detector for two autoinducers controls gene expression. EMBO J 22:870–881
8. Waters CM, Bassler BL (2006) The Vibrio harveyi quorum-sensing system uses shared regulatory components to discriminate between multiple autoinducers. Genes Dev 20: 2754–2767
9. Tu KC, Bassler BL (2007) Multiple small RNAs act additively to integrate sensory information and control quorum sensing in Vibrio harveyi. Genes Dev 21:221–233
10. Bassler BL, Miller MB (2013) Quorum sensing. In: The prokaryotes. Springer, New York, pp 495–509
11. Banik SK, Fenley AT, Kulkarni RV (2009) A model for signal transduction during quorum sensing in Vibrio harveyi. Phys Biol 6:046008–046008
12. Long T, Tu KC, Wang Y, Mehta P, Ong NP, Bassler BL, Wingreen NS (2009) Quantifying the integration of quorum-sensing signals with single-cell resolution. PLoS Biol 7

13. Fenley AT, Banik SK, Kulkarni RV (2011) Computational modeling of differences in the quorum sensing induced luminescence phenotypes of Vibrio harveyi and Vibrio cholerae. J Theor Biol 274:145–153
14. Hunter GAM, Vasquez FG, Keener JP (2013) A mathematical model and quantitative comparison of the small RNA circuit in the Vibrio harveyi and Vibrio cholerae quorum sensing systems. Phys Biol 10(4):046007
15. Hunter GAM, Keener JP (2014) Mechanisms additive and redundant qrr phenotypes in *Vibrio harveyi* and *Vibrio cholerae*. J Theor Biol 340:38–49
16. Lenz DH, Mok KC, Lilley BN, Kulkarni RV, Wingreen NS, Bassler BL (2004) The small RNA chaperone Hfq and multiple small RNAs control quorum sensing in Vibrio harveyi and Vibrio cholerae. Cell 118:69–82
17. Levine E, Zhang Z, Kuhlman T, Hwa T (2007) Quantitative characteristics of gene regulation by small RNA. PLoS Biol 5:e229–e229
18. Levine E, Hwa T (2008) Small RNAs establish gene expression thresholds. Curr Opin Microbiol 11:574–579
19. Mehta P, Goyal S, Wingreen NS (2008) A quantitative comparison of sRNA-based and protein-based gene regulation. Mol Syst Biol 4:221–221
20. Mitarai N, Andersson AM, Krishna S, Semsey S, Sneppen K (2007) Efficient degradation and expression prioritization with small RNAs. Phys Biol 4:164–171
21. Mitarai N, Benjamin JA, Krishna S, Semsey S, Csiszovszki Z, Massé E, Sneppen K (2009) Dynamic features of gene expression control by small regulatory RNAs. Proc Natl Acad Sci USA 106:10655–10659
22. Chatterjee J, Miyamoto CM, Meighen EA (1996) Autoregulation of luxR: the Vibrio harveyi lux-operon activator functions as a repressor. Mol Microbiol 20:415–425
23. Teng SW, Schaffer JN, Tu KC, Mehta P, Lu W, Ong NP, Bassler BL, Wingreen NS (2011) Active regulation of receptor ratios controls integration of quorum-sensing signals in Vibrio harveyi. Mol Syst Biol 7:491–491
24. Mehta P, Goyal S, Long T, Bassler BL, Wingreen NS (2009) Information processing and signal integration in bacterial quorum sensing. Mol Syst Biol 5:325–325
25. Teng SW, Wang Y, Tu KC, Long T, Mehta P, Wingreen NS, Bassler BL, Ong NP (2010) Measurement of the copy number of the master quorum-sensing regulator of a bacterial cell. Biophys J 98:2024–2031
26. Svenningsen SL, Tu KC, Bassler BL (2009) Gene dosage compensation calibrates four regulatory RNAs to control Vibrio cholerae quorum sensing. EMBO J 28:429–439
27. Cai L, Friedman N, Xie XS (2006) Stochastic protein expression in individual cells at the single molecule level. Nature 440:358–362
28. Friedman N, Cai L, Xie XS (2006) Linking stochastic dynamics to population distribution: an analytical framework of gene expression. Phys Rev Lett 97:168302–168302
29. Rosenfeld N, Young JW, Alon U, Swain PS, Elowitz MB (2005) Gene regulation at the single-cell level. Science 307:1962–1965
30. Rosenfeld N, Perkins TJ, Alon U, Elowitz MB, Swain PS (2006) A fluctuation method to quantify in vivo fluorescence data. Biophys J 91:759–766
31. Timmen M, Bassler BL, Jung K (2006) Ai-1 influences the kinase activity but not the phosphatase activity of LuxN of Vibrio harveyi. J Biol Chem 281:24398–24404
32. Anetzberger C, Reiger M, Fekete A, Schell U, Stambrau N, Plener L, Kopka J, Schmitt-Kopplin P, Hilbi H, Jung K (2012) Autoinducers act as biological timers in *Vibrio harveyi*. PLoS ONE 7:e48310
33. Tu KC, Long T, Svenningsen SL, Wingreen NS, Bassler BL (2010) Negative feedback loops involving small regulatory RNAs precisely control the Vibrio harveyi quorum-sensing response. Mol Cell 37:567–579
34. Rutherford ST, van Kessel JC, Shao Y, Bassler BL (2011) AphA and LuxR/HapR reciprocally control quorum sensing in Vibrios. Genes Dev 25(4):397–408
35. van Kessel JC, Rutherford ST, Shao Y, Utria AF, Bassler BL (2013) Individual and combined roles of the master regulators AphA and LuxR in control of the Vibrio harveyi quorum-sensing regulon. J Bacteriol 195(3):436–443

Chapter 3
Stochastic Effects in Quorum Sensing

Marc Weber and Javier Buceta

3.1 Introduction

All of us have surely played the "broken telephone." In that game a group of people arrange in a circle and one participant passes a message to one of his/her neighbors. The message is whispered/mumbled, such that it is difficult to understand, and passed progressively along the participants until it reaches the original messenger. The funny part of the game consists in comparing the original message and the one that finally arrives (normally they have nothing to do with each other!). The "broken telephone" nicely illustrates how noise interferes with the signal in communication processes. Since quorum sensing (QS) is nothing but that, a communication mechanism, one may wonder how noise interferes with it, how bacteria cope with fluctuations, and how to provide a modeling framework for addressing these questions.

Yet, what do we mean by noise? Over the past decade a number of studies have shown that the level and activity of the species involved in gene regulatory circuits fluctuate [1]. While extrinsic factors are in some cases the source of these fluctuations (e.g., light fluctuations in circadian clocks [2]), in most situations they are mainly due to the inherent randomness of biochemical reactions when the number of molecules is very low [3]. Under these conditions, the value of the mean and the variance are of the same order and consequently the deterministic description fails. Notably, biochemical noise, either intrinsic or extrinsic, is not

M. Weber
Co.S.Mo. Lab (Computer Simulation and Modeling), Parc Cientific de Barcelona, C/Baldiri Reixac 4-8, Barcelona 08028, Spain

J. Buceta (✉)
Department of Chemical and Biomolecular Engineering, Lehigh University, 111 Research Drive, Room D316 Bethlehem, PA 18015, USA
e-mail: jbuceta@gmail.com

S.J. Hagen (ed.), *The Physical Basis of Bacterial Quorum Communication*, Biological and Medical Physics, Biomedical Engineering, DOI 10.1007/978-1-4939-1402-9_3

necessarily a nuisance but a biological component that is essential and has a positive functional role in many situations [4]: for example, improving cellular regulation [5].

In the particular case of QS, the detection of the freely diffusing signaling molecule, the autoinducer, is subject to intense molecular noise [6]. Still, QS bacteria cope with these fluctuations reliably. For example, the typical volume of *Vibrio fischeri* bacteria is $0.35\,\mu m^3$, and a concentration of 10 nM of autoinducer already induces a QS response [7]. This means that just $\sim$2 signaling molecules per cell are enough to be sensed by this small marine bacterium. The low number of signaling molecules inside the cell, together with the other possible sources of noise, indicates that the fluctuations at the autoinducer level must be taken under consideration for a deep understanding of the QS pathway activation and functioning. Moreover, the stochastic effects in QS pose the intriguing question of how cells achieve a coordinated response in the presence of noise. Indeed, the QS mechanism may produce a robust and synchronized behavior at the level of the population [8]. However, how this behavior at the collective level arises from the stochastic dynamics of individual cells is puzzling. At the end, a collective response means a precise information exchange in the colony: the quantification of the number of cells, the density, in the colony. Consequently, how can a bacterial population estimate its number of constituents precisely if such information is fuzzy at the single cell level?

At the most fundamental level, cell communication by QS relies on the diffusion of a signaling molecule through the cell membrane. Recent studies have shown that diffusion reduces the noise at the level of the autoinducer [9]; however, the interplay between the diffusion process and some standard sources of stochasticity (transcriptional and biochemical noise) has remained elusive until very recently [10]. Moreover, while in eukaryotes the diffusion seems to contribute for enhancing the precision of regulatory processes [11], similar effects have not been reported in the context of QS. Thus, a first central question is to elucidate how the diffusion process influences, and interplay with, the fluctuations in the signaling molecule.

Another relevant point refers to the relation between the QS signaling network architecture and its ability to filter and/or enhance and/or suppress noise. While this question is case dependent, general clues and answers can be obtained by studying simple QS systems, e.g. the LuxI/LuxR system, as the underlying signaling motif in most QS species is a positive feedback loop leading to phenotypic bistability [12]. As a matter of fact, a number of studies have shown that noise plays an important role in bistable systems [13–17]. In the context of QS, it has been recently revealed how noise at different levels of the signaling network controls the precision of the collective response [18] and, ultimately, how noise modifies the phenotypic landscape that produces the observed heterogeneity in QS colonies.

Herein we shed light on these aspects of the stochasticity in QS communication by reviewing recent advances in the field. Altogether, the results suggest that bacteria have adapted their communication mechanisms in order to improve the signal-to-noise ratio and to adjust the intensity of the fluctuations depending on the environmental conditions. The chapter is organized as follows. We first illustrate by

means of a toy model how, at the onset of the QS transition, the autoinducer diffusion process conditions the QS dynamics and that the interplay between different sources of noise establishes ranges of diffusion values that minimize the noise at the autoinducer level. We then show by means of a detailed model of the LuxI/LuxR system how fluctuations interfere with the synchronization of the cell activation process and lead to a bimodal phenotypic distribution. In this context, we review the concept of precision in order to characterize the reliability of the QS communication process in the colony. In terms of the network architecture, we show that increasing the noise in the expression of LuxR helps cells to get activated at lower autoinducer concentrations but, at the same time, slows down the global response. Some of the observed properties are rather counterintuitive, e.g. noise at the level of LuxR helps cell to become activated at low autoinducer values but above a certain threshold of the autoinducer concentration the fluctuations stabilize the cell at the unactivated phenotype. As we will see, the latter can be explained by analyzing how noise modifies the phenotypic landscape. Finally, we present the main conclusions and discuss the applicability and relevance of these studies in the context of noise in QS communication.

3.2 Diffusion and Noise

QS communication relies on the diffusion of the signaling molecule through the cell membrane. On top of that, the autoinducer is subjected to different sources of noise and the following question naturally arises: what is the interplay between the diffusion process and the autoinducer stochastic dynamics? In this regard, a recent study has shown that diffusion, together with a fast turnover of the QS transcriptional regulator, attenuates low-frequency components of extrinsic noise at the level of the autoinducer [9]. These authors have coined the term “diffusional dissipation” that emphasizes the importance of fast signal turnover (or dissipation) by diffusion in QS. Other studies have used some characteristics of the diffusion process in Gram-negative bacteria (the permeability of the cell membrane to the autoinducer and the symmetry of autoinducer diffusion) to demonstrate that the extracellular noise is required for a stable synchronization in the colony [19].

These studies assume a constitutive expression of the QS master regulators. However, QS communication also relies on situations when the levels of transcription/translation are very low and the system lacks autoinduction. Thus, at low cell density, *luxI* gene expression is either repressed by a high concentration of its repressor or activated at a very low level by its activator. Under these conditions, very few *luxI* transcripts are produced and the feedback regulation of the *luxI* gene leading to autoinduction can be disregarded. Such infrequent transcription events have been observed in many bacterial operons. For example, single molecule experiments have shown that the infrequent dissociation of the lac repressor produces rare transcription events leading to just one mRNA molecule [20, 21]. Importantly, when the transcription rate is very low, the so-called transcriptional noise is a major source of stochasticity [3].

In this section we focus on the interplay between the diffusion process and the transcriptional and intrinsic noises. We aim at understanding how the communication mechanism and different sources of noise determine the dynamics of the autoinducer. We restrict ourselves to the study of the aforementioned problems below the QS activation threshold where we can assume that the transcription events produce basal constitutive levels of mRNA of at most one molecule per cell at a time and the regulatory feedback loop can be neglected.

3.2.1 Modeling the LuxI mRNA Leaky Dynamics

Below the activation (autoinduction) threshold, it can be assumed that rare (basal) transcription events produce individual *luxI* transcripts. Under these conditions the dynamics of the mRNA can be then described by means of a Markovian dichotomous process [22],

$$M_0^i \underset{\alpha}{\overset{\beta}{\rightleftarrows}} M_1^i \tag{3.1}$$

where $M_{0,1}^i = 0, 1$ stands for the number of mRNA molecules at cell i and α and β for the transition rates between these states; i.e., α and β account for the mRNA degradation rate and the transcription frequency, respectively. Notice that the fluctuations of the mRNA dynamics are not memoryless, i.e. white. Once an mRNA molecule is produced, and until it becomes degraded, the cell keeps producing the autoinducer. That is, the transcriptional noise is a colored noise, and its autocorrelation decays exponentially with a characteristic time scale $\tau_c = (\alpha + \beta)^{-1}$ [22].

Once an mRNA molecule is produced it leads to the appearance of functional LuxI synthetases. It has been shown that the amount of the synthetase substrate is not a limiting factor for the production of the autoinducer [23, 24]. As a consequence, the levels of the signaling molecule depend directly on the expression levels of the synthetase. Ignoring intermediate biochemical steps in the autoinducer synthesis reduces the number of noise sources and may even change, under some circumstances, the observed dynamics [25]. Still, it is a valid approximation in most cases and one can assume that the translation of the synthetase and the subsequent synthesis of the autoinducer, A, can be effectively described by a single chemical step with rate k_+. In addition, the autoinducer becomes degraded at a rate k_-, that is,

$$M_1^i \xrightarrow{k_+} M_1^i + A^i \tag{3.2}$$

$$A^i \xrightarrow{k_-} \varnothing \tag{3.3}$$

$$A_{\text{ext}} \xrightarrow{k_-} \varnothing \ . \tag{3.4}$$

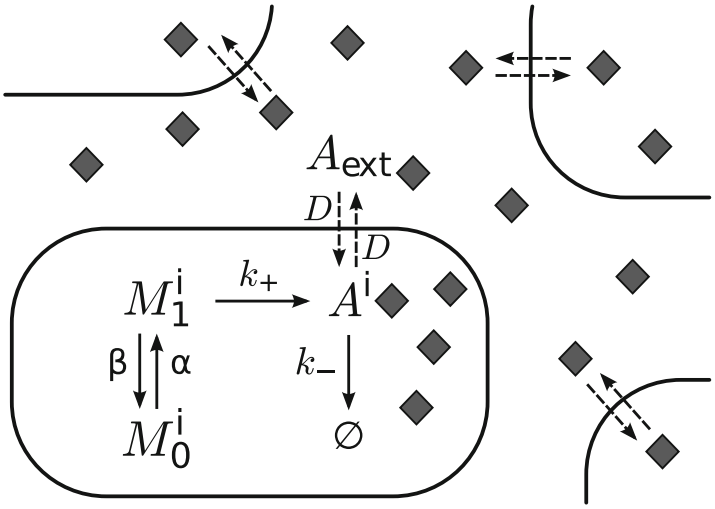

Fig. 3.1 Scheme of a simplified biochemical QS network near the activation threshold. Schematic representation of the biochemical processes considered for describing the dynamics of the signaling molecule, A (*diamonds*), in cell i. The mRNA dynamics follow a dichotomous process with state values $M_{0,1}$ corresponding to zero and one molecule, respectively. Once the autoinducer has been produced, it can diffuse into and out of the cell leading to cell communication

where A_{ext} accounts for the number of signaling molecules in the extracellular medium. Passive diffusion in and out the cell of the autoinducer can be implemented by means of the reaction:

$$A^i \underset{rD}{\overset{D}{\rightleftarrows}} A_{\text{ext}} \tag{3.5}$$

where D stands for the diffusion rate and $r = V/V_{\text{ext}}$ represents the ratio of the volume of a cell to the total extracellular volume. Figure 3.1 schematically represents the biochemical processes described by the set of reactions (3.1)–(3.5).

3.2.2 Null-intrinsic Noise Approximation

Two stochastic contributions drive the dynamics of A: the mRNA fluctuations due to the random switching and the intrinsic noise due to low copy number of the resulting autoinducer. As of the latter, it can be neglected if over the course of time $A^i/\left(A^i+1\right) \simeq 1$ ("large" number of autoinducer molecules). While such approximation is not justified (see parameters values below), it is useful to implement it in order to discriminate between the effects caused by different stochastic contributions and to obtain analytical expressions. In this case, it is

straightforward to demonstrate that the dynamics of the autoinducer, (3.1)–(3.5), can be described by the following coupled stochastic equations:

$$\dot{c}_{A^i} = k_+ c_{M_1^i}(t) - k_- c_{A^i} + D\left(c_{A_{\text{ext}}} - c_{A^i}\right) \tag{3.6}$$

$$\begin{aligned}\dot{c}_{A_{\text{ext}}} &= -k_- c_{A_{\text{ext}}} + rD\sum_{i=1}^{N}\left(c_{A^i} - c_{A_{\text{ext}}}\right) \\ &= -k_- c_{A_{\text{ext}}} + rDN\left(\langle c_A\rangle - c_{A_{\text{ext}}}\right),\end{aligned} \tag{3.7}$$

where $c_{A^i} = A^i/V$, $c_{M_1^i}(t) = M_1^i/V$, and $c_{A_{\text{ext}}} = A_{\text{ext}}/V_{\text{ext}}$ stand for the concentration of species A and M_1^i at cell i and for species A_{ext} at the extracellular medium, respectively, N is the bacterial colony size, and $\langle\cdot\rangle$ represents the population average. In Eq. (3.6) the term $c_{M_1^i}(t)$ accounts for a dichotomous stochastic process characterized by the rates and states (α, β) and $(0, 1/V)$, respectively, and describes the fluctuating dynamics of the mRNA concentration.

By implementing a quasi-steady approximation for the dynamics of the external autoinducer, i.e. $\dot{c}_{A_{\text{ext}}} = 0$ we obtain that,

$$c_{A_{\text{ext}}} = \langle c_A\rangle \frac{1}{1+\frac{k_-}{NDr}}\,. \tag{3.8}$$

By substituting (3.8) into (3.6) we obtain a rate equation for the concentration of the signaling molecule inside a given cell that depends on the average $\langle c_A\rangle$ (the index i has been dropped),

$$\dot{c}_A = k_+ c_{M_1}(t) - D\left(1+\frac{k_-}{D}\right)c_A + \langle c_A\rangle \frac{D}{1+\frac{k_-}{NDr}}\,. \tag{3.9}$$

In the absence of diffusion, Eq. (3.9) reveals that the concentration of the signaling molecule reaches a maximum value of $c_A^+ = k_+/(k_- V)$ when $c_{M_1}(t) = V^{-1}$. In terms of c_A^+ and the time scale $t_c = 1/k_-$ (the typical lifetime of a signaling molecule), the dimensionless version of (3.9) reads

$$\dot{\tilde{c}}_A = \hat{c}_{M_1}(\tilde{t}) + k_+^{\text{eff}}\left(\langle\tilde{c}_A\rangle\right) - k_-^{\text{eff}}\tilde{c}_A\,, \tag{3.10}$$

where

$$\tilde{D} = D/k_- \tag{3.11}$$

$$k_-^{\text{eff}} = 1 + \tilde{D} \tag{3.12}$$

$$k_+^{\text{eff}}\left(\langle\tilde{c}_A\rangle\right) = \langle\tilde{c}_A\rangle\,\frac{\tilde{D}}{1+\frac{1}{N\tilde{D}r}}\,; \tag{3.13}$$

$\hat{c}_{M_1}(\tilde{t})$ being a Markovian dichotomous noise with states $\{\hat{c}_{M_1}\} = 0, 1$ and rates $\tilde{\alpha} = \alpha/k_-$ and $\tilde{\beta} = \beta/k_-$. Equation (3.10) can be formally closed by invoking the following self-consistency condition:

$$\langle \tilde{c}_A \rangle = \int_{\tilde{\Omega}} \tilde{c}_A \, \rho\left(\tilde{c}_A; \langle \tilde{c}_A \rangle\right) \mathrm{d}\tilde{c}_A, \tag{3.14}$$

$\rho\left(\tilde{c}_A; \langle \tilde{c}_A \rangle\right)$ being the probability density solving (3.10) and $\tilde{\Omega}$ its support (see below) [22]:

$$\rho\left(\tilde{c}_A; \langle \tilde{c}_A \rangle\right) = \mathscr{N}\left(k_-^{\mathrm{eff}} \tilde{c}_A - k_+^{\mathrm{eff}}\left(\langle \tilde{c}_A \rangle\right)\right)^{\frac{\tilde{\beta}}{k^{\mathrm{eff}}} - 1} \tag{3.15}$$

$$\left(1 + k_+^{\mathrm{eff}}\left(\langle \tilde{c}_A \rangle\right) - k_-^{\mathrm{eff}} \tilde{c}_A\right)^{\frac{\tilde{\alpha}}{k^{\mathrm{eff}}} - 1}, \tag{3.16}$$

with

$$\mathscr{N} = \frac{\left(1 + \tilde{D}\right) \Gamma\left[\frac{\tilde{\alpha}+\tilde{\beta}}{1+\tilde{D}}\right]}{\Gamma\left[\frac{\tilde{\alpha}}{1+\tilde{D}}\right] \Gamma\left[\frac{\tilde{\beta}}{1+\tilde{D}}\right]} \tag{3.17}$$

being the normalization constant. The condition (3.14) can be exactly solved and leads to the following value for the average concentration of autoinducer:

$$\langle \tilde{c}_A \rangle = \frac{1 + \tilde{D} N r}{1 + \tilde{D} N r + \tilde{D}} \frac{\tilde{\beta}}{\tilde{\alpha} + \tilde{\beta}} = \frac{1 + \tilde{D} N r}{1 + \tilde{D} N r + \tilde{D}} \langle \tilde{c}_A \rangle|_{\tilde{D}=0} \tag{3.18}$$

where $\langle \tilde{c}_A \rangle|_{\tilde{D}=0} = \tilde{\beta}/\left(\tilde{\alpha} + \tilde{\beta}\right)$ is the average concentration of the signaling molecule in the absence of diffusion. For the sake of concision, on what follows we drop in the notation of $\rho\left(\tilde{c}_A; \langle \tilde{c}_A \rangle\right)$ the term $\langle \tilde{c}_A \rangle$ from the argument. Note that $\rho\left(\tilde{c}_A\right)$ has two states (barriers) that define its support. That is, the minimum and maximum values that the concentration of the autoinducer can reach as a function of the diffusion are:

$$\tilde{c}_A^- = \frac{\tilde{D}^2 N r}{(1 + \tilde{D})(1 + \tilde{D} + \tilde{D} N r)} \frac{\tilde{\beta}}{\tilde{\alpha} + \tilde{\beta}} \tag{3.19}$$

$$\tilde{c}_A^+ = \tilde{c}_A^- + \frac{1}{1 + \tilde{D}}. \tag{3.20}$$

Moreover, it is easy to prove that the probability density $\rho\left(\tilde{c}_A\right)$ shows a single extremum if

$$\tilde{\alpha}, \tilde{\beta} \lesssim k_-^{\mathrm{eff}}, \tag{3.21}$$

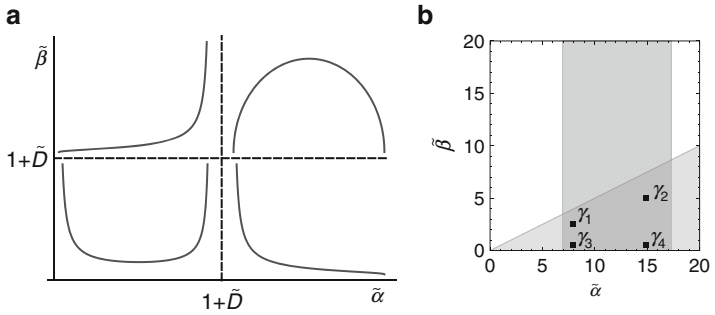

Fig. 3.2 Probability densities of the signaling molecule and parameter space. (**a**) Sketch of the different probability densities of the autoinducer concentration depending on the value of $\tilde{\alpha}$ and $\tilde{\beta}$ with respect to $\tilde{D}$. Given a set of values $(\tilde{\alpha}, \tilde{\beta})$ the dynamics of the autoinducer shows different behaviors depending on the value of the diffusion parameter since the transition lines are located at $\tilde{\alpha}, \tilde{\beta} = 1 + \tilde{D}$. The constraints set by the approach (one mRNA at a time) make the region on the top-left corner non-accessible. (**b**) Parameter space diagram $(\tilde{\alpha}, \tilde{\beta})$ indicating the sets of parameters used in simulations (*solid squares*): $\gamma_1 = (8, 2)$, $\gamma_2 = (15, 5)$, $\gamma_3 = (8, 0.5)$, $\gamma_4 = (15, 0.5)$. The experimental values reported for the degradation rate of the mRNA leads to a biological meaningful range for $\tilde{\alpha}$ (*rectangular region*). The low constitutive expression assumption is prescribed by the constraint $\tilde{\alpha} > 2\tilde{\beta}$ (*triangular region*)

where the extremum is a maximum if $\tilde{\alpha}, \tilde{\beta} > k_{-}^{\text{eff}}$ and a minimum if $\tilde{\alpha}, \tilde{\beta} < k_{-}^{\text{eff}}$. In other cases the probability density does not display any extrema. Therefore, as a function of $\tilde{\alpha}$ and $\tilde{\beta}$, the probability density $\rho(\tilde{c}_A)$ may show four different behaviors depending on the value of the diffusion coefficient as schematically represented in Fig. 3.2a. However, given the constraints on the parameters of our modeling not all regions, i.e. behaviors, are accessible to the autoinducer dynamics. In particular, we have assumed a low constitutive expression such that only a single mRNA molecule can be transcribed at a time. The latter implies that $\tilde{\beta} < \tilde{\alpha}$ (the degradation rate of the mRNA is larger than the transcription rate) in order to assure that a maximum of one mRNA molecule is present in a cell at any given time. As a consequence, and independently of the diffusion value, the dynamics leading to the probability density shown at the top-left region of Fig. 3.2a (for which $\tilde{\beta} > \tilde{\alpha}$) cannot be considered as physical in the context of a *luxI* leaky mRNA dynamics.

Finally, the noise of the autoinducer concentration can be estimated by computing the ratio between the variance and the mean[1]:

$$\eta^2_{\tilde{c}_A} = \frac{\sigma^2_{\tilde{c}_A}}{\langle \tilde{c}_A \rangle^2} = \frac{\tilde{\alpha}\left(1+\tilde{D}+\tilde{D}Nr\right)^2}{\tilde{\beta}\left(1+\tilde{D}\right)\left(1+\tilde{D}Nr\right)^2\left(1+\tilde{D}+\tilde{\alpha}+\tilde{\beta}\right)} \tag{3.22}$$

[1]Note that "noise" has been used with two different meanings: a stochastic contribution and, in this case, a quantity that effectively measures the effects of that stochastic contribution.

where $\sigma^2_{\tilde{c}_A} = \langle \tilde{c}_A^2 \rangle - \langle \tilde{c}_A \rangle^2$. Note that in a purely deterministic system $\eta^2_{\tilde{c}_A} = 0$. On the other hand, in systems where fluctuations play a relevant role in the dynamics $\eta^2_{\tilde{c}_A} \gtrsim 1$.

3.2.3 QS Switch at the Onset: Parameter Values

Herein we are particularly interested in the role played by the fluctuations of the signaling molecule, A, when its concentration is close, yet below, to the activation threshold of the QS switch such that autoinduction doesn't play a role and the basal leaky dynamics of the luxI mRNA holds. Therefore, we fix the mean concentration of the autoinducer and modulate the rest of the parameters in order to keep constant this value. According to some recent experiments [6], a value of $c_A^0 = 25$ nM is reasonable for most of the bacterial species when the value of the so-called sensing potential, $\nu = (rN)^{-1}$, is $\nu \sim 10^3$. In our simulations we choose $N = 10^2$ and then $V_{\text{ext}} = \nu N V = 10^5 V$ (i.e., $r = 10^{-5}$). Keeping ν to a constant value necessarily requires an external dilution protocol for maintaining constant the cell density and compensate for cell growth at a rate, $\sim 2 \cdot 10^{-2}$ min^{-1} (i.e., cell cycle duration $\sim$50 min). In addition, we notice that most autoinducer molecules are rather stable. For example, the degradation rate of the homoserine lactone 3-oxo-C6-AHL has been measured in vitro: $\sim 3 \cdot 10^{-4}$ min^{-1} [26]. The values in vivo has been also estimated [6]: $\sim 5 \cdot 10^{-3}$–$2 \cdot 10^{-2}$ min^{-1}. Consequently, the dilution process constitutes the main source of effective degradation of A, both inside and outside the cell.

As for the luxI mRNA dynamics, the half-lives of all mRNAs of *Staphylococcus aureus* have been recently measured during the mid-exponential phase. Most of the transcripts (90 %) have half-lives shorter than 5 min [27, 28]. According to these studies we restrict the mRNA degradation rate to the range $\ln(2)/5$ min^{-1} $< \alpha <$ $\ln(2)/2$ min^{-1} and consequently $\tilde{\alpha} > 1$. As for the frequency of the transcription events, β is determined by particular characteristics of the gene regulatory process under consideration, like the affinity of the regulatory proteins to the operator site and the initiation rate of transcription. Due to the assumption of low constitutive transcription, we choose values of parameter β satisfying the relation $\alpha > \beta$. In particular in our simulations we implement the more restrictive condition $\alpha > 2\beta$. Figure 3.2b recapitulates the different sets of α and β values that we use in our simulations and analytical calculations. Summarizing, N, r, and k_- are kept fixed and we explore the parameter space α, β, and D within the ranges and constraints mentioned above. In every particular situation we determine the value of k_+, see Eq. (3.18), in order to keep $\langle c_A \rangle = 25$ nM.

3.2.4 Passive versus Active Transport in QS

The rate of passive diffusion has been estimated for the 3-oxo-C6-AHL autoinducer [9]: $\sim 10^3$ min^{-1}. Under these conditions the typical value for the normalized parameter $\tilde{D}$ is of the order of 10^4. Yet, active transport mechanisms for the autoinducer lead to much smaller effective diffusion values. For example, in the bacterial species *Pseudomonas aeruginosa*, C4-HSL can freely diffuse but C12-HSL, a larger signaling molecule, is subjected to active influx and efflux where its importation and exportation rates are of the order of $\sim 10^{-2}$ min^{-1} and $\sim 10^{-1}$ min^{-1}, respectively [29]. Other example corresponds to the AI-2 signaling molecule. The latter is present in many Gram-positive and Gram-negative species and it is believed to allow for interspecies communication [30]. In *Escherichia coli* and *Salmonella enterica* extracellular AI-2 accumulates during the exponential phase, but then decreases drastically upon entry into the stationary phase. This reduction is due to the import and processing of AI-2 by the Lsr transporter [30,31]. Moreover, excretion from the cell of this autoinducer also appears to be an active process involving the putative transport protein YdgG (or alternatively named TqsA) [32]. In the case of *E. coli* these rates have been estimated by computational and experimental means: $D_{\text{out}} \simeq 10^{-1}$ min^{-1} and $D_{\text{in}} \simeq 10^{-3} - 10^{-2}$ min^{-1} [33].

In principle our model does not account for active diffusion processes, but transport driven by concentration differences. Still, our simple model is valid when the active transport mechanism can be described by two symmetric first-order transport reactions. If we assume that the excretion and uptake systems follow the Michaelis–Menten kinetics then, in the regime where the concentration of autoinducer (substrate) is much smaller than the K_m of the enzymatic reaction, the transport rate can be approximated by a first-order reaction with rates $D_{\text{in}} c_{A_{\text{ext}}}$ and $D_{\text{out}} c_a$. If, in addition, we assume that the transport rates are symmetric, $D_{\text{in}} = D_{\text{out}}$, the resulting dynamics are identical to the case of passive diffusion. Under these conditions, the rates of active transport in the QS systems described above would fit in our model with a normalized diffusion coefficient in the range $\tilde{D} \in [10^{-1}, 10]$. All in all, the transport rates when driven by active processes are four orders of magnitude smaller than the diffusion rate of small molecules through the membrane. Hence, transport rates in QS systems can be categorized into two main, well-separated, classes: small transport rates due to active process, and large diffusion rates due to passive mechanisms.

3.2.5 Dynamics and Population Heterogeneity driven by Diffusion

According to the analytical results, as a function of $\tilde{D}$ one can expect a rich phenomenology since the transition lines in the parameter space $(\tilde{\alpha}, \tilde{\beta})$ shift as a function of the diffusion (see Fig. 3.2a). By taking as a reference the case

γ_2, that is $(\tilde{\alpha}, \tilde{\beta}) = (15, 5)$, Fig. 3.3 shows the effect of the diffusion on the distribution (left column) and dynamics (center column) of c_A in a given cell. The results were obtained by means of numerical simulations of the set of reactions (3.1)–(3.5) using the Gillespie algorithm in an N-cells system [34]. The system initially displays a single-peak distribution and by increasing the diffusion rate we observe transitions to other behaviors (monotonically decreasing and double-peak distributions). For $\tilde{D} = 10$, the diffusion is already large enough to remove signaling molecules between consecutive mRNA burst events, thus leading to a monotonically decreasing distribution. Increasing the diffusion rate to $\tilde{D} = 100$ leads to the situation where both $\tilde{\alpha}$ and $\tilde{\beta}$ become smaller than $1 + \tilde{D}$ and a bistable dynamics develops. Note that, counterintuitively, increasing the diffusion leads to a population heterogeneity instead of homogenizing the colony. As the diffusion further increases, e.g. $\tilde{D} = 2 \cdot 10^3$, the autoinducer molecules diffusing from the external medium into the cell set a constitutive level of this species. The latter explains the presence of A molecules in the cell even if no mRNA is produced. Finally, at very large values of $\tilde{D}$, e.g. $\tilde{D} = 5{\cdot}10^4$, the low constitutive concentration of the autoinducer increases due to the influx of molecules when no mRNA is present whereas the concentration of A that is internally produced decreases due to the efflux of molecules. In this case, the whole N-cells system can be considered as a single volume with no diffusive barriers between cells. Thus, the burst events average out and, as a consequence, a single effective peak again develops for the concentration of the autoinducer.

Figure 3.3 shows that the theoretical distribution captures the essential features of the dynamics obtained in the numerical simulations. Note that the noticeable deviations are due to the intrinsic noise (i.e., to the low number of molecules) of the signaling molecule A that are not considered in the theoretical analysis. Moreover, notice that as the diffusion increases those deviations seem to be larger. Yet, we stress that as $\tilde{D}$ changes we modulate the production rate k_+ so that the average number of autoinducer molecules per cell remains constant. Consequently, the deviations between the simulations and the theoretical analysis cannot be ascribed to a putative decrease of the number of A molecules (i.e., to an increase of the intrinsic noise).

In order to ensure that the intrinsic fluctuations are not actually increasing due to diffusion we first perform the following *in silico* control experiment. We consider a modification of the system such that a single mRNA molecule transcript leads to two autoinducer molecules that are considered to be distinguishable: A_1^i and A_2^i. Following [35], by plotting the distribution of c_{A_1} as a function of c_{A_2} we can then discern a putative increase of the intrinsic fluctuations. Right column of Fig. 3.3 shows that the width of the distribution in a direction perpendicular to the diagonal (a measure of the intrinsic fluctuations) does not vary and consequently so does not the intrinsic noise. Thus, we must conclude that as the diffusion increases the balance between the mRNA and the intrinsic fluctuations get modified. Indeed, as shown in Eq. (3.22) the noise due to the mRNA dynamics behaves as $\sim 1/\tilde{D}$ for large values of $\tilde{D}$. Therefore, the deviations between the theoretical and the numerical

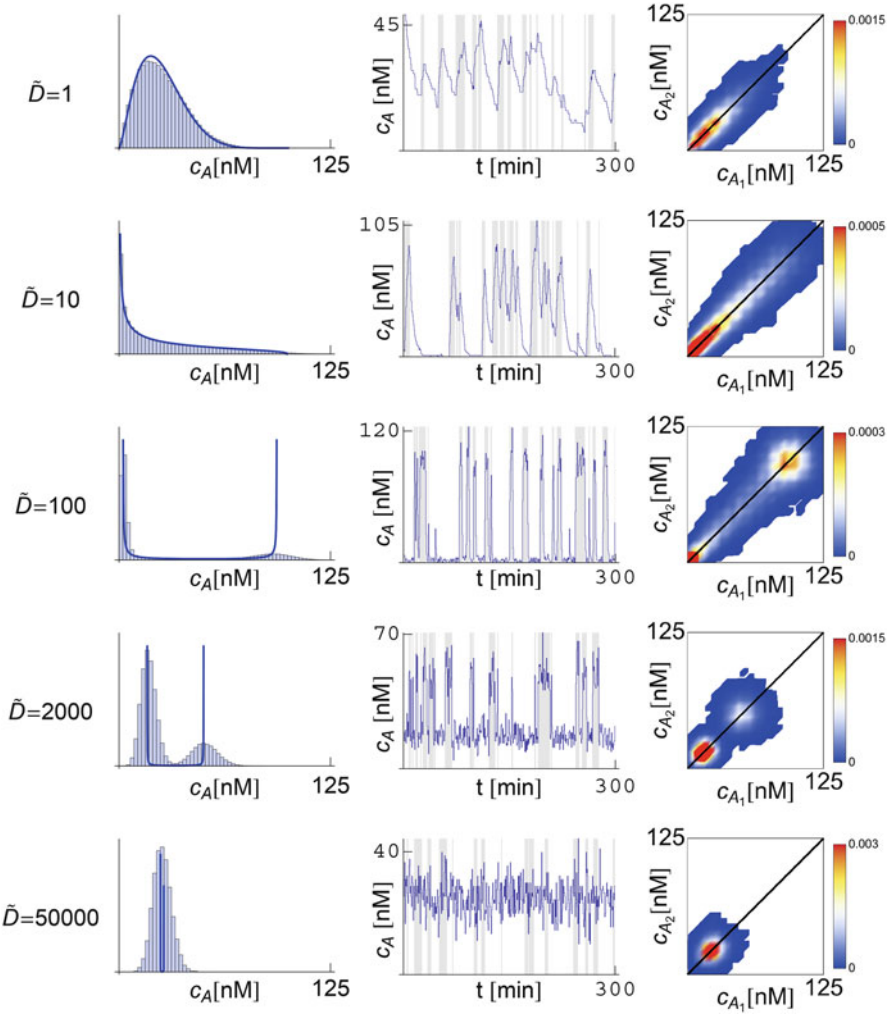

Fig. 3.3 Distributions and dynamics of the signaling molecule. Distributions (*left column*) and dynamics (*center column*) of c_A at steady-state for different values of $\tilde{D}$. In all cases the parameters set $(\tilde{\alpha}, \tilde{\beta})$ is γ_2 (see Fig. 3.2b). The production rate $\tilde{k}_+$ is modulated as a function of $(\tilde{\alpha}, \tilde{\beta}, \tilde{D})$ in order to maintain constant the average $\langle c_A \rangle = 25$ nM. The histograms obtained in the stochastic simulations (*blue bars, left column*) are in qualitative agreement with the probability densities from the analytical calculations (*blue line, left column*). When increasing the diffusion coefficient the system explores different dynamics as revealed by the trajectories shown in the center column. The *gray-shaded background* shown in the trajectories of c_A indicates the presence of an mRNA molecule in the cell. In order to discern a putative increase in the molecular noise we perform stochastic simulations of a modified system in which a single mRNA molecule produces two distinguishable autoinducer molecules A_1 and A_2. The density plots (*right column*) of the distribution of c_{A_2} vs c_{A_1} reveal that the diffusion does not contribute to an increase of the intrinsic noise since the spreading of the distributions in a direction perpendicular to the diagonal does not grow when increasing $\tilde{D}$

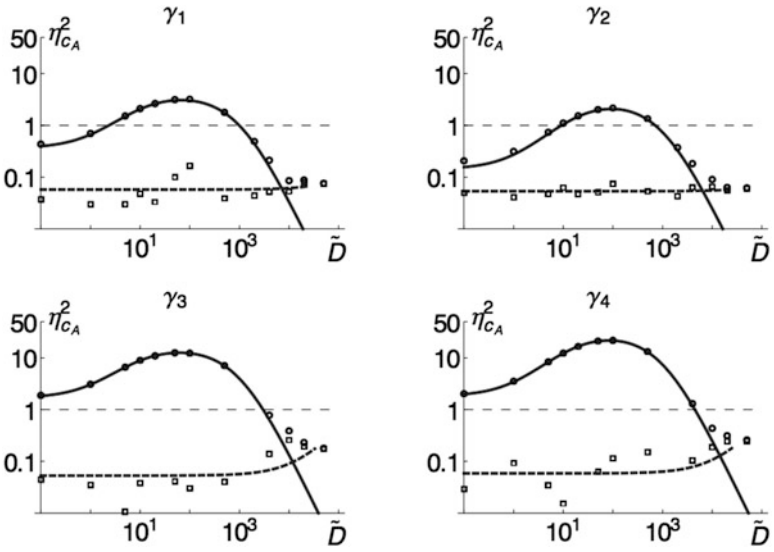

Fig. 3.4 Total noise in the signaling molecule as a function of the diffusion coefficient. Total noise $\eta^2_{c_A}$ as a function of diffusion coefficient $\tilde{D}$ for the sets of parameters $\gamma_{1,2,3,4}$ (see Fig. 3.2b): stochastic simulations (*circles*) and analytical expression (3.22) (*solid line*). The difference between the computational and the theoretical distributions quantifies the amount of intrinsic noise (*squares*). The latter remains constant and is the main contribution to the total noise only for large diffusion values, $\tilde{D} > 10^4$. The function is non-monotonic and has a maximum value above $\eta^2_{c_A} > 1$ for all parameter sets, showing that the variance is larger than the mean for intermediate ranges of $\tilde{D}$

approaches are due to a drop of the fluctuations related to the mRNA dynamics such that for large enough diffusion rates, the intrinsic noise constitutes the main source of stochasticity.

3.2.6 Total Noise in QS Communication Lacking Autoinduction

It is interesting to place these results in the context of the total noise present in the autoinducer concentration. Figure 3.4 reveals that $\eta^2_{c_A}$ shows a non-monotonic behavior. As a function of $\tilde{D}$ the total noise first increases and reaches a maximum at $\tilde{D} \sim 10^2$ and then decreases as the diffusion becomes larger. Note that for a large range of $\tilde{D}$ values the analytical calculations, that just account for the transcriptional noise, are in agreement with the numerical simulations, that account for both the transcriptional and the intrinsic noise. This indicates that the main contribution to the total fluctuations for a large range of diffusion values is the transcriptional noise. Yet, as mentioned above, the latter diminishes as the diffusion increases while the

intrinsic fluctuations remain constant. Consequently, the contribution of the intrinsic noise must become more relevant than the mRNA stochasticity beyond some value of $\tilde{D}$. One can address the relative importance of the noisy sources by using the decomposition $\eta^2_{c_A} = \eta^2_{c_A,\text{int}} + \eta^2_{c_A,\text{tran}}$, where $\eta^2_{c_A,\text{int}}$ and $\eta^2_{c_A,\text{tran}}$ stand, respectively, for the intrinsic and the transcriptional contributions to the total noise [36]. Thus, by subtracting the analytical expression of the transcription noise given by Eq. (3.22) to the total noise obtained in the numerical simulations we are able to compute the intrinsic noise as a function of the diffusion (see Fig. 3.4). By performing a linear regression of the points that corresponds to the intrinsic noise we obtain that the slope of the curve is indeed zero in practical terms ($2 \cdot 10^{-7}$ for parameter set γ_2). Therefore, in agreement with the results obtained in Fig. 3.3 (right column), the intrinsic noise remains constant ($\eta^2_{c_A,\text{int}} = 0.054 \pm 0.003$ for parameter set γ_2) as the diffusion increases and is the main stochastic component if $\tilde{D} \gtrsim 10^4$.

The non-monotonic behavior of the total noise as a function of the diffusion rate suggests a new interpretation of the role of noise regulation by the QS mechanism. As mentioned above, the values of the diffusion rates in QS systems fall into two distinctive categories: either large values corresponding to passive transport mechanism, $\tilde{D} \sim 10^4$, or small values when an active transport mechanism applies, $\tilde{D} \sim 10^{-1} - 10$. Surprisingly, these two QS classes avoid diffusion rates that maximize the total noise, $\tilde{D} \sim 5 \cdot 10^1 - 10^2$. While the modeling presented herein is certainly very simple and the derived consequences should be carefully taken, the latter suggests that bacteria have developed mechanisms for coping with the noise and keep their functional QS regime away from the region where $\eta^2_{c_A} > 1$. Notice that the maximum noise in the level of autoinducer means large fluctuations that may perturb the activation of the QS pathway. When looking at the dynamics of the autoinducer for $\tilde{D} = 100$ (see Fig. 3.3) we observe the population heterogeneity such that the autoinducer "jumps" between a low state with few molecules and a high state around 100 nM. If the activation threshold lies in between these two values (as it actually does), the QS pathway could get randomly activated due to the fluctuations only in a subpopulation and the colony would lack a synchronous behavior. Yet, our results point towards the direction that bacteria have adapted their communication mechanisms in order to improve the signal-to-noise ratio and produce a more reliable information exchange.

In the next section we further explore the relation between noise, network architecture, and synchronous collective behavior by introducing the concept of precision in a more detailed model.

3.3 Non-stationary Signaling, Network Structure, and Noise

The seminal work of Nealson and coworkers described the QS phenomenon as a *sudden* activation of the bioluminescence in a culture of growing *V. fischeri* cells [37]. It was not until recently that the behavior of individual cells has been shown

to differ significantly from the bulk behavior, revealing large inter-cell variations in the expression level of QS genes. Thus, Pérez and Hagen [38] were able to measure the weak bioluminescence of a single bacterium and observed a large cell-to-cell variability in the level of emission and in the onset time for the response. Importantly, this heterogeneity seemed not to be related to the specificities of *V. fischeri* and has been also reported in other QS bacterial species, as *Vibrio harveyi* [39], *P. aeruginosa* [40], and synthetic *E. coli luxI/luxR-GFP* strains [41].

As shown above, noise plays an important role in the QS activation phenomenon and the aforementioned cell-to-cell heterogeneity may be caused by the random fluctuations that unavoidably affect cell regulation and signaling. Yet, answering this question in deep requires a case-dependent approach since the underlying network architecture conditions how noise is filtered, enhanced, and/or suppressed. Moreover, many QS systems may sense and use different autoinducers and the design principles of these multi-input systems remain puzzling particularly in the framework of QS stochasticity. Recent advances include the study of *V. fischeri* cells that is regulated by two HSL signals. The results show that at the single-cell level the heterogeneity in the lux response depends only on the average degree of activation, so that the noise in the output is not reduced by the presence of the second signal [42]. Still, most QS systems share the same underlying network motif, a two component positive feedback loop. Thus, by studying a canonical QS system one can address questions and raise conclusions about the relation between network architecture and noise regulation.

In *V. fischeri* cells, the canonical activation pathway is controlled by LuxR, the receptor of the signaling molecule, and LuxI, the synthetase of the signaling molecules. Therefore, fluctuations at the expression levels of these two proteins can potentially influence the variability in the QS transition. Interestingly, experiments have revealed the presence of additional regulatory interactions for controlling the LuxR noise levels [44]. Yet, the regulatory interactions that control the wild-type lux operon in *V. fischeri* are more complex than first thought [45,46]. Those include both positive and negative regulation of the *luxR* gene depending on the concentration of the autoinducer [47]. In this regard, simplified synthetic constructs in *E. Coli*, such as *lux01* and *lux02* [43], retain the minimal LuxI/LuxR regulatory motif and lack the structural genes responsible for light emission that may also play a regulatory role, e.g. *luxD* [48]. These constructs reproduce the main features of the wild-type operon as revealed by the GFP fluorescence assays reporting the promoter activity [43]. In this section, we make use of the simplified network architecture of these synthetic strains in order to study how the cell-to-cell variability changes when we modulate independently the intensity of gene expression noise of LuxR and LuxI and raise general conclusions about the relation between noise and network architecture.

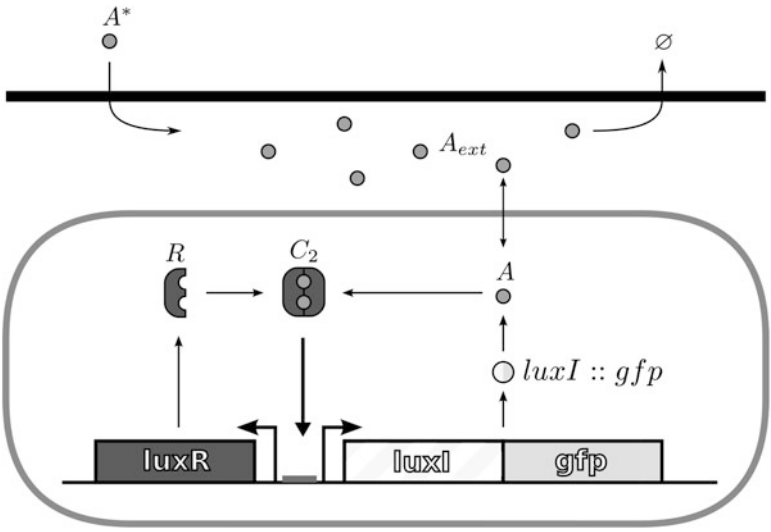

Fig. 3.5 Scheme of the LuxI/LuxR regulatory network in lux01 and lux02 strains. The LuxR (R) protein activates the operon upon binding to autoinducer molecules (A). The *lux01* operon lacks the *luxI* gene and therefore cells cannot produce their own autoinducer and exogenous signaling molecules, A^*, are needed to activate the expression of *luxR* and GFP [43]. On the other hand, the *lux02* operon carries a *luxI::gfp* fusion and allows for the production of autoinducer and self-induction

3.3.1 Synthetic Strains: A LuxR/LuxI System with No Frills

The *lux01* operon is a truncated divergently transcribed *lux* operon, capable of expressing LuxR but lacking the *luxI* gene. All the transcripts normally downstream of the promoter are replaced with *gfp*. Thus, bacteria carrying the *lux01* operon cannot produce the autoinducer and an exogenous autoinducer is required for GFP expression. On the other hand, the *lux02* operon carries a *luxI::gfp* fusion and is capable of expressing LuxI and synthesize the autoinducer [43]. Figure 3.5 shows schematically the regulatory interactions present in these strains as well as the control of the autoinducer levels by means of exogenous signaling molecules. These interactions and the *DNA* duplication process can be formally written as a set of chemical reactions:

$$
\begin{aligned}
DNA &\xrightarrow{\alpha_R k_R} DNA + mRNA_{\text{luxR}} \\
DNA &\xrightarrow{\alpha_I k_I} DNA + mRNA_{\text{luxI::gfp}} \\
DNA \cdot (luxR \cdot A)_2 &\xrightarrow{k_R} DNA \cdot (luxR \cdot A)_2 + mRNA_{\text{luxR}} \\
DNA \cdot (luxR \cdot A)_2 &\xrightarrow{k_I} DNA \cdot (luxR \cdot A)_2 + mRNA_{\text{luxI::gfp}}
\end{aligned}
$$

$$
\begin{aligned}
mRNA_{\text{luxR}} &\xrightarrow{p_R} mRNA_{\text{luxR}} + luxR \\
mRNA_{\text{luxI::gfp}} &\xrightarrow{p_I} mRNA_{\text{luxI::gfp}} + luxI::gfp \\
luxI::gfp &\xrightarrow{k_A} A + luxI::gfp \\
luxR + A &\underset{k_1^-}{\overset{k_1^-/K_{d1}}{\longleftrightarrow}} luxR \cdot A \\
2\,(luxR \cdot A) &\underset{k_2^-}{\overset{k_2^-/K_{d2}}{\longleftrightarrow}} (luxR \cdot A)_2 \\
(luxR \cdot A)_2 + DNA &\underset{k_{\text{lux}}^-}{\overset{k_{\text{lux}}^-/K_{\text{dlux}}}{\longleftrightarrow}} DNA \cdot (luxR \cdot A)_2 \\
A &\underset{rD}{\overset{D}{\longleftrightarrow}} A_{\text{ext}} \\
A &\xrightarrow{d_A} \varnothing \\
A_{\text{ext}} &\xrightarrow{d_A} \varnothing \\
mRNA_{\text{luxR}} &\xrightarrow{d_{\text{mR}}} \varnothing \\
mRNA_{\text{luxI::gfp}} &\xrightarrow{d_{\text{mI}}} \varnothing \\
luxR &\xrightarrow{d_R} \varnothing \\
luxI::gfp &\xrightarrow{d_I} \varnothing \\
(luxR \cdot A)_2 &\xrightarrow{d_{C_2}} \varnothing \\
luxR \cdot A &\xrightarrow{d_C} \varnothing \\
DNA &\xrightarrow{ln(2)/\tau} DNA + DNA \\
DNA \cdot (luxR \cdot A)_2 &\xrightarrow{ln(2)/\tau} DNA \cdot (luxR \cdot A)_2 + DNA.
\end{aligned}
\tag{3.23}
$$

As revealed by the set of reactions (3.23) the regulatory complex $(luxR \cdot A)_2$ activates the transcription of both *luxI* and *luxR* upon binding to the *DNA*. Since *lux01* lacks the *luxI* gene, the autoinducer, A, cannot be synthesized, i.e. in that case $k_A = 0$. Note that in agreement with Sect. 3.2.1, we include basal transcriptional rates, $\alpha_R k_R$ and $\alpha_I k_I$, even though the regulatory complex $(luxR \cdot A)_2$ is not bound to the promoter region of the *DNA*.

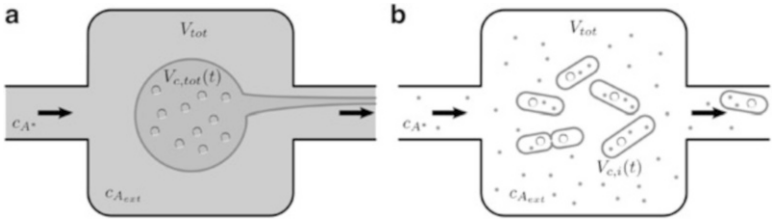

Fig. 3.6 Scheme of the deterministic and stochastic modeling approaches. (**a**) In the deterministic model, the population of cells is described by a unique volume with average and continuous concentrations of all species, including the DNA carrying the QS network (*small circles*). Cellular growth is also taken into account in this approach. (**b**) In the stochastic model, cells are modeled as individual compartments that can grow and divide and all molecular species are represented as discrete entities. In both cases we assume that all species are well stirred inside the cells and in the medium. In order to maintain a constant cell density, as in the experiments we aim to model, a dilution protocol is implemented (see text). In the deterministic model the dilution removes continuously cytoplasmic material in order to compensate the cell growth. In the stochastic model individual cells are removed every time a new cell is born

3.3.2 *Bulk and Single-Cell Approaches: Cell Growth, Division, and External Dilution Protocol*

The set reactions (3.23) can be sampled exactly by means of the Gillespie algorithm [34] (stochastic approach). The latter is suitable for the characterization of the system at the single cell level. Complementary to this, if we consider the colony as a whole and the number of molecules of the species is large enough, we can assume that intrinsic fluctuations average out and the set of ordinary differential equations (ODEs) that derive from reactions (3.23) describe the bulk behavior (deterministic description). Still, as shown below in Sect. 3.3.6, the intrinsic fluctuations can actually modify the behavior of the system in a more profound way. Herein we make use of both deterministic and stochastic descriptions. The former is particularly useful to fit the simulation results to experimental data in order to obtain values of the parameters.

As for the deterministic model, we consider that all cells share their cytoplasm in a *single* volume $V_{c,\mathrm{tot}}$ (see Fig. 3.6). Chemical species X inside *the* cell are described by their concentration, c_X, in $V_{c,\mathrm{tot}}$ and the chemical kinetics formalism leads to a set of ODEs that describes the population average dynamics:

$$\dot{c}_{\mathrm{luxI::gfp}} = p_I c_{mRNA_{\mathrm{luxI::gfp}}} - \left(\frac{ln(2)}{\tau} + d_I\right) c_{\mathrm{luxI::gfp}} \tag{3.24}$$

$$\dot{c}_{\mathrm{luxR}} = -\frac{k_1^-}{K_{d1}} c_A c_{\mathrm{luxR}} + k_1^- c_{\mathrm{luxR}\cdot A} + p_R c_{\mathrm{mRNA_{luxR}}} - \left(\frac{ln(2)}{\tau} + d_R\right) c_{\mathrm{luxR}} \tag{3.25}$$

$$\dot{c}_{\mathrm{mRNA_{luxI::gfp}}} = \alpha_I k_I c_{\mathrm{DNA}} + k_I c_{\mathrm{DNA}\cdot(\mathrm{luxR}\cdot A)_2} - \left(\frac{ln(2)}{\tau} + d_{\mathrm{mI}}\right) c_{\mathrm{mRNA_{luxI::gfp}}} \tag{3.26}$$

$$\dot{c}_{\text{mRNA}_{\text{luxR}}} = \alpha_R k_R c_{\text{DNA}} + k_R c_{\text{DNA}\cdot(\text{luxR}\cdot A)_2} - \left(\frac{ln(2)}{\tau} + d_{\text{mR}}\right) c_{\text{mRNA}_{\text{luxR}}} \tag{3.27}$$

$$\dot{c}_{\text{luxR}\cdot A} = -k_1^- c_{\text{luxR}\cdot A} + \frac{k_1^-}{K_{d1}} c_A c_{\text{luxR}} - 2\frac{k_2^-}{K_{d2}} [c_{\text{luxR}\cdot A}]^2 + 2k_2^- c_{(\text{luxR}\cdot A)_2} \tag{3.28}$$

$$- \left(\frac{ln(2)}{\tau} + d_C\right) c_{\text{luxR}\cdot A} \tag{3.29}$$

$$\dot{c}_{(\text{luxR}\cdot A)_2} = \frac{k_2^-}{K_{d2}} [c_{\text{luxR}\cdot A}]^2 - k_2^- c_{(\text{luxR}\cdot A)_2} - \frac{k_{\text{lux}}^-}{K_{\text{dlux}}} c_{(\text{luxR}\cdot A)_2} c_{\text{DNA}} \tag{3.30}$$

$$+k_{\text{lux}}^- c_{\text{DNA}\cdot(\text{luxR}\cdot A)_2} - \left(\frac{ln(2)}{\tau} + d_{C_2}\right) c_{(\text{luxR}\cdot A)_2} \tag{3.31}$$

$$\dot{c}_{\text{DNA}} = -\frac{k_{\text{lux}}^-}{K_{\text{dlux}}} c_{(\text{luxR}\cdot A)_2} c_{\text{DNA}} + k_{\text{lux}}^- c_{\text{DNA}\cdot(\text{luxR}\cdot A)_2} \tag{3.32}$$

$$+\frac{ln(2)}{\tau} \left(c_{\text{DNA}} + c_{\text{DNA}\cdot(\text{luxR}\cdot A)_2}\right) - \frac{ln(2)}{\tau} c_{\text{DNA}} \tag{3.33}$$

$$\dot{c}_{\text{DNA}\cdot(\text{luxR}\cdot A)_2} = \frac{k_{\text{lux}}^-}{K_{\text{dlux}}} c_{(\text{luxR}\cdot A)_2} c_{\text{DNA}} - k_{\text{lux}}^- c_{\text{DNA}\cdot(\text{luxR}\cdot A)_2} - \frac{ln(2)}{\tau} c_{\text{DNA}\cdot(\text{luxR}\cdot A)_2} \tag{3.34}$$

$$\dot{c}_A = k_1^- c_{\text{luxR}\cdot A} - \frac{k_1^-}{K_{d1}} c_A c_{\text{luxR}} + k_A c_{\text{luxI::gfp}} + D\left(c_{A_{\text{ext}}} - c_A\right) \tag{3.35}$$

$$- \left(\frac{ln(2)}{\tau} + d_A\right) c_A \tag{3.36}$$

$$\dot{c}_{A_{\text{ext}}} = rD\left(c_A - c_{A_{\text{ext}}}\right) + \gamma \frac{V_{\text{tot}}}{V_{\text{ext}}} c_{A^*} - (\gamma + d_A) c_{A_{\text{ext}}} \tag{3.37}$$

The experiments reveal that the temporal scale for reaching a steady-state is much larger than the cell cycle duration (see, for instance, Figure S6 in [43]). Thus, we need to take into account the cell growth. If cells are maintained in the exponential phase with doubling time τ, then the dynamics of the volume of *the* cell is $V_{c,\text{tot}}(t) = V_{0,\text{tot}} 2^{t/\tau}$, where $V_{0,\text{tot}} = N V_0$, N being the number of cells in the colony and V_0 the volume of a single cell at the beginning of the cell cycle. As a consequence, the cellular growth introduces dilution terms, $-c_X \frac{ln(2)}{\tau}$, in the r.h.s. of the ODEs of all species, with the exception of the autoinducer in the medium A_{ext}. On the other hand, cell division events lead to the duplication of the genetic material. The latter is taken into account by adding the term $+\frac{ln(2)}{\tau}\left(c_{\text{DNA}} + c_{\text{DNA}\cdot(\text{luxR}\cdot A)_2}\right)$ to the ODE that describes the concentration of *DNA*. Note that this term compensates for the dilution.

In the experiments that reported the properties of the *lux01* and *lux02* QS strains the cell density is kept constant by means of an external dilution protocol that compensates for cell proliferation [43]. In order to compare quantitatively with those experiments, we keep the volume $V_{c,\text{tot}}$ constant and define the external volume, V_{ext}, such that the total volume of the cell culture reads $V_{\text{tot}} = V_{\text{ext}} + V_{c,\text{tot}}$. Accordingly, the parameter r, see reactions (3.23), reads $r = V_{c,\text{tot}}/V_{\text{ext}}$. Notice that the external dilution protocol also removes from the medium autoinducer molecules [43]. This is

compensated by an influx of exogenous autoinducer in the dilution buffer. The influx of exogenous autoinducer molecules, together with the efflux of culture medium, can be represented by the following reaction

$$A_{\text{ext}} \underset{\gamma c_{A^*} V_{\text{tot}}}{\overset{\gamma}{\longleftrightarrow}} \varnothing. \tag{3.38}$$

where $\gamma = ln(2)/\tau$. That is, an efflux removes autoinducer molecules from the external volume at a rate γ and an influx introduces signaling molecules in the external volume at a rate $\gamma c_{A^*} V_{\text{tot}}$. In the deterministic description, this reaction leads to an additional term at the r.h.s. of the ODE for the concentration of A_{ext} : $+\gamma \left(c_{A^*} \frac{V_{\text{tot}}}{V_{\text{ext}}} - c_{A_{\text{ext}}} \right)$. In the absence of synthesis (e.g., *lux01* strain) and taking into account that the degradation is slower than the diffusion and the influx rate, it is easy to see that the concentration of autoinducer, both inside and outside *the* cell, tends to c_{A^*}: the desired control value of the autoinducer concentration.

As for the single-cell, stochastic, description, each bacterium is described as a single cell carrying a copy of the regulatory network. As in the deterministic case, cell growth introduces a dilution of the molecules in a cell. Cell growth is implemented by allowing the volume of cell i to change in time as

$$V_{c,i}(t) = V_0 2^{t/\tau_i}, \tag{3.39}$$

where V_0 is the volume of a cell at the beginning of the cell cycle, τ_i is the duration of the cell cycle of cell i, and t is referred to the precedent division event. When $t = \tau_i$ the cell i has doubled its volume and a new division takes place. At this time the internal clocks and volumes of daughter cells are reset to zero and V_0, respectively. The duration of the cell cycle, τ_i, is different for each cell and is set independently after a division according to the following stochastic rule [49],

$$\tau_i = \lambda \tau + (1 - \lambda) \tilde{\tau}, \tag{3.40}$$

where τ and $\tilde{\tau}$ denote, respectively, the deterministic and stochastic components of the cell cycle duration, and $\lambda \in [0, 1]$ is a parameter that weights their relative importance. The stochastic component accounts for the period of time between events driven by a Poissonian process and satisfies an exponential distribution,

$$\rho(\tilde{\tau}) = \frac{e^{-\frac{\tilde{\tau}}{\tau}}}{\tau}. \tag{3.41}$$

According to these definitions, the average duration and standard deviation of the cell cycle are τ and $(1 - \lambda)\tau$, respectively. When a cell divides, proteins, mRNAs, and signaling molecules inside the cell are binomially distributed [50] between daughter cells and one copy of the DNA is given to each cell (regulatory complexes bound to the DNA are detached prior to the distribution between daughter cells).

As in the case of the deterministic description, the cell density is kept constant due to a compensating efflux that wash away cells in the culture: each time a division takes place a cell is picked at random and "deleted." In relation to the effect of the cell volume of individual cells on the diffusion rate of the autoinducer, we note that in this case

$$r_i(t) = \frac{V_{c,i}(t)}{V_{\text{tot}} - \sum_{j=1}^{N} V_{c,j}(t)}. \tag{3.42}$$

A model as comprehensive as the one introduced here requires to know the value of a large number of parameters. Some of those have been characterized and measured in previous experiments, e.g. the dissociation constant of LuxR to A [51], while others have to be estimated or fitted. In the case of the synthetic strains reviewed herein most of the parameters can be estimated by fitting the results obtained in numerical simulations of the deterministic system to experimental data reporting on the colony bulk behavior [43]. We refer the reader to [18] for the fitting procedure and the list of estimated parameters.

3.3.3 Noise Intensity Regulation: Burst Size

In experiments there are two possible ways to regulate the intensity of the intrinsic noise keeping the same average values of protein concentration. On the one hand, one can scale up the number of molecules and the volume while keeping the same ratio, i.e. the same concentration. This approach has been indeed implemented in bacterial cultures by inhibiting the septation process [52]. The downside of this method is than one cannot actually control the noise level since during the time course of an experiment it diminishes progressively. On the other hand, one can control the so-called burst size that quantifies the translational efficiency. During translation mRNA molecules are translated into proteins following a bursting dynamics [3, 20, 53]. The so-called burst size, b_X, is defined as the ratio between the protein X production rate and the mRNA X degradation rate. It has been shown that b_X is directly related to the intensity of gene expression noise [54]. Thus, for the same average protein concentration, the larger b_X, the more fluctuating is the expression dynamics of X. Herein we use this approach and tune independently the noise intensity of *luxI* and *luxR* in our simulations in order to elucidate the role of fluctuations at the level of the main components of the QS switch architecture. Unless explicitly indicated otherwise, the bursting size in the stochastic simulations is $b_R = b_I = 20$ [44, 53].

3.3.4 LuxR Noise Levels and the Induction Time Control the Features of the QS Switch

In order to analyze the behavior of individual cells and reveal how noise affects the QS switch, we perform stochastic simulations of a population of growing and dividing cells. As described above, the *in silico* cell culture grows in a medium at a (nearly) fixed autoinducer concentration. We measure the activation of the QS network by reporting the concentration of GFP in single cells. The transition of an individual cell between the low (no signal from the GFP reporter) and the high state (signal from the GFP reporter) is intrinsically random and depends, among others, on the levels of autoinducer. Thus, inside a population some cells will jump while others remain in their current state leading to a bimodal phenotypic distribution. We compute the proportion of cells that are below and above a threshold of GFP equal to half-maximum GFP concentration; we consider the distribution of cells to be bimodal when the proportion of cells in either the low or the high state is below 90 %. According to this, we define the range of autoinducer concentration $[c_{A^*_{b1}}, c_{A^*_{b2}}]$ for which there is bimodality. For low concentrations of autoinducer, $c_{A^*} < c_{A^*_{b1}}$, the collective response of the cell population is unactivated, and for high concentrations, $c_{A^*} > c_{A^*_{b2}}$, most of the cells are activated leading to a global response of the colony. On the other hand, within the bimodality range, the response is distributed between two subpopulations, thus failing to achieve a global coordination in the colony. In order to characterize this behavior, we introduce the concept of *precision* in the QS switch as the inverse of the c_{A_*} concentration range for which the cells response distribution (phenotypes) is bimodal. That is, the larger the bimodal range, the less precise the switch is in order to generate a global response in the colony. We point out that the precision of the switch in a noise-free situation (deterministic case) is infinite since all cells achieve global coordination simultaneously.

Figure 3.7 shows, by means of a color density plot, the probability of a cell to have a particular GFP expression level after either 10 or 100 h of induction as a function of c_{A^*}. For a large range of autoinducer concentrations, both *lux01* and *lux02*, display a bimodal distribution after 10 h of induction. Some cells of the colony are induced at a concentration lower than the critical concentration of the deterministic model at the steady state (black line). Still, the concentration for which more than 90 % of the cells are induced requires up to four times more autoinducer than under deterministic conditions. Thus, on the one hand, noise helps cells to get induced at lower autoinducer concentrations but, on the other hand, amplifies the non-stationary effects for achieving global coordination. If the same experiment is performed with a larger induction time (100 h), the situation changes dramatically. In that case, the precision of the switch increases (tenfold change) and cells achieve global coordination at (*lux01*) or before (*lux02*) the critical deterministic concentration. In any case, the simulations reveal that the behavior of the QS switch is highly dynamic and the precision of the switch is a transient quantity that crucially depends on the duration of induction.

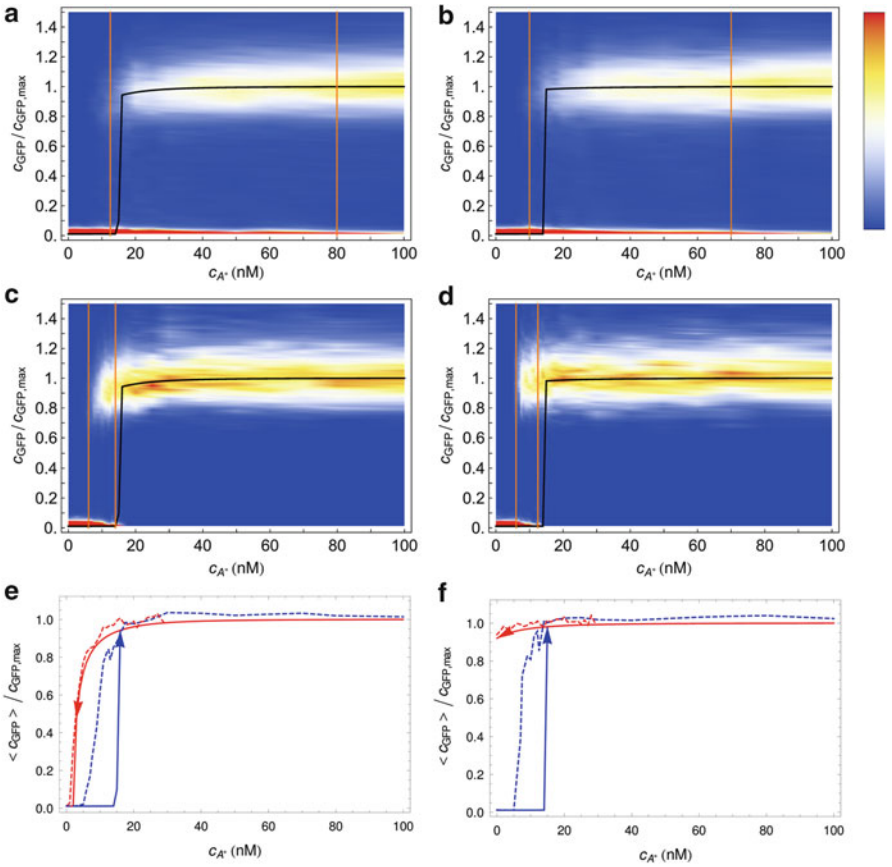

Fig. 3.7 Cell response distribution. Cell response probability after 10 h (*top*: **a**, **b**) and 100 h (*middle*: **c**, **d**) of induction at different autoinducer concentrations for the *lux01* (*left*: **a**, **c**) and *lux02* (*right*: **b**, **d**) operons in the stochastic model. The distribution reveals the coexistence of two subpopulations with low and high GFP expression when the cells are induced at intermediate autoinducer concentrations. The region of bistability (precision) is defined by the range of c_{A^*} for which the response is bimodal according to the following criterion: the lower/upper limit of the bistable region (*orange lines*) is defined by the value of c_{A^*} for which 90 % of the cells are in the low/high state. The *black line* stands for the concentration of GFP (normalized) as a function of c_{A^*} in the deterministic model at the steady state. After 10 h of induction (*top*: **a**, **b**) most cells are still in a transient state if $c_{A^*} < 70$ nM. After 100 h of induction (*middle*: **c**, **d**), the bimodality region shrinks and the precision increases. The population average curves of the induction and dilution experiments in the stochastic model (*bottom*: **e**, **f**, *dashed lines*) show that the intrinsic noise allows cells to jump to the high state inside the deterministic bistable region. On the other hand, the transition from high to low follows the deterministic path, thus indicating that the switching rate in this case is close to zero

For the same concentration of the external autoinducer, the stochastic dynamics of the regulatory network arises from the noise at the level of LuxI and LuxR. By taking the *lux02* operon as a reference case, we analyze the individual contribution

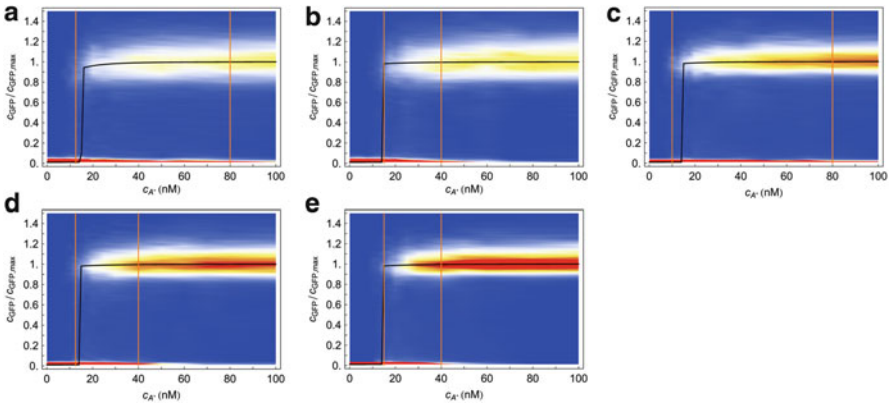

Fig. 3.8 Cell response distribution in the transient regime for different burst size values. Cell response distribution (jumping probability) after 10 h of induction (transient state) at different autoinducer concentrations for the *lux02* operon in the stochastic model and different burst sizes. Burst size values (**a**) $b_R = b_I = 20$ (**b**) $b_R = 4,\ b_I = 20$ (**c**) $b_R = 20,\ b_I = 4$ (**d**) $b_R = b_I = 4$ (**e**) $b_R = b_I = 0.01$. Width of bistable region: (**a**) = 60 nM (**b**) 25 nM (**c**) 70 nM (**d**) 27.5 nM (**e**) 25 nM. The *black line* stands for the concentration of GFP (normalized) as a function of c_{A^*} in the deterministic model at the steady state

of those network components by modulating the burst size of LuxR and LuxI (b_R and b_I, respectively). Thus, in Fig. 3.8 we plot the GFP expression probability for the *lux02* operon after 10 h of induction and for different values of the burst size b_R and b_I. Notice that the region of bimodality does not vary when changing the burst size for LuxI. However, decreasing the burst size in LuxR reduces the region of bimodality, thus increasing the precision of the switch. Furthermore, the noise at the level of LuxR helps some cells to become activated at lower concentration levels of the autoinducer. Once more, this phenomenon does not depend on the levels of noise of LuxI. That is, while the global coordination increases as the noise of LuxR decreases, more concentration of the autoinducer is required to start activating cells. On the other hand, Fig. 3.9 shows that under long induction time conditions (100 h) the precision of the switch remains constant regardless of the value of the burst size of LuxR or LuxI.

3.3.5 Activation Time Statistics: QS Cells Jump on the Bandwagon

Further insight about the role of noise of individual components and the induction time in the activation process for regulating the precision of the QS switch can be obtained by computing the so-called mean first passage time (MFPT). This quantity evaluates the average time it takes to a cell to become activated (high state)

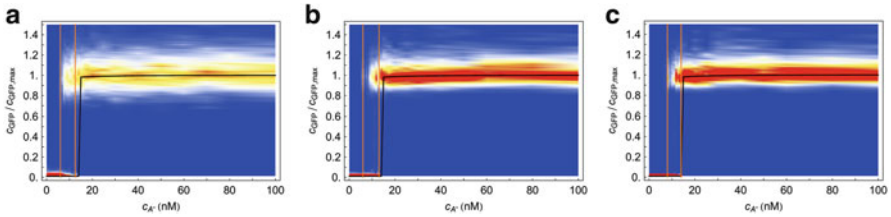

Fig. 3.9 Cell response distribution at the steady-state for different burst size values. Cell response distribution at the steady-state (100 h induction), at different autoinducer concentrations for the *lux02* operon in the stochastic model for different burst size values: (**a**) $b_R = b_I = 20$ (**b**) $b_R = b_I = 4$ (**c**) $b_R = b_I = 0.01$. The probability density of getting a particular GFP expression level is indicated by means of a density plot. The width of bistable region barely depends on the stochasticity levels, ≈ 7 nM. The *black line* stands for the concentration of GFP (normalized) as a function of c_{A^*} in the deterministic model at the steady state

starting in an unactivated situation (low state) [55]. Taking again the *lux02* case as a reference, Fig. 3.10 shows the MFPT as a function of c_{A^*} and for different values of the burst size of LuxR and LuxI. For the sake of comparison, we also compute the MFPT for the deterministic solution. As for the latter, we note that the MFPT inside the bistable region is infinite, since the deterministic system cannot spontaneously jump from one stable state to the other without the help of noise. In agreement with the results shown above, changing the burst size of LuxI does not modify the mean first passage time whereas changing the noise at the level of LuxR clearly modifies the jumping statistics. Moreover, the results reveal a nontrivial behavior of the MFPT as a function of the concentration of the autoinducer. On the one hand, with respect to the activation dynamics, when c_{A^*} is below $\sim$ 25 nM, an increase in LuxR noise decreases the mean time of the activation. That is, LuxR noise helps cells to get activated quicker. On the other hand, above $\sim$ 25 nM of autoinducer concentration, the effect is the opposite: an increase in LuxR noise slows down the cell activation. We also note that, surprisingly, when the autoinducer concentration is above the critical concentration of the deterministic system, $c_{A^*} \approx 25$ nM, the stochastic system always takes more time to get activated than the deterministic case. That is, in that case the noise does not help cells to get activated but to remain in the unactivated state.

By computing additional statistical properties of the first passage time we can clarify the behavior of the precision depending on the induction time. In particular, one can compute the times t_{low} and t_{high} for which, at a given c_{A^*} concentration, the probabilities of finding an FPT$< t_{\text{low}}$ and an FPT$> t_{\text{high}}$ are 10 %, i.e. the 10 % and 90 % quantiles, respectively. The shadings in Fig. 3.10 delimit these regions for the cases $b_R = b_I = 20$ and $b_R = b_I = 0.01$. Thus, the precision of the switch after n hours of induction is directly related to the width of the shaded region at $\langle \text{FPT} \rangle = n$ hours: at any given time, this width indicates which is the minimal concentration of autoinducer for getting 10 % of cells already activated and also the concentration beyond which more than 90 % of cells have been activated. Thus, in agreement

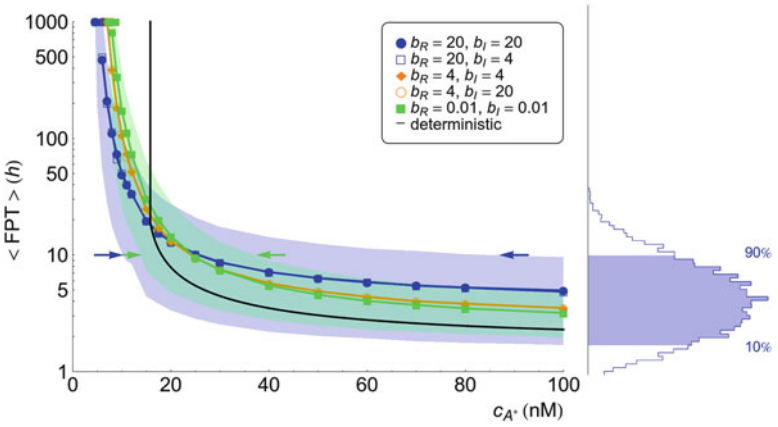

Fig. 3.10 Mean first passage time of cell activation for different burst size values for the lux02 case. Mean first passage time of cell activation (*lines*) as a function of autoinducer concentration for different values of the burst size for LuxR (b_R) and LuxI (b_I) and for the deterministic solution. The *lower* (*upper*) limit of the *shaded regions* is the 10 % (90 %) quantile curve of the distribution of FPT for the cases $b_R = b_I = 20$ (*blue shaded region*) and $b_R = b_I = 0.01$ (*green shaded region*). The distribution of the FPT for $c_{A^*} = 100$ nM, $b_R = b_I = 20$ is plotted on the side as an example. The MFPT reveals a nontrivial behavior: for low autoinducer concentration noise helps cells to jump quicker to the high state, while for high autoinducer concentration noise slows down the cells activation. Intersections of the quantile 10 % and quantile 90 % curves with a horizontal line at $t = 10$ h indicate the autoinducer concentration for which 10 % of cell trajectories have jumped to the high state (*left arrow*) and the concentration for which 90 % of cell trajectories have been activated (*right arrow*). The precision after 10 h of induction (inversely proportional to the width of the region delimited by the *arrows*) increases when decreasing the noise in LuxR

with Fig. 3.7, the induction time clearly modifies the precision: it increases (the width of the shading decreases) as the induction time becomes larger and becomes independent of the noise intensity for large induction times. Note also that as the LuxR noise weakens the precision increases.

3.3.6 *Solving a Noisy Mystery: The Fluctuations Modify the Phenotypic Landscape*

The analysis of the FPT statistics poses an intriguing question about the role of noise in the QS switch. Namely, below a "critical" concentration of autoinducer LuxR noise helps cells to become activated and above LuxR noise helps cells to remain in the unactivated state. The complexity of the detailed model presented above makes very difficult to find the reasons for this counterintuitive behavior. However, the fact that this effect is independent of the LuxI noise levels points towards the direction that the underlying reason does not depend on the communication process but on

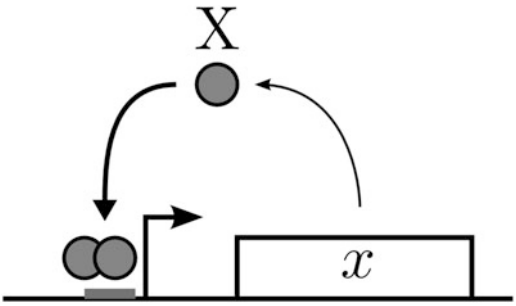

Fig. 3.11 Scheme of the genetic auto-activating switch model. The expression of gene x leads to protein X that after oligomerization binds to its own promoter acting as an self-activator

the network architecture. Therefore, we can analyze a "simple" system that shares the network motif driven by LuxR and try to draw conclusions.

The basic motif underlying regulation in QS is a positive feedback loop. In that regard, the simplest system that shares such network scheme is the so-called auto-activating switch [56, 57]. In this genetic circuit, a protein forms an oligomer that binds to the promoter region of its own gene and activates its expression (see Fig. 3.11). As shown elsewhere [16], this regulatory process can be effectively described by the Hill function formalism and leads to the following deterministic equation for the concentration, x, of protein:

$$\dot{x} = r + \frac{ax^n}{K_d + x^n} - k_5 x \tag{3.43}$$

where r is the basal expression rate (due to promoter leakiness), a the maximum production rate (efficiency of the auto-activation), n the cooperativity (oligomerization index), K_d the concentration of protein yielding half-maximum activation, and k_5 the degradation rate. In this simple model x and a play the role of the GFP expression levels and the external concentration of autoinducer in the QS switch, respectively.

Alternatively, the dimensionless version of (3.43) reads

$$\dot{\tilde{x}} = \tilde{r} + \tilde{a}\frac{\tilde{x}^n}{1 + \tilde{x}^n} - \tilde{x} \tag{3.44}$$

with $\tilde{x} = \frac{x}{\sqrt[n]{K_d}}$, $\tilde{t} = k_5 t$, $\tilde{a} = \frac{a}{k_5 \sqrt[n]{K_d}}$, $\tilde{r} = \frac{r}{k_5 \sqrt[n]{K_d}}$.

If $n \geqslant 2$ and $\left(3\sqrt{3}\right)^{-1} > \tilde{r} > 0$, then the system exhibits a bistable behavior (phenotypic variability) for a range of values of $\tilde{a}$. Here we choose $n = 2$ and $\tilde{r} = 0.12$ such that there is a bistable region as in the case of the QS switch. The points (x_0, a_0) that define the bistable region correspond to the solutions of the polynomial equations [58],

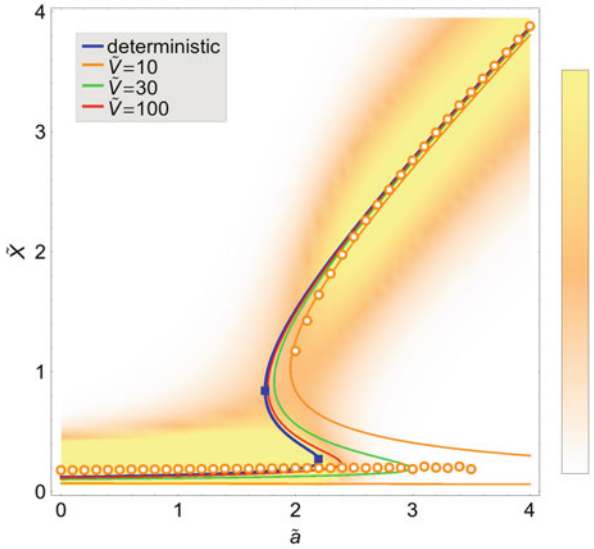

Fig. 3.12 Bifurcation diagram (phenotypic landscape) of the genetic auto-activating switch model. Bifurcation diagram of the autoactivating switch under deterministic (*blue line*) and stochastic conditions: *red, green, and orange lines* stand for the analytical location of the probability extrema for different noise intensities (see legend). The *open circles* indicate the results of numerical simulations of the case $\tilde{V} = 10$. The probability density of that case is also depicted by means of a density plot (logarithmic scale). The bistable region of the deterministic system gets delimited by the points (x_0, a_0) (*squares*). Note that noise stabilizes the low state and the bistable region expands

$$0 = \tilde{r} + \frac{\tilde{a}_0 \tilde{x}_0^2}{1 + \tilde{x}_0^2} - \tilde{x}_0 \tag{3.45}$$

$$0 = \frac{2\tilde{a}_0 \tilde{x}_0}{(1 + \tilde{x}_0^2)^2} - 1. \tag{3.46}$$

Figure 3.12 shows the stationary solution, $\tilde{x}_{\mathrm{st}}$, as a function of $\tilde{a}$ where set of points (x_0, a_0) are highlighted. Note that this bifurcation diagram reflects a situation akin to that of the QS switch.

If we now consider the biochemical fluctuations, the stochastic description of the system reads [16, 59]

$$\dot{\tilde{x}} = \tilde{r} + \tilde{a}\frac{\tilde{x}^2}{1 + \tilde{x}^2} - \tilde{x} + \xi(t)\sqrt{\tilde{r} + \tilde{a}\frac{\tilde{x}^2}{1 + \tilde{x}^2} + \tilde{x}} \tag{3.47}$$

where the noise term must be interpreted according to Itō and the statistical properties of the fluctuations are

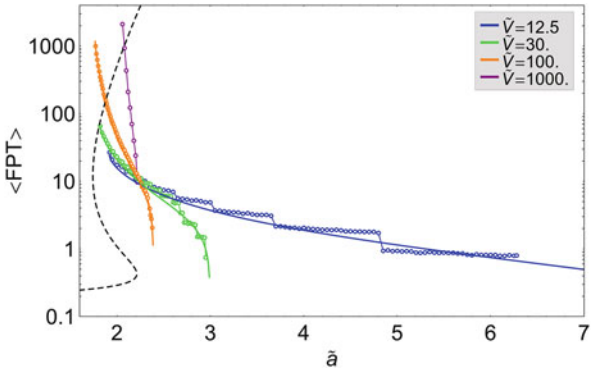

Fig. 3.13 First passage time and switching rate for the genetic switch. Mean first passage time (MFPT) for the genetic switch from the low stable state to the high state for different volume sizes, i.e. noise intensities (see legend). The *solid lines* correspond to the analytical solution and the *circles* to the Gillespie simulations. The deterministic bifurcation curve (*dashed line*) is depicted with an arbitrary y-scale in order to visualize the deterministic bistable region. Depending on the value of $\tilde{a}$, the MFPT increases or decreases with the intrinsic noise intensity

$$\langle \xi(t) \rangle = 0 \tag{3.48}$$

$$\langle \xi(t)\xi(t') \rangle = \tilde{\sigma}^2 \delta\left(t - t'\right). \tag{3.49}$$

In this case, the intensity of the fluctuations is related with the cellular volume such that $\tilde{\sigma}^2 = 1/\tilde{V}$, where $\tilde{V} = V \sqrt[n]{K_d}$ is the dimensionless volume.

Interestingly, the location of the bifurcation points that define the bistable region gets modified by the noise such that the low protein concentration state becomes more stable. An effect referred to as the *stochastic stabilization* of a phenotypic state [58]. Figure 3.12 shows this effect and reveals that the low state extends its stability with respect to the deterministic system.

The FPT statistics is related to the structure of the bifurcation diagram since the former evaluates the amount of time required to jump to a stable state. Thus, Fig. 3.13 shows the MFPT as a function of the control parameter $\tilde{a}$ for different volumes, namely noise intensities. We can observe the same counterintuitive behavior reported on the QS switch: depending on the value of $\tilde{a}$ (equivalent to the concentration of autoinducer in the QS switch), the MFPT increases or decreases with the intrinsic noise intensity. This effect can be now easily explained in terms of the modification of the bifurcation diagram due to noise that extends the stability of the low state. Up to the value of the control parameter where there is the bifurcation point of the deterministic system, the fluctuations help cells to jump to the high state. Beyond that point, the deterministic system "immediately" jumps. However, the stochastic system gets "trapped" in the low state. This causes the FPT to increase with respect to the deterministic situation such that the larger the noise the larger the FPT since the low state becomes more stable. In the context of the QS switch these results reveal that LuxR noise controls the precision by modifying

the phenotypic landscape and at the same time raises the following question: how comes LuxI noise has no effect on the QS phenotypic landscape? Note that LuxI fluctuations are transmitted to the autoinducer at the end. Yet, the diffusion process effectively averages out the fluctuations of the signaling molecule (see Sect. 3.2.5). That is, the effective cellular volume "perceived" by LuxI is the total volume of the cells. This is not possible for LuxR which is not driven by diffusion and is kept within the cell. As a result, the activation complex is susceptible to the fluctuations of LuxR but not to those of LuxI.

3.4 Discussion

In this chapter we have reviewed some studies that reveal the importance of stochasticity in QS. We first explored the role played by cell–cell communication and transcriptional noise in QS systems near the activation threshold where *luxI* is expressed at a low constitutive level such that the feedback regulation (autoactivation) can be disregarded. Under these conditions we have shown that the interplay between the diffusion and the mRNA dynamics plays a crucial role for regulating the total amount of noise. Thus, transcriptional noise is the main contribution to the total noise for a large range of diffusion values and only for large values of the diffusion the intrinsic noise is the major source of stochasticity. Importantly, we have shown that the total noise shows a non-monotonic behavior as a function of the diffusion rate that indicates a mechanism to reduce the signal to noise ratio.

Herein we have also introduced the concept of precision in the QS switch: a meaningful measure of the synchronization of the cells based on the *homogeneity* of the collective cell response. A small precision means a bimodal response over a broad range of autoinducer concentrations, producing a graded response at the population level. A high precision means a response that is mainly monomodal and a bimodal response over a narrow range of autoinducer concentrations, providing a steep response at the population level. The precision is highly dynamic and critically depends on the induction time and, importantly, on the noise levels of LuxR that influences the probability of a cell to jump from the deactivated to the activated state (change of phenotype). In addition, we have revealed that the noise at the level of LuxI does not modify the phenotypic landscape and consequently has no effect on the precision of the QS switch.

Interestingly, recent experiments have revealed the presence of additional regulatory interactions for controlling the LuxR noise levels. For example, C8HSL molecules, a secondary QS signal in *V. fischeri*, has been suggested to reduce the noise in bioluminescence output of the cells at low autoinducer concentrations [42]. In the same direction, in *V. harveyi*, the number of LuxR dimers is tightly regulated indicating a control over LuxR intrinsic noise [44]. In fact, wild-type *V. harveyi* strains have two negative feedback loops that repress the production of LuxR [60] and this kind of regulatory circuit is known to reduce noise levels [61]. In this context, the results reviewed here provide a feasible explanation for the network

structure in wild-type strains: since noise in LuxR controls the phenotypic variability of LuxR/LuxI QS systems, bacteria may have evolved mechanisms to control its noise levels. An additional argument in this regard arises from the simulation results about the deactivation process: once cells are fully induced the reversibility of the phenotype is a pretty rare event (FPT larger than 100 h). Thus, it makes sense that wild-type strains have additional interactions that regulate negatively *luxR* [45–47]. Moreover, it indicates that synthetic strains as *lux01* and *lux02* may summarize most features of the wild-type operon during the activation process but they fail to capture aspects of the deactivation phenomenon.

In regards to the importance of non-stationary effects, most works assume steady conditions. However, we have shown that the time for reaching a steady state of cell response distribution is much larger than the duration of the cell cycle. This is in agreement with experimental results [43] as well as with another stochastic model of QS transition in *Agrobacterium tumefaciens* [62]. In our simulations, the population of cells needs $\sim$30 h to reach a steady-state when induced at 50 nM of autoinducer and that this time is even larger close to the critical concentration of activation [18]. In most laboratory experiments studying the QS transition, the typical experimental run or time of culture growth before measurement rarely exceeds 20 h [43,44,57,63, 64], after which the expression of genes is assumed to reach a steady-state. While a modeling approach is certainly a crude simplification of the real genetic network, the results suggest that special care should be taken about transient effects when studying the population-wide QS response. Indeed, bistable gene networks are often associated with slow response time compared to graded-response gene networks [65, 66].

While speculative, these results about the importance of non-stationary effects can be extrapolated to growing colonies where the cell density is not kept constant as in our simulations or in the experiments we reproduced [18,43]. A good supply of nutrients implies short induction times since the concentration of autoinducer will quickly grow (exponentially) as the population size does. According to our results, this fast growing condition decreases the precision of the switch and, consequently, promotes variability at the population level (see Fig. 3.14, fast growth line). In addition, the full collective activation of the system would require a large population size (i.e., more autoinducer).

On the other hand, if the colony grows in an environment poor in nutrients, the concentration will increase slowly and the system will have time to reach the steady-state response (see Fig. 3.14, slow growth line). In this case, the precision would increase, the variability would be diminished, and full activation would require smaller colony sizes. Most phenotypic changes induced by the QS mechanism refer to bacterial strategies for survival and/or colonization. In this context, these results suggest that both the QS activation threshold and the phenotypic variability might depend on the growth rate of the colony and, as a consequence, on the environmental conditions. This is in fact in agreement with recent studies that show that the collective response of a population of cells depends not only on the underlying genetic circuit and the environmental signals but also on the speed of variation of these signals [67].

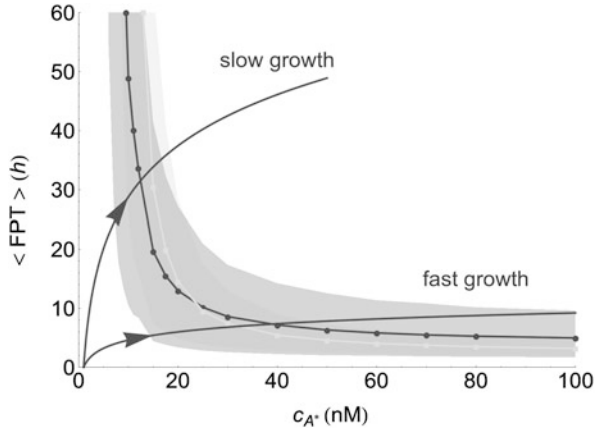

Fig. 3.14 The growth rate conditions the phenotypic variability. In the context of a growing colony, the autoinducer concentration increases as the colony does: *arrow lines* show schematically two exponential growth conditions for the autoinducer concentration as a function of time. Our results on the MFPT, valid at fixed autoinducer concentrations, can be extrapolated, qualitatively, to the case of increasing autoinducer levels. Fast growth results in a large cell variability and large critical colony size for achieving a global response, while slow growth produces reduced cell variability and a smaller critical population size. Increasing fluctuations in LuxR have two opposite effects: in the slow growth case, increasing the noise (*dark circles/shading*: $b_R = 20$; *light squares/shading*: $b_R = 0.01$) decreases the critical population size while hardly changing the variability, in the fast growth case, increasing noise increases the critical population size and increases greatly the variability

Finally, we have observed a counterintuitive effect of LuxR gene expression noise in the dynamics of the QS activation. For high concentration of autoinducer (above $\sim$25 nM) an increase in the noise intensity slows down the mean activation time. This effect is the opposite of what would be expected in the case of a bistable autoactivating switch with additive noise or extrinsic fluctuations [68]. In order to address this puzzling result, we have introduced a simple model that summarizes the underlying LuxR/LuxI motif: the autoactivating switch with a positive feedback loop. Thus, we have shown that intrinsic noise modifies the bifurcation diagram (phenotypic landscape) and stabilizes the low state of the cells; an effect that we call *stochastic stabilization*.

Our final comment refers to the possibility of considering other sources of stochasticity that may play a crucial role in QS. Cell-to-cell variability and extrinsic noise have been proved key in many cell processes [35, 49, 50, 69]. In the context of the problems studied herein, the results suggest that variability, either at the level of the mRNA dynamics or at the level of the diffusion rate, can effectively lead to significant changes in the reported phenomenology. However, theoretical studies [19, 70] suggest that the QS synchronization is robust to the variability in the diffusion rate and extracellular noise. Thus, whether or not these additional noise sources may generate new effects in the framework of QS is not clear yet

and further research is needed. In any case, stochasticity in QS is key for describing adequately the bacterial communication phenomena and therefore it is a promising field of research that will continue flourishing in next years.

References

1. Raj A, van Oudenaarden A (2008) Cell 135:216
2. Ullner E, Buceta J, Díez-Noguera A, García-Ojalvo J (2009) Biophys J 96:3573
3. Kaern M, Elston TC, Blake WJ, Collins JJ (2005) Nat Rev Genet 6:451
4. Eldar A, Elowitz MB (2010) Nature 467:167
5. Cai L, Dalal CK, Elowitz MB (2008) Nature 455:485
6. Pai A, You L (2009) Mol Syst Biol 5:286
7. Kaplan H, Greenberg E (1985) J Bacteriol 163:1210
8. Danino T, Mondragón-Palomino O, Tsimring L, Hasty J (2010) Nature 463(7279):326. DOI: 10.1038/nature08753
9. Tanouchi Y, Tu D, Kim J, You L (2008) PLoS Comput Biol 4:e1000167
10. Weber M, Buceta J (2011) BMC Syst Biol 5:11
11. Erdmann T, Howard M, ten Wolde PR (2009) Phys Rev Lett 103:2
12. Waters CM, Bassler BL (2005) Annu Rev Cell Dev Biol 21:319
13. Zhu XM, Yin L, Hood L, Ao P (2004) J Bioinformatics Comput Biol 2:785
14. Tian T, Burrage K (2006) PNAS 103:8372
15. Wang J, Zhang J, Yuan Z, Zhou T (2007) BMC Syst Biol 1:50
16. Frigola D, Casanellas L, Sancho JM, Ibañes M (2012) PLoS ONE 7:e31407
17. Kepler T, Elston T (2001) Biophys J 81:3116
18. Weber M, Buceta J (2013) BMC Syst Biol 7:6
19. Hong D, Saidel WM, Man S, Martin JV (2007) J Theor Biol 245:726
20. Yu J, Xiao J, Ren X, Lao K, Xie XS (2006) Science 311:1600
21. Choi PJ, Cai L, Frieda K, Xie XS (2009) Science 322:442
22. Horsthemke W, Lefever R (1984) Noise-induced transitions: theory and applications in physics, chemistry and biology. Springer, New York
23. More MI, Finger LD, Stryker JL, Fuqua C, Eberhard A, Winans SC (1996) Science 272:1655
24. Parsek MR, Val DL, Hanzelka BL, Cronan JE, Greenberg EP (1999) PNAS 96:4360
25. Shahrezaei V, Swain PS (2008) PNAS 105:17256
26. Kaufmann G, Sartorio R, Lee S, Rogers C, Meijler M, Moss J, Clapham B, Brogan A, Dickerson T, Janda K (2005) PNAS 102:309
27. Roberts C, Anderson KL, Murphy E, Projan SJ, Mounts W, Hurlburt B, Smeltzer M, Overbeek R, Disz T, Dunman PM (2006) J Bacteriol 188:2593
28. Anderson KL, Dunman PM (2009) Int J Microbiol 2009:525491
29. Pearson J, Van Delden C, Iglewski B (1999) J Bacteriol 181:1203
30. Xavier K, Bassler B (2005) J Bacteriol 187:238
31. Wang L, Hashimoto Y, Tsao C, Valdes J, Bentley W (2005) J Bacteriol 187:2066
32. Herzberg M, Kaye I, Peti W, Wood T (2006) J Bacteriol 188:587
33. Li J, Wang L, Hashimoto Y, Tsao CY, Wood TK, Valdes JJ, Zafiriou E, Bentley WE (2006) Mol Syst Biol 2:67
34. Gillespie D (1977) J Phys Chem 81:2340
35. Elowitz MB, Levine AJ, Siggia ED, Swain PS (2002) Science 297:1183
36. Swain P, Elowitz M, Siggia E (2002) PNAS 99:12795
37. Nealson K, Platt T, Hastings J (1970) J Bacteriol 104:313
38. Pérez PD, Hagen SJ (2010) PLoS ONE 5:e15473
39. Anetzberger C, Pirch T, Jung K (2009) Mol Microbiol 73:267

40. Boedicker JQ, Vincent ME, Ismagilov RF (2009) Angew Chemie 48:5908
41. Hagen SJ, Son M, Weiss JT, Young JH (2010) J Biol Phys 36:317
42. Pérez PD, Weiss JT, Hagen SJ (2011) BMC Syst Biol 5:153
43. Williams JW, Cui X, Levchenko A, Stevens AM (2008) Mol Syst Biol 4:234
44. Teng SW, Wang Y, Tu KC, Long T, Mehta P, Wingreen NS, Bassler BL, Ong NP (2010) Biophys J 98:2024
45. Lyell NL, Dunn AK, Bose JL, Stabb EV (2010) J Bacteriol 192:5103
46. Septer AN, Stabb EV (2012) PLoS ONE 7:e49590
47. Sitnikov D, Shadel G, Baldwin T (1996) Mol General Genet 252:622
48. Shadel G, Baldwin T (1992) J Biol Chem 267:7690
49. Canela-Xandri O, Sagués F, Buceta J (2010) Biophys J 98:2459
50. Rosenfeld N, Young JW, Alon U, Swain PS, Elowitz MB (2005) Science 307:1962
51. Urbanowski M, Lostroh C, Greenberg E (2004) J Bacteriol 186:631
52. Süel GM, Kulkarni RP, Dworkin J, García-Ojalvo J, Elowitz MB (2007) Science 315:1716
53. Cai L, Friedman N, Xie XS (2006) Nature 440:358
54. Ozbudak EM, Thattai M, Kurtser I, Grossman AD, van Oudenaarden A (2002) Nat Genet 31:69
55. Gardiner C (1985) Handbook of stochastic methods: for physics, chemistry and the natural sciences. Springer, New York
56. Isaacs FJ, Hasty J, Cantor CR, Collins JJ (2003) PNAS 100:7714
57. Ozbudak E, Thattai M, Lim H, Shraiman B, Van Oudenaarden A (2004) Nature 427:737
58. Weber M, Buceta J (2013) PLoS ONE 8:e73487
59. Gillespie D (2000) J Chem Phys 113:297
60. Tu KC, Long T, Svenningsen SL, Wingreen NS, Bassler BL (2010) Mol Cell 37:567
61. Balázsi G, van Oudenaarden A, Collins JJ (2011) Cell 144:910
62. Goryachev AB, Toh DJ, Wee KB, Zhang HB, Zhang LH, Lee T (2005) PLoS Comput Biol 1:e37
63. Long T, Tu KC, Wang Y, Mehta P, Ong NP, Bassler BL, Wingreen NS (2009) PLoS Biol 7:e68
64. Anetzberger C, Schell U, Jung K (2012) BMC Microbiol 12:209
65. Savageau Ma (2002) Math Biosci 180:237
66. Tiwari A, Ray JCJ, Narula J, Igoshin Oa (2011) Math Biosci 231:76
67. Nené NR, García-Ojalvo J, Zaikin A (2012) PLoS ONE 7:e32779
68. Zheng XD, Yang XQ, Tao Y (2011) PLoS ONE 6:e17104
69. Shahrezaei V, Ollivier J, Swain P (2008) Mol Syst Biol 4:196
70. Mina P, di Bernardo M, Savery NJ, Tsaneva-Atanasova K (2013) J Roy Soc Interface Roy Soc 10:20120612

Chapter 4
Spatial Structure of Microbes in Nature and the Biophysics of Cell–Cell Communication

James Q. Boedicker, Katie Brenner, and Douglas B. Weibel

4.1 Introduction to Microbial Structure

Microbes are social organisms and their language is chemical. Microbial communities provide cells with structures that facilitate chemical communication and enable them to adapt to environmental pressure. Fossil records demonstrate that microbial communities existed several billion years ago [1] and a wide variety of observations point to the importance of these structures today [2]. The spatial organization of communities provides organisms with advantages for growth and adaptation in fluctuating environmental conditions.

We are surrounded by visible examples of spatial and temporal organization in macro-biological communities that confer growth advantages, including: structured forest ecosystems [3], mussel beds [4], islands [5], and soils [6]. These examples have informed evolutionary ecology for over a century; such ecosystems are frequently highlighted in literature in the context of their disruption and resulting collapse [7]. In contrast, studies of physical structure in microbial communities have been limited until recently by a lack of experimental tools and by the

J.Q. Boedicker (✉)
Department of Physics and Astronomy, Seaver Science Center (SSC) 223, University of Southern California, 920 Bloom Walk, Los Angeles, CA 90089, USA
e-mail: boedicke@usc.edu

K. Brenner
Department of Biochemistry, University of Wisconsin-Madison, Madison, WI 53706, USA

D.B. Weibel
Department of Biochemistry, University of Wisconsin-Madison, Madison, WI 53706, USA

Department of Biomedical Engineering, University of Wisconsin-Madison, Madison, WI 53706, USA

Department of Chemistry, University of Wisconsin-Madison, Madison, WI 53706, USA

S.J. Hagen (ed.), *The Physical Basis of Bacterial Quorum Communication*, Biological and Medical Physics, Biomedical Engineering, DOI 10.1007/978-1-4939-1402-9_4

century-old mindset that these organisms operate only as single cells and lack community structure and organization. Yet there is strong evidence that concepts from landscape ecology, for example, can inform our understanding and aid in making predictions about microbial community structure [8] and provide insight into the chemical language of microbes. The prevalence and importance of microbial communities suggests that understanding their spatiotemporal structure may be critical to maintaining terrestrial homeostasis [7, 9] and human health [10, 11], and may also stimulate the development of new technologies in future decades [12].

Recent interest in microbial structures has largely focused on bacterial biofilms, colonies, and aggregates. Microbes frequently form biofilms at interfaces between different forms of matter (i.e., solid, liquid, and gas). Aggregates are produced during biofilm growth as groups of cells break away from these communities or in response to flow patterns that promote grouping and cell–cell adhesion [13, 14]. Micro-environments in biofilms and aggregates shelter cells from mechanical stress, flow, and antimicrobial compounds [15, 16] including toxic metals [17], while sequestering nutrients, signals, and DNA [18], and facilitating the exchange of chemical signals between cells. Cells in biofilms and aggregates differentiate [19], communicate [20], share resources [14, 21], and exchange genes [18]. Therefore, studying the relationship between the physical structure of these communities, the exchange of molecules, and cellular function will elucidate the role structure plays in microbial behavior and evolution.

In this chapter, we discuss structured microbial communities—including biofilms and aggregates—and the principles of chemical communication from a biophysical perspective by: (1) providing examples of structured communities and mechanisms by which their physical arrangement is formed and maintained; (2) highlighting biophysical models that provide insight into the length and time scales of microbial communication; (3) examining recent advances that will accelerate the study of microbial community structure; and (4) exploring advances in engineering cell/cell communication and community structure.

4.2 Microbial Structures in Nature

4.2.1 Structures in the Environment

Biofilm studies in the laboratory have yielded insight into the multitude of structures that microbes form, and the surprisingly rapid transition from uni- to multi-cellular behavior exhibited by microbes in the context of environmental stresses [2, 22]. Biofilms enable coordinated cellular activity by spatially sequestering signals and metabolites and thereby elevating concentrations of molecules that regulate cell behavior within the community. For example, the structure of *Pseudomonas aeruginosa* biofilms makes it possible to retain important signaling factors and metabolites inside the biofilm, leading to a chemical gradient that extends from the center of

the biofilm to outside of the community [23]. Within these multi-cellular structures microbes differentiate: that is, changes in transcription or biochemistry create subpopulations of cells with altered behavior and physiology. The death of cells in *Bacillus subtilis* biofilms creates structures that project spore-forming bodies [24]. *Myxococcus xanthus* differentiates into swarmer cells that "ripple" quickly over surfaces consisting of prey cells that consume nutrients, thereby optimizing both nutrient uptake and cell migration speed [25]. This behavior culminates in a pattern of programmed cell death that leads to fruiting body formation and the release of spores [26]. These intriguing examples of microbial structure studied in pure culture in the laboratory inspire a closer examination of structures in natural settings, where multiple species often grow together in close association and form symbiotic relationships.

4.2.1.1 Water

A close look at slime-covered rocks in a stream or at the bottom of the ocean reveals surprising cooperation between microbes. In stream biofilms and other benthic layers, fluid flow impacts the size and shape of biofilms. In areas of unidirectional flow, biofilms form ripple-like patterns consistent with the prevailing flow direction while in areas of isotropic flow, biofilms form star-shaped clusters [27]. Microorganisms can also engineer ecosystems by actively changing surrounding flow patterns [28]. In some cases, for example, bacteria in microbial communities depend upon algae to influence the flow of fluids. Algae grow in ridged, patterned biofilms under turbulent conditions, and form filamentous structures and nets under laminar flow. Bacteria co-habiting with algae experience predictable flow patterns created in proximity to a mature algal population (Fig. 4.1a) [28]. This symbiosis is poorly understood, and it is possible that algae benefit from the presence of bacteria by cross feeding or that the relationship is commensal and only benefits bacteria. In either case, the overall microbial structure clearly optimizes bacterial adhesion and persistence in the environment.

In the ocean or sea, organic particles bind to inorganic materials to create aggregates with millimeter length scales. Behavior of these aggregates can be accurately modeled by agar particles that are ∼4 mm in diameter [29]. In oceans, the density of the aggregates makes them sink and they provide a mechanism for cells to transition from suspension to benthic environments. These aggregates act as reservoirs for pathogenic bacterial species and harbor a higher density of microbes that feed higher organisms than would be found suspended in fluids. Microbes within the particles interact and may exhibit density-dependent behaviors (e.g., quorum sensing). Growth of microbes in marine aggregates primarily benefits bacteria and other microorganisms because the physical structure traps nutrients—akin to the function of a filter feeding organism—and thereby enables bacteria to access 60 % more nutrients than are typically available in planktonic growth [30]. Aggregation has a direct benefit on cell growth and replication.

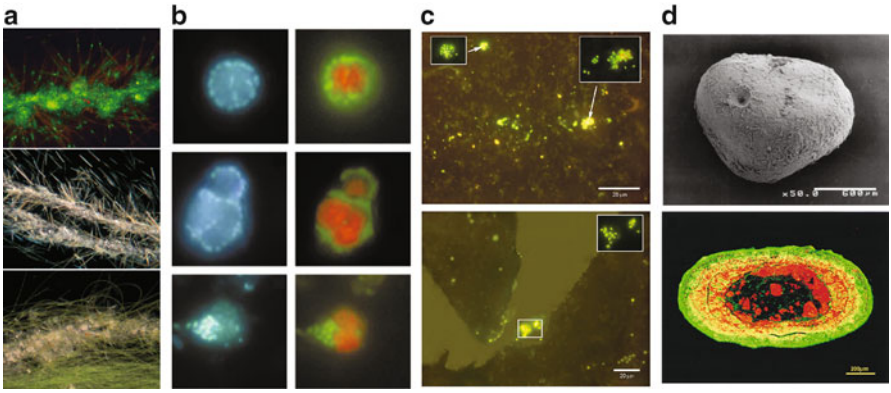

Fig. 4.1 Microbes exhibit structure in nature. (**a**) In streams, bacterial biofilms form streamers which recruit diatoms (*top panel*, epifluorescence and *middle panel*, dark field). Over time, algae overgrow the streamers to form a mat and eventually provide a predictable flow pattern for the bacteria (*bottom panel*) [28]. (**b**) Three examples of methane-oxidizing microbial aggregates that form near exposed methane-hydrate layers in the deep sea. DAPI staining (*left panels*) and fluorescent probes (*right panels*) allow differentiation between archaea (*red*) and bacteria (*green*) [31]. (**c**) FISH-stained bacteria in sandy forest soil (*top panel*) and sandy agricultural soil (*bottom panel*) demonstrate that there are more bacteria that are metabolically active in forest soil [33]. (**d**) Thermophilic methanogenic granules form with bacteria surrounding archaea in anaerobic waste-water reactors that bear striking resemblance to those featured in (**b**) [35]

Near exposed methane hydrate layers in the deep sea, the aggregation of microorganisms mediates anaerobic oxidation of methane (Fig. 4.1b). In their mature form, aggregated consortia consist of archaea growing in clusters of approximately 100 cells surrounded by sulfate-reducing bacteria. However, early consortia containing a nucleus of only 1–3 archaea surrounded by sulfate-reducers also exist and suggest that new consortia grow out of these small aggregates [31]. In this case, a physical organization of cells enables their mutualistic metabolism and directly benefits the growth of both community members.

4.2.1.2 Soil

The structure of soil is often overlooked, and yet it is strikingly complex; the composition of soil includes aggregates or "continents" inhabited by particular residents surrounded by "oceans" inhabited by other microbes, and its surface is divided into layers of different life forms positioned at different depths, which suggests a structure with a striking resemblance to an upside-down rainforest canopy. Much can be learned about the earth's ecosystem and its trajectory and resilience by examining soil carefully [6]. Communities of bacteria co-exist with multi-cellular eukaryotes in soil, including arthropods and plants. Relationships between soil organisms are mediated by physical interactions and chemical signaling between them.

Microbial communities shape the chemical and physical properties of soil as well as the structure of vegetation on land. Soil microbes that are symbionts of one plant species may deter growth of other plant species. In some cases, seedlings of one species in proximity to adults of the same species suffer because host-specific soil pathogens which surround the adult plant make the region inhospitable to the plant's seeds (i.e., the Janzen Connell hypothesis) [32]. This effect benefits the overall ecosystem as it promotes biodiversity. The evolutionary rise of such complexity is still a fascinating puzzle for ecologists. It is also clear that different types of soil host different sizes and species of microbial aggregates [33]. Sandy soils contain large, abundant aggregates compared to loamy soils. Additionally, samples from forested soils contain more metabolically active microbes than samples from farmland soils [33] (Fig. 4.1c). On a local scale, the plant rhizosphere secretes flavonoids and other signaling factors that cause closely associated fungi to transcribe nodulation genes. In response, microbial populations living in the rhizosphere export signaling factors that alter gene expression in their neighbors. It is not clear how far-reaching the impact of a single plant's signaling factors may be, however given the relay that can accompany microbial signaling—based upon the signaling cascade they initiate in neighboring microbe populations—it is possible that root signals can influence biology at a distance that extends beyond the diffusion of chemical signals through a granular medium such as soil [6, 32]. Effects such as these make clear that a full understanding of microbial community structure requires spatial and temporal studies across several orders of magnitude: from minutes to years and microns to kilometers.

4.2.1.3 Bioremediation

Soils and bodies of water are sites of interest from the standpoint of studying naturally occurring microbial consortia as highlighted above, and particularly to identify consortia that have the ability to degrade pollutants and promote environmental remediation. In a classic example of a soil-based microbial consortium, Wolfaardt et al. [34] identified nine bacterial species and one alga that grow together in a biofilm and cooperate to degrade the herbicide diclofop-methyl. Cells degrade the compound in batch culture; however, degradation was more efficient when glass beads were introduced into the environment to promote biofilm formation, highlighting the impact community spatial structure can have on community function.

Bioengineers are already harnessing the natural abilities of microbes to degrade recalcitrant compounds that are pollutants. For example, in waste-water purification reactors, thermophilic methanogenic sludge granules form in which bacteria grow in an outer layer surrounding archaea (Fig. 4.1d) [35]. Scientists have reproduced similar structured communities in the lab. When grown together with a specific spatial arrangement, *Sphingobium chlorophenolicum*, a pentachlorophenol (PCP) degrader, surrounded by *Ralstonia metallidurans*, a mercuric ion (Hg(II)) reducer, degraded both PCP and Hg(II) from a mixture [36]. The particular spatial

arrangement of the two species is paramount in this case; if *R. metallidurans* instead surrounds *S. chlorophenolicum* the consortium no longer degrades PCP efficiently. The physical arrangement of this consortium is organized over a distance of 200 μm and degradation takes place over several days.

4.2.2 Structures in the Human Body

In recent years it has become increasingly evident that human health is modulated not only by activities of human cells, but also by the behavior and physiology of resident microorganisms. We often think about microbes in the context of wound infections, oral plaques, and digestive difficulty, but we also have many beneficial interactions with our microbiota. A closer examination of each niche reveals intricate physical structures that govern symbioses among microbes and between microbes and the human host. A better understanding of these structures, the chemical communication that occurs within them, and the exchange of chemical signals between microbiota and eukaryotic cells may be critical in guiding therapeutic efforts.

4.2.2.1 Wounds

In wound infections, it is evident that physical structure arises due to the different growth properties of species in the biofilm. For example, when colonizing a wound together with other species, *P. aeruginosa* always inhabits the leading edge of the wound infection and forms tendril-like projections that consist of swarmer cells producing more virulence factors and exhibiting greater antibiotic resistance than other cells in the wound [37]. *P. aeruginosa* usually outcompetes other bacteria in close spatial proximity, however in wounds it grows in intimate association with other species and this close physical association across length scales on the order of millimeters reduces the susceptibility of *P. aeruginosa* to antibiotics. Additionally, during co-infection, *P. aeruginosa* detects peptidoglycan released from neighboring Gram-positive bacteria and up-regulates production of lytic factors in response, which kill both prokaryotic and human cells [38]. The cytotoxicity of *P. aeruginosa*—as occurs in the context of cystic fibrosis or a wound—may therefore be a side effect of an evolved response to competition with Gram-positive cells and might be mitigated by eradication of Gram-positive bacteria that are physically proximate to *P. aeruginosa*.

4.2.2.2 Mouth

When the “wrong” bacteria thrive in the mouth, the outcome is gingivitis, caries, and even dysfunction throughout the host gastrointestinal (GI) tract. Microbial communities that form on the surfaces of teeth exhibit intricate spatial structure.

In addition to structure at micron length scales, microbes in the mouth influence microbial colonization throughout the human gut. In the mouth, the order in which microbes colonize tooth surfaces can influence the subsequent composition of the community. Microbes in the mouth form layered biofilms, and colonization of the basement layer by particular species is required for other beneficial commensal species to thrive [39]. These pioneer species inform the composition of the mature biofilms by promoting the adherence of specific species to the subsequent biofilm layers. For example, streptococci such as *Streptococcus gordonii* DL1 recognize receptor polysaccharides (RPS) on the cell surface of streptococci such as *Streptococcus oralis* 34 [40]. Recognition promotes intimate association between the two strains, presumably facilitating a metabolic interaction in which small molecules are exchanged. Pathogenic bacteria also organize spatially to promote tooth decay. *Porphyromonas gingivalis* (harbinger of gingivitis) grows faster when co-localized with *Treponema denticola* because it can metabolize succinate produced by *T. denticola* and the isobutyric acid excreted by *T. denticola* also stimulates its growth [41, 42].

4.2.2.3 Gut

The spatial structure of microbes in the gut is also associated with human health. Crohn's disease can be diagnosed by examining the physical location of gut microbes within the feces of sick patients. Habitual bacterial species that are distributed throughout the feces in healthy humans are found only on the surface of feces from sick patients. Additionally, the physical form of bacterial communities is very different between feces from the two groups: healthy individuals have a higher proportion of bacterial mats and webs, whereas the feces of sick patients exhibit spheroidal and striated colonies. These observations demonstrate that the physical structure of commensal microbes in the gut differs between healthy and sick individuals. The role that these structures play in disease progression is yet to be elucidated [43].

It is also known that obesity affects the composition of the gut microbiome. In the gut of obese mice, Bacteroidetes are reduced by 50 % compared to lean mice, with a proportional increase in Firmicutes [10]. Community composition influences transcriptional and metabolite profiles [44], although little is known about the physical structure of these gut communities. Does composition vary because of changes in the topology of the gut biofilm due to obesity? Do changes in the spatial structure of the gut microflora enable more efficient caloric harvesting resulting in obesity? A spatiotemporal understanding of microbial communities in the gut will answer fundamental questions such as these, and yield insight into the influence of the microbiome upon human health, development, and behavior.

4.3 Biophysics of the Spatial Structure of Microbial Communities

In the previous sections, we highlighted examples in which microbes develop complex spatial structures, and discussed the effect that spatial structure has on the physiology and behavior of microorganisms in these systems. Microbes have evolved to form structures in response to biological and physical cues from their environment (e.g., surface properties, nutrient availability, and the presence of other species). The location of cells within these communities influences chemical communication between cells and enables them to adapt to extracellular changes. In this section we develop a framework for applying biophysical concepts to understand, predict, and dissect the role of spatial structure in microbial communication and physiology.

4.3.1 Diffusion Sets a Length and Time Scale of Signal Exchange Between Microbes

Diffusion helps to define the scale over which spatial structure influences cellular activity. Diffusion is the process by which molecules spread from areas of higher concentration into areas of lower concentration. Individual cells use diffusion to exchange signaling molecules with neighbors. For example, synthetase enzymes inside cells produce molecular signals that are exported out of the cell and drift away from the producing cell until they reach neighboring cells, thereby relaying a chemical message, as depicted in Fig. 4.2. In this process, each individual signaling molecule undergoes a random walk, bumping into other molecules in the environment, and produces a characteristic pattern of molecular concentrations in time and space that is described by Fick's laws of diffusion [45].

Fick's first law states that the flux of signals from one cell to another will be proportional to the gradient of the concentration of the signal—that is, how sharply the signal concentration changes with distance,

$$J = -D \, \mathrm{d}C/\mathrm{d}x. \tag{4.1}$$

The constant D in this relationship is known as the diffusion coefficient. For simplicity, consider the case of diffusion in one dimension. Fick's second law defines how the gradient of the signal will change over time,

$$\mathrm{d}C/\mathrm{d}t = D \, \mathrm{d}^2C/\mathrm{d}x^2. \tag{4.2}$$

With knowledge of the geometry of the space in which cells are located, the boundary conditions (e.g., how the production of the signal changes over time and whether the signal accumulates or is consumed at the receiver cell), and the

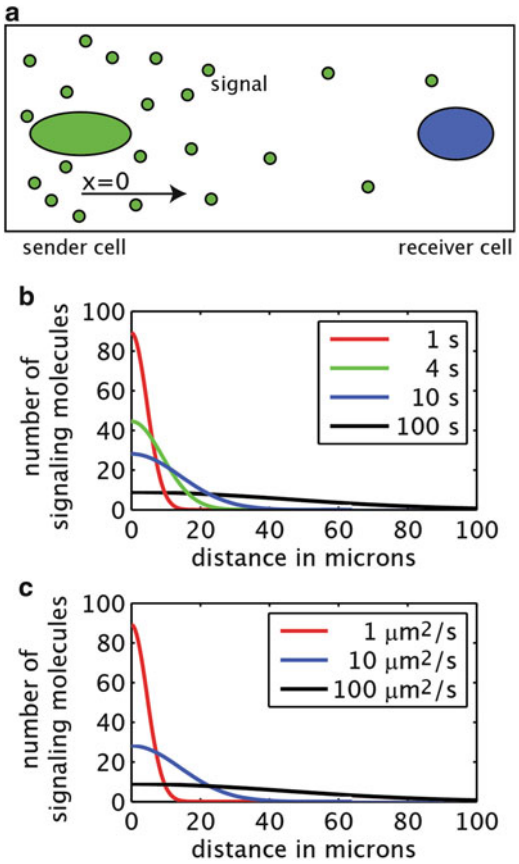

Fig. 4.2 Diffusion of signals between cells. (**a**) At $t = 0$ the green sender cell emits a burst of 1,000 signal molecules (*small green circles*). The signal molecules diffuse toward the *blue* receiver cell. (**b**) The gradient of signal molecule after 1, 4, 10, and 100 s with a diffusion coefficient of 10 $\mu m^2/s$. (**c**) The gradient of signal molecule after 10 s for diffusion coefficients of 1, 10, and 100 $\mu m^2/s$

stability of the signaling molecule (i.e. whether it is degraded) during its journey between cells, Fick's laws can be used to predict how the exchange of signals between two cells evolves over time. In many cases an exact solution to the diffusion equations is not possible, although analytical approaches can be used to approximate the formation and dynamics of diffusive gradients. As a concrete example, Fig. 4.2 shows the solution to the diffusion equation for the case in which a burst of signal is created by a producing cell and diffuses in one dimension. For mathematical details describing the derivations of such gradients from Fick's laws, we refer the reader to [45, 46].

As seen in Fig. 4.2, the gradient of signal molecules between two cells changes over time. Signal molecules spread from the producing cell to the receiving cell. A signal with a diffusion coefficient of 10 $\mu m^2/s$ (Fig. 4.2b), requires more than 10 s

to reach a receiving cell 50 μm away. The time it takes a signal to reach the receiving cell depends upon its distance from the producing cell, as shown in Fig. 4.2b, and also upon the diffusion coefficient, D, of the signal in its medium, as shown in Fig. 4.2c.

Often we want to know the approximate amount of time it will take for a signal to reach a receiving cell at a set distance. A useful approximation for the relationship between distance and time for a simple diffusion problem such as the one depicted in Fig. 4.2 is:

$$x = (2Dt)^{0.5} \tag{4.3}$$

This rule of thumb enables one to estimate how long it will take a signal to reach a cell at a distance x or, conversely, how far a signal will diffuse in time t. Using this approximation, Table 4.1 estimates how far typical signals will travel in 1 s, 1 min, 1 h, and 1 day.

Table 4.1 demonstrates that diffusion is effective for signal exchange over length scales from μm to mm, however it will take more than 10 years for a small molecule signal to travel 1 m. Based on Eq. (4.3), it will take signal molecules four times as long to diffuse twice as far, limiting the ability to relay chemical signals over long distances. Diffusion is typically only used to exchange signals between cells separated by several millimeters or less.

The medium through which diffusion occurs also plays an important role in modulating the time and length scales of signaling. As seen in Table 4.1, the diffusion coefficient of methanol in air is a factor of 10^4 higher than it is in water. Gels such as the extracellular polysaccharide matrix (EPS) of biofilms also slow transport rates, although for proteins diffusing in 4 % agarose, diffusion coefficients are reduced only by a factor of 2 or less. Larger molecules typically have smaller diffusion coefficients than small molecules. The pore sizes of gel matrices such as EPS can also produce non-linear behavior for diffusion of larger molecules such as proteins. In the cellular cytoplasm, the diffusion coefficient of proteins scales approximately as $\mathrm{MW}^{-0.7}$ [51]. For larger objects, such as phage particles or whole cells, the diffusion coefficients are even smaller, such that these objects take two to three orders of magnitude longer to diffuse 1 mm than a typical small molecule signal.

4.3.2 *The Temporal Scale of the Biochemical Processes Involved in Cell–Cell Signaling*

Diffusion is one process that sets the timescale of cell–cell signaling. How do transport times compare with the other cellular processes involved in detecting and responding to a signal? Cells use a variety of molecular mechanisms to detect chemical signals, including two-component signaling systems, extracytoplasmic function (ECF) sigma factors, and one-component signaling systems [52].

Table 4.1 Diffusion time and distances estimated using Eq. (4.3) for representative compounds in different media

			Diffusion distance after				Time needed to reach			
Signal	Medium	~D ($\mu m^2/s$)	1 s	1 min	1 h	1 day	1 μm	1 mm	1 m	Ref.
Glycine	Water	1,000	45 μm	350 μm	2.7 mm	13 mm	500 μs	8.3 min	16 year	[47]
Sucrose	Water	540	33 μm	250 μm	2.0 mm	9.7 mm	930 μs	15 min	29 year	[47]
Protein (14 kD)	Water	140	17 μm	130 μm	1.0 mm	4.9 mm	3.5 ms	1.0 h	110 year	[48]
Protein (67 kD)	Water	94	14 μm	110 μm	820 μm	4.0 mm	5.3 ms	1.5 h	170 year	[48]
T7 phage	Water	9.5	4.4 μm	34 μm	260 μm	1.3 mm	52 ms	15 h	1,700 year	[47]
Whole microbe	Water	0.5	1.0 μm	7.8 μm	60 μm	290 μm	1.0 s	12 day	32,000 year	[49]
Protein (14 kD)	4 % agarose	110	15 μm	110 μm	890 μm	4.4 mm	4.5 ms	1.3 h	140 year	[48]
Protein (67 kD)	4 % agarose	48	9.8 μm	76 μm	590 μm	2.9 mm	10 ms	2.9 h	330 year	[48]
Methanol	Water	1,500	55 μm	420 μm	3.3 mm	16 mm	330 μs	5.6 min	11 year	[47]
Methanol	Air	1.5×10^7	5.5 mm	42 mm	330 mm	1.6 m	33 ns	33 ms	9.3 h	[50]

Two-component signaling systems detect changes in the chemical environment using histidine kinase sensors containing a periplasmic or extracellular domain. Once activated by signal binding, the sensor donates a phosphate group to a transcription factor known as a response regulator, changing its ability to bind to the genome and influence gene expression [53]. Sensing a signal and activating (or sometimes deactivating) a transcription factor enables the cell to relay chemical messages at sub-second timescales [54]. The chemosensory system in bacterial cells is the canonical example of a two-component signaling system and has been the center of several decades of biochemical studies [55].

ECF sigma factors are another type of sensor and regulator system that controls gene expression in response to external chemical stimuli. Sigma factors are proteins that bind to the promoter regions of genes to facilitate binding between the RNA polymerase and specific promoters. Typical ECF sigma factors are regulated by external sensor proteins in the cell membrane, known as anti-sigma factors. Anti-sigma factors bind and sequester ECF sigma factors, inhibiting gene regulation. When a signal molecule binds to an anti-sigma factor it induces a conformational change that releases the sigma factor [52, 56]. As in the case of signal transduction for a two-component system, the ligand binding and conformational changes needed to release an ECF sigma factor occur on a sub-second timescale.

In one-component signaling systems, a signal binds directly to a regulator protein. In the canonical example of *P. aeruginosa* quorum sensing signaling, homoserine lactones (HSLs) are exchanged between cells. Variants of HSL with short acyl chains freely partition across the cell membrane, whereas some variants are actively transported and require several minutes to reach steady-state [57]. In the cytoplasm, signals bind and dimerize receptor proteins [58]. These activated receptor proteins are transcription factors that increase expression of proteins associated with community structure, including HSL synthases and receptor proteins. Dimerization of the transcriptional regulator through binding of a ligand at μM concentrations occurs on sub-second timescales [46].

After a signal has been received, a response is elicited through the production of new proteins, which may take considerable time. Association between an active transcription factor and the promoter region to which it binds is likely the rate-determining step. A single Lac repressor can take 3–5 min to find a single promoter region, although the response time is decreased when multiple copies of Lac repressor are present [59]. The copy numbers of RNA polymerase with common sigma factors have been measured to be >1,000 [60], suggesting that binding between RNA polymerase and an activated promoter should not be rate limiting. Because transcription produces mRNA at ~50 nucleotides per second and translation occurs at a rate of 20 residues per second [61], it takes ~11 s to make an unfolded peptide chain of 100 amino acids. Folding times can be as short as hundreds of μs [62] and many proteins exhibit folding times of <1 s [63]. Protein maturation can be slow—derivatives of green fluorescent protein require 5–30 min to become functional [64]. Some proteins require cleavage to become activated, which increases the response time. Overall, it takes between 10 s and 10 min, on average, for protein to be produced in response to a signal.

Table 4.2 Approximate timescales of the processes involved in cell–cell signaling

Process	∼Timescale
External signal activating response regulator in two-component system	<1 s
External signal activating ECF sigma factor	<1 s
Short chain HSL partitioning across membrane	30 s
Long chain HSL partitioning across membrane	5 min
Ligand binding to protein	<1 s
Activated TF binding to target promoter	1–5 min
Transcription and translation of 100 amino acid peptide	10 s
Folding time of typical protein	ms–min
Doubling time of most microbes	10 min–1 day
Enacting full response to β-galactosidase stimulation	30 min
Small molecule diffusing 1 mm	10 min

See text for more details and references

The approximations above suggest that cellular responses to incoming signals occur on a timescale of seconds to minutes. However, enacting a full cellular response to the signals can take significantly longer. Long-term responses to chemical signals may require activating an entire gene network, increasing the response time. The response may also involve accumulating high intercellular concentrations of proteins, requiring many cycles of transcription, translation, and folding. Beta-galactosidase can take a full cell cycle to reach steady-state levels upon stimulation [65]. Although at some distances diffusion of signals may be a rate limiting step in the ability of cells to communicate, protein expression may also govern response times and several division cycles may elapse before cells mount full responses to some chemical messages.

Having defined these timescales, see Table 4.2 for a summary, we can calculate a length scale over which signal exchange by diffusion is effective. Given that production of and response to a signal occur in minutes, Eq. (4.3) specifies that communication by diffusion between cells at distances of 100 μm will not be limited by transport rates. Another length scale to keep in mind is the doubling time. As cell division consumes significant energy and resources, it may be beneficial to relay chemical messages to neighboring cells within the division time. Microbial division times typically range from 10 min to several hours. Within a few hours, signals may travel several millimeters.

4.3.3 Biophysical Detection Limits

In addition to the rate of transport, another parameter that influences the spatial scaling of signal exchange is signal sensitivity (i.e., the lowest detectable concentration of a signal). In the previous section we assumed that a receiving cell will detect any amount of signal, a suitable assumption for the estimates

made using Eq. (4.3). However, the noise inherent in single molecule diffusion and binding provides a limit to the concentration of signal that individual cells can detect. Cells overcome this biophysical limit by, for example, time averaging binding events [66, 67]. Above the limit of signal sensitivity, cells can control the threshold concentration of signal to which they will respond. Cooperative binding of ligands or multimerization of transcription factors can regulate the sharpness of the threshold [68]. The value of the threshold concentration can also be tuned through a combination of reactions that activate and repress the response, especially if the activation is super-linear, as has been shown in the case of blood coagulation [69]. Together these features enable cells to tune their response function, and thereby the timescale of the response. The range of signal concentration to which a cell responds is an important feature that helps set the time and length scales of signaling.

4.3.4 Gradients Over Short Length Scales

Diffusion creates well-mixed conditions inside a 1-μm long cell within milliseconds. However, if signals are bound at timescales equivalent to or shorter than the diffusion time, gradients of signaling molecules can be observed within a cell [70]. One example in which cells create and respond to gradients formed over micron length scales occurs with the filamentous cyanobacteria *Anabaena. Anabaena* forms chains of interconnected cells. These filaments are heterogeneous and consist of a mixture of cell types that are formed when *Anabaena* differentiates. Under nitrogen starvation, heterocyst cells capable of fixing nitrogen develop approximately every ten cells [71]. The spatial pattern of cellular differentiation stems from production of an inhibitory signal in heterocyst cells [72]. Current models suggest that diffusion of this inhibitory signal within the chain creates a gradient of inhibition around each heterocyst. New heterocysts only form at distances of several cell lengths from an existing heterocyst, where the gradient of this diffusing inhibitor falls below a threshold concentration [73]. This example demonstrates how cells can experience steep signaling gradients over short length scales.

There is emerging evidence that intracellular structures exist to promote signaling between neighboring cells. Nanotubes form between adjacent cells—even different species of cells—and efficiently exchange molecules between cells, including proteins and genetic material [74]. Transport mechanisms in these nanostructures are not yet characterized. However, if the transport process is diffusive, signal exchange between adjacent cells should be rapid. In addition to molecular exchange, there is evidence that some species use direct cell-to-cell connections such as nanotubes to transmit electrical signals [75]. These direct cytoplasmic connections may facilitate signal exchange, catalyze formation of larger physical structures, and coordinate group behavior in communities of cells.

4.3.5 Gradients Over Long Length Scales

Long timescales are needed for signals to diffuse over long distances. Recall that in Table 4.1 we estimated that a small molecule will take 10 years to diffuse a distance of 1 m. It is not yet clear whether microbes in nature exchange signals over long distances. As discussed in Sect. 4.2.1.2 on soil microorganisms, the distribution of microbes is ordered across length scales ranging from microns to kilometers. Large-scale patterns may emerge in microbial networks as diffusive signaling leads to a local spatial structure that propagates to neighboring clusters of cells, thus creating order over long distances [6, 32]. Volatile signals also play a role in long distance communication. Because small molecules exhibit large diffusion coefficients in air, volatile signals reach neighboring cells meters away in less than a day. Many microbes produce volatile compounds that are thought to participate in communication with insects [76] and volatile compounds produced in the rhizosphere trigger plant growth [77]. The plant pathogen *Ralstonia solanacearum* uses the volatile signal 3-hydroxpalmitic acid methyl ester to regulate virulence [78] and microbes can be engineered to respond to airborne volatiles [79], yet it is not yet clear to what extent volatile signals mediate microbe–microbe interactions.

Several additional mechanisms make it possible for microbes to overcome the slow rate of long distance diffusion. First, transport is rarely purely diffusive. In real environments, advection—or the directed bulk flow of materials—transports released signals away from a sender cell rapidly. For example, directed transport has an influence on signal exchange within *P. aeruginosa* biofilms [80], thus potentially increasing the length scale over which signaling occurs. In systems such as the gastrointestinal (GI) tract, there is directed flow of material over a length scale of $\sim$10 m. This flow should transport signals, secondary metabolites, and metabolic waste from cells in the upper GI tract to cells in the lower GI tract, however it is yet unclear whether signal exchange occurs and how essential it is to the function of this ecosystem.

Microbes also communicate over long distances using motility. Due to the low diffusion coefficient of large objects—such as a micron-sized cells—dispersion primarily by diffusion has significant limitations at short timescales. Many microbes overcome diffusion limitations overcome diffusion limitations using motility mechanisms such as flagella that are coupled to chemosensory systems to direct cell movement. Table 4.1 estimates that a cell takes $\sim$1 h to diffuse 60 μm. As the effective swimming velocity of *Escherichia coli* cells—which use flagella for propulsion in fluids—in a gradient of chemoattractant is $\sim$7 μm/s [81], they cover the same distance (60 μm) in 9 s. Many microbes can detect chemical signals in the environment using chemotactic systems that direct their motion. When motile cells localize to similar areas, signaling by diffusion is much more efficient, reducing the time required to coordinate group activities. The dispersal of signaling molecules in dynamic, high-density communities of bacteria can be hyperdiffusive, which may enhance long range communication between cells [82].

4.3.6 Efficient Signaling Can Sometimes Be Detrimental

We have discussed mechanisms that increase the rate of signal transmission; however, in some cases it is beneficial for cells to prevent diffusion of signaling molecules. For example, cells release enzymes to digest complex food sources and it is detrimental if the enzymes diffuse too far away. To limit diffusive losses, microbial cells are hypothesized to gauge the transport properties of their local environment by sending out test signals in a process called "diffusion sensing" [83]. If the test signal accumulates to a high concentration around the cell, energetically costly degradation enzymes are released. Cells actively reduce the rate of diffusion by producing and secreting extracellular materials, including EPS, that effectively decrease the diffusion coefficient of released molecules. Transport rates can be further reduced if the matrix material has an affinity for the diffusing molecules, for example through electrostatic or hydrophobic interactions [84].

4.4 Engineering the Spatial Structure of Microbes in the Laboratory

In light of the critical role that the spatial arrangement of cells has on the activity of cellular communities, many experimental approaches have been developed to actively manipulate the spatial structure of microbes in the lab. In this section, we organize these approaches into three classes based on the type of spatial parameter that is varied: (1) arrangement of cells; (2) arrangement of chemical gradients and activity; and (3) physical parameters. Manipulating these parameters has enabled new studies of the role of "space" in regulating and coordinating the behavior of microbial consortia. We present and discuss seminal work in each of these areas; however, we do not provide a comprehensive overview of all of the research in this area, and often a specific experiment implements a combination of several themes.

4.4.1 Controlling the Arrangement of Cells

To examine the effects of communication upon cellular activity, a variety of techniques are available for manipulating the spatial arrangement of cells in laboratory culture.

4.4.1.1 Engineering Cell Organization at the Macroscale

It is possible to study the effect of cellular communication that occurs over macroscopic distances—that is thousands of cell lengths—by inoculating a pattern of cells on agar media plates. Early uses of this approach included inoculating sister colonies of microbes on opposite sides of a Petri dish to examine how chemical

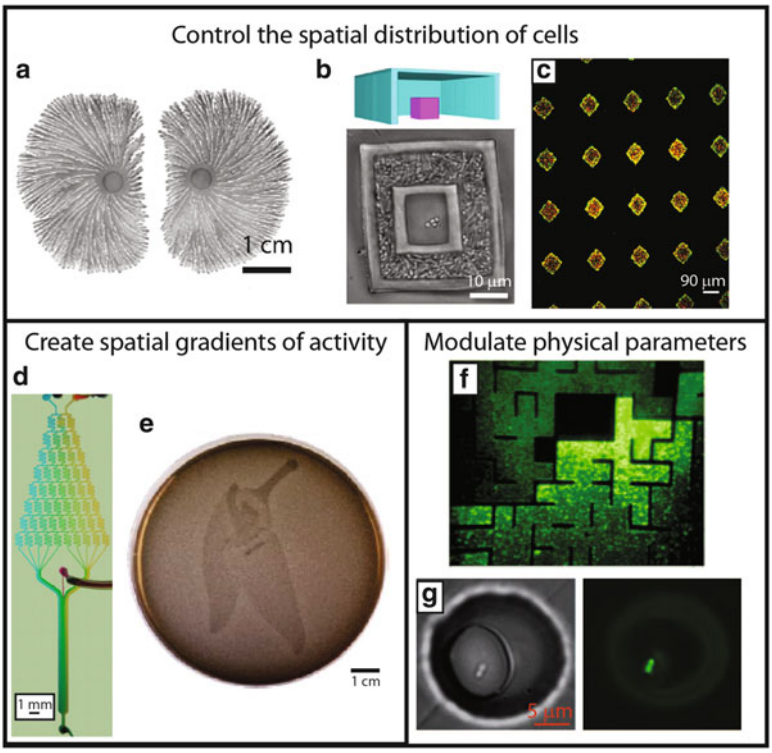

Fig. 4.3 Engineering spatial structure in the lab. (**a**) Interactions between colonies of *Paenibacillus dendritiformis* shape the growth patterns observed on agar plates [85]. (**b**) Multiphoton lithography traps a cluster of *Staphylococcus aereus* microns away from a dense colony of *P. aeruginosa* [96]. (**c**) Microfabrication techniques pattern an array of biofilms with controlled shape and position [93]. (**d**) A microfluidic device creates microscale chemical gradients for microbial chemotaxis experiments [99]. (**e**) Optogenetics controls the expression of reporter genes in response to either red or green light, enabling the transfer of the *red* and *green* image of chili peppers onto a lawn of bacteria [100]. (**f**) The movement of *E. coli* in a microscale maze depends on the local arrangement of physical boundaries, resulting in non-uniform cell clustering, magnification 400X [101]. (**g**) A *P. aeruginosa* cell confined within a femtoliter droplet activates the high-density behavior of quorum sensing in response to the accumulation of released autoinducer [102]

signals emanating from a colony influence growth patterns on the plate, such as the repulsive growth pattern shown in Fig. 4.3a [85]. This pattern formation was the result of a simple reaction diffusion system. To further explore these reaction–diffusion patterns, *E. coli* cells harboring a synthetic quorum sensing system have been embedded in thin strips of an agarose gel through which quorum sensing signals freely diffuse [86, 87]. Such studies may elucidate tuning parameters that are useful in engineering communication systems for synthetic microbial communities [87].

Research in this area also focuses on the interaction between different cells and cell types. Phenotypic assays place microbes in spatial proximity to screen

for interactions mediated by diffusible signals [88]. Signal exchange between colonies can be imaged by MALDI mass spectrometry to identify genes and gene products involved in cell communication. The response of engineered microbes to a diffusing signal may be dependent on the position in which the cells are sampling a gradient [89]. These examples demonstrate that methods of patterning cells at macroscale distances can provide great insight about how space shapes the dynamics of multi-cellular systems. Next we will see that recent technologies enable precise manipulation of microbial communities even at cellular—that is micrometer—length scales.

4.4.1.2 Engineering Cell Organization at the Microscale

Several technologies enable control of microbial habitats at the micron length scale, including: optical traps [90], microelectromechanical systems [91], and microfluidics [92]. Microfluidics enables users to precisely manipulate individual cells and small volumes of liquids (e.g., microliters, nanoliters, and femtoliters). By incorporating microscale and nanoscale features into microfluidic channels, researchers can direct the exchange of chemical information within spatially patterned networks of cells. Figure 4.3c demonstrates microscale control of the shape and position of biofilms [93], and similar techniques position different species of microbes at fixed distances. Using this technique, it was shown that the spatial arrangement of colonies of three soil microbes plays a critical role in balancing interactions within this microbial community [94].

Another promising approach to positioning cells at the microscale is to trap them in a material, for example by isolating individual cells in micron-sized particles or droplets of liquid [95]. Particles can be partitioned such that each section of the structure contains a different microbe [36]. Microbes can also be actively trapped in gel microstructures. These "bacterial cages," shown in Fig. 4.3b, enable researchers to probe the influences of aggregation and of proximity to other species upon gene regulation and phenotypic response [96]. Alternatively, light can be used to hold cells in place. Optical traps grab and position individual cells within a hydrogel, where they can be stimulated and monitored for many hours [90]. Cells can also be positioned by printing them on agarose gels using inkjet printers or fluorescence activated cell sorters [97, 98]. By programming patterns of cells with varying complexity, it is possible to study how microbial spatial structures impact physiology and behavior.

4.4.2 Spatially Controlling Cellular Activity

An alternative approach to positioning cells is to create spatial patterns of cellular activity. One method for patterning activity is to control the location of chemical gradients within a system. Early work by Winogradsky demonstrated that the

formation of macroscale gradients of nutrients and oxygen led to striation of cellular activity and influenced the overall activity within a complex ecosystem of microorganisms. Microfluidic approaches, such as the device shown in Fig. 4.3d, enable precise control over chemical gradients on micron length scales [99, 103]. In one example, a nanofabricated ecosystem of *E. coli* cells was created by connecting picoliter-volume chambers with micrometer and nanometer scale channels, and used to explore the development of antibiotic resistance in a spatially heterogeneous environment [104]. In another example, researchers injected plumes of nutrients into a microchannel and tracked the rapid aggregation of marine microbes around a food source [105]. These are just two of many examples in which microfluidic systems can be used to control chemical gradients.

Optogenetics is a recently developed method of regulating cellular activity. In optogenetics, cellular engineering controls gene regulation in response to light. When cells are illuminated with a specific wavelength of light, an optically controlled chemical transformation in a biomolecule occurs that leads to a change in gene regulation. Although initially developed for neuroscience [106, 107], this technique has been applied to control the activity of microbes with precise temporal and spatial resolution. Figure 4.3e demonstrates cells programmed to change the expression of multiple target genes in response to different wavelengths of light [100, 108].

4.4.3 Manipulating Physical Parameters

The physical parameters of a microbial system are key regulators of the spatiotemporal patterns of signal exchange. Microbes sense physical barriers to transport through the accumulation of released signals or metabolites, and these perturbations to the chemical environment around each cell induce physiological changes. For example, *E. coli* introduced into a microscale maze clustered in the "dead-ends," as shown in Fig. 4.3f. The distribution of chemotactic signals was patterned by the maze itself, resulting in a cellular response dependent on the local structure of the maze [101].

Microdroplets provide another method for introducing barriers to signal exchange between cells. Encapsulating microbes or small groups of microbes in microdroplets enable an examination of cellular physiology in physical confinement. This technique has been used to monitor the activity of small groups of isolated microbes [109, 110]. Cells in microdroplets can activate high-density behaviors, such quorum sensing as shown in Fig. 4.3g. As droplets can contain small numbers of individual cells, the stochastic, heterogeneous nature of single cell activity becomes prominent [102]. Interactions among a mixture of microbial strains can also be studied within and between microdroplets containing specified species [111, 112].

Experimental techniques have also been used to regulate the transport of chemical signals between cells. For example, the flow rate of the bulk liquid nutrient media above a dense cluster of cells influences the activation of quorum sensing regulated genes [113]. In another study, the flow rate shifted the cell density required to initiate quorum sensing [80]. Understanding the role of convection in signaling is critical, as microbes in natural settings experience a wide range of transport environments.

4.5 Next Steps in Understanding and Utilizing Spatial Regulation Within Microbial Communities

The study of microbial spatial structure is an emerging field that is likely to play a major role in microbiology, health, and biotechnology in the future. There are many potential avenues of exploration and development. Here we discuss three key areas: (1) quantifying spatial structure in natural systems; (2) manipulating spatial structure in the lab to discover new biology; and (3) applying engineered spatial structure to tackle real-world problems.

4.5.1 Exploring the Spatial Structure of Real-World Niches, Environments, and Ecosystems

Our understanding of and appreciation for microbial spatial structure is still in its infancy. Section 4.2 discussed several examples of natural systems exhibiting spatial structure, however in many cases the relationship between structure, physiology, and function is not yet clear. Understanding these relationships is an important step forward in altering microbial community behavior to improve the environment and human health.

New deep sequencing technologies make it possible to identify and catalog microbial species found in the human gastrointestinal tract, and to identify trends relating community composition to the development of gastrointestinal disorders, including Crohn's disease and irritable bowel syndrome [43]. However, the spatial structure of gut microbial communities has yet to be closely examined due to the challenges associated with accessing and imaging these structures. As discussed in Sect. 4.2.2.2, the intricate processes that control the nucleation and maturation of multispecies oral biofilms are relevant to human health and remain largely unexplored beyond the identification of the organisms involved [11, 40]. An important next step in this area is to connect genomic data revealing the identity of microbes to their spatial organization in vivo. Extending this challenge to other areas in the human body—beyond the gut and mouth and including wound infections containing different organisms—will likely yield new biology and contribute to health and disease.

In addition to uncovering spatial structure in specific contexts, there are many fundamental unanswered questions regarding the regulation and formation of microbial spatial structures. Mechanisms that influence the nucleation and maturation of multispecies aggregates such as those that form near methane vents on the ocean floor or in waste-water treatment reactors are not fully understood [114]. Understanding the mechanisms of aggregate formation may enable precise manipulation of aggregate spatial structure and composition, and bring to light new strategies to disrupt the formation of aggregates during biofouling.

Effort should also be focused on understanding how microbes regulate structure over longer length scales. In many environments such as soils and in the ocean, microbes exhibit spatial structure over kilometer length scales [32]. An unsolved challenge is to predict how large-scale microbial patterns respond to global environmental changes, as they may introduce important feedbacks into the processes driving global climate change. A quantitative understanding of the mechanisms that regulate large-scale community structure should bring us closer to the ability to rationally and precisely manipulate microbial processes on a global scale.

Revealing mechanisms that regulate microbial structure at multiple scales will inform studies of the adaption and evolution of these structures. Some of the mechanisms underlying the formation of specific spatial structures are encoded in the genome, yet is often unclear how spatial structure emerges from the interactions of these components. Some structures are regulated by interactions between multiple species, suggesting the processes that govern spatial structure would have coevolved. Indeed, such coevolution of spatial structure has been observed in the lab [115]. Elucidating the evolutionary changes that lead to the spatial structures that exist today should give us clues as to how to create, alter, or evolve spatial structure in microbial systems.

4.5.2 Manipulating Spatial Structure in the Lab

There is growing interest in manipulating and engineering microbial community spatial structure in the lab. As new experimental tools become available and are used to decipher the organization of microbial communities, a next step will be to recreate these structures in the lab, and study how they evolve and adapt. As discussed in Sect. 4.4, there are a growing number of techniques available to specify patterns of cell placement and activity in laboratory experiments. We can also manipulate cell function by adjusting physical parameters within these systems (e.g., by varying signal diffusion and mass transport rates, and anisotropy). Undoubtedly, developments in this area will continue.

An important motivation for the development of new approaches to manipulate cell function is addressing key biological problems that remain unresolved. For example, one scientific challenge that the study of spatial structure may solve is the so called “culturability problem.” Over 99 % of the microbes that have been identified by sequencing in nature cannot be cultured in the lab using the methods

and techniques currently available. Although laboratory conditions are inherently limited [116], still, adjusting the spatial structure of laboratory cultures may promote cell growth. Several precedents have been reported. Positioning marine microbial isolates in proximity to native communities using a nanoporous membrane enabled the cultivation of new marine microbes [117]. Another approach confines cells to induce growth. Physical confinement can lead to the accumulation of factors necessary to induce cell growth [118]. Confining pairs of cells increases the strength of interactions between species [111], and close proximity may be required to cultivate species involved in syntrophic interactions, which involve obligate cross feeding. Devices and microsystems that engineer and manipulate spatial structure may prove to be a major component in discovering and cultivating the next generation of laboratory strains.

One hurdle to quantifying multispecies interactions in any environment is the inability to easily test predictions made using global measurements of community composition and function. Analysis of "omics" data—that is large data sets from techniques such as high throughput sequencing and metabolic profiling—reveals patterns such as the association of specific species or metabolites with global aspects of such systems [44, 119, 120], such as disease states. Testing these correlations has been hindered by difficulties in designing laboratory experiments that support the interactions required to reproduce target community functions. One solution may be creating systems of intermediate complexity, consisting of subsets of microbes from the original community. Some community subsets may contain the minimal set of microbes and interaction pathways necessary to test predictions based on correlations observed in the more complicated original system. Recreating essential interactions within these intermediate communities may require reproducing key aspects of the spatial structure of the initial community. Building such laboratory experiments with simplified cellular networks should lead to a more precise understanding of which interactions in large microbial ecosystems shape community outputs.

4.5.3 Solving Problems with Engineered Microbial Systems

In addition to expanding the repertoire of techniques that can be used to study communities in the lab, engineering the spatial structure of cells has applications in health, biotechnology, and the environment. Advances in understanding the role of microbial spatial structure throughout the body will be matched by incorporating aspects of spatial structure into innovative therapies and more accurate diagnostic tools. In ecosystems such as the microbiota of the gut, the composition of communities is remarkably stable over time, yet as changes in composition occur, they may have a dramatic impact on health [44]. Currently, it is unclear to what extent community composition in these systems is malleable.

Relatively simple perturbations to the system—such as introducing a single new species—do not always result in a permanent change within the community [121].

Studying the role of spatial structure in compositional robustness may reveal new opportunities for altering community composition. There are several far-reaching questions in this area. Could introducing pre-structured microbial mixtures into communities yield better control over community composition? Can physiology be controlled by modulating the interactions within the community that maintain spatial and community structure?

In biotechnology, microbial engineering has deeply influenced chemical production and processing. What role will organized community structure and multispecies communities play in these advances? It has been suggested that using "division of labor" to distribute biological processes across species within a community could have several advantages in design and modularity [12]. It is very likely that the spatial structure of these synthetic communities will be essential to maintaining the community composition and regulating functions.

In the environment, interactions within complex communities of microbes are key regulators of global geochemical cycles. Can we apply our knowledge of the influence of microbial spatial structure on community physiology to manipulate these processes on a global scale? At smaller scales, there are many examples of spatial structure influencing environmental processes such as toxin degradation, as detailed in Sect. 4.2.1.3. Potential opportunities are present for engineered spatial structure to modulate rates of these processes occurring in the environment.

4.5.4 Concluding Remarks

Ecosystems exhibit numerous examples of spatially and temporally organized microbes. We have reviewed many examples of these structures in nature, and discussed the theoretical and experimental approaches that can be used to quantitatively understand how spatial structures form and influence microbial physiology. As future research continues to create and explore spatially structured microbial communities, new opportunities will arise for translating these efforts into advances in ecology, human health, and biotechnology. The impact of this area of science on technology is poised to be tremendous.

References

1. Hall-Stoodley L, Costerton JW, Stoodley P (2004) Bacterial biofilms: from the natural environment to infectious diseases. Nat Rev Microbiol 2:95–108
2. Claessen D, Rozen DE, Kuipers OP, Søgaard-Andersen L, van Wezel GP (2014) Bacterial solutions to multicellularity: a tale of biofilms, filaments and fruiting bodies. Nat Rev Microbiol 12:115–124
3. Connell JH, Slatyer RO, The S, Naturalist A, Dec NN (1977) Mechanisms of succession in natural communities and their role in community stability and organization. Am Nat 111:1119–1144

4. Liu Q-X, Doelman A, Rottschäfer V, de Jager M, Herman PMJ, Rietkerk M, van de Koppel J (2013) Phase separation explains a new class of self-organized spatial patterns in ecological systems. Proc Natl Acad Sci U S A 110:11905–11910
5. Lyons M, Ward J, Gaff H, Hicks R, Drake J, Dobbs F (2010) Theory of island biogeography on a microscopic scale: organic aggregates as islands for aquatic pathogens. Aquat Microb Ecol 60:1–13
6. Young IM, Crawford JW, Nunan N, Otten W, Spiers A (2008) Microbial distribution in soils: physics and scaling. Adv Agron 100:81–121
7. Silliman BR, McCoy MW, Angelini C, Holt RD, Griffin JN, van de Koppel J (2013) Consumer fronts, global change, and runaway collapse in ecosystems. Annu Rev Ecol Evol Syst 44:503–538
8. Battin TJ, Sloan WT, Kjelleberg S, Daims H, Head IM, Curtis TP, Eberl L (2007) Microbial landscapes: new paths to biofilm research. Nat Rev Microbiol 5:76–81
9. Andersen R, Chapman SJ, Artz RRE (2013) Microbial communities in natural and disturbed peatlands: a review. Soil Biol Biochem 57:979–994
10. Ley RE, Ba F, Turnbaugh P, Lozupone CA, Knight RD, Gordon JI (2005) Obesity alters gut microbial ecology. Proc Natl Acad Sci U S A 102:11070–11075
11. Kuramitsu HK, He X, Lux R, Anderson MH, Shi W (2007) Interspecies interactions within oral microbial communities. Microbiol Mol Biol Rev 71:653–670
12. Brenner K, You L, Arnold FH (2008) Engineering microbial consortia: a new frontier in synthetic biology. Trends Biotechnol 26:483–489
13. Costerton JW, Lewandowski Z, DeBeer D, Caldwell D, Korber D, James G (1994) Biofilms, the customized microniche. J Bacteriol 176:2137–2142
14. Stoodley P, Sauer K, Davies DG, Costerton JW (2002) Biofilms as complex differentiated communities. Annu Rev Microbiol 56:187–209
15. Fux CA, Costerton JW, Stewart PS, Stoodley P (2005) Survival strategies of infectious biofilms. Trends Microbiol 13:34–40
16. Hoffman LR, D'Argenio DA, MacCoss MJ, Zhang Z, Jones RA, Miller SI (2005) Aminoglycoside antibiotics induce bacterial biofilm formation. Nature 436:1171–1175
17. Harrison JJ, Ceri H, Turner RJ (2007) Multimetal resistance and tolerance in microbial biofilms. Nat Rev Microbiol 5:928–938
18. Molin S, Tolker-nielsen T (2003) Gene transfer occurs with enhanced efficiency in biofilms and induces enhanced stabilisation of the biofilm structure. Curr Opin Biotechnol 14:255–261
19. Vlamakis H, Aguilar C, Losick R, Kolter R (2008) Control of cell fate by the formation of an architecturally complex bacterial community. Genes Dev 22:945–953
20. Parsek MR, Greenberg EP (2005) Sociomicrobiology: the connections between quorum sensing and biofilms. Trends Microbiol 13:27–33
21. Brenner K, Arnold FH (2011) Self-organization, layered structure, and aggregation enhance persistence of a synthetic biofilm consortium. PLoS One 6(2):e16791
22. Shapiro JA (1998) Thinking about bacterial populations as multicellular organisms. Annu Rev Microbiol 52:81–104
23. Julou T, Mora T, Guillon L, Croquette V, Schalk IJ, Bensimon D, Desprat N (2013) Cell–cell contacts confine public goods diffusion inside *Pseudomonas aeruginosa* clonal microcolonies. Proc Natl Acad Sci U S A 110:12577–12582
24. Branda SS, González-Pastor JE, Ben-Yehuda S, Losick R, Kolter R (2001) Fruiting body formation by *Bacillus subtilis*. Proc Natl Acad Sci U S A 98:11621–11626
25. Berleman JE, Chumley T, Cheung P, Kirby JR (2006) Rippling is a predatory behavior in *Myxococcus xanthus*. J Bacteriol 188:5888–5895
26. O'Connor KA, Zusman DR (1991) Development in *Myxococcus xanthus* involves differentiation into two cell types, peripheral rods and spores. J Bacteriol 173:3318–3333
27. Hödl I, Mari L, Bertuzzo E, Suweis S, Besemer K, Rinaldo A, Battin TJ (2014) Biophysical controls on cluster dynamics and architectural differentiation of microbial biofilms in contrasting flow environments. Environ Microbiol 16(3):802–812

28. Besemer K, Singer G, Limberger R, Chlup A-K, Hochedlinger G, Hödl I, Baranyi C, Battin TJ (2007) Biophysical controls on community succession in stream biofilms. Appl Environ Microbiol 73:4966–4974
29. Kiørboe T, Tang K, H-P G, Ploug H (2003) Dynamics of microbial communities on marine snow aggregates: colonization, growth, detachment, and grazing mortality of attached bacteria. Appl Environ Microbiol 69:3036–3047
30. Logan BE, Hunt JR (1987) Advantages to microbes of growth in permeable aggregates in marine systems l. Limnol Oceanogr 32:1034–1048
31. Boetius A, Ravenschlag K, Schubert CJ, Rickert D, Widdel F, Gieseke A, Amann R, Jùrgensen BB, Witte U, Pfannkuche O (2000) A marine microbial consortium apparently mediating anaerobic oxidation of methane. Nature 407:623–626
32. Bever JD, Platt TG, Morton ER (2012) Microbial population and community dynamics on plant roots and their feedbacks on plant communities. Annu Rev Microbiol 266:265–283
33. Eickhorst T, Tippkötter R (2008) Detection of microorganisms in undisturbed soil by combining fluorescence in situ hybridization (FISH) and micropedological methods. Soil Biol Biochem 40:1284–1293
34. Wolfaardt GM, Lawrence JR, Robarts RD, Caldwell DE (1994) The role of interactions, sessile growth, and nutrient amendments on the degradative efficiency of a microbial consortium. Can J Microbiol 40:331–340
35. Sekiguchi Y, Kamagata Y, Nakamura K, Ohashi A, Harada H (1999) Fluorescence in situ hybridization using reveals localization of methanogens and selected uncultured bacteria in mesophilic and thermophilic sludge granules fluorescence in situ hybridization using 16S rRNA-targeted oligonucleotides reveals localization o. Appl Environ Microbiol 65: 1280–1288
36. Kim HJ, Du W, Ismagilov RF (2011) Complex function by design using spatially pre-structured synthetic microbial communities: degradation of pentachlorophenol in the presence of Hg(ii). Integr Biol 3:126–133
37. Dalton T, Dowd SE, Wolcott RD, Sun Y, Watters C, Griswold JA, Rumbaugh KP (2011) An in vivo polymicrobial biofilm wound infection model to study interspecies interactions. PLoS One 6:e27317
38. Korgaonkar A, Trivedi U, Rumbaugh KP, Whiteley M (2013) Community surveillance enhances *Pseudomonas aeruginosa* virulence during polymicrobial infection. Proc Natl Acad Sci U S A 110:1059–1064
39. Foster JS, Kolenbrander PE (2004) Development of a multispecies oral bacterial community in a saliva-conditioned flow cell development of a multispecies oral bacterial community in a saliva-conditioned flow cell. Appl Environ Microbiol 70:4340–4348
40. Palmer RJ, Gordon SM, Cisar JO, Kolenbrander PE (2003) Coaggregation-mediated interactions of streptococci and actinomyces detected in initial human dental plaque coaggregation-mediated interactions of streptococci and actinomyces detected in initial human dental plaque. J Bacteriol 185:3400–3409
41. Grenier D (1992) Nutritional interactions between two suspected periodontopathogens, *Treponema denticola* and *Porphyromonas gingivalis*. Infect Immun 60:5298
42. Yamada M, Ikegami A, Kuramitsu HK (2005) Synergistic biofilm formation by *Treponema denticola* and *Porphyromonas gingivalis*. FEMS Microbiol Lett 250:271–277
43. Swidsinski A, Loening-Baucke V, Vaneechoutte M, Doerffel Y (2008) Active Crohn's disease and ulcerative colitis can be specifically diagnosed and monitored based on the biostructure of the fecal flora. Inflamm Bowel Dis 14:147–161
44. Ridaura VK, Faith JJ, Rey FE, Cheng J, Duncan AE, Kau AL, Griffin NW, Lombard V, Henrissat B, Bain JR, Muehlbauer MJ, Ilkayeva O, Semenkovich CF, Funai K, Hayashi DK, Lyle BJ, Martini MC, Ursell LK, Clemente JC, Van Treuren W, Walters WA, Knight R, Newgard CB, Heath AC, Gordon JI (2013) Gut microbiota from twins discordant for obesity modulate metabolism in mice. Science 341:1241214
45. Berg HC (1983) Random walks in biology. Princeton University Press, Princeton

46. Phillips RB, Kondev J, Theriot J (2009) Physical biology of the cell. Taylor & Francis Group, New York
47. Freitas Jr RA (1999) Nanomedicine. In: Basic capabilities, vol I. Landes bioscience, Georgetown
48. Karlsson D, Zacchi G, Axelsson A (2002) Electronic speckle pattern interferometry: a tool for determining diffusion and partition coefficients for proteins in gels. Biotechnol Prog 18: 1423–1430
49. Bray D (2001) Cell movements: from molecules to motility, vol 2. Garland Science
50. Lugg GA (1968) Diffusion coefficients of some organic and other vapors in air. Anal Chem 40:1072–1077
51. Kalwarczyk T, Tabaka M, Holyst R (2012) Biologistics-diffusion coefficients for complete proteome of *Escherichia coli*. Bioinformatics 28:2971–2978
52. Staron A, Sofia HJ, Dietrich S, Ulrich LE, Liesegang H, Mascher T (2009) The third pillar of bacterial signal transduction: classification of the extracytoplasmic function (ECF) sigma factor protein family. Mol Microbiol 74:557–581
53. Stock AM, Robinson VL, Goudreau PN (2000) Two-component signal transduction. Annu Rev Biochem 69:183–215
54. Groban ES, Clarke EJ, Salis HM, Miller SM, Voigt CA (2009) Kinetic buffering of cross talk between bacterial two-component sensors. J Mol Biol 390:380–393
55. Sourjik V, Wingreen NS (2012) Responding to chemical gradients: bacterial chemotaxis. Curr Opin Cell Biol 24:262–268
56. Missiakas D, Raina S (1998) The extracytoplasmic function sigma factors: role and regulation. Mol Microbiol 28:1059–1066
57. Pearson JP, Van Delden C, Iglewski BH (1999) Active efflux and diffusion are involved in transport of *Pseudomonas aeruginosa* cell-to-cell signals. J Bacteriol 181:1203–1210
58. Fuqua C, Parsek MR, Greenberg EP (2001) Regulation of gene expression by cell-to-cell communication: acyl-homoserine lactone quorum sensing. Annu Rev Genet 35:439–468
59. Hammar P, Leroy P, Mahmutovic A, Marklund EG, Berg OG, Elf J (2012) The lac repressor displays facilitated diffusion in living cells. Science 336:1595–1598
60. Grigorova IL, Phleger NJ, Mutalik VK, Gross CA (2006) Insights into transcriptional regulation and sigma competition from an equilibrium model of RNA polymerase binding to DNA. Proc Natl Acad Sci U S A 103:5332–5337
61. Bremer HD, Dennis PP (1996) Modulation of chemical composition and other parameters of the cell by growth rate. In: Neidhardt FC et al (eds) *Escherichia coli* and salmonella: cellular and molecular biology. American Society for Microbiology, Washington, pp 1553–1569
62. Kubelka J, Hofrichter J, Eaton WA (2004) The protein folding 'speed limit'. Curr Opin Struct Biol 14:76–88
63. Naganathan AN, Munoz V (2005) Scaling of folding times with protein size. J Am Chem Soc 127:480–481
64. Iizuka R, Yamagishi-Shirasaki M, Funatsu T (2011) Kinetic study of de novo chromophore maturation of fluorescent proteins. Anal Biochem 414:173–178
65. Rosenfeld N, Elowitz MB, Alon U (2002) Negative autoregulation speeds the response times of transcription networks. J Mol Biol 323:785–793
66. Mora T, Wingreen NS (2010) Limits of sensing temporal concentration changes by single cells. Phys Rev Lett 104(24):248101
67. Berg HC, Purcell EM (1977) Physics of chemoreception. Biophys J 20:193–219
68. Zhang Q, Bhattacharya S, Andersen ME (2013) Ultrasensitive response motifs: basic amplifiers in molecular signalling networks. Open Biol 3(4):130031
69. Kastrup CJ, Runyon MK, Shen F, Ismagilov RF (2006) Modular chemical mechanism predicts spatiotemporal dynamics of initiation in the complex network of hemostasis. Proc Natl Acad Sci U S A 103:15747–15752
70. Kholodenko BN (2006) Cell-signalling dynamics in time and space. Nat Rev Mol Cell Biol 7:165–176

71. Golden JW, Yoon HS (1998) Heterocyst formation in Anabaena. Curr Opin Microbiol 1: 623–629
72. Risser DD, Callahan SM (2009) Genetic and cytological evidence that heterocyst patterning is regulated by inhibitor gradients that promote activator decay. Proc Natl Acad Sci U S A 106:19884–19888
73. Zhu M, Callahan SM, Allen JS (2010) Maintenance of heterocyst patterning in a filamentous cyanobacterium. J Biol Dyn 4:621–633
74. Dubey GP, Ben-Yehuda S (2011) Intercellular nanotubes mediate bacterial communication. Cell 144:590–600
75. El-Naggar MY, Wanger G, Leung KM, Yuzvinsky TD, Southam G, Yang J, Lau WM, Nealson KH, Gorby YA (2010) Electrical transport along bacterial nanowires from Shewanella oneidensis MR-1. Proc Natl Acad Sci U S A 107:18127–18131
76. Davis TS, Crippen TL, Hofstetter RW, Tomberlin JK (2013) Microbial volatile emissions as insect semiochemicals. J Chem Ecol 39:840–859
77. Ortiz-Castro R, Diaz-Perez C, Martinez-Trujillo M, del Rio RE, Campos-Garcia J, Lopez-Bucio J (2011) Transkingdom signaling based on bacterial cyclodipeptides with auxin activity in plants. Proc Natl Acad Sci U S A 108:7253–7258
78. Flavier AB, Clough SJ, Schell MA, Denny TP (1997) Identification of 3-hydroxypalmitic acid methyl ester as a novel autoregulator controlling virulence in *Ralstonia solanacearum*. Mol Microbiol 26:251–259
79. Weber W, Daoud-El Baba M, Fussenegger M (2007) Synthetic ecosystems based on airborne inter- and intrakingdom communication. Proc Natl Acad Sci U S A 104:10435–10440
80. Kirisits MJ, Margolis JJ, Purevdorj-Gage BL, Vaughan B, Chopp DL, Stoodley P, Parsek MR (2007) Influence of the hydrodynamic environment on quorum sensing in *Pseudomonas aeruginosa* biofilms. J Bacteriol 189:8357–8360
81. Berg HC, Turner L (1990) Chemotaxis of bacteria in glass-capillary arrays – *Escherichia-coli*, motility, microchannel plate, and light-scattering. Biophys J 58:919–930
82. Copeland MF, Weibel DB (2009) Bacterial swarming: a model system for studying dynamic self-assembly. Soft Matter 5:1174–1187
83. Redfield RJ (2002) Is quorum sensing a side effect of diffusion sensing? Trends Microbiol 10:365–370
84. Stewart PS (1998) A review of experimental measurements of effective diffusive permeabilities and effective diffusion coefficients in biofilms. Biotechnol Bioeng 59:261–272
85. Be'er A, Ariel G, Kalisman O, Helman Y, Sirota-Madi A, Zhang HP, Florin EL, Payne SM, Ben-Jacob E, Swinney HL (2010) Lethal protein produced in response to competition between sibling bacterial colonies. Proc Natl Acad Sci U S A 107:6258–6263
86. Dilanji GE, Langebrake JB, De Leenheer P, Hagen SJ (2012) Quorum activation at a distance: spatiotemporal patterns of gene regulation from diffusion of an autoinducer signal. J Am Chem Soc 134:5618–5626
87. Brenner K, Karig DK, Weiss R, Arnold FH (2007) Engineered bidirectional communication mediates a consensus in a microbial biofilm consortium. Proc Natl Acad Sci U S A 104:17300–17304
88. Barger SR, Hoefler BC, Cubillos-Ruiz A, Russell WK, Russell DH, Straight PD (2012) Imaging secondary metabolism of Streptomyces sp Mg1 during cellular lysis and colony degradation of competing *Bacillus subtilis*. Antonie Van Leeuwenhoek 102:435–445
89. Basu S, Gerchman Y, Collins CH, Arnold FH, Weiss R (2005) A synthetic multicellular system for programmed pattern formation. Nature 434:1130–1134
90. Mirsaidov U, Scrimgeour J, Timp W, Beck K, Mir M, Matsudaira P, Timp G (2008) Live cell lithography: using optical tweezers to create synthetic tissue. Lab Chip 8:2174–2181
91. Ingham CJ, van Hylckama Vlieg JE (2008) MEMS and the microbe. Lab Chip 8:1604–1616
92. Weibel DB, DiLuzio WR, Whitesides GM (2007) Microfabrication meets microbiology. Nat Rev Microbiol 5:209–218
93. Eun Y-J, Weibel DB (2009) Fabrication of microbial biofilm arrays by geometric control of cell adhesion. Langmuir 25:4643–4654

94. Kim HJ, Boedicker JQ, Choi JW, Ismagilov RF (2008) Defined spatial structure stabilizes a synthetic multispecies bacterial community. Proc Natl Acad Sci U S A 105:18188–18193
95. Schmitz CHJ, Rowat AC, Koester S, Weitz DA (2009) Dropspots: a picoliter array in a microfluidic device. Lab Chip 9:44–49
96. Connell JL, Ritschdorff ET, Whiteley M, Shear JB (2013) 3D printing of microscopic bacterial communities. Proc Natl Acad Sci U S A 110:18380–18385
97. Merrin J, Leibler S, Chuang JS (2007) Printing multistrain bacterial patterns with a piezoelectric inkjet printer. PLoS One 2(7):e663
98. Choi WS, Ha D, Park S, Kim T (2011) Synthetic multicellular cell-to-cell communication in inkjet printed bacterial cell systems. Biomaterials 32:2500–2507
99. Englert DL, Manson MD, Jayaraman A (2009) Flow-based microfluidic device for quantifying bacterial chemotaxis in stable, competing gradients. Appl Environ Microbiol 75: 4557–4564
100. Tabor JJ, Levskaya A, Voigt CA (2011) Multichromatic control of gene expression in *Escherichia coli*. J Mol Biol 405:315–324
101. Park S, Wolanin PM, Yuzbashyan EA, Lin H, Darnton NC, Stock JB, Silberzan P, Austin R (2003) Influence of topology on bacterial social interaction. Proc Natl Acad Sci U S A 100:13910–13915
102. Boedicker JQ, Vincent ME, Ismagilov RF (2009) Microfluidic confinement of single cells of bacteria in small volumes initiates high-density behavior of quorum sensing and growth and reveals its variability. Angew Chem Int Ed Engl 48:5908–5911
103. King KR, Wang S, Jayaraman A, Yarmush ML, Toner M (2008) Microfluidic flow-encoded switching for parallel control of dynamic cellular microenvironments. Lab Chip 8:107–116
104. Zhang Q, Lambert G, Liao D, Kim H, Robin K, Tung C-K, Pourmand N, Austin RH (2011) Acceleration of emergence of bacterial antibiotic resistance in connected microenvironments. Science 333:1764–1767
105. Stocker R, Seymour JR, Samadani A, Hunt DE, Polz MF (2008) Rapid chemotactic response enables marine bacteria to exploit ephemeral microscale nutrient patches. Proc Natl Acad Sci U S A 105:4209–4214
106. Williams SCP, Deisseroth K (2013) Optogenetics. Proc Natl Acad Sci U S A 110:16287
107. Knoepfel T, Lin MZ, Levskaya A, Tian L, Lin JY, Boyden ES (2010) Toward the second generation of optogenetic tools. J Neurosci 30:14998–15004
108. Toettcher JE, Voigt CA, Weiner OD, Lim WA (2011) The promise of optogenetics in cell biology: interrogating molecular circuits in space and time. Nat Methods 8:35–38
109. Martin K, Henkel T, Baier V, Grodrian A, Schon T, Roth M, Kohler JM, Metze J (2003) Generation of larger numbers of separated microbial populations by cultivation in segmented-flow microdevices. Lab Chip 3:202–207
110. Jakiela S, Kaminski TS, Cybulski O, Weibel DB, Garstecki P (2013) Bacterial growth and adaptation in microdroplet chemostats. Angew Chem Int Ed Engl 52:8908–8911
111. Park J, Kerner A, Burns MA, Lin XN (2011) Microdroplet-enabled highly parallel co-cultivation of microbial communities. PLoS One 6(2):e17019
112. Bai Y, Patil SN, Bowden SD, Poulter S, Pan J, Salmond GPC, Welch M, Huck WTS, Abell C (2013) Intra-species bacterial quorum sensing studied at single cell level in a double droplet trapping system. Int J Mol Sci 14:10570–10581
113. Connell JL, Wessel AK, Parsek MR, Ellington AD, Whiteley M, Shear JB (2010) Probing prokaryotic social behaviors with bacterial "Lobster Traps". MBio 1(4): pii:e00202-10
114. Barr JJ, Cook AE, Bond PL (2010) Granule formation mechanisms within an aerobic wastewater system for phosphorus removal. Appl Environ Microbiol 76:7588–7597
115. Hansen SK, Rainey PB, Haagensen JAJ, Molin S (2007) Evolution of species interactions in a biofilm community. Nature 445:533–536
116. Stewart EJ (2012) Growing unculturable bacteria. J Bacteriol 194:4151–4160
117. Kaeberlein T, Lewis K, Epstein SS (2002) Isolating "uncultivable" microorganisms in pure culture in a simulated natural environment. Science 296:1127–1129

118. Kaprelyants AS, Gottschal JC, Kell DB (1993) Dormancy in non-sporulating bacteria. FEMS Microbiol Lett 104:271–286
119. Huttenhower C, Gevers D, Knight R, Abubucker S, Badger JH, Chinwalla AT, Creasy HH, Earl AM, FitzGerald MG, Fulton RS, Giglio MG, Hallsworth-Pepin K, Lobos EA, Madupu R, Magrini V, Martin JC, Mitreva M, Muzny DM, Sodergren EJ, Versalovic J, Wollam AM, Worley KC, Wortman JR, Young SK, Zeng Q, Aagaard KM, Abolude OO, Allen-Vercoe E, Alm EJ, Alvarado L, Andersen GL, Anderson S, Appelbaum E, Arachchi HM, Armitage G, Arze CA, Ayvaz T, Baker CC, Begg L, Belachew T, Bhonagiri V, Bihan M, Blaser MJ, Bloom T, Bonazzi V, Brooks JP, Buck GA, Buhay CJ, Busam DA, Campbell JL, Canon SR, Cantarel BL, Chain PSG, Chen IMA, Chen L, Chhibba S, Chu K, Ciulla DM, Clemente JC, Clifton SW, Conlan S, Crabtree J, Cutting MA, Davidovics NJ, Davis CC, DeSantis TZ, Deal C, Delehaunty KD, Dewhirst FE, Deych E, Ding Y, Dooling DJ, Dugan SP, Dunne WM, Durkin AS, Edgar RC, Erlich RL, Farmer CN, Farrell RM, Faust K, Feldgarden M, Felix VM, Fisher S, Fodor AA, Forney LJ, Foster L, Di Francesco V, Friedman J, Friedrich DC, Fronick CC, Fulton LL, Gao H, Garcia N, Giannoukos G, Giblin C, Giovanni MY, Goldberg JM, Goll J, Gonzalez A, Griggs A, Gujja S, Haake SK, Haas BJ, Hamilton HA, Harris EL, Hepburn TA, Herter B, Hoffmann DE, Holder ME, Howarth C, Huang KH, Huse SM, Izard J, Jansson JK, Jiang H, Jordan C, Joshi V, Katancik JA, Keitel WA, Kelley ST, Kells C, King NB, Knights D, Kong HH, Koren O, Koren S, Kota KC, Kovar CL, Kyrpides NC, La Rosa PS, Lee SL, Lemon KP, Lennon N, Lewis CM, Lewis L, Ley RE, Li K, Liolios K, Liu B, Liu Y, Lo C-C, Lozupone CA, Lunsford RD, Madden T, Mahurkar AA, Mannon PJ, Mardis ER, Markowitz VM, Mavromatis K, McCorrison JM, McDonald D, McEwen J, McGuire AL, McInnes P, Mehta T, Mihindukulasuriya KA, Miller JR, Minx PJ, Newsham I, Nusbaum C, O'Laughlin M, Orvis J, Pagani I, Palaniappan K, Patel SM, Pearson M, Peterson J, Podar M, Pohl C, Pollard KS, Pop M, Priest ME, Proctor LM, Qin X, Raes J, Ravel J, Reid JG, Rho M, Rhodes R, Riehle KP, Rivera MC, Rodriguez-Mueller B, Rogers Y-H, Ross MC, Russ C, Sanka RK, Sankar P, Sathirapongsasuti JF, Schloss JA, Schloss PD, Schmidt TM, Scholz M, Schriml L, Schubert AM, Segata N, Segre JA, Shannon WD, Sharp RR, Sharpton TJ, Shenoy N, Sheth NU, Simone GA, Singh I, Smillie CS, Sobel JD, Sommer DD, Spicer P, Sutton GG, Sykes SM, Tabbaa DG, Thiagarajan M, Tomlinson CM, Torralba M, Treangen TJ, Truty RM, Vishnivetskaya TA, Walker J, Wang L, Wang Z, Ward DV, Warren W, Watson MA, Wellington C, Wetterstrand KA, White JR, Wilczek-Boney K, Wu Y, Wylie KM, Wylie T, Yandava C, Ye L, Ye Y, Yooseph S, Youmans BP, Zhang L, Zhou Y, Zhu Y, Zoloth L, Zucker JD, Birren BW, Gibbs RA, Highlander SK, Methe BA, Nelson KE, Petrosino JF, Weinstock GM, Wilson RK, White O (2012) Human microbiome project C structure, function and diversity of the healthy human microbiome. Nature 486:207–214
120. Muller EEL, Glaab E, May P, Vlassis N, Wilmes P (2013) Condensing the omics fog of microbial communities. Trends Microbiol 21:325–333
121. McNulty NP, Yatsunenko T, Hsiao A, Faith JJ, Muegge BD, Goodman AL, Henrissat B, Oozeer R, Cools-Portier S, Gobert G, Chervaux C, Knights D, Lozupone CA, Knight R, Duncan AE, Bain JR, Muehlbauer MJ, Newgard CB, Heath AC, Gordon JI (2011) The impact of a consortium of fermented milk strains on the gut microbiome of gnotobiotic mice and monozygotic twins. Sci Transl Med 3(106):106ra106

Chapter 5
Functionality of Autoinducer Systems in Complex Environments

B.A. Hense, C. Kuttler, and J. Müller

5.1 Introduction

Cell-to-cell signalling via small diffusible molecules, usually termed quorum sensing (QS), represents a common behaviour in bacteria. This signalling regulates life style switches in many, if not most symbiotic microbial species either beneficial or pathogenic for their eukaryotic hosts, but is also involved in controlling environmental processes such as biofouling, degradation processes in sewage plants or environmental pollutions and N cycling [1–4]. Biochemically, the core of a generic system comprises a cytoplasmatic signal synthase (or several involved enzymes), a small, diffusible signal which is released into the environment, and a signal receptor located in the cell membrane or in the cytoplasma. The signal-receptor complex directly or indirectly controls the expression of target genes (Fig. 5.1). The signal was termed autoinducer (AI), because the same cells produce and react on the signal molecules. For an overview on the various chemical realizations of AI systems see, e.g. Atkinson and Williams [5]. Originally, three main types of AI molecules have been described: (a) Mainly gram-negative proteobacteria, but also

B.A. Hense (✉)
Helmholtz Zentrum München, Institute of Computational Biology, Ingolstädter Landstr. 1, 85764 Neuherberg/Munich, Germany
e-mail: burkhard.hense@helmholtz-muenchen.de

C. Kuttler
Technical University München, Centre for Mathematical Sciences, Boltzmannstr. 3, 85747 Garching, Germany

J. Müller
Helmholtz Zentrum München, Institute of Computational Biology, Ingolstädter Landstr. 1, 85764 Neuherberg/Munich, Germany

Technical University München, Centre for Mathematical Sciences, Boltzmannstr. 3, 85747 Garching, Germany

S.J. Hagen (ed.), *The Physical Basis of Bacterial Quorum Communication*, Biological and Medical Physics, Biomedical Engineering, DOI 10.1007/978-1-4939-1402-9_5

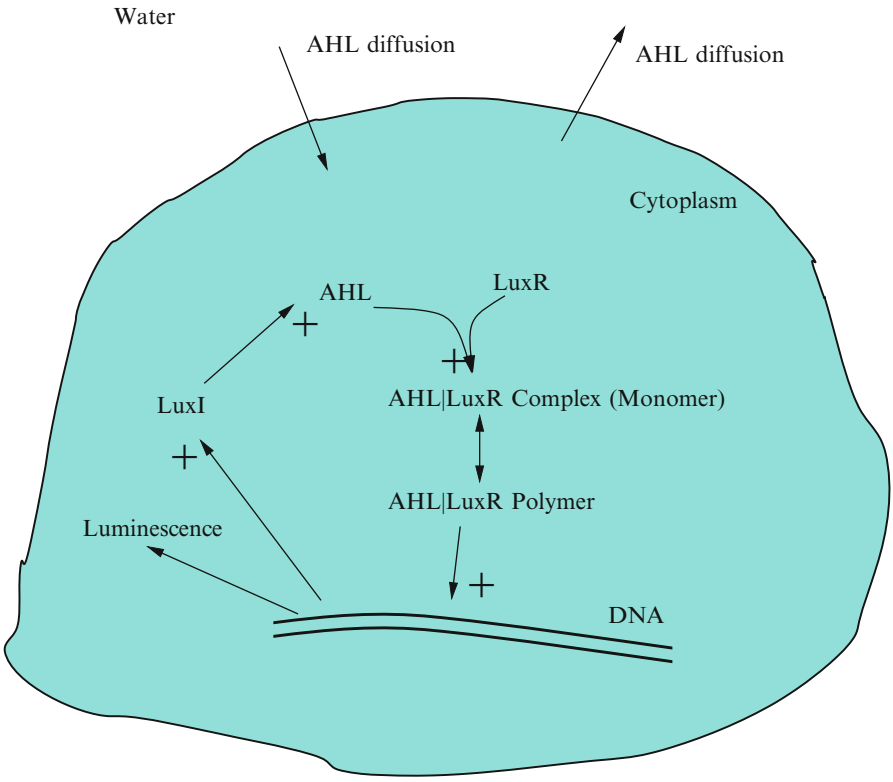

Fig. 5.1 Sketch of the basics of a typical autoinducer system in a cell, exemplarily for the LuxI/luxR.system of *Vibrio fischeri*, including an intracellular autoinducer synthase (LuxI), the autoinducer AHL and an intracellular autoinducer receptor LuxR, which binds after polymerization (often dimerization) of the LuxR–AHL complex to promoter regions of the DNA to control gene expression. The controlled target genes include usually parts of the autoinducer system (here: luxI expression is up-regulated), and a set of other target genes—in this examples involving those responsible for bioluminescence

some cyanobacteria and archaebacteria employ molecules of the acylhomoserine lactone (AHL) group as AIs, (b) oligopeptide AIs occur in gram-positive bacteria, and (c) AI2 has been described as a universal signal for interspecies communication. Recently, a still increasing number of AIs belonging to various chemical classes have been discovered.

The generic system is adapted in various ways, specifically for each species. For example, several oligopeptide AIs are post-translationally intra- or extracellularly modified, and the AI transfer through the plasma membrane might be passive (by diffusion) or active. Two properties relevant for the ecological function have been described for most, but not all AI systems, introducing feedback and non-linearity into the regulation architecture: (1) Autoregulation, i.e. AIs positively regulate their own activity on gene expression level, e.g. via expression of their synthase, and (2) Cooperativity of the AI effect (Hill factor >1), e.g. via

di(multi)merization of receptor/AI complexes. As a consequence, for an appropriate parameter range bistability and hysteresis might occur. In fact, AI systems tend to react in switch-like manner. This behaviour supports a synchronous all-or-none behaviour of cells in a population. However, existence of bistability was reported to depend on the stability of receptor/AI complexes, and thus may not exist in many AI systems in vivo [6].

Another aspect that is poorly understood is the dependence of the AI-circuit on other processes. AI activity at least often depends on the cell state. Ulitzur [7] showed for example that starvation may enhance QS. The function of these interdependencies of different regulation systems with respect to homoeostasis of cells and ecological function deserves more intensive attention. The situation is even more complex if several feedback loops are existent or more than one interconnected AI systems co-exist in one species. The appropriate description of the interaction between AI system and interconnected regulatory pathways forms a foundation for interpretations and theories of the ecological function of AIs. The original interpretation of AI regulation as a mechanism to control target gene expression by cell density was quite narrow.

Mathematical modelling has been involved in the study of AI systems for a long time. (For an overview see, e.g. [8].) They are employed for parameter estimation from experiments, for predictions in a kind of virtual experiments, or for analysis of the evolutionary stability of the systems. Furthermore, they play an important role for the development of theories or concepts with respect to the in situ functionality of AI regulation.

Mainly from the latter perspective, this chapter will focus on four aspects[1]:

(A) What is the ecological function of AI systems?
(B) Case study: QS and luminescence
(C) Integration of nutrients in AI regulation—Purpose?
(D) Relevance of locality for QS

Following the argumentation of, for example, Winzer et al. [9] and Diggle et al. [10, 11] we apply a rather strict definition of these terms “signalling”, “signal molecule” and “communication”. We limit them to systems, in which there are direct or indirect evolutionary benefits for the receiver to response, and the response of the receiver has to be beneficial for the sender. Thus we exclude coercion and eavesdropping.

5.2 What Is the Ecological Function of AI Systems?

The original quorum sensing concept, which focussed on the relevance of cell density (or quorum) for the gene expression regulation via AIs, was derived

[1]The book chapter partly bases on a recent journal article Hense and Schuster [77] (in preparation).

from experimental observation in homogeneously mixed batch cultures [12, 13]. Its ecological purpose was interpreted as limiting certain joint activities to a population size or cell density, which allows these activities to be effective. An example was bioluminescence which might only be effective, i.e. visible, if produced by a sufficiently large number of cells. It was assumed that this was ensured by an AI-controlled synchronous all-or-none behaviour of the cells. Consequently, most mathematical models—especially the early ones—use cell density as input variable to analyse, e.g. the induction dynamic of the system.

However, in situ most bacterial cells exist in spatially structured environments. They live in heterogeneous matrices like soils or eukaryotic hosts and in colonies/biofilms. Recent interpretations acknowledge that other influences such as spatial cell organization and diffusion rates also have an impact on the AI concentration (for an overview see [14]). The resulting concepts have mainly been developed on the basis of theoretical considerations, partly on modelling, but the relevance of the additional factors for AI regulation has been confirmed experimentally (e.g. [15–19]). Most of these interpretations identify cell density, cell distribution (i.e. relative spatial location of cells with respect to each other) and/or mass transfer properties of the environment (including space limitations, diffusion rates and flow conditions) as the primary important factors influencing AI systems. Note that the cell density and cell distribution are sometimes subsumed into a term called “local cell density”, suggesting that both aspects are not independent and may be transformed in each other [14]. A careful consideration of the term cell density is necessary. The simple counting of cell numbers per volume will not always work, as cells in clusters as well as homogeneously distributed cells may yield similar cell densities, but behave differently with respect to AI induction of the cells (Fig. 5.2). The spatial scale—a reference volume included in the term “density”—plays a crucial role, but a reasonable reference volume is impossible to be defined. Consequently, we prefer to differentiate between cell distribution and cell density. Both can be calculated independently. Exemplarily, one method to analyse clustering is the radial distribution function (RDF), which bases on the ratio of the probability of finding a particle pair, separated by a distance r, normalized by the same probability for a randomly distributed mixture.

As Platt and Fuqua [14] pointed out, the emerging multitude of concepts and concept names, focussing specifically on different influencing factors, led to unnecessary confusion. In reality, usually a mixture of these three aspects will influence the AI concentration to which the cells are exposed. The relative relevance or contribution of each influencing factor will spatio-temporally vary dependent on the specific environmental conditions, and the cells usually will not be able to distinguish between them [14, 20]. In fact, recent experimental studies support the idea that a combination of the influencing factors is responsible for the induction behaviour of AI systems [19, 21, 22]. It is to expect that the system yields reasonable results over a wide range of parameters and in different geometries, i.e. largely independent on the relative contribution of the factors.

Thus, different attempts have been made to unify the different concepts [20, 23]. The approach of Hense et al. [20], named efficiency sensing (ES), focuses on

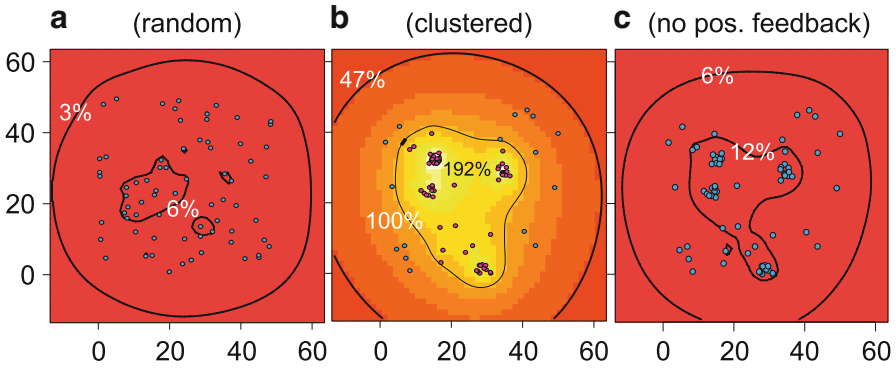

Fig. 5.2 Autoinducer pattern for a population of 70 cells in a volume of $50 \times 50 \times 10$ μm^3 on a solid surface. Induction threshold = 50 nM AI. Lines indicate identical AI concentrations. Values given indicate AI concentration in % of threshold concentration. *Cyan cells*: not induced. *Red cells*: induced. The 3D domain is viewed from the top, onto an impermeable surface at the bottom. As the domain is otherwise infinite, the autoinducer can diffuse away. (**a**) cells randomly distributed, (**b**) cells clustered, (**c**) cells clustered, but lacking the positive feedback via AI dependent up-regulation of AI synthase. Clearly, clustering promotes induction by achieving high local autoinducer concentrations, which is further strengthened by the positive feedback loop. The figure was taken from [20]. For more details see there

understanding the regulation system from the perspective of its ecological or evolutionary purpose instead from the perspective of which factors affect it.[2] The ES concept assumes that the ecologically relevant function of AI sensing is to assess the efficiency of producing extracellular effectors (public goods) such as exoenzymes, siderophores or antibiotica, whose extracellular concentration pattern will be influenced by the same combination of influencing factors that affect the concentration pattern of AIs. AI systems integrate the net-influence of these factors into a single readout. AI can therefore function as a proxy to predict the environmental pattern of the more expensive released effectors. As AIs consists of small molecules and regulate multiple genes, they can act as significant cost savers

[2]Here, we will use the term "quorum sensing" in its original restricted way, i.e. as a strategy to the control gene activity in dependency of *cell density*, although now a tendency exists to interpret it in a wider way, comprehending other influencing aspects like cell distribution and mass transfer properties. The wider concept we term more neutrally as "AI sensing". We do this just for clarity of terming within this text.

Note that the authors here which have been involved in the introduction of the ES concept, did not intend to add an additional quagmire or substitute the term "quorum sensing" by the term "efficiency sensing", but to reshape thinking about what the ecological function of AIs might be. The term "quorum sensing" gained wide acceptance in the scientific community. Thus, to our opinion, it might be kept, but consistently be interpreted in a much broader sense than "cell density dependent gene regulation". Unfortunately, due to the fact that phrasing often determines thinking, to our feeling still very often the function of AI regulation tends to be interpreted in the latter, narrow sense.

by limiting costly activity of AI regulated genes to conditions, where this activity is cost-effective (= efficient). ES unifies the concepts of what cells sense, why cells sense and the evolutionary hypotheses of the fitness benefits derived from AI sensing. Other factors affecting the AI and regulated effectors in a non-correlated way, e.g. degradation processes, are not defined as influence factors in our sense, but simply as disturbances, which decrease the reliability of the system. If these factors are independently recognizable by the cells (e.g. pH affecting the stability of certain AI), their disturbance potential on the signalling may, at least theoretically, be compensated.

In fact, most AI systems control genes connected with effector releases. Usually AI systems do not control single targets genes, but rather life style switches, e.g. from opportunistic to virulent in pathogens [24–27]. Thus, not each single gene, but rather the life style switch itself may be connected with effector release, to make an efficiency control via AIs beneficial.

5.3 Case Study: AI Regulation and Luminescence

The original interpretation of the ES concept described above, although thought to explain most cases of QS, probably has been too strict (narrow). One aspect covered only incompletely by ES is the AI control of intracellular, i.e. non-released enzymes, which interfere with environmental properties respectively with substances that are connected with cellular stress. Examples are intracellular enzymes controlling oxidative stress or acidification [28–31].

The ecological and evolutionary benefit of the light-producing luciferase reaction is usually assumed to be connected with visibility or camouflage. This, however, has been questioned to be the sole purpose as there are bioluminescing species that live in the gut of certain beetles or even the soil [32–36]. As the O_2 consuming luciferase reaction is able to reduce oxidative stress, an alternative hypothesis proposes that detoxification of oxidative stress has been the original purpose of the luciferase reaction evolutionarily, and light emission is only a secondary effect [37–40]. Timmins et al. [38] suggested that, although detoxification has been the original purpose during the evolution of the luciferase reaction in former times, removing of O_2 via ATP consuming luciferase reaction may be inefficient nowadays due to the higher environmental O_2 concentration. Thus, recently light emission, resp. visibility may be the only benefit.

In a recent publication, Müller and Hense [41] (in preparation) investigated the functionality of an AI regulated intracellular luciferase reaction, as it exists, e.g. in *Vibrio fischeri* using an AHL as autoinducer.

The model for a hemispherical colony attached to an impermeable surface consists of two equations:

$$A_t = D_A \Delta A + \rho(x) \left(\alpha + \beta A^n / \left(A^n + A_\tau^n\right)\right)$$

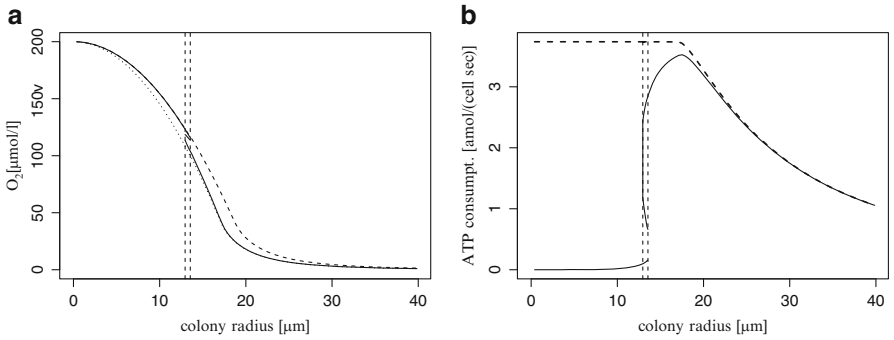

Fig. 5.3 *Left panel*: O_2 concentration in the colony centre over colony size. *Dashed-dotted line*: only aerobic respiration; *dashed line*: respiration plus constitutively induced luciferase reaction; *solid line*: aerobic respiration plus autoinducer regulated luciferase reaction; *vertical line*: range of induction. *Right panel*: Mean ATP consumption by luciferase reaction for varying colony sizes. *Solid line*: autoinducer controlled luciferase production; *dashed line*: constitutively production of luciferase at induced level; *vertical lines*: range of induction. The figure was taken from [41]. For more details see there

and

$$O_t = D_O \Delta O - \rho(x) \frac{O^2 K_{\text{cat},1}}{O^2 + K_{m,1}^2} - \rho(x) \frac{O^2 K_{\text{cat},2}}{O^2 + K_{m,2}^2} \frac{A^n}{A^n + A_\tau^n}.$$

(with radius R, cell concentration $\rho(|x|)$, AHL concentration A, AHL concentration of half-maximal AHL production rate A_τ, Hill factor n, background concentration of O_2 (e.g. in the open sea) O_0, O_2 concentration O, O_2 consumption described by K_m denoting the concentration with half-maximal reaction rate resp. K_{cat} the maximal reaction rate, $K_{x,1}$ resp. $K_{x,2}$ denoting the O_2 consumption via respiration resp. luciferase reaction, diffusion coefficient D_A and D_O for AHL resp. O_2).

The ATP consumption due to oxygen consumption by luciferase is assumed to be proportional to

$$\rho(x) \frac{O^2 K_{\text{cat},2}}{O^2 + K_{m,2}^2} \frac{A^n}{A^n + A_\tau^n}$$

As a proof of principle the model outcome indicated that by controlling luciferase reaction via autoinducer the cells might be able to optimize efficiency of the reaction for O_2 removal even under current environmental O_2 conditions (Fig. 5.3). This optimization effect is also true under other conditions, e.g. in semi-confined space (cave with limited access) where mass transfer limitations exists.

The concentrations of O_2 and AHL depend in a similar way on colony size (i.e. cell number), cell respectively colony distribution and mass transfer limitations. Exemplarily, both the O_2 depletion and the AHL accumulation towards the centre of a colony become stronger in a correlated way with increasing colony size.

Hence, AHL seems to be a rather reliable predictor for the achievable reduction of the O_2 concentration. It can be used as a control for the efficiency of luciferase with respect to O_2 removal. As an increasing AHL concentration is connected to a larger achievable reduction of the O_2 concentration, AHL acts here as an inverse indicator (or proxy) for the reachable O_2 concentration.

As shown by this example, the prediction of the efficiency of a target activity is thus not limited to released public goods, but can also be employed for other behaviours. As long as the efficiency of the target behaviour can be predicted by the environmental pattern of the AI concentration, i.e. as long as AIs can be used as proxies (or inverse proxies), employing them for target gene regulation enables the cells to save costs.

5.4 Integration of Stress Responses in AI Regulation and Its Purpose?

Most interpretations of AI systems base on the assumption that QS active cells constitutively produce AIs at a constant low basic rate, and that in case of positive feedbacks the induced cells produce AIs with a second, increased production rate. It is assumed that this sufficiently reflects the scenario of homogeneously mixed plankton population under constant environmental conditions, e.g. in a chemostat which has reached its equilibrium state. Some biofilm models include terms for the dependency of AI production on nutrient concentration, connecting a lower AI production rate/cell to lower nutrient conditions [16, 42, 43].

However, there is increasing evidence that AI systems' activities are under direct or indirect control of a number of environmental and physiological factors. Exemplarily, AI systems often regulate responses to starvation [44–47]. In the present section, we try to understand the ecological benefit of that fact. We start off with discussing some characteristics of the dependency of QS on nutrient concentration. Then, we identify situation where this control rules central aspects of bacterial communities, and situations where this nutrient-dependency may only play a minor role. These considerations give an input for the discussion of the purpose of this dependency in the third part of the section.

5.4.1 Characteristics of the Control

The still few existing quantitative experimental analyses suggest non-linear or even non-monotonous relations between activity of AI systems and degree of starvation [7, 48]. In *V. fischeri*, at least in certain nutrient concentration range, nutrient deficiency promotes AI activity (Fig. 5.4). Only at severe starvation AI production finally abolishes [7]. Such a regulation design reminds to the stress

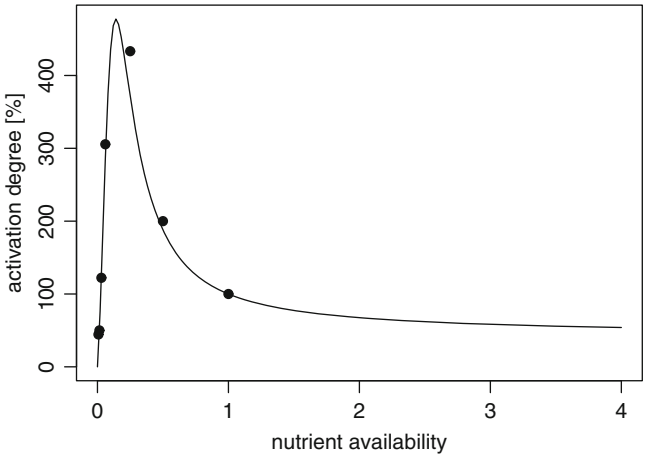

Fig. 5.4 Fit of modulation of the AHL system by nutrient availability. *Dots* are data from [7], *the solid line* indicates the fit. Activation degree denotes the relative autoinducer production: production rate with standard medium was set to 100 %. Nutrient availability: dilution of standard medium. The figure was taken from [49]. For more details see there

gradient hypothesis developed mainly in plant ecology, which suggests that certain facilitative interactions, at least under some environmental conditions, are promoted by the presence of mild stress [50].

5.4.2 Nutrient Control in Different Situations

In homogeneously mixed plankton, all cells experience the same nutrient concentration and the same AI concentration. That is, modifying the AI production rate by nutrient does not add new information about the cells' environment. (Note that this does not rule out the possibility that other reasons support the utility of such a regulation architecture under planktonic conditions). This is different in systems, where physico-chemical gradients may evolve. In this case, some cells may starve while others do not, and it may be useful for the total population to communicate this situation to all bacteria. Typical scenarios for spatially structured populations are microcolonies and biofilms. Most bacterial cells live under such conditions.

In order to investigate the consequences of spatial structure superimposed by microcolonies, a model (similar to the model in the section before) has been developed [49]. The parameters used are based on quantitative data for nutrient concentration/AI production relationship in a QS system of *V. fischeri* [7]. Basically it assumes that the AI production is not only influenced by AI itself, but additionally by the nutrient concentration.

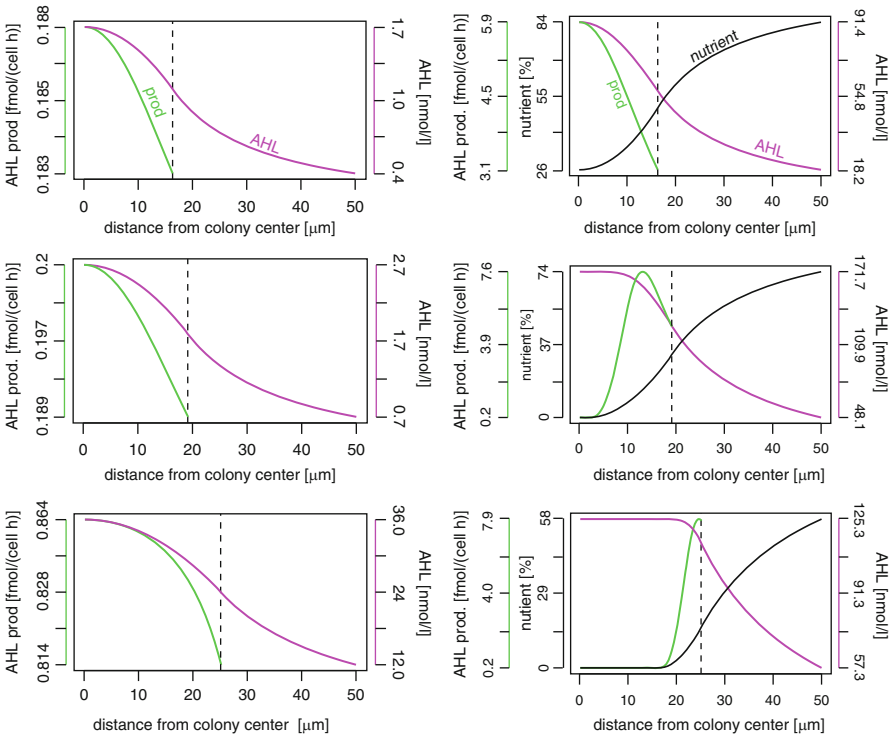

Fig. 5.5 Profiles of autoinducer production (*green curve*), autoinducer concentration (*magenta curve*) and nutrient concentration (*black curve*) in colonies of different sizes (*vertical line*); *left*: without nutrient influence, *right*: with nutrient influence. The figure was taken from [49]. For more details see there

The outcome of this model was that nutrient influence increases the spatial complexity of AI activity within the colony. Especially, the area of maximum AI activity, e.g. of the AI production rate, shifts between the centre of the colony and its outer edge depending on the colony size, the nutrient concentration in the bulk fluid, and the emerging nutrient gradient within the colony (Fig. 5.5). In contrast, AI models without nutrient effects usually lead to an almost synchronous up-regulation of the complete colony (or for certain rather artificial parameter sets the colony is up-regulated in its centre first, depending on, for example, the strength of the positive feedback). In extreme cases, not only small colonies consisting of only non-induced cells, but also a very large colony size could result in a down-regulation of the AI system (due to severe nutrient starvation). Note that the maximum AI concentration itself is almost always found in the colony centre, also with nutrient influence, although the AI production rate may be not due to too severe starvation (see Fig. 5.4). Only scenarios with large AI degradation rates and/or low diffusion rates could change this.

The reason for the increased spatial complexity is that the nutrient depletion naturally starts at the centre of the colony, i.e. we have two overlying spatial gradients of AHL and nutrients in the colony, both affecting AI activity.

Note that the spatial gradients of the chemical, e.g. nutrient conditions in colonies may be reflected by temporal changes in batch culture experiments. The relative relevance of cell density compared with the relevance of chemical conditions for the observed induction under batch culture conditions is widely unknown, but the necessarily artificial experimental setup in batch cultures most likely leads to effects (as transition from rich nutrient to nutrient depletion) that mimic spatial gradients. Probably, this effect affects interpretation of experimental results. Conversely, AI-controlled temporal dynamics of gene expression patterns found in batch cultures [24] may occur in nature rather at least partly as spatial patterns in colonies/biofilms, which often represent more realistic growth scenarios.

Thus relation between AI signalling and outcome can be variable and counter-intuitive. One example presents a dilution event such as a rainfall, which decreases both cell density and nutrients concentration and thus could result in an induction or de-induction of the AI system (depending on whether cell density or nutrient effect dominates). The scenario is further complicated as nutrients are not the only environmental aspects that have an impact on AI systems [51].

5.4.3 Ecological Rationale

The question emerges, what receiving cells can learn from such variable signalling, i.e. what is the ecological benefit of it.

Referring to the terminology in industrial production processes, we have proposed the term "hybrid push/pull control" for this kind of regulation [49, 52]. We can understand push and pull as follows.

AI systems are mainly considered to be sampling the local environment, including the cells living there, for its suitability with respect to attainable effect of the regulated phenotype, e.g. for the influencing factors cell density, distribution and mass transfer properties. These external factors determine the potential strength of the coordinated target activity and could be regarded as *push* factors ("Do it, when your activity can reach a certain vigour" or "Do it, when you can do it").

However, when environmental stress and hence, the physiological state of the cell, directly controls the activity of AI systems, the amount of released AI can be connected to the demand of the cell for the target activity. As an example, AIs, which often control stress responses, are up-regulated by, e.g. nutritional stress [53]. Indicators of opportunities can also upregulate AI production, e.g. the host stress hormone epinephrine promotes AI-controlled virulence in the opportunistic pathogen *Pseudomonas aeruginosa* [54]. Other examples are certain plant produced flavonoids and opines, which affect AI systems in plant associated bacteria and thereby seem to promote development of symbiosis [55, 56]. Interlinking the

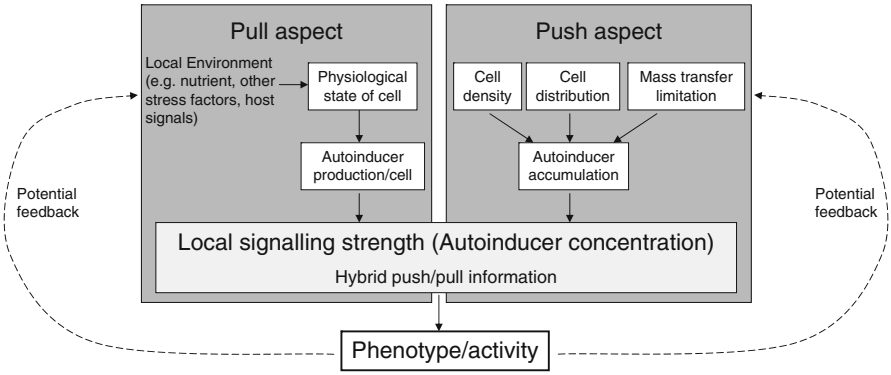

Fig. 5.6 Scheme of the push/pull regulation. Autoinducer regulation systems integrate information affecting the cells demand (*pull aspect*) with those about the potential cooperative strength of the regulated activity (*push aspect*; dependent on cell density, cell distribution and mass transfer limitations) into local autoinducer concentration. The regulated phenotype can influence both the pull aspect (e.g. if the availability of nutrients is increased by exoenzymes) and the push aspect (e.g. if a changed migratory behaviour influences the cell density or distribution). The figure was taken from [49]

cell's need, its internal ability and/or the opportunity for the target phenotype with the AI production rate adds an internal demand or *pull* aspect to AI system ("Do it, when you want/need it—and ask others to give you a hand".)

Thus, environmental AI concentration sensed by the receptor cell carries integrated hybrid information about independent pull and push factors (Fig. 5.6). Note that there is a difference between "push" and "pull". While the push aspect works effectively for isolated single cells as well as for populations as microcolonies [20], this is not the case for the pull aspect. Here, in microcolonies some cells (that do not starve in the example above) may be directed into the activation of a phenotype that is not directly beneficial for themselves but for the population. In the example of bioluminescing *V. fischeri*, this concerns the outer ring of cells, the induction of which is promoted by the high AHL production of starving cells in the centre of the colony, but which are themselves only to a limited degree protected from toxic effects of oxygen, as there is still a certain oxygen concentration in their environment, whereas towards the colony centre the substance depletes [49]. Such self-sacrifice is not uncommon in cooperating groups and can be explained in terms of kin or group selection [10, 11, 57, 58]. Thus, the pull aspect is strongly connected to cooperation. To explain the same aspect from information perspective: for a single cell in a confined space, integration of nutrient restriction resp. intracellular starvation signals in the up-regulation of AI production does not supply the cell with new information about its environment.

AI systems integrate pull and push information and transform them into the local AI concentration. Which aspect dominates depends on the regulation architecture and the actual environmental and cellular conditions. Consequently, interpreting the function of AI systems allowing mainly for a cell density dependent gene regulation, only modified/modulated by additional factors, seems inadequate.

As all of these pull and push factors influence the cost-effectivity of the regulated activity on the population level (and indirectly also for single cells—although some of them may sacrifice themselves), we hypothesize that the "core" purpose of this regulation systems is to promote a gene control based on pre-assessment of the efficiency of the target gene resp. target behaviour.

The integrated information may be an explanation for the existence of multiple AI systems in the same species: Assume that each AI system is responsive to a different combination of environmental or physiological factors which may vary over time. Then the environmental concentration of different AIs released and sensed by each cell at a certain time carries different pull information, although the push information may be largely identical. Multiple AI systems allow a sophisticated regulation of different targets genes, whose efficiency and thus benefit may depend on different pull aspects.

Regulating the AI system itself by an up-regulation, instead of directly the target genes, allows each unit (cell) to send pull information, varying spatio-temporally within the colony. Sensing the combined pull/push information carried by the AIs enables each cell to a contextual interpretation of the state of the neighbouring cells relative to its own state and of the push factors [59]. This results in an adaptive behaviour of cells within the colony, highly dynamic in space and time. Cooperativity and division of work can emerge, the flexibility of which goes beyond those of real multicellular organisms, as depending, e.g. on changing environmental conditions and colony size the function of each cell as well as the spatial organization of the whole colony adaptively changes. This remarkable phenotypic plasticity enables an adaptive life style optimization of the entire colony under the actual current conditions with respect to the fitness.

Generally, the relation between the localization of a cell within a colony and its AI activity is governed by several aspects, e.g. the target of nutrient influence (i.e. the AI synthase or AI receptor), the shape of the correlation function between different nutrients and the AI activity, flow and diffusion properties of the bulk matrix, the nutrient concentration in the matrix and the colony size. Thus, it varies between different AI systems, and even within one species if different culture media are used. This may help to understand the variation of areas showing the first/strongest AI activity between species as well as conflicting experimental results for one species in different media (*Pseudomonas aeruginosa*) [60–62]. Indeed for *P. aeruginosa* a nutrient influence on AI regulation was experimentally shown [48].

For *V. fischeri*, the system can result in spatial distinction between cells strongly promoting cooperative activity (represented by high AI production) and those which are asked to do it (exposed to high AI concentration).

Interestingly, in mixed planktonic populations, i.e. where spatial gradients of pull aspect are absent pull aspects may be largely identical for all cells, thus from this point of view sending pull information by increased AI production seems a waste of costs. However, this argument does not hold if, e.g. multiple subpopulations with different functions and thus potentially different pull strength exist.

5.5 Relevance of Locality

Based on results from batch cultures it has been assumed that AIs are intended for communication on the level of a whole population, i.e. all cells within the population talk and listen simultaneously to each other. However, especially models of spatially heterogeneously structured populations, i.e. microcolonies or biofilms have challenged this view [20, 42, 49]. Communication seems to be stronger for cells within rather than between cell clusters. The existence of flow in the bulk fluid probably strengthens this restriction as shown in a modelling study [63]. Such a (partial) restriction of AI regulated cooperation to colonies also supports the evolutionary stability against cheater mutants, which do not contribute to cooperation and thus safe resources, but benefit from the cooperation of the others [64]. Fluctuating transitions through bottlenecks in transiently isolated subpopulations, as, e.g. in new colonies emerging from single attached cells, can prevent an outcompeting of the honest cells by cheaters [65]. Although to our knowledge not yet investigated explicitly in laboratory experiments, some results indirectly support the idea that AI based communication is in some cases at least partly restricted to subpopulations, i.e. within colonies [19].

As direct chemical measurements of AI distribution patterns in such microstructured populations are difficult to conduct, we choose a model approach.

The model describes the situation of (small) bacterial colonies on a flat, non-diffusible surface. The bacteria are assumed to live in a biofilm/mucus layer of a certain thickness. We use a deterministic model which combines AI production in the cells, abiotic degradation of AI and diffusion (in the cells and the extracellular medium) in form of a reaction–diffusion equation. It is in some sense a simplified version of a model approach first introduced in Müller et al. [66]. The variable u (dependent on time t and spatial position x) describes the concentration of AI. The reaction–diffusion equation is formulated as follows:

$$\frac{\partial u\,(x,t)}{\partial t} = D_{\mathrm{AI}} \Delta u\,(x,t) - \gamma u\,(x,t) + \sum_{i=1}^{N} f_{\mathrm{AI}}\,(u\,(x,t))\,\chi_{|x-x_i|<R}$$

for $x \in \Omega$, where x_i describes the position of cell i, R the radius of the cells, γ the abiotic degradation rate of AI and D_{AI} the diffusion rate of AI.

The production only takes place where bacterial cells are localized, which is modelled by the so-called characteristic function $\chi_{|x-x_i|<R}$. It assumes the value 1 inside the cells and 0 everywhere else. The strength of the production is described by the function f_{AI} and includes the typical positive feedback loop:

$$f_{\mathrm{AI}}\,(u\,(x,t)) = \alpha_{\mathrm{AI}} + \frac{\beta_{\mathrm{AI}} u(x,t)^n}{u_{\mathrm{thresh}}^n + u(x,t)^n}.$$

α_{AI} denotes the non-induced and β_{AI} the induced AI production rate; u_{thresh} describes the threshold AI concentration for induction. In general, we use n as the

Table 5.1 Parameter values used for simulations in Fig. 5.7

Parameter	Value	Meaning	Source
D_{AI}	3,232,542 μm/h	Diffusion rate AHL in water	[76]
α_{AI}	$2.3*10^{-19}$ mol/(cell*h)	Non-induced production rate of AHL	[67]
β_{AI}	$2.3*10^{-18}$ mol/(cell*h)	Induced production rate of AHL	[67]
μ_{thresh}	$70*10^{-9}$ mol/L	Threshold of AHL concentration between low and increased activity (or between non-induced and induced)	[67]
n	2.5	Hill factor; polymerization degree	[67]
γ	0.00427	Abiotic degradation rate of AHL	[68]

degree of receptor multimerization; for the simulation it is usually used for dimers, i.e. $n = 2$. We neglect cell division in order to keep the model as simple as possible.

Examplarily, we consider a squared region with edges of length 1,000 μm with homogeneous Dirichlet boundary conditions, which means

$$u(x,t) = 0 \quad \text{for} \quad x \in \partial\Omega$$

From a biological point of view, this means that all AI molecules arriving at the boundary (e.g. via diffusion) are lost for the system. By using these boundary conditions, we underestimate the accumulating AI, however, as the region is chosen quite large compared to the size of a bacterium, it might play a minor role.

Parameter values used in the simulations are given in Table 5.1.

The simulations start with the initial condition

$$u(x,0) = 0 \quad \text{for} \quad x \in \Omega$$

i.e. with a newly colonized region without any already accumulated AI.

All simulations assume 100 cells on a flat square of $1{,}000 \times 1{,}000$ μm^2, located (a) in just one central colony, (b) in four colonies, each of them containing 25 cells and (c) in 25 microcolonies, each consisting of only four cells, spread on the given surface. The simulations run until the AI level has approximately reached equilibrium level. The simulation showed strong spatial differences of AI concentration (Fig. 5.7), which can be considered quantitatively with this simple modelling and simulation approach. The strength of these differences depends on the inhomogeneity of cell resp. colony distribution, but also on factors as diffusion rates and flow conditions, and the strength of positive feedback loop. The same factors influenced the maximum AI concentration, e.g. the more "colonised" the cells are, the higher AI concentrations they can accumulate, even though the total number of cells in the region of interest is kept constant.

Summarized, within spatially structured populations strong gradients of AI can arise, promoting differences in activities of AI-controlled genes between neighboured colonies. The degree of isolation of communication depends on the

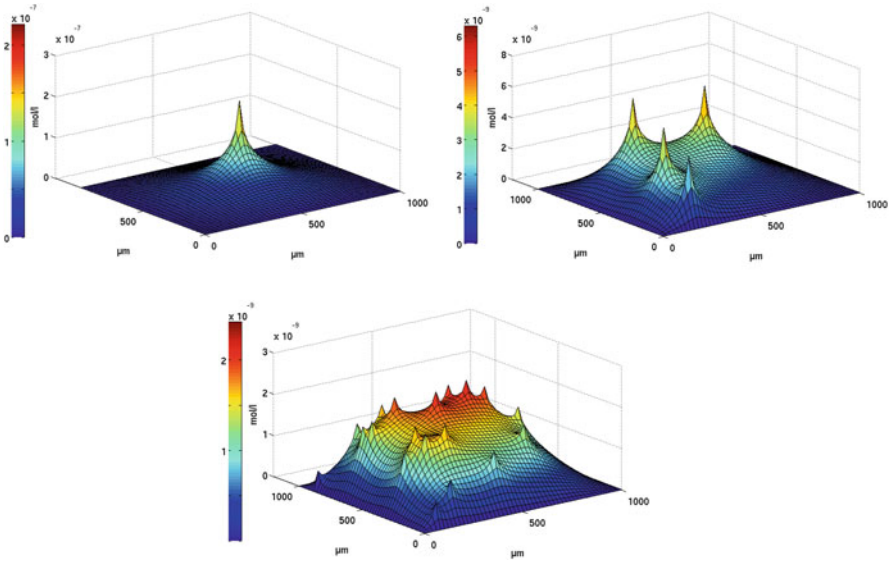

Fig. 5.7 Distribution pattern of AI concentration for a population of 25 cells growing in a single colony (*upper left graphics*), 4 colonies of 25 cells each (*upper right*) and 25 colonies of 4 cells each (*lower*). The colonies are located below the peaks

conditions in the cells environment. It is strengthened by, e.g. distance between colonies, by flow conditions (washing AI between colonies away) or low diffusion rates within the matrix between cells/colonies (keeping the AI next to the colonies and thus promoting high local AI concentrations peaks). In fact, a limitation of between-colony communication via AI was indicated by Meyer et al. [19], which conducted a combined experimental and modelling study with *Pseudomonas putida* IsoF. As the authors discussed, it could be evolutionary beneficial for colonies to limit—or even interrupt—cooperation with neighbouring, potentially non-related colonies competing, e.g. for nutrients, even if they belong to the same species/strain. They speculate that AI degrading enzymes which are possibly released by an AI active species might be connected with such a function.

The high localization of AI peaks in spatially structured populations (partly) explains confusing results of AI relevance of bacteria associated with human (or other) hosts. Many human pathogens are known to employ AI systems, usually connected with virulence control [2]. Thus, understanding the functionality of AI systems in these species is of high relevance, e.g. for the development of new anti-pathogen treatment strategies [69]. A number of studies describe effects of certain AHLs on cells of the human immune system or other tissues [70]. Surprisingly, almost all of these effects occur at AHL concentrations in the micromolar range, whereas most AHL systems become induced in nM range in the bacteria themselves. AHL concentrations up to >600 µm have been reported in in vitro biofilms. However, such high values are almost never measured in human or mouse samples,

e.g. of lung or gastrointestinal tract, although AHL producing bacteria are known to occur there, and AI regulated activities are of relevance in this habitat, e.g. often such connected with virulence [71, 72]. AHLs are even hardly ever detected at all in, e.g. gut samples [73]. How can these contradictions be solved?

AHL producing bacteria tend to live in colonies in their host, and often the environment matrix has a lower diffusion rate compared to water (see, e.g. [28, 74, 75]). This applies, e.g. in mucus of gut or lung epithets, but also in the gut lumen. Patients with cystic fibrosis, which produce mucus with significantly higher viscosity, are especially prone to pathogenic infections with the AHL producing *P. aeruginosa*.

The seemingly contradictory results are at least partly explainable by the fact that mostly the samples for chemical analyses are taken in volume ranges of milliliters. Furthermore, the original matrix often was mixed before sampling, which destroyed the original spatial structure, e.g. in sputum. With respect to our model results, such an averaging of spatial structures necessarily leads to a strong underestimation of the achieved local AI concentration maxima. Furthermore, it also can lead to an underestimation of the involved local amount of cells, e.g. in colonies. For a real estimation of cell and AHL pattern and—connected with that—for the development of treatment strategies, new analytical methods allowing high spatially resolution on microscale are required.

5.6 Conclusions

Based on a combination of modelling and experimental data, we discussed that the purpose of bacterial autoinducer systems is the cost-benefit optimization of the efficiency of regulated target behaviour. We showed that this concept works for releases of effectors, but also for intracellular enzymatic activities, as long as the efficiency of the target behaviour can be predicted by the environmental pattern of the AI concentration. Beyond pure cell density measurement, this efficiency is also affected by cell distribution and mass transfer properties of the matrix,

Furthermore, environmental and cellular factors directly influence activity of AI systems. This hybrid push/pull control ensures for each cell a contextual adaptation to the conditions to which the cell itself and the neighbour cells are exposed. These systems are able to integrate a range of environmental information into a consistent picture that guides the decision for the optimal life style, where the word “optimal” has to be interpreted with caution and only relates to a given situation.

The integration of push as well as of pull factors into AI-controlled decisions impedes interpretations of experimental results. Exemplarily, in batch cultures not only the cell density, but almost certainly (but usually not experimentally analysed) relevant pull factors change over time. In other words, in batch cultures with relatively low growth rate, but relevant shifts in the environmental conditions due to bacterial metabolic activity, AI systems probably rather function as nutrient (or chemical environment) sensing than as quorum sensing.

We argue that cell-to-cell communication may often/usually rather occur on local (micro-)scale than on global (macro-) scale level. This has impact on the discussion about evolutionary stability of QS regulated cooperation. Furthermore, the analytical methods for detection of, e.g. autoinducers or autoinducer regulated gene products need to be adjusted adequately, e.g. by very high spatial resolution.

Acknowledgment We thank Martin Schuster for the fruitful discussion of our article.

References

1. Valle A, Bailey MJ, Whiteley AS, Manefield M (2004) *N*-acyl-L-homoserine lactones (AHLs) affect microbial community composition and function in activated sludge. Environ Microbiol 6:424–433
2. Antunes LCM, Ferreira RBR, Buckner MMC, Finlay BB (2010) Quorum sensing in bacterial virulence. Microbiology 156:2271–2282
3. De Clippeleir H, Defoirdt T, Vanhaecke L, Vlaeminck SE, Carballa M, Verstraete W, Bonn N (2011) Long-chain acylhomoserine lactones increase the anoxic ammonium oxidation rate in an OLAND biofilm. Appl Microbiol Biotechnol 90:1511–1519
4. Shrout JD, Nerenberg R (2012) Monitoring bacterial twitter: Does quorum sensing determine the behaviour of water and wastewater treatment biofilms? Environ Sci Technol 46:1995–2005
5. Atkinson S, Williams P (2009) Quorum sensing and social networking in the microbial world. J R Soc Interface 6:959–978
6. Goryachev AB (2009) Design principles of the bacterial quorum sensing gene networks. WIREs Syst Biol Med 1:45–60
7. Ulitzur S (1989) The regulatory control of the bacterial luminescence system—a new view. J Biolumin Chemilumin 4:317–325
8. Goryachev AB (2011) Understanding bacterial cell–cell communication with computational modeling. Chem Rev 111:238–250
9. Winzer K, Hardie KR, Williams P (2002) Bacterial cell-to-cell communication: sorry, can't talk now—gone to lunch! Curr Opin Microbiol 5:216–222
10. Diggle SP, Gardner A, West S, Griffin AS (2007) Evolutionary theory of bacterial quorum sensing: when is a signal not a signal? Phil Trans R Soc Lond B 362:1241–1249
11. Diggle SP, Griffin AS, Campbell GS, West SA (2007) Cooperation and conflict in quorum-sensing bacterial populations. Nature 450:411–414
12. Miller MB, Bassler BL (2001) Quorum sensing in bacteria. Annu Rev Microbiol 55:165–199
13. Whitehead NA, Barnard AML, Slater H, Simpson NJL, Salmond GPC (2001) Quorum-sensing in gram-negative bacteria. FEMS Microbiol Rev 25:65–404
14. Platt TG, Fuqua C (2010) What's in a name? The semantics of quorum sensing. Trends Microbiol 18:383–387
15. Shompole S, Henon KT, Liou LE, Dziewanowska K, Bohach GA, Bayles KW (2003) Biphasic intracellular expression of *Staphylococcus aureus* virulence factors and evidence for Agr-mediated diffusion sensing. Mol Microbiol 49:919–927
16. Kirisits MJ, Margolis JJ, Purevdorj-Gage BL, Vaughan B, Chopp DL, Stoodley P, Parsek MR (2007) Influence of the hydrodynamic environment on quorum sensing in *Pseudomonas aeruginosa* biofilms. J Bacteriol 189:8357–8360
17. Dulla G, Lindow SE (2008) Quorum size of *Pseudomonas syringae* is small and dictated by water availability on the leaf surface. Proc Natl Acad Sci U S A 105:3082–3087
18. Carnes EC, Lopez DM, Donegan NP, Cheung A, Gresham H, Timmins GS, Brinker CJ (2010) Confinement-induced quorum sensing of individual *Staphylococcus aureus* bacteria. Nat Chem Biol 6:41–45

19. Meyer A, Megerle JA, Kuttler C, Müller J, Aguilar C, Eberl L, Hense BA, Rädler JO (2012) Dynamics of AHL mediated quorum sensing under flow and non-flow conditions. Phys Biol 9:026007. doi:10.1088/1478-3975/9/2/026007
20. Hense BA, Kuttler C, Müller J, Rothballer M, Hartmann A, Kreft J-U (2007) Does efficiency sensing unify diffusion and quorum sensing? Nat Rev Microbiol 5:230–239
21. Connell JL, Wessel AK, Parsek MR, Ellington AD, Whiteley M, Shear JB (2010) Probing prokaryotic social behaviors with bacterial "lobster traps". MBIO 1:e00202–e00210. doi:10.1128/mBio.00202-10
22. Whitaker RD, Pember S, Wallace BC, Brodley CE, Walt DR (2011) Single cell time-resolved quorum responses reveal dependence on cell density and configuration. J Biol Chem 286:21623–21632
23. Alberghini S, Polone E, Corich V, Carlot M, Seno F, Trovato A, Squartini A (2009) Consequences of relative cellular positioning on quorum sensing and bacterial cell-to-cell communication. FEMS Microbial Lett 292:149–161
24. Schuster M, Lostroh CP, Ogi T, Greenberg EP (2003) Identification, timing, and signal specifity of *Pseudomonas aeruginosa* quorum-controlled genes: a transcriptome analysis. J Bacteriol 185:2066–2079
25. Willcox MDP, Zhu H, Conibear TCR, Hume EBH, Givskov M, Kjelleberg S, Rice SA (2008) Role of quorum sensing by *Pseudomonas aeruginosa* in microbial keratitis and cystic fibrosis. Microbiology 154:2184–2194
26. Coggan KA, Wolfgang MC (2012) Global regulatory pathways and cross-talk control *Pseudomonas aeruginosa* environmental lifestyle and virulence phenotype. Curr Issues Mol Biol 14:47–69
27. Suppiger A, Schmid N, Aguilar C, Pessi G, Eberl L (2013) Two quorum sensing systems control biofilm formation and virulence in members of the *Burkholderia cepacia* complex. Virulence 4:400–409
28. Hassett DJ, Ma JF, Elkins JG, Ochsner UA, West SEH, Huang C-T (1999) Control of catalase and superoxide dismutase by quorum sensing in *Pseudomonas aeruginosa*: catalase is important is resistance of biofilm organisms to hydrogen peroxide. Mol Microbiol 34:1082–1093
29. Pontes MH, Babst MH, Lochhead R, Oakeson K, Smith K, Dale C (2008) Quorum sensing primes the oxidative stress response in the insect endosymbiont, *Sodalis glossinidius*. PLoS One 3:e3541
30. Studer SV, Mandel MJ, Ruby EG (2008) AinS quorum sensing regulates the *Vibrio fischeri* acetate switch. J Bacteriol 190:5915–5923
31. Pierson LS III, Pierson EA (2010) Metabolism and function of phenazines in bacteria: impacts on the behaviour of bacteria in the environment and biotechnological processes. Appl Microbiol Biotechnol 86:1659–1670
32. Poinar GO, Thomas G, Haygood M, Nealson KH (1980) Growth and luminescence of the symbiotic bacteria associated with the terrestrial nematode, *Heterorhabditis bacteriophora*. Soil Biol Biochem 12:5–10
33. Diggles BK, Moss MA, Carson J, Anderson CD (2000) Luminous vibriosis in rock lobster *Jasus verreauxi* (Decapoda: Palinuridae) phyllosoma larvae associated with infection by *Vibrio harveyi*. Dis Aquat Organ 43:127–137
34. Dunlap PV, Kita-Tsukamoto K (2006) Luminous bacteria, 3rd ed., vol 2, The prokaryotes: a handbook on the biology of bacteria. Springer, New York, pp 863–892. doi:10.1007/0-387-30742-7_27
35. Krin E, Chakroun N, Turlin E, Givaudan A, Gaboriau F, Bonne I et al (2006) Pleiotropic role of quorum-sensing autoinducer AI-2 in *Photorhabdus luminescens*. Appl Environ Microbiol 72:6439–6451
36. Münch A, Stingl L, Jung K, Heermann R (2008) *Photorhabdus luminescens* genes induced upon insect infection. BMC Genomics 9:1–17
37. McElroy WD, Seliger HH (1962) Origin and evolution of bioluminescence. In: Kasha M, Pullman B (eds) Horizons in biochemistry. Academic, New York, pp 91–101

38. Timmins GS, Jackson SK, Swartz HM (2001) The evolution of bioluminescent oxygen consumption as an ancient oxygen detoxification mechanism. J Mol Evol 52:321–332
39. Szpilewska H, Czyz A, Wegrzyn G (2003) Experimental evidence for the physiological role of bacterial luciferase in the protection of cells against oxidative stress. Curr Microbiol 47: 379–382
40. Lyzen R, Wegrzyn G (2005) Sensitivity of dark mutants of various strains of luminescent bacteria to reactive oxygen species. Arch Microbiol 183:203–208
41. Müller J, Hense BA. Efficiency sensing of colonies and environmental engineering, in preparation
42. Chopp D, Kiritis M, Moran B, Parsek M (2002) A mathematical model of quorum sensing in a growing bacterial biofilm. J Ind Microbiol Biotechnol 29:339–346
43. Goryachev A, Toh D, Wee K, Lee T, Zhang H, Zhang L (2005) Transition to quorum sensing in an *Agrobacterium* population: a stochastic model. PLoS Comput Biol 1:45–60. doi:10.1371/journal.pcbi.0010037
44. Ulitzur S, Dunlap PV (1995) Regulatory circuitry controlling luminescence autoinduction in *Vibrio fischeri*. Photochem Photobiol 62:625–632
45. Dunlap PV (1999) Quorum regulation of bioluminescence in *Vibrio fischeri*. J Mol Microbiol Biotechnol 1:5–12
46. Chatterjee J, Miyamoto CM, Zouzoulas A, Lang BF, Skouris N, Meighen EA (2002) MetR and CRP bind to *Vibrio harveyi lux* promotors and regulate luminescence. Mol Microbiol 46: 101–111
47. De Lay N, Gottesman S (2009) The Crp-activated small noncoding regulatory RNA CyaR (RyeE) links nutritional status to group behaviour. J Bacteriol 191:461–476
48. Mellbye B, Schuster M (2014) A physiological framework for the regulation of quorum-sensing-dependent public goods in *Pseudomonas aeruginosa*. J Bacteriol 196:1155–1164
49. Hense BA, Müller J, Kuttler C, Hartmann A (2012) Spatial heterogeneity of autoinducer regulation systems. Sensors 12:4156–4171
50. Holmgren M, Schefer M (2010) Strong facilitation in mild environments: the stress gradient hypothesis revisited. J Ecol 98:1269–1275
51. Boyer M, Wisniewski-Dye F (2009) Cell-cell signalling in bacteria: not simply a matter of quorum. FEMS Micobiol Ecol 70:1–19
52. Olhager J, Östlund B (2009) An integrated push–pull manufacturing strategy. Eur J Oper Res 45:135–142
53. Van Delden C, Comte R, Bally M (2001) Stringent response activates quorum sensing and modulates cell density dependent gene expression in *Pseudomonas aeruginosa*. J Bacteriol 183:5376–6384
54. Hedge M, Wood TK, Jayaraman A (2009) The neuroendocrine hormone norepinephrine increases *Pseudomonas aeruginosa* PA14 virulence through the las quorum sensing pathway. Appl Microbiol Biotechnol 84:763–776
55. Newton JA, Fray RG (2004) Integration of environmental and host-derived signals with quorum sensing during plant-microbe interactions. Cell Microbiol 6:213–224
56. Perez-Montano F, Guasch-Vidal B, Gonzalez-Barroso S, Lopez-Baena FJ, Cubo T, Ollero FJ, Gil-Serrano AM, Rodriguez-Carvajal MA, Bellogin RA, Espuny MR (2011) Nodulation-gene-inducing flavonoids increase overall production of autoinducers and expression of *N*-acyl homoserine lactone synthesis genes in rhizobia. Res Microbiol 164:749–760
57. Kaiser D (1986) Control of multicellular development: *Dictyostelium* and *Myxococcus*. Ann Rev Genet 20:539–566
58. Kreft JU (2004) Conflicts of interest in biofilms. Biofilms 1:265–276
59. Jacob E, Shapira Y, Tauber A (2006) Seeking the foundations of cognition in bacteria: from Schroedinger's negative entropy to latent information. Physica A 369:495–524

60. De Kievit T, Gillis R, Marx S, Brown C, Iglewski B (2001) Quorum sensing genes in *Pseudomonas aeruginosa* biofilms: their role and expression patterns. Appl Environ Microbiol 67:1865–1873
61. Lenz A, Williamson K, Pitts B, Stewart P, Franklin M (2008) Localized gene expression in *Pseudomonas aeruginosa* biofilms. Appl Environ Microbiol 74:4463–4471
62. Perez-Osorio A, Williamson K, Franklin M (2010) Heterogeneous rpoS and rhlR mRNA levels and 16S rRNA/rDNA (rRNA gene) ratios within *Pseudomonas aeruginosa* biofilms, sampled by laser capture microdissection. J Bacteriol 192:2991–3000
63. Uecker H, Mueller J, Hense BA (2014) Individual-based model for quorum sensing with background flow. Bull Math Biol. doi:10.1007/s11538-014-9974-2
64. Drescher K, Nadell CD, Stone HA, Wingreen NS, Bassler BL (2014) Solutions to the public goods dilemma in bacterial biofilms. Curr Biol 24:50–55
65. Chuang JS, Rivoire O, Leibler S (2009) Simpson's paradox in a synthetic microbial system. Science 323:272–275
66. Müller J, Kuttler C, Hense BA, Rothballer M, Hartmann A (2006) Cell–cell communication by quorum sensing and dimension–reduction. J Math Biol 53:672–702
67. Fekete A, Kuttler C, Rothballer M, Hense BA, Fischer D, Buddrus-Schiemann K, Lucio M, Müller J, Schmitt-Kopplin P, Hartmann A (2010) Dynamic regulation of *N*-acyl-homoserine lactone production and degradation in *Pseudomonas putida* IsoF. FEMS Microbiol Ecol 72: 22–34
68. Englmann M, Fekete A, Kuttler C, Frommberger M, Li X, Gebefügi I, Fekete J, Schmitt-Kopplin P (2007) The hydrolysis of unsubstituted *N*-acylhomoserine lactones to their homoserine metabolites. Analytical approaches using ultra performance liquid chromatography. J Chromatogr A 1160:184–193
69. LaSarre B, Federle MJ (2013) Exploiting quorum sensing to confuse bacterial pathogens. Microbiol Mol Biol Rev 77:73–111
70. Cooley M, Chhabra SR, Williams P (2008) *N*-acylhomoserine lactone-mediated quorum sensing: a twist in the tail and a blow for host immunity. Chem Biol 15:1141–1147
71. Charlton TS, de Nys R, Netting A, Kumar N, Hentzer M, Givskov M, Kjelleberg S (2000) A novel and sensitive method for the quantification of N-3-oxoacyl homoserine lactones using gas chromatography–mass spectrometry: application to a model bacterial biofilm. Environ Microbiol 2:530–541
72. Bernatowicz R, Binder T, Noessner E, Rothballer M, Perez-Velazquez J, Hense BA, Kuttler C, Griese M, Eickelberg O, Hartmann A, Krauss-Etschmann S. 3oxoC12-Homoserine lactone from *P. aeruginosa* impairs multiple human dendritic cell functions required for priming of T cells. J Immun
73. Swearingen MC, Sabag-Daigle A, Ahmer BMM (2013) Are there acyl-homoserine lactones within mammalian intestines? J Bacteriol 195:173–179
74. Hassett DJ, Sutton MD, Schurr MJ, Herr AB, Caldwell CC, Matu JO (2009) *Pseudomonas aeruginosa* hypoxic or anaerobic biofilm infection within cystic fibrosis airways. Trends Microbiol 17:1130–1138
75. Worlitzsch D, Tarran R, Ulrich M, Schwab U, Cekici A, Meyer KC et al (2002) Effects of reduced mucus oxygen concentration in airway *Pseudomonas* infections of cystic fibrosis patients. J Clin Invest 109:317–325
76. Hobbie, R.K.: Intermediate Physics for Medicine and Biology, 2nd ed. Wiley & Sons, Incorporated, John, 1988, p. 624.
77. Hense, B.A. and Schuster, M.; Unifying principles of microbial autoinducer systems, submitted

Chapter 6
Localization of Quorum Sensing by Extracellular Polymeric Substances (EPS): Considerations of In Situ Signaling

Alan W. Decho

6.1 Overview

Attached bacteria exhibit remarkable capabilities to resist, persist, and adapt to changing environments. A few examples range from the diverse commensal and pathogenic flora exposed to the human immune system and antibiotics, to the changing environmental conditions of hypersaline lakes and oceans. These bacteria can exist as single strains, but most often as multiple species/genera, and form complex and diverse communities [1] having hundreds to thousands of OTUs (i.e., operational taxonomic units or in plainer terms, types of bacteria that can be distinguished from each other using sequencing). Bacteria and other microorganisms release small molecules to the extracellular environment, which under some conditions act as signals, environmental sensors, agonists, or antagonists, and perhaps provide other information to cells.

The process of quorum sensing (QS) is a form of chemical communication, which allows cells in proximity to sense one another, and coordinate group activities, and is used by bacteria in symbioses, infections and virulence, antibiotic production, and biofilm formation [2–6]. It also used for other forms of chemical sensing by cells [7, 8], and has been studied for over three decades since the initial discovery and characterization of an autoinducer signal [9–11]. QS appears to be conducted most efficiently over relatively short distances (e.g., micrometers to tens of micrometers), and is often occur localized within a biofilm, where groups of cells are spatially arranged in proximity in 3-dimensions and enclosed within a matrix of extracellular polymeric substances (or secretions) (EPS) produced by the cells

A.W. Decho (✉)
Microbial Interactions Laboratory, Department of Environmental Health Sciences, Arnold School of Public Health, University of South Carolina, Columbia, SC 29208, USA
e-mail: awdecho@mailbox.sc.edu

S.J. Hagen (ed.), *The Physical Basis of Bacterial Quorum Communication*, Biological and Medical Physics, Biomedical Engineering, DOI 10.1007/978-1-4939-1402-9_6

[12–15]. The EPS matrix can potentially influence the movement and efficiency of signaling within a biofilm.

There are currently many different classes of signal molecules, which are likely just a subset of those utilized by bacteria. Major signal classes include acylhomoserine lactones (AHL), autoinducer-2 (AI2), diffusive signaling factors (DSF), and autoinducing peptides (AIP), and *p*-coumaroyl homoserine lactones and have been reviewed elsewhere [16–19]. Most recently photopyrones have been found in association with insects [20]. In this review, AHLs and their interactions with EPS will be the main focus since they have been the most extensively studied bacterial signals.

6.2 Signal Properties and Diffusion

Diffusion is a critical process driving the movement of small, free molecules (and ions) in water and is the primary process known to influence the movement of most signal molecules between cells. Signaling molecules, such as AHL, occur in a range of molecular sizes, which mostly reflects the number of carbons (e.g., C4–C18) in their acyl chain. Passive or "simple" diffusion of relatively small molecules (e.g., <500 g/mol) in a water medium is most strongly influenced by the spherical diameter (i.e., hydrodynamic radius) of the molecule at a constant temperature in pure water and is best described by Fick's Law [21]. This predicts that in pure water relatively small AHLs (e.g., C4- or C6-AHL) will diffuse more rapidly than a larger AHLs (e.g., C14- or C18-AHL), all else being equal. It was noted by Decho and colleagues [22] that while diffusivities in pure water remain predictable based on molecular size, a complicating issue becomes the relative solubilities (in water) of larger signals. Short-chained AHLs are easily water-soluble while relatively larger signals consisting of longer acyl chains are more hydrophobic; a property that limits their relative solubility. It becomes surprising that relatively long chain AHLs are able to function effectively as signals between cells using a diffusion-mediated transport simply due to solubility issues. However, being less soluble during extracellular transit may offer an additional degree of protection against hydrolyses. With an increase in molecular size, the AHLs present in water become more prone to associate with hydrophobic moieties (e.g., particle surfaces) or organic phases (e.g., during chemical extractions). One result is that as AHLs become larger, they become more "sticky" and tend to partition (in a chromatographic sense) with the stationary phase (e.g., sediment particles, extracellular polymers, or other organics) rather than water (i.e., mobile-phase). Given their structure, a minimum of 99.9 % of AHLs with log $K_{oc} \geq 3$ would be expected to partition into the organic phase. In practical terms, this suggests that the strictly diffusive movement of AHLs having a mw > 350 g/mol (e.g., >C14-AHL) should become negligible.

Assuming simple Newtonian diffusion in water, how far can signals such as AHLs travel and still elicit gene responses by a receptor cell? This was experimentally examined on plant surfaces by Gantner and colleagues [23] using an engineered reporter strain of *Pseudomonas putida* that produces fluorescence (i.e.,

upon excitation by photons) when (i.e., C6–C12) AHL-mediated quorum sensing was occurring. They determined that the majority of cell–cell signaling occurs over relatively short distances, less than 10 micrometers (μm), which they termed the cell–cell "calling distance." They found, however, that AHL signals were able to travel up to 78 μm and still induce quorum sensing as evidenced by fluorescence of the reporter strain.

EPS is considered a highly hydrated matrix. The hydrated properties of many EPS (see below) result from water that is localized in the spaces between individual polymer molecules, rather than "bound" to polymers [24]. Therefore, within a biofilm, solute diffusion occurs through the localized water within the matrix. Interestingly, experimental and theoretical evidence by physicists suggest that free water molecules exist in clusters of five, six, and eight molecules, held together by transient hydrogen bonds, a process which contributes to the unusual temperature-density dependence of water [25, 26]. It follows that in the localized water within a biofilm, diffusion of signals such as AHLs will consist of random movements in between water molecule clusters rather than between individual water molecules.

6.2.1 Measurements of Diffusion Within Biofilms

One assumes that during diffusion (in a biofilm) the solute does not interact with, or sorb to, the matrix polymer molecules (i.e., EPS). Under these conditions, solute molecules should exhibit diffusivities approximating those observed in pure water (i.e., all else the same). However, the EPS consists of polymers that interact to a high degree with each other, and with nearby molecules and ions. Diffusion rates, therefore, will be guided (i.e., slowed) to some degree by interactions with the EPS matrix.

Early speculation was raised in the study of biofilm-based infections, that the EPS matrix prevented antibiotics from reaching pathogenic cells. A large number of studies since have examined the diffusion of antibiotics, metal ions, fluorescent probes, and other molecules into biofilms with varying results [27–37]. Studies have utilized microprobes, fluorescent tracers coupled to confocal microscopy-based measurements such as fluorescence recovery after photobleaching (FRAP), fluorescence correlation spectroscopy (FCS), and fluorescence lifetime imaging microscopy (FLIM). In general, this was found not to be the case. The biofilm matrix does not exclude antibiotics, per se, from entering the matrix and reaching cells, but rather shows differing degrees of diffusion-slowing properties.

A key assumption in all water-based diffusional studies is that the solute whose penetration is being analyzed does not sorb or react with other molecules. In the biofilm, this assumption does not appear to hold. Some results have shown that diffusivities of molecules in biofilms are quite rapid, and in some cases approach those of molecules in free water [28, 38]. For example, the fluorophore Rhodamine B (479.02 Da) diffused into large cell clusters (200–600 μm dia) within a few minutes [33]. Mean diffusion coefficients were calculated to be 3.7×10^{-7} cm^2 s^{-1} or just 11 % of the value in pure water. Fluorescein, a

slightly smaller fluorophore (332.31 g/mol), diffused more rapidly, with a diffusion coefficient = 1.6×10^{-6} cm^2 s^{-1}, or 32 % of the value in water. Waharte and colleagues [39] found differences in diffusion rates of (fluorescent) 150 kDa FITC-dextrans into biofilms from *Lactobacillus lactis* ($D = 10$ μm^2 s) and *Stenotrophomonas maltophila* ($D = 20$ μm^2 s), and attributed this to differences in the spatial architectures of their respective EPS. These studies provided direct confirmation that solutes the size of many antibiotics and biocides can diffuse relatively rapidly into biofilms but are slowed compared to simple diffusion rates calculated for pure water. When several different time-resolved fluorescent approaches (FRAP, FCS, and FLIM) were used in combination [40, 41] additional spatiotemporal resolution was achieved. During these studies it was concluded that a significant portion of vancomycin (approx. 30–50 %) was "sorbed" to biofilm matrix components, even though free vancomycin reached all depths (approx. 30 μm) of the *S. aureus* biofilms. Using FCS in conjunction with fluorescent-nanobeads and -dextrans, diffusion models were developed to show that diffusion-slowing of solutes in biofilms is related to the molecular size and charges of the solute, and its interaction with the EPS matrix [29]. Here, rates were found to be up to 50 times smaller than comparable rates measured in pure water. Together, these studies began to suggest that the EPS matrix is acting as a "membrane" which slows, but does not halt, diffusion of solutes. A complicating factor appears when the solutes being measured are produced and released (from cells) more rapidly than diffusion or other forms of mass transfer can remove them [42]. This results in localized accumulations and sharp gradients of ions, such as O_2, Ca^{2+} and H^+ [38, 43–48].

6.2.2 Is There a Size Limit to Diffusion in a Biofilm?

To examine if diffusion of larger-sized molecules and particles could be stopped by the EPS matrix, nanoparticles were used in conjunction with fluorescent dextrans [49]. Diffusion coefficients of the smallest nanoparticles (<5 nm dia) were 60–80 % of those found in water. For larger particles (>50 nm dia) diffusion was effectively negligible. Diffusion coefficients decreased exponentially with the square of the solute radius. From these and other studies, the model(s) developed to explain diffusion of solutes (including signals) within a biofilm must encompass additional factors, which include interactions of solute with extracellular polymeric substances (EPS), and the sieve or membrane effects of the polymer network.

6.3 The EPS Matrix

The biofilm is a 3D structure of cells and EPS. What is poorly understood and underappreciated at present is how the network of EPS molecules may potentially reduce the 3-D volume for diffusion. Can EPS through its 3D architecture constrain the directions of diffusion, to reduce diffusion to less than 3-dimensions and hasten

the movement of signals? In contrast, can EPS also form "barriers" to diffusion through interactions with the signal, and thus "localize" signal accumulation. This will, in part, depend on the heterogeneity of EPS arrangements at molecular scales.

The EPS matrix that surrounds biofilm cells has been infrequently addressed with regard to quorum sensing. Yet it constitutes the medium through which signal exchange occurs between cells. The relationship between quorum sensing and biofilm formation speaks to the interactive role(s) of both together in facilitating a wide range of bacterial processes [4, 50]. Therefore, the EPS component is central to understanding the physico-chemical movement of signal molecules within a biofilm, yet it is highly diverse in chemical composition, properties, and structure, and likely varies in all of these over the small spatial scales (e.g., micrometers). Information on small-scale variations in EPS, however, is limited. Of importance to the movement of signal molecules, is the ability of the signal (solute) to interact with the EPS molecules.

The EPS matrix consists of polymeric molecules with water-filled pore spaces in between adjacent molecules [51]. Polymers are embedded in a water solvent to form a 3-dimensional hydrogel network, which has microenvironments that are in thermodynamic equilibrium with the surrounding medium [52]. The extracellular matrix is composed of a vast, and sometime very dense, network of interacting molecules, which include polysaccharides, proteins, peptides, extracellular DNA (called *e*DNA), and lipids, but additionally proteoglycans, glycoproteins, lipopolysaccharides, and perhaps even RNA [15, 53, 54] (Fig. 6.1). The matrix results from both active secretion and cellular lysates. The secretions can be metabolic excess by-products (i.e., overabundance of C relative to limiting N, or P). In laboratory cultures this occurs due to excess glucose or some other carbon source being present during stationary phase. It also occurs in natural cells during the later stages of plankton blooms, as a metabolic excess product, where it facilitates the vertical movement of cells to deeper and more nutrient-rich, reaches of the water column. EPS is also secreted purposefully by cells to buffer and even manipulate their immediate extracellular microenvironment. Specific polysaccharides have been isolated from bacteria such as *P. aeruginosa*, which are associated with the structural stability of the greater mucoid colony [55–58].

While extractions and analyses of bulk EPS can contribute important compositional information, these data do not offer insight into the microspatial arrangements of EPS, and hence their physico-chemical functioning at molecular scales. A vast literature exists on the monomeric compositions of bacterial EPS polysaccharides grown under different conditions, and will not be addressed here (for reviews, see [12, 42, 59]). When extracted and dry, EPS consist of long polymeric fibrils that can reach greater than 300 kDa. When in a hydrated state, these same polymers link to form an intricate network. The linkages between adjacent polymers can be the result of covalent bonds, cation (e.g., divalent Ca^{2+}, Mg^{2+} ions) bridges, resulting from dehydration reactions, hydrogen bonds and hydrophobic, electrostatic and Van der waals interactions, London forces, peptide linkages with many of these transient in nature [15, 60].

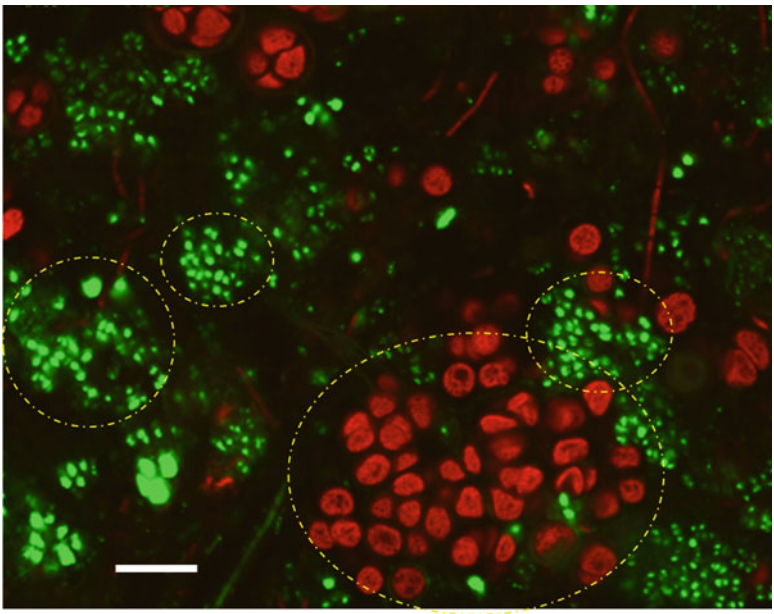

Fig. 6.1 Bacteria in natural environments such as microbial mats exhibit much microspatial heterogeneity in their cell distributions. Confocal scanning laser microscopy (CSLM) image showing microspatial clustering of cells within a natural microbial mat. Clusters of sulfate reducing bacteria (stained with a *dsrA* probe *green fluor*) are shown in proximity to photosynthetic cells (*red autofluorescence*) and highlighted with *dashed yellow circles*. Here quorum sensing is likely occurring among cells within a cluster, and possibly between clusters. Do different clusters talk to each other? (Scale bar is 10 μm)

The presence of *e*DNA in biofilms was detected long ago, but was thought to result from lysed cells. During analyses of activated sludge, however, DNA was abundantly found within EPS [61] and later in pure cultures of the bacterium *Pseudomonas putida*. Since that time, *e*DNA has been found in *P. aeruginosa* biofilms [62] and those of other bacteria [63]. It is now realized to play significant roles as a structuring agent of some EPS [64, 65]. In *Staphylococcus aureus* biofilms, the *cidA* gene has been shown to control cell-lysis and subsequent release of genomic DNA, which then results in important structural property changes in the biofilms [66]. As an interesting aside, inhalants containing the enzyme DNAse have been found to be helpful (to patients) in dissolving dense aggregations during lung infections, further suggesting a role of *e*DNA in the structural rigidity of EPS [67]. Here, quorum sensing using AHLs is known to occur under these conditions, and has been an additional target for therapies [68].

A signal molecule, released by a cell, has potential to be photochemically or geochemically modified to different molecular forms before being received by a receiver-cell, and potentially become environmental sensors. This has been extensively discussed elsewhere [22]. A study by Ferry and colleagues [69]

determined that a C6-AHL can be converted to an *oxo*-C6-AHL in the presence of photo-generated oxidants. This suggests that environmental conditions can change identity of a signal during transit between cells.

The environmental conditions in which biofilms exist, fluctuate on both short (e.g., min.) and long (e.g., mo.) temporal scales. The EPS polymers provide a relatively stable and non-dispersing network, which can exist as tangled, hydrophobic, or ionic linkages, and can readily expand or contract [70]. Hence, certain portions of gels (e.g., tangled networks) can change size and density rapidly, responding to pH, ionic concentration, or temperature, while other portions (i.e., covalently linked networks) can remain relatively stable.

6.3.1 Constraining Diffusion in EPS Gels

The density of EPS can vary over small spatial scales (e.g., micrometers) due to changes in linkages between adjacent molecules. Purified EPS, especially certain polysaccharides such as alginate, can be manipulated in bulk in the laboratory to create hydrogels having varying viscosity and water-retention capacities [71]. Very dense gels have also been observed during in the EPS of mucoid *Pseudomonas aeruginosa* related to cystic fibrosis lung infections [56, 68].

Polysaccharide gels, owing to their inherent properties, are realized to consist of local areas or "microdomains" where certain chemical properties can be different from the bulk gel [72]. Microdomains have the potential to change the chemical properties of EPS over small spatial scales (e.g., nm to μm) [73, 74]. EPS can be carefully probed with fluorescent lectins, which bind to specific arrangements of sugar monomers. The resulting patterns of lectin fluorescence indicate areas of concentration (of lectins) within EPS, as noted by Neu and colleagues [75–77]. Other biofilm polysaccharides show similar trends [78].

Some microdomains result from areas of highly ordered H-bonding between adjacent EPS molecules, which exclude water, and result in net hydrophobic microzones. EPS acetylation, for example, has been associated with formation of hydrophobic domains through London dispersion forces [79]. The functional result of such microdomains in largely hydrophilic EPS is the occurrence of small localized hydrophobic areas [74].

Under natural conditions, geochemical and photochemical transformations of EPS occur, further modifying their composition. Natural EPS, therefore, will be composed of a "continuum" of molecular sizes and compositions. From a signaling standpoint, it is important to determine which specific molecules will contribute to the binding of signal molecules. The functional relevance of EPS compositions will relate to how specific monomers, or more specifically their functional groups, interact with signals. Carbohydrate monomers that occur in EPS include charged and uncharged forms such as D-glucose, D-galactose, D-mannose, L-fucose, L-rhamnose; uronic acids such as D-glucuronate, D-galacturonate, L-glucuronate, D-mannuronate; and *N*-acetyl-D-glucosamine, and *N*-acetyl-D-galactosamine [42].

Functional groups such as carboxyls, hydroxyls, phosphates, amines, and sulfates, which are present on charged EPS monomers, are especially significant in guiding molecule–molecule interactions [80].

Certain sugar monomers on EPS are highly labile to heterotrophic bacteria, and hence could be selectively removed during bacterial degradation of EPS. Microbial mat bacteria rapidly utilize uronic acids and other monomers [81]. Removal of specific moieties can change the polymeric solubility, flexibility, and steric conformations of EPS polysaccharide components [42]. Steric conformational changes of an EPS molecule will affect which functional groups are unavailable (i.e., hidden) for interactions with signal molecules. Steric conformational changes in a molecule, in part, reflect which portions (i.e., moieties) of the molecule are exposed and available for complexation. These steric modifications have dramatic effects on their physical properties. Small changes in pH, hydration, and partial degradation can change the steric configuration of a molecule, and has the potential to make available functional groups.

6.3.2 Packaging of Signals Within EPS

EPS can serve as a signal storage facility. Bacteria are known to utilize lipid vesicles as packaging outposts. This allows signals, and other molecules (e.g., antibiotics, enzymes) to be remotely located within the EPS matrix and assist the cells. The vesicles originate from the outer cell membrane in Gram negative-bacteria and are "blebbed" off into EPS [82]. Vesicles as facilitate the movement of larger and more hydrophobic, signal molecules called *P. aeruginosa* quinolone signals (PQS) are known to be packaged within such lipid vesicles. Under natural conditions, the lipid vesicles can be quite abundant within EPS [83, 84] and could protect an AHL from degradation during transit from one cell to another.

Signals, such as AHLs, can persist outside of the cell for extended periods of time (e.g., months) under the right conditions. The water-retention properties of EPS are well-documented and are known to enhance the resiliency of biofilms by slowing water loss during desiccation [85–89]. However, certain saccharide components and polysaccharides can protect signal molecules during desiccation and heat exposure, which normally denatures the signal. These components of EPS can be used to protect and preserve cells, and extracellular enzymes and chemical signals that are localized in the EPS matrix during desiccation, and are currently under investigation (Decho, unpublished). During the slow dehydration of hypersaline microbial mats, signals released by cells may remain *in-transit* outside of cells for as long as several months (during desiccation of the mat) before being received by another cell. Upon rehydration, the signals (and extracellular enzymes) quickly become active again (within 1 h) as cells are rehydrated, and signaling quickly resumes.

Hydrogen bonds can provide a major interaction in the overall binding forces between EPS molecules. EPS is often observed to be very dense in its physical texture and can become even dehydrated in places. How do EPS change their

density and conformations outside of the cell? An emerging possibility is that EPS undergoes condensation, which results in dense, relatively water-poor areas of EPS through the exclusion of water from the polymer. This process is called "syneresis," and is best illustrated in the formation of the curd and whey during cheese production. Syneresis involves the spontaneous formation of abundant hydrogen bonds among adjacent (EPS) molecules, and the squeezing out of water (i.e., whey) from the aggregate (i.e. curd). The triggers for such a process, however, have remained elusive to polymer chemists. An important point is that the condensation of EPS during syneresis is not thought to be related to extracellular enzyme activities, but rather the spontaneous formation of abundant H bonds between adjacent molecules, which drives the exclusion of water.

6.4 Interactions of EPS and Signals

In natural biofilms, the water-filled spaces between EPS do not consist of pure water but rather contain a wide range of dissolved organic carbon (DOC) molecules and ions, which may interact with signal molecules. Therefore, the movement of signals via diffusion will be slowed by their interactions with: (1) the EPS itself and (2) molecules/ions contained in the water of EPS pore spaces. The spatial and temporal patterns of signaling that can be seen in biofilms with bacteria using reporter genes for quorum sensing [90] likely are the combined result of cell density differences, localization of signals by EPS.

Sharp microspatial changes in gradients or chemical heterogeneity are a trademark of conditions within the EPS of many biofilms. They are the combined result of activities of microbial cells and diffusion-slowing properties of the surrounding EPS [91]. Rather than physical exclusion entirely, the very rapid consumption of solutes by certain microbes can result in low measurable concentrations. This has been termed the *reaction-diffusion theory* [31], and the measured profiles of many chemical species are consistent with this idea. Oxygen profiles are one such example where the near surface of a biofilm may contain high O_2 concentrations while areas just a few tens of micrometers below this conditions may be anoxic [43, 44]. Stewart [31] calculated that O_2 and similar size solutes will diffuse through the EPS matrix at a rate that is approx 60 % of the rate in pure water (i.e., absence of a matrix). Similarly, there are likely to be sharp microspatial gradients in concentrations of chemical signals such as AHLs within a biofilm, although such measurements over the very small spatial scales (e.g., micrometers), required to be relevant, are not yet possible [22]. Diffusion of AHLs may be slowed through interactions with other molecules in areas simply due to high localized concentrations of DOC that is similar in molecular size and properties to the AHLs. Diffusivities of AHLs will be in contrast to those observed for pure water.

How might bacteria construct or modify the EPS matrix to enhance chemical communication? One possibility is that a recently divided bacterial cell will move away from its twin cell creating a tunnel through the EPS. This has been shown

to occur in bacteria that colonize biofilms [92]. The tunneling efforts will create conduits in dense EPS for diffusion to follow. This has the potential to create water channels and reduce diffusion to less than a full 3 dimensions.

One of the most dramatic examples of QS in EPS is the bioluminescence of aggregate-associated bacteria in plankton blooms in oceans. Coordinated signaling by bacteria can appear to occur over very large scales during plankton blooms containing bioluminescent bacteria. This has been footnoted (in history) in the logs by ship captains as the "milky ocean" phenomenon at night. This was documented more recently using satellite imagery, and occurred over an area of 15,400 km^2 in the northwest Indian Ocean over three consecutive nights [93, 94]. Bacteria in such ocean plankton blooms tend to form suspended aggregates (i.e., flocs) consisting cells plus EPS. This potentially allows cells to remain in proximity to one another in order to conduct quorum sensing.

6.5 Emerging Approaches for Understanding In Situ EPS/Signaling Interactions

The EPS matrix is proving to be considerably more-complex than initially conceived. It is now realized that bacterial cells can sense, communicate, and exchange molecules and perhaps energy over both short (i.e., μm) and long (i.e., cm) distances using "nanowires" [95], which are postulated to extend over centimeter distances in natural sediments. Nanotubes [96], which directly connect several bacterial cells with each other, are known to allow exchange of cytoplasmic molecules. A key to understanding the EPS matrix lies in chemically probing and imaging the very small-scale structural detail of the matrix. Chemically probing the interactions among molecules such as steric conformations, availability of functional groups, spacing and types of linkages among adjacent EPS molecules will require non-destructive methods. These properties, which contribute to the adaptive nature and viscoelastic properties of EPS for microbial cells, can most effectively be approached examining EPS in situ at molecular- to atomic-scales.

6.5.1 Raman/SERS/Raman-Confocal Microscopy

The use of photons to interrogate the complex EPS matrix of and provide detailed chemical and/or biological information represents a potentially non-destructive approach to investigating biofilms in situ. Such information is derived from the simple principle that a photon (of a given energy) can cause predictable vibrational changes in a molecule, due to chemical bonds or groups of bonds between atoms. These changes can be measured and interpreted. This property, when can analyzed properly can provide detailed chemical information in a rapid and non-destructive manner for systems such as biofilms.

Raman spectroscopy is a type of "vibrational" spectroscopy. It is especially suited to being non-destructive because little or no preparation of samples is needed. Raman spectral profiles are based on the scattering of photons and target the backbone of a molecule. This is in contrast to infrared spectroscopy approaches, whose spectra are based on the absorption of photons and target the outer functional groups of a molecule. Infrared spectra are complicated by the presence of water. However, water does not cause problems for interpreting Raman spectra, therefore, fully hydrated and intact biofilms can be analyzed.

Raman can be adapted to microscopy to collect spectra pixel by pixel, and hence can be used to probe for the presence/absence of specific molecules, and decipher variations in molecular composition over very small xy plane spatial scales (e.g., 1×1 μm). Through adaptation to confocal changes in the z-axis (e.g., depth in a biofilm) can also be differentiated [97]. A technical drawback to Raman is its compromised sensitivity. However, when certain types (e.g., Ag) of nanoparticles (i.e., 1–100 nm dia) are added to a sample, sensitivities can be increased dramatically and in some cases have made single molecule detection possible. This process is referred to as surface-enhanced Raman scattering (SERS) and can be used with Raman-confocal microscopy [98]. A number of other adaptations are now possible such as combining Raman and atomic-force microscopy (AFM), where Raman spectra correspond to the location of the cantilever tip of the AFM. Another Raman-related approach is coherent anti-Stokes Raman scattering (CARS) microscopy; a technique that has much greater sensitivity than conventional Raman and does not require label [99]. Although technically challenging at this point, these approaches provide information on chemical composition of a biofilm at unprecedented spatial scales, and can be used to gain information on microspatial arrangements of EPS and perhaps signaling molecules within a biofilm.

3-Dimensional Cryo-TEM Tomography is a unique form of transmission electron microscopy that allows the sample to be frozen in a hydrated state, then sliced into blocks (500 nm thick) then observed without the use of stains to enhance electron density. Through imaging and successive reorientation of the block, a high resolution 3-dimensional image of the specimen can be created. Intact cellular structures (cell membranes, proteins, etc.) can be observed with high resolution. This approach has been used to examine bacterial cells, capsules, and vesicles. EPS is still difficult to image due to its high water content and light elemental composition, but can be enhanced through binding of soluble electron dense metals such as U(VI) or Mn(II)/(III) [100, 101]. This has the potential to provide the first look at changes in the in situ arrangements of EPS polymers within biofilms (Fig. 6.2).

Over the past two decades our understanding of the EPS matrix has evolved considerably. The matrix is now realized to be a complex and spatially organized milieu, especially with regard to chemical communication. In order to more fully understand this matrix, which is laden with vesicles, nanotubes, nanowires, and diffusible channels, future studies will require high-resolution and high-sensitivity chemical mapping at nm spatial scales.

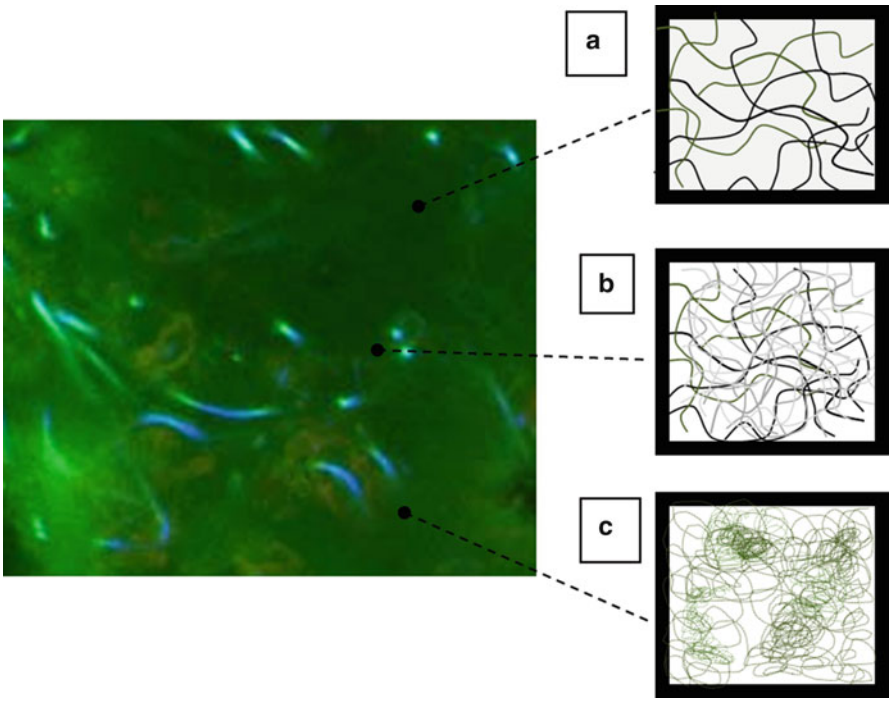

Fig. 6.2 EPS forms a 3-dimensional arrangement of polymer molecules having vastly different conformations over small spatial scales. Above is a confocal scanning laser micrograph (CSLM) showing EPS stained with the fluorescent lectin concanavalin-A; cyanobacteria are long *white/blue* structures within EPS. Although EPS may appear relatively homogeneous when viewed with light microscopy, however, at molecular scales (*diagramed at right*) the individual polymers can range from loosely interacting linear molecules to closely interacting branching combs to dense tangled networks. Spaces in between polymer molecules contain pore-water water and contribute to the highly hydrated nature of many EPS. It is through the water-filled pore spaces that diffusion of chemical signals such as acylhomoserine lactones (AHLs) occurs during quorum sensing. (**a**) EPS can be loosely arranged having much free water in between polymers. (**b**) When EPS are closely linked together they form dense gels having relatively small water pores for diffusion. (**c**) They can even form hydrophobic microdomains, where EPS are very closely linked, usually in linear arrangements, and have very little free water. These changes in conformation and density likely vary over small spatial scales (e.g., nanometers to micrometers) and will affect the diffusivities of solutes (e.g., signal molecules) through the matrix

References

1. Boles BR, Thoendel M, Singh PK (2004) Self-generated diversity produces "insurance effects" in biofilm communities. Proc Natl Acad Sci U S A 101:16630–16635
2. Miller MB, Bassler BL (2001) Quorum sensing in bacteria. Annu Rev Microbiol 55:165–199
3. Fuqua WC, Greenberg EP (2002) Listening in on bacteria: acyl-homoserine lactone signaling. Nat Rev Mol Cell Biol 3:685–695
4. Camilli A, Bassler BL (2006) Bacterial small-molecule signaling pathways. Science 311:1113–1116

5. Keller L, Surette MG (2006) Communication in bacteria: an ecological and evolutionary perspective. Nat Rev Microbiol 4:249–258
6. Dandekar AA, Chugani S, Greenberg EP (2012) Bacterial quorum sensing and metabolic incentives to cooperate. Science 338:264–266
7. Redfield RJ (2002) Is quorum sensing a side effect of diffusion sensing? Trends Microbiol 10:365–370
8. Hense BA, Kuttler C, Müller J, Rothballer M, Hartmann A, Kreft J-U (2007) Does efficiency sensing unify diffusion and quorum sensing? Nat Rev Microbiol 5:230–239
9. Nealson KH, Platt T, Hastings JW (1970) Cellular control of synthesis and activity of bacterial luminescent systems. J Bacteriol 104:313–322
10. Nealson KH, Hastings JW (1979) Bacterial bioluminescence: its control and ecological significance. Microbiol Rev 43:496–518
11. Eberhard A, Burlingame AL, Eberhard C, Kenyon GL, Nealson KH, Oppenheimer NJ (1981) Structural identification of autoinducer of *Photobacterium fischeri* luciferase. Biochemistry 20:2444–2449
12. Decho AW (1990) Microbial exopolymer secretions in ocean environments: their role(s) in food webs and marine processes. Oceanogr Mar Biol Ann Rev 28:73–154
13. Wingender J, Neu TR, Flemming H-C (1999) Microbial extracellular polymeric substances. Springer, Berlin
14. Neu TR, Manz B, Volke F, Dynes JJ, Hitchcock AP, Lawrence JR (2010) Advanced imaging techniques for assessment of structure, composition and function in biofilm systems. FEMS Microbiol Ecol 72:1–21
15. Flemming H-C, Wingender J (2010) The biofilm matrix. Nat Rev Microbiol 8:623–633
16. Schauder S, Bassler BL (2001) The languages of bacteria. Genes Dev 15:1468–1480
17. Diggle SP, Griffin AS, Campbell GS, West SA (2007) Cooperation and conflict in quorum sensing bacterial populations. Nature 450:411–414
18. Geske GD, O'Neill JC, Blackwell HE (2008) Expanding dialogues: from natural autoinducers to non-natural analogues that modulate quorum sensing in Gram-negative bacteria. Chem Soc Rev 37:1432–1447
19. Schaefer AL, Greenberg EP, Oliver CM, Oda Y, Huang JJ, Bittan-Banin G, Peres CM, Schmidt S, Juhaszova K, Sufrin JR, Harwood CS (2008) A new class of homoserine lactone quorum-sensing signals. Nature 454:595–599
20. Schulz S (2014) A new bacterial chemical signal: mapping the chemical space used for communication. Chembiochem 15:498–500
21. Brogioli D, Vailati A (2001) Diffusive mass transfer by non-equilibrium fluctuations: Fick's law revisited. Phys Rev E 63:012105
22. Decho AW, Frey RL, Ferry JL (2011) Chemical challenges to bacterial AHL signaling in the environment. Chem Rev 111:86–99
23. Gantner S, Schmid M, Dürr C, Schuheggar R, Steidle A, Hutzler P, Langebartels C, Eberl L, Hartmann A, Dazzo FB (2006) In situ quantitation of the spatial scale of calling distances and population density independent *N*-acyhomoserine lactone-mediated communication by rhizobacteria colonized on plant roots. FEMS Microbiol Ecol 56:188–194
24. Schmidt J, Flemming H-C (1999) Water binding in biofilms. Water Sci Technol 39:77–82
25. Smith JD, Cappa CD, Wilson KR, Cohen RC, Geissler PL, Saykally RJ (2005) Unified description of temperature-dependent hydrogen bond rearrangements in liquid water. Proc Natl Acad Sci U S A 102:14171–14174
26. Tokmachev AM, Tchougreeff AL, Dronskowski RR (2010) Hydrogen-bond networks in water clusters: an exhaustive quantum-chemical. Eur J Chem Phys Phys Chem 11:384–388
27. Nichols WW, Dorrington SM, Slack MP, Walmsley HL (1988) Inhibition of tobramycin diffusion by binding to alginate. Antimicrob Agents Chemother 32:518–523
28. Stewart PS (1998) A review of experimental measurements of effective diffusive permeabilities and effective diffusion coefficients in biofilms. Biotechnol Bioeng 59:261–272

29. Guiot E, Georges P, Brun A, Fontaine-Aupart MP, Bellon-Fontaine MN, Briandet R (2002) Heterogeneity of diffusion inside microbial biofilms determined by fluorescence correlation spectroscopy under two-photon excitation. Photochem Photobiol 75:570–578
30. Stone G, Wood P, Dixon L, Keyhan M, Matin A (2002) Tetracycline rapidly reaches all the constituent cells of uropathogenic *Escherichia coli* biofilms. Antimicrob Agents Chemother 46:2458–2461
31. Stewart PS (2003) Diffusion in biofilms. J Bacteriol 185:1485–1491
32. Jefferson KK, Goldmann DA, Pier GB (2005) Use of confocal microscopy to analyze the rate of vancomycin penetration through *Staphylococcus aureus* biofilms. Antimicrob Agents Chemother 49:2467–2473
33. Rani SA, Pitts B, Stewart PS (2005) Rapid diffusion of fluorescent tracers into *Staphylococcus epidermidis* biofilms visualized by time lapse microscopy. Antimicrob Agents Chemother 49:728–732
34. Gilbert Y, Deghorain M, Wang L, Xu B, Pollheimer PD, Gruber HJ, Errington J, Hallet B, Haulot X, Verbelen C, Hols P, Dufrêne YF (2007) Single-molecule force spectroscopy and imaging of the vancomycin/D-Ala-D-Ala interaction. Nano Lett 7:796–801
35. Briandet R, Lacroix-Gueu P, Renault M, Lecart S, Meylheuc T, Bidnenko E, Steenkeste K, Bellon-Fontaine M-N, Fontaine-Aupart M-P (2008) Fluorescence correlation spectroscopy to study diffusion and reaction of bacteriophages inside biofilms. Appl Environ Microbiol 74:2135–2143
36. Stewart PS, Davison WM, Steenbergen JN (2009) Daptomycin rapidly penetrates a *Staphylococcus epidermidis* biofilm. Antimicrob Agents Chemother 53:3505–3507
37. Zhang Z, Nadezhina E, Wilkinson KJ (2010) Quantifying diffusion in a biofilm of *Streptococcus mutans*. Antimicrob Agents Chemother 55:1075–1081
38. De Beer D, Stoodley P, Lewandowski Z (1997) Measurements of local diffusion coefficients in biofilms by microinjection and confocal microscopy. Biotechnol Bioeng 53:151–158
39. Waharte F, Steenkeste K, Briandet R, Fontaine-Aupart MP (2010) Diffusion measurements inside biofilms by image-based fluorescence recovery after photobleaching (FRAP) analysis with a commercial confocal laser scanning microscope. Appl Environ Microbiol 76:5860–5869
40. Daddi-Oubekka S, Briandet R, Wharate F, Fontaine-Aupart M-P, Steenkeste K (2011) Image-based fluorescence recovery after photobleaching (FRAP) to dissect vancomycin diffusion–reaction processes in *Staphylococcus aureus* biofilms. SPIE-OSA Clin Biomed Spectrosc Imaging II 8087 11:1–8
41. Daddi-Oubekka SD, Briandet R, Fontaine-Aupart M-P, Steenkeste K (2012) Correlative time-resolved fluorescence microscopy to assess antibiotic diffusion–reaction in biofilms. Antimicrob Agents Chemother 56:3349–3358
42. Sutherland IW (2001) The biofilm matrix – an immobilized but dynamic microbial environment. Trends Microbiol 9:222–227
43. De Beer D, Stoodley P, Roe F, Lewandowski Z (2004) Effects of biofilm structure on oxygen distribution and mass transport. Biotechnol Bioeng 43:1131–1133
44. Visscher PT, Reid RP, Bebout BM (2000) Microscale observations of sulfate reduction: correlation of microbial activity with lithified micritic laminae in modern marine stromatolites. Geology 28:919–922
45. Braissant O, Cailleau G, Dupraz C, Verrechia EP (2003) Bacterially induced mineralization of calcium carbonate in terrestrial environments: the role of exopolysaccharides and amino acids. J Sediment Res 73:485–490
46. Braissant O, Decho AW, Dupraz C, Glunk C, Przekop KM, Visscher PT (2007) Exopolymeric substances of sulfate-reducing bacteria: interactions with calcium at alkaline pH and implications for formation of carbonate minerals. Geobiology 5:401–411
47. Braissant O, Decho AW, Przekop KM, Gallagher KL, Glunk C, Dupraz C, Visscher PT (2009) Characteristics and turnover of exopolymeric substances in a hypersaline microbial mat. FEMS Microbiol Ecol 67:293–307

48. Decho AW, Visscher PT, Ferry J, Kawaguchi T, He L, Przekop KM, Norman RS, Reid RP (2009) Autoinducers extracted from microbial mats reveal a surprising diversity of *N*-acylhomoserine lactones (AHLs) and abundance changes that may related to diel pH. Environ Microbiol 11:409–420
49. Peulen T-O, Wilkinson KJ (2011) Diffusion of nanoparticles in a biofilm. Environ Sci Technol 45:3367–3373
50. Davies DG, Parsek MR, Pearson JP, Iglewski BH, Costerton JW, Greenberg EP (1998) The involvement of cell-to-cell signals in the development of a bacterial biofilm. Science 280: 295–299
51. Decho AW (1999) Imaging an alginate polymer gel matrix using atomic force microscopy. Carbohydr Res 315:330–333
52. Verdugo P, Alldredge AL, Azam F, Kirchman DL, Passow U, Santschi PH (2004) The oceanic gel phase: a bridge in the DOM–POM continuum. Mar Chem 92:67–85
53. Flemming H-C, Neu TR, Wozniak DJ (2007) The EPS matrix: the "house of biofilm cells". J Bacteriol 189:7945–7947
54. Dupraz C, Reid RP, Braissant O, Decho AW, Norman RS, Visscher PT (2009) Processes of carbonate precipitation in modern microbial mats. Earth-Sci Rev 96:141–162
55. Nivens DE, Ohman DE, Williams J, Franklin MJ (2001) Role of alginate and its O acetylation in formation of *Pseudomonas aeruginosa* microcolonies and biofilms. J Bacteriol 183: 1047–1057
56. Friedman L, Kolter R (2004) Two genetic loci produce distinct carbohydrate-rich structural components of the *Pseudomonas aeruginosa* biofilm matrix. J Bacteriol 186:4457–4465
57. Jackson KD, Starkey M, Kremer S, Parsek MR, Wozniak DJ (2004) Identification of *psl*, a locus encoding a potential exopolysaccharide that is essential for *Pseudomonas aeruginosa* PAO1 biofilm formation. J Bacteriol 186:4466–4475
58. Ma L, Jackson KD, Landry RM, Parsek MR, Wozniak DJ (2006) Analysis of *Pseudomonas aeruginosa* conditional Psl variant reveals roles for the Psl polysaccharide in adhesion and maintaining biofilm structure post attachment. J Bacteriol 188:8213–8221
59. Wotton RS (2004) The ubiquity and many roles of exopolymers (EPS) in aquatic systems. Oceanogr Mar Biol Annu Rev 42:57–94
60. Dupraz C, Visscher PT (2005) Microbial lithification in marine stromatolites and hypersaline mats. Trends Microbiol 13:429–438
61. Palmgren R, Nielsen, PH (1996) Accumulation of DNA in the exopolymeric matrix of activated sludge and bacterial cultures. Water Sci Technol 34(5–6):233–240
62. Allesen-Holm M, Barken KB, Yang L, Klausen M, Webb JS, Kjelleberg S, Molin S, Givskov M, Tolker-Nielsen T (2006) A characterization of DNA release in *Pseudomonas aeruginosa* cultures and biofilms. Mol Microbiol 59:1114–1128
63. Böckelmann U, Janke A, Kuhn R, Neu TR, Wecke J, Lawrence JR, Szewzyk U (2006) Bacterial extracellular DNA forming a defined network-like structure. FEMS Microbiol Lett 262:31–38
64. Whitchurch CB, Tolker-Nielsen T, Ragas PC, Mattick JS (2002) Extracellular DNA required for bacterial biofilm formation. Science 295:1487
65. Tang L, Schramm A, Neu TR, Revsbech NP, Meyer RL (2013) Extracellular DNA in adhesion and biofilm formation of four environmental isolates: a quantitative study. FEMS Microbiol Ecol 86:394–403
66. Rice KC, Mann EE, Endres JL, Weiss EC, Cassat JE, Smeltzer MS, Bayles KW (2007) The *cidA* murein hydrolase regulator contributes to DNA release and biofilm development in *Staphylococcus aureus*. Proc Natl Acad Sci U S A 104:8113–8118
67. Tolker-Neilsen T, Høiby N (2009) Extracellular DNA and F-actin as targets in anti-biofilm cystic fibrosis therapy. Future Microbiol 4:645–647
68. Bjarnsholt T, Pø Jensen MJ, Fiandaca JP, Hansen CR, Andersen CB, Pressler T, Givskov M, Høiby N (2009) *Pseudomonas aeruginosa* biofilms in the respiratory tract of cystic fibrosis patients. Pediatr Pumonol 44:547–558

69. Cui Y, Frey RL, Ferry JL, Ferguson PL (2009) Identification of hydroxyl radical oxidation products of *N*-hexanoyl-homoserine lactone by reversed-phase high performance liquid chromatography coupled with electrospray ionization tandem mass spectrometry. Rapid Commun Mass Spectrom 23:1212–1220
70. Tanaka T (1992) Phase transitions of gels. ACS Sym Ser 480:1–21
71. Späth R, Flemming H-C, Wuertz W (1998) Sorption properties of biofilms. Water Sci Technol 37:2007–2210
72. Decho AW (2000) Exopolymer microdomains as a structuring agent for heterogeneity within microbial biofilms. In: Riding RE, Awramik SM (eds) Microbial sediments. Springer, New York, pp 1–9
73. Lawrence JR, Swerhone GD, Kuhlicke U, Neu TR (2007) In situ evidence for microdomains in the polymer matrix of bacterial microcolonies. Can J Microbiol 53:450–458
74. Aldeek F, Schneider R, Fontaine-Aupart M-P, Mustin C, Lécart S, Merlin C, Block J-C (2013) Patterned hydrophobic domains in the exopolymer matrix of *Shewanella oneidensis* MR-1 biofilms. Appl Environ Microbiol 79:1400–1402
75. Neu TR, Swerhone GDW, Lawrence JR (2001) Assessment of lectin-binding analysis for in situ detection of glycoconjugates in biofilm systems. Microbiology 147:299–313
76. Böckelmann U, Manz W, Neu TR, Szewzyk U (2002) Investigation of lotic microbial aggregates by a combined technique of fluorescent in situ hybridization and lectin-binding-analysis. J Microbiol Methods 49:75–87
77. Zippel B, Neu TR (2011) Characterization of EPS glycoconjugates in tufa forming biofilms by means of 2 fluorescence lectin-binding analysis. Appl Environ Microbiol 77:505–516
78. Strathmann M, Wingender J, Flemming H-C (2002) Application of fluorescently labelled lectins for the visualization and biochemical characterization of polysaccharides in biofilms of *Pseudomonas aeruginosa*. J Microbiol Methods 50:237–248
79. Mayer C, Moritz R, Kirschner C, Borchard W, Wingender J, Flemming H-C (1999) The role of intermolecular interactions: studies on model systems for bacterial biofilms. Int J Biol Macromol 26:3
80. Flemming H-C (1995) Sorption sites in biofilms. Water Sci Technol 32:27–33
81. Decho AW, Visscher PT, Reid RP (2005) Production and cycling of natural microbial exopolymers (EPS) within a marine stromatolite. Palaeogeogr Palaeoclimatol Palaeoecol 219:71–86
82. Mashburn LM, Whiteley M (2005) Membrane vesicles traffic signals and facilitate group activities in a prokaryote. Nature 437:422–425
83. Schooling SR, Beveridge TJ (2006) Membrane vesicles: an overlooked component of the matrices of biofilms. J Bacteriol 188:5945–5947
84. Mashburn-Warren L, Mclean RJC, Whiteley M (2008) Gram-negative outer membrane vesicles: beyond the cell surface. Geobiology 6:214–219
85. Ophir T, Gutnik DL (1994) A role for exopolysaccharides in the protection of microorganisms from desiccation. Appl Environ Microbiol 60:740–745
86. Potts M (1994) Desiccation tolerance in prokaryotes. Microbiol Rev 58:755–805
87. Potts M (1999) Mechanisms of desiccation tolerance in cyanobacteria. Eur J Phycol 34:319–326
88. Potts M (2001) Desiccation tolerance: a simple process? Trends Microbiol 9:553–559
89. Buitink J, Leprince O (2004) Glass formation in plant anhydrobiotes: survival in the dry state. Cryobiology 48:215–228
90. Yarwood JM, Bartels DJ, Volper EM, Greenberg EP (2004) Quorum sensing in *Staphylococcus aureus* biofilms. J Bacteriol 186:1838–1850
91. Stewart PS, Franklin MJ (2008) Physiological heterogeneity in biofilms. Nat Rev Microbiol 6:199–210
92. Houry A, Gohar M, Deschamps J, Tischenko E, Aymerich S, Gruss A, Briandet R (2012) Bacterial swimmers that infiltrate and take over the biofilm matrix. Proc Natl Acad Sci U S A 109:13088–13093

93. Miller SD, Haddock SHD, Elvidge CD, Lee TF (2005) Detection of a bioluminescent milky sea from space. Proc Natl Acad Sci U S A 102:14181–14184
94. Nealson KH, Hastings JW (2006) Quorum sensing on a global scale: massive numbers of bioluminescent bacteria make milky seas. Appl Environ Microbiol 72:2295
95. Gorby YA, Yanina S, McLean JS, Rosso KM, Moyles D, Dohnalkova A, Beveridge TJ, Chang I, Kim BH, Kim KS, Culley DE, Reed SB, Romine MF, Saffarini DA, Hill EA, Shi L, Elias DA, Kennedy DW, Pinchuk G, Watanabe K, Ishii S, Logan B, Nealson KH, Fredrickson JK (2006) Electrically conductive bacterial nanowires produced by *Shewanella oneidensis* strain MR-1 and other microorganisms. Proc Natl Acad Sci U S A 103:11358–11363
96. Dubey GP, Ben-Yehuda S (2011) Intercellular nanotubes mediate bacterial communication. Cell 144:590–600
97. Chao Y, Zhang T (2012) Surface-enhanced Raman scattering (SERS) revealing chemical variation during biofilm formation: from initial attachment to mature biofilm. Anal Bioanal Chem 404:1465–1475
98. Zeiri L, Bronk BV, Shabtai Y, Eichler J, Efrima S (2004) Surface-enhanced Raman spectroscopy as a tool for probing specific biochemical components in bacteria. Appl Spectrosc 58:33–40
99. Pezacki JP, Blake JA, Danielson DC, Kennedy DC, Lyn RK, Singaravelu R (2011) Chemical contrast for imaging living systems: molecular vibrations drive CARS microscopy. Nat Chem Biol 7:137–145
100. Hunter RC, Beveridge TJ (2005) High-resolution visualization of *Pseudomonas aeruginosa* PAO1 biofilms by freeze-substitution transmission electron microscopy. J Bacteriol 187:7619–7630
101. Dohnalkova AC, Marshall MJ, Arey BW, Williams KH, Buck EC, Fredrickson JK (2011) Imaging hydrated microbial extracellular polymers: comparative analysis by electron microscopy. Appl Environ Microbiol 77:1254–1262

Chapter 7
Swimming in Information? Physical Limits to Learning by Quorum Sensing

Stephen J. Hagen

7.1 Physical Interpretation of QS Behavior

A standard description of bacterial quorum sensing is that it allows a colony of bacteria to detect and respond to its own population density [1]. However, given the diversity and complexity of bacterial quorum sensing mechanisms that have been discovered and characterized, it is apparent that QS is much more than just a scheme for population counting [2, 3]. QS networks often respond to many environmental inputs in addition to population density. These include pH, temperature and nutrient, as well as signals produced by other species. Many bacterial species employ multiple autoinducer signals and they detect those signals using multiple sensing networks [1]. The architecture of QS networks can be very complex [4], leading to intriguing dynamics that can involve nonlinearity, hysteresis, bistability, stochastic switching, and more. Such sophisticated systems allow QS populations to respond in complex fashion to environmental stimuli.

Researchers have also suggested that, in addition to performing a social function, QS behavior may also allow individual cells to gather information about purely physical properties of their environment: geometrical parameters of confinement, clustering, or rates of advective flow could in principle be accessible to a cell that both secretes and detects a diffusible signal [5–8]. This perspective sets aside the social context of QS and focuses on the physical problem of one individual cell (or a few cells) swimming in a diffuse cloud of its own autoinducer. Is such a mechanism effective for the cell? As a QS regulatory network is ultimately a detector, or at least a device for translating an input signal into a regulatory output, we should attempt to understand some of its physical capabilities and limitations at the microscopic level. What are the physical limits on the information that a bacterium can acquire

S.J. Hagen (✉)
Physics Department, University of Florida, PO Box 118440, Gainesville, FL 36211-8440, USA
e-mail: sjhagen@ufl.edu

S.J. Hagen (ed.), *The Physical Basis of Bacterial Quorum Communication*, Biological and Medical Physics, Biomedical Engineering, DOI 10.1007/978-1-4939-1402-9_7

by sensing a diffusing signal? This chapter aims to give a general introduction to some of the physical constraints. By focusing on QS at the microscopic level, rather than in its social context, we hope to better understand how the benefits to the individual—or the information available to one cell—differ from the group benefits that accrue in a population-averaged sense to a bulk culture of QS bacteria.

Redfield took a provocative step in viewing the physical side of QS apart from its social context by considering a solitary, isolated cell that synthesizes an autoinducer and releases it into the environment [8]: The local concentration of autoinducer measured by this single cell is not a measure of the cell population. It does however measure the rate at which the autoinducer diffuses (or is otherwise transported) away from the cell. If the cell is confined in a small volume, its autoinducer should accumulate, signaling to the cell that it occupies a small volume, and that any of its secreted enzymes or other products will tend to remain nearby. This viewpoint reinterprets the social behavior of QS as an autonomous "diffusion sensing" (DS) behavior aimed at probing the character of local diffusion in order to establish whether to invest in the secretion of costly goods. Hense et al. [6] subsequently pointed out that the signal concentration does not perfectly reveal either the population or the local diffusion properties. Rather the concentration is one measurable quantity that depends on a complex combination of environmental factors: the local population density, the spatial distribution of other proximal cells, and the rates of advection and diffusion [6, 9]. If the regulatory circuit is optimized to measure this composite—the overall efficiency associated with production of a diffusible product—then the behavior involves elements of both QS and DS and could be referred to as "efficiency sensing" (ES).

The possibility that solitary cells or small clusters could benefit from deploying their QS circuits inspired researchers to test whether QS circuits of individual cells could be activated by confinement to microscopic volumes [10–12]. Boedicker et al. [10] showed that as few as 1–3 cells of *Pseudomonas aeruginosa* confined to a microfluidic chamber could activate their QS network. Similarly the LuxI/LuxR system of *Vibrio fischeri* was also activated in individual cells that were confined to picoliter volumes [12]. More generally, through the use of novel microfabrication techniques, researchers can manipulate the diffusive and advective coupling between a few locally confined cells and the rest of the physical and chemical world, and thus explore the full range of ES responses, in scenarios ranging from complete isolation of a cell to high density living [13, 14].

Of course the fact that QS circuits can respond to purely physical parameters of the environment does not mean that bacteria use them for this purpose. There are at least two separate questions here: Are QS circuits "intended" to sense microscopic properties of the environment? And if so are they good at it?

The first question is difficult to answer because the physical consequences of one cell's secreting and detecting the same molecule are the same, regardless of the "intent" of the behavior: demonstrating a use for a tool does not necessarily tell us how it is typically used. QS behavior develops in the context of the organism's social environment, which may span a range from highly social and related (many closely related and potentially cooperating organisms) to solitary and

unrelated (non-cooperating organisms), with many environments lying somewhere in between [7]. As discussed by West and Diggle [15], autoinducer production in these intermediate cases offers benefits that do not lie purely within either a solitary (DS) or social (QS) description. Those authors further point out that one cannot argue that a particular QS circuit may have evolved to serve the individual rather than its close relatives, as evolution does not make a distinction between these two cases. Evolution is expected to maximize the "inclusive fitness" of the organism, meaning the reproductive success of both the individual and its closest relatives. Therefore it does not seem plausible that evolution could favor one benefit or the other [15]. Just as the autoinducer sensing system cannot distinguish between inefficient diffusion and high population density, the evolutionary scheme that optimizes that system does not distinguish between individual and group benefits. Consequently we should hesitate to name new subcategories of QS behaviors according to different adaptive functions they may serve in different situations. Platt and Fuqua [7] have argued that the term "quorum sensing" can continue to refer generically to gene regulation through the secretion and detection of diffusible autoinducers. It is not necessary to restrict its meaning to "a social behavior of regulating gene expression in response to bacterial population density."

However we must still ask the physical question of how well a QS circuit may work in these different possible roles. What do the physics of diffusible signals allow a QS bacterium to learn about its environment? We begin by considering some basic properties of autoinducer diffusion and its consequences for diffusion sensing behavior.

7.2 Possibilities and Limits in Diffusion Sensing

Different QS bacteria employ different autoinducers with a range of chemical and physical properties. These include the acyl homoserine lactones (AHLs) that are used by many Gram negative microbes, the peptides used by many Gram positives, and a variety of other small molecules. Some of these are transported by complex mechanisms. The quinolones of *P. aeruginosa*, for example, are packaged into vesicles [16] for transport. However, we focus here on the AHLs, which are believed generally to travel by diffusion and advection. In the absence of stirring or flow, gene activation from a diffusing signal should then develop in a way that is governed by the diffusion equation:

$$\frac{\partial C}{\partial t} = D\nabla^2 C \tag{7.1}$$

Here $C(\boldsymbol{r}, t)$ is the concentration of the autoinducer at location $\boldsymbol{r}$ and time t and D is the diffusion coefficient. (Equation (7.1) can also be modified to account for the synthesis and degradation of the autoinducer.) From this equation it is straightforward to calculate the concentrations and gradients of autoinducer that will

surround individual cells or small clusters in an open environment, and to find the relationship between intercellular distances and quorum sensing activation in such clusters [5]. Here we consider the DS or ES picture of a cell that is confined to a finite volume. We can ask how well the autoinducer concentration reveals the size of that volume.

The most straightforward method for detecting the boundaries of one's environment would be to emit a signal that travels as a wave and reflects from the boundary: As in echolocation, the round trip time for the emitted signal to reflect from the boundary and return to the source provides all the information that is required. This behavior is completely uncharacteristic of the diffusion equation, and so this scenario may seem far fetched. Interestingly however, even fairly simple theoretical models of QS circuits—in which the autoinducer travels solely by diffusion—may permit wavelike excitations to travel through a spatially extended colony [17, 18]. For example, in a model of the LuxI/LuxR QS circuit of *V. fischeri*, the excitation of the *lux* system was found to be capable of propagating as a wave: If cells at all locations synthesize AHL at basal levels, any localized activation or excess AHL at one location can produce a pulse of diffusing AHL that can push neighboring cells over the threshold of activation, leading to a traveling wave [17]. Wave behavior certainly can be designed into a synthetic QS system [19]. In fact, laboratory studies of wild-type *V. fischeri* also showed wavelike excitations of the QS-regulated bioluminescence traveling over centimeter distances in an extended colony [20]. However, as the biological significance of such mechanisms is still a matter of speculation, we set aside traveling waves here. Instead we focus on the information that a cell can extract simply by sensing the diffusional spreading of its autoinducer.

We imagine a cell that is located at the center of a spherical confining volume that has radius R. The confining volume initially contains no autoinducer or other sources of autoinducer. Starting at time $t = 0$, the cell begins secreting autoinducer at a steady rate γ (with units of concentration × volume). This autoinducer travels radially outward by diffusion (diffusion coefficient D) and reaches the impermeable wall of the container, which is located outside the cell, at R. Figure 7.1 shows the growth of the autoinducer concentration $C(a,\ t)$ at the location $a = 1$ μm, obtained by solving the diffusion equation. Although the exact solution for the time dependence of this concentration is somewhat complicated, it is fairly well approximated by the sum of two simple terms:

$$C\ (a,t) \simeq 3\gamma t / \left(4\pi R^3\right) + \gamma / 4\pi D a \tag{7.2}$$

The relative importance of the two terms depends on how t compares to a characteristic time scale $t^* = R^3/Da$. At early times $t < t^*$ (i.e., for relatively large R, or for slow diffusion D), the second term dominates and C is virtually a constant, $C \simeq \gamma/4\pi Da$. This describes the time scale before the diffusing particles have reached the confining wall (Fig. 7.2). The secreted particles are "lost" to the cell after they have diffused a short distance. The cell detects only the local concentration that is due to the flux of outwardly moving particles. However at later times $t > t^*$ (i.e., for smaller R or faster diffusion D), the first term dominates

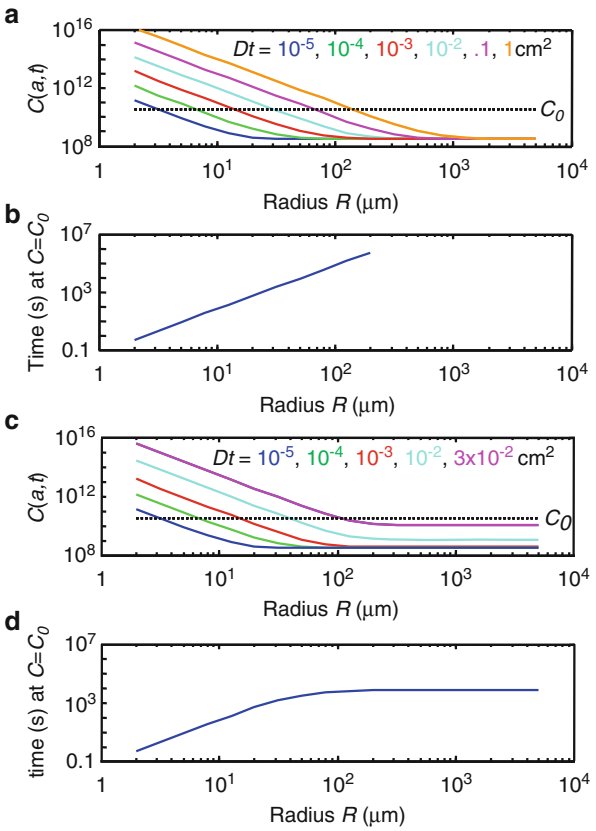

Fig. 7.1 Accumulation of diffusible autoinducer in a spherical volume of radius R, due to a source that is located at $r = 0$ and produces autoinducer at a rate $\gamma = 2$ particles/s. The figures show the accumulated concentration $C(a, t)$ as measured at radius $a = 1$ μm after production for time t, assuming that the autoinducer diffuses with $D = 5 \times 10^{-6}$ cm^2/s. (**a**) At early times ($Dt \ll R^3/a$), for a single (non-dividing) cell producing autoinducer, $C(a, t) \simeq \gamma/(4\pi Da)$, independent of R. At later times ($Dt \gg R^3/a$), $C(a, t) \propto 1/R^3$. (**b**) If $C_0 > \gamma/4\pi Da$, then the time required for $C(a, t)$ to reach threshold (here $C_0 = 100\gamma/4\pi Da$) scales as R^3; (**c**) For a bacterium that divides with a doubling time $t_D = 1{,}200$ s, the concentration $C(a, t)$ for large R steadily rises with time, owing to increasing autoinducer production by daughter cells; (**d**) The time required for $C(a, t)$ to reach the threshold $C_0 = 100\gamma/4\pi Da$ is sensitive to R only for small R

and $C \simeq 3\gamma\, t/4\pi R^3$. Here the secreted molecules have time to diffuse and mix reasonably well throughout the volume of the sphere. Only at these later times, or equivalently in smaller volumes, is the signal concentration at the cell sensitive to the size of the containing volume.

We can say that sensing may occur when C at the cell exceeds a threshold C_0 that triggers activation of the QS circuit. In the case above, only a sufficiently large threshold $C_0 > \gamma/4\pi Da$ gives the cell any chance of diffusion sensing successfully:

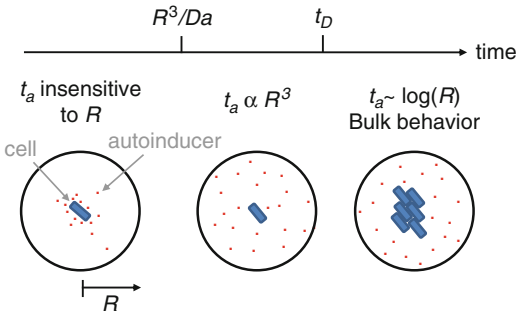

Fig. 7.2 For a bacterium growing at the center of a closed volume of radius R, the activation time t_a required for the autoinducer concentration $C(a, t)$ to reach a threshold C_0 exhibits different sensitivity to R, depending on the diffusion time scale R^3/Da and the population doubling time t_D. For a low threshold C_0, slow diffusion or large R, such that the sensing time scale $t \ll R^3/Da$, the activation time t_a is independent of R. For a higher threshold, faster diffusion or smaller R, such that $t \gg R^3/Da$, then $t_a \propto R^3$. If the sensing process occurs more slowly than the population growth ($t_a \gg t_D$), then t_a scales logarithmically in R, as in a well-stirred bulk culture

"Measuring" R requires that the time t needed to reach the threshold C_0 be sensitive to R. Equation (7.2) shows that at late times (or equivalently for small R^3/Da) the time to reach the threshold scales as R^3 and diffusion sensing behavior is possible. Moderate rates of degradation of the autoinducer do not significantly change this picture, as autoinducer molecules will likely have diffused far from the source cell by the time that they degrade.

The possibility of bacterial growth introduces some complications. Under favorable nutrient conditions a single bacterial cell may divide on a time scale of tens of minutes, with each of its daughter cells producing additional autoinducer. In the simplest description the number N of cells in the confining volume grows as

$$N \simeq 2^{t/tD} = \exp(\mu t).$$

Here t_D is the population-doubling time, which is related to the growth rate μ by $t_D = \log(2)/\mu$. For a culture of cells growing exponentially in a finite volume, the production of autoinducer will also grow exponentially. We can consider the implications for the diffusion sensing scenario by considering a cell located at the center of a confining spherical volume, where the cell divides at rate μ into daughter cells that also secrete autoinducer at the same rate γ, from the same central location. Again the concentration C at $r = a$ and time t is well approximated by the sum of two terms:

$$C(a,t) \simeq 3\gamma \ (\exp(\mu t) - 1)/4\pi\mu R^3 + \gamma \exp(\mu t)/4\pi Da \qquad (7.3)$$

Again the relative size of the two additive terms—and the sensitivity of $C(a, t)$ to R—depends on t and R. In particular it depends on how t compares to both the doubling time t_D and the characteristic diffusion time t^*. During the earliest stages

of growth ($t \ll t_D$) the situation is not different from the non-growth case above: In a large confining volume the concentration never reaches any threshold C_0 that is greater than $\gamma/4\pi Da$, while in a small confining volume the activation time is sensitive to R, scaling as $t \propto R^3$.

Once exponential growth is well underway, with $t \gg t_D$, then both terms in Eq. (7.3) grow exponentially in time. Once this happens, the time required to reach C_0 is at best only weakly sensitive to R. For example, if R is "large" in the sense that the second term in Eq. (7.3) dominates, then the time required for $C(a, t)$ to reach its threshold C_0 is independent of R and the QS circuit is insensitive to R. Instead the time to reach threshold is sensitive to the growth rate. On the other hand, if R is "small" so that the first term dominates, then the time t_a required for $C(a, t)$ to reach its threshold C_0 is determined by $C_0 \sim \gamma \exp(\mu t_a)/\mu R^3$, which means that $t_a \propto \log(R)$. That is, during exponential growth, the QS circuit's sensitivity to its confining volume is either poor (i.e., logarithmic in R) or nonexistent. In fact the logarithmic case applies only to a small range of R; it requires the general time scale t of sensing to be much larger than t_D while the container volume is not too large, $R^3 < Da/\mu$. If $D \simeq 10^{-7}$ cm^2/s, $a \sim 1$ μm, then this implies R must be less than about 20 μm. As the scenario also requires $t \gg t_D \sim 1{,}000$ s, it appears to describe the case in which a cluster of cells inhabits a volume as large as ∼30,000 μm^3, which is sufficient to contain ∼10,000 cells.

This last case is not very different from the case of a well-stirred bulk culture, in which many cells inhabit a much larger volume, and where again the time to reach threshold C_0 scales logarithmically with the volume of the container. The only difference is that here the cell is detecting the autoinducer of nearby cells, as opposed to that of distant cells in the bulk culture. Therefore, when the bacteria are actively growing the time scale for their QS activation grows at best logarithmically with the confining volume, the number of confined cells is large, and the overall physical picture is not very different from that of a bulk culture.

In short, diffusion sensing appears plausible for a QS circuit that exhibits a threshold response to its own signal. However the parameter regime in which it can acquire some information about the volume of its container is limited. Specifically, diffusion sensing is not physically dissimilar from bulk QS except in the narrow regime where the concentration threshold C_0, system size R, and growth rate $\mu \propto 1/t_D$ are such that $t \ll t_D$ and also $t > R^3/Da$ (Fig. 7.2).

7.3 Noise in Detection

A robust threshold response to autoinducer could allow an individual cell to gain useful information about its environment. However the response of real QS networks is not in general highly deterministic. Feedback and nonlinearity in the regulatory network may lead to hysteresis, in which the prior activation history of the circuit shapes its response to the present autoinducer signal level [9, 21]. The network is also subject to noise, which may in principle arise both in the signal input and in

the processing of that signal. We do not expect that the signal input will introduce significant noise in the QS response, even at low concentrations. The Berg–Purcell estimate [22] for the precision with which a concentration C of a diffusible signal in a finite detection volume can be measured over an integration time t is

$$\delta C/C \simeq 1/\sqrt{(DtaC)}.$$

If the radius of the detection volume is $a \simeq 1$ μm, the autoinducer diffusion coefficient $D \simeq 10^{-7}$ cm^2/s, and the concentration C of signal is ∼10 nM, then by measuring for $t \sim 100$ s the cell can determine C to a precision $\delta C/C \sim 1$ %. Therefore a QS circuit can in principle measure even a low concentration of signal to rather good precision.

The obstacle to a consistent response by an individual cell is not the small magnitude of the input signal, but rather noise in the QS regulatory pathway [23]. This noise arises from variability in the copy number of key regulatory molecules [24] as well as the underlying stochasticity of the chemical processes associated with transcription and translation [25–27]. Studies of QS activation in individual cells show that even in the presence of a uniform concentration of autoinducer, the QS networks that regulate the native bioluminescence of *Vibrio harveyi* [28, 29] and *V. fischeri* [30, 31] give a heterogeneous output. The LuxI/LuxR circuit of *V. fischeri,* for example, responds to *N*-3-oxohexanoyl L-homoserine lactone (3OC6HSL); Fig. 7.3 shows that even if this AHL is present at concentrations that saturate the bioluminescence output of a bulk culture, the light output from individual cells varies tenfold over a population. The distribution of responses is similar to a gamma distribution [31, 32] and is no sharper as the population-averaged activation level increases. Even in a brightly luminescing culture, many individual cells show little if any sign of activation; some 20–30 % of the cells are virtually dark, showing little if any bioluminescence. In addition the time scale of the response to the autoinducer signal is also heterogeneous, varying by at least a factor of ten across the population [30]. Similarly when autoinducer is supplied to *V. harveyi*, roughly 25 % of live cells exhibit only a small fraction of the luminescence of the brightest activated cells [28].

Given the noise in the QS circuit we cannot expect the individual cell to gather much useful information by diffusion sensing. When small numbers of cells carrying the LuxI/LuxR QS circuit were confined to a volume of a few picoliters, the time scale for their activation of a *gfp* reporter varied by roughly a factor of two [12]. Therefore, although a sixfold increase in the confining volume (3 pl → 18 pl) increased the average activation time, the increase was smaller than the cell-to-cell variation in any one volume. In this sense, the solitary cell confinement experiments (above) that can be viewed as evidence for the viability of the DS mechanism are more likely evidence against it: the time scale for activation of one cell's QS circuit is a very poor indicator of the cell's physical environment. In the following section we make this idea of information gathered (or lack thereof) by the QS network quantitative, using some ideas of information theory.

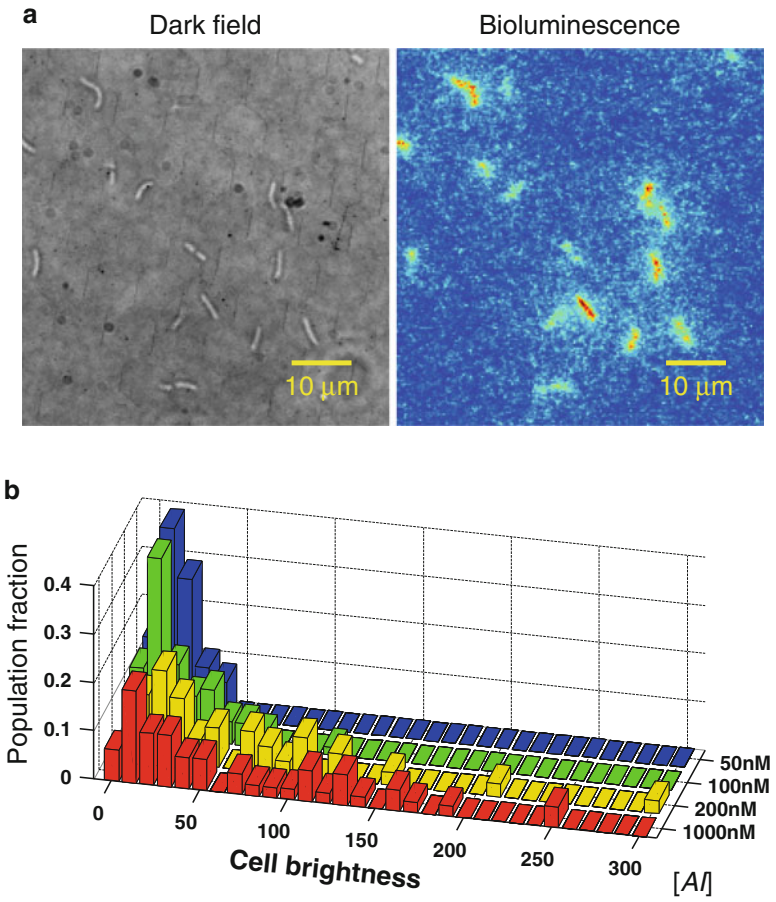

Fig. 7.3 Noise in the bioluminescence output of the LuxI/LuxR QS circuit of *V. fischeri*. The light output by individual cells in the presence of the 3OC6HSL autoinducer is highly variable. (**a**) Dark field and bioluminescence (false color) images of the same group of cells in saturating autoinducer (500 nM 3OC6HSL), showing highly variable luminescence output; (**b**) Histogram showing a broad distribution of luminescence output in a population of cells. Even at the highest autoinducer concentration (AI) the coefficient of variation in output is close to 100 % [30]

Because the noise arises in the regulatory circuit itself, simply increasing the signal concentration does not improve the information-gathering capacity of the QS system. Doubling the concentration of 3OC6HSL signal certainly does not improve the signal-to-noise ratio of the *V. fischeri* response. However, adding an additional signal input—i.e., introducing a parallel receptor channel that senses an additional autoinducer—is a potentially useful strategy, and many quorum sensing bacteria (including *Vibrio* species) do employ multiple autoinducer species and detectors. Further, since the average response of a group of cells is more reliable than the response of one individual cell, one may construct theoretical models for effective

quorum sensing communication based on the idea of clusters of cells interacting collectively with other clusters via multiple, diffusing signal species [33]. In general however, one key difference between QS networks and other chemical sensing systems (e.g., chemotaxis) seems to be that only at the level of the population-average is the output a very useful reporter of the input.

Nevertheless the QS circuit serves the microbe by gathering information about its environment. To better understand the microscopic-level performance of QS circuits in this task, we would like to quantify the information that they gather. Information theory provides the basis for calculating the amount of information that the output of a regulatory network provides about its inputs. Therefore in the following section we provide a brief introduction to information theory in its applications to QS.

7.4 The Information Carried in a Signal

Information theory in the more general context of chemical signaling and other types of biological communication has been reviewed elsewhere [34, 35]. Here we review a few basic ideas from information theory that may provide insight into the performance and optimization of QS circuits.

Suppose that X describes an environmental parameter that can take different values: a measurement of X yields a particular value x with a probability $P_X(x)$. How much information does the organism gain by measuring X? Information theory finds that the average gain is equal to the entropy $S(X)$ of the probability distribution $P_X(x)$, where the entropy is defined as [34]

$$S(X) = -\int \mathrm{d}x \; P_X(x) \log_2 P_X(x) \tag{7.4}$$

Here the integral extends over all observable values of x, and the appearance of the base-2 logarithm means that the information is measured in units of bits. The entropy $S(X)$ is a property of the parameter X—or really a property of its probability distribution $P_X(x)$—and not the specific result x obtained in one measurement. We note that $S(X)$ is larger if $P_X(x)$ is a broader, flatter distribution than if $P_X(x)$ is sharply peaked around a specific value of x. One gains little information by measuring a variable whose probability distribution is so narrow that the outcome of the measurement is highly predictable.

In QS, X could represent the concentration C of an autoinducer measured in a finite volume that contains an emitting cell. If the cell releases a small, finite quantity of autoinducer at $t = 0$, the concentration C is initially large near the cell and is very small at distant locations. Therefore the range of observable values for C is large. Consequently the probability distribution $P(C)$ for measurement of C is a broad distribution, and a measurement of C is capable of yielding information; it can be used, for example, to calculate the distance between the location where C was measured and the source of the signal. However, as time

passes, the autoinducer spreads diffusively and C becomes more uniform throughout the volume. Eventually, only a narrow range of values for C is now observable, and the probability distribution $P(C)$ becomes more sharply peaked at a single value. The measurement of C is now less informative. Diffusion of the signal reduces the amount of information that is present in its concentration profile $C(\boldsymbol{r}, t)$. This example illustrates a fundamental problem with using a diffusible signal (i.e., a QS mechanism) to gather information: generally the diffusional spreading of the autoinducer signal is accompanied by loss—not gain—of information. We should be somewhat skeptical that a cell can learn much about its environment by secreting a diffusible signal.

The bacterium uses a regulatory circuit to convert the environmental input X to an output Y, such as production of an exoenzyme. Because Y is sensitive to X and $P_X(x)$, and the regulatory circuit also introduces noise, Y is associated with a probability distribution $P_Y(y)$. Therefore the information gained in a measurement of Y is determined by the entropy $S(Y)$ that is calculated from Eq. (7.4) above. Clearly the QS system is not useful unless the regulatory output Y provides some information about X. The amount of information about X that is gained on average from a measurement of Y (and vice versa) is known as the mutual information $I(X, Y)$. Its value depends on $P_X(x)$, $P_Y(y)$ and the joint probability $P(x, y)$ for the measurement of X and Y together. It can be calculated from the expression [34]

$$I(X,Y) = \iint \mathrm{d}x\, \mathrm{d}y\; P(x,y) \log_2 \frac{P(x,y)}{P_X(x) P_Y(y)} \tag{7.5}$$

The integral extends over all observable values of x and y. If X and Y are statistically independent, such that $P(x, y) = P_X(x)\, P_Y(y)$, then this mutual information is found to be zero, because a measurement of Y yields no information about X.

If we make the plausible hypothesis that QS circuits are designed to optimize the information that their output provides about the environment, then we can hope that evaluating $I(X, Y)$ for real QS networks will generate insight into how those organisms use their QS networks to gather information. For many QS circuits we have a good idea of the function that relates X to Y. Often the regulated output can be represented as a Hill function of the autoinducer concentration x, with a source of noise as well,

$$y = \frac{x^n}{x^n + K^n} + (\text{noise}) \tag{7.6}$$

Here n is a Hill coefficient and K is an equilibrium constant [36]. If we have some information about the noise term, then we can in principle calculate the mutual information between the input and output. If the QS circuit employs multiple autoinducers (e.g., signals X_1 and X_2), we can also evaluate the mutual information between different variables, such as $I(X_1, Y)$, $I(X_2, Y)$, or $I((X_1, X_2), Y)$, etc. In the following we discuss a few instances where experimental data on QS systems have allowed researchers to pursue this approach.

The QS network that regulates the bioluminescence of the marine bacterium *V. harveyi* receives input from three autoinducers which are designated AI-1, AI-2, and CAI-2 [1]. The signals are detected by three receptors LuxPQ, LuxN, and CqsS. Signals from the three receptors are integrated through their kinase activity in phosphorylating a single enzyme LuxU, which relays the collected signal downstream by phosphorylating LuxO. Long et al. found the dose response to AI-1 and AI-2 to be symmetric and additive, in the sense that both autoinducer concentrations contribute equally and additively to the bioluminescence circuit output Y [29, 37]. Given the measured noise in the output Y—which was actually the activity of a *gfp* reporter—Mehta et al. [37] estimated the total mutual information $I((X_1, X_2), Y)$ between the output and the two (AI-1 and AI-2) inputs as roughly 1.5 bits. That is, the system exhibits almost three ($\simeq 2^{1.5}$) output states in responding to the state of the two input AHL concentrations. However, if only one of the two inputs (e.g., AI-1) is specified, while the other input is unknown, then the mutual information between the one input and the overall output Y is significantly lower. The authors estimated that this situation reduces the mutual information between X_1 and Y to roughly 0.6–0.8 bits. That is, if the concentration of the second autoinducer is not specified, then it can be known only probabilistically and it therefore becomes a source of uncertainty or interference in the circuit. If the circuit output is used to estimate just one input signal, the lack of knowledge of the other, unknown signal reduces the information throughput.

Moreover, the sensitivity of the two channels needs to be balanced in order to maximize the information throughput. If the kinase activity of one AHL receptor is very different from that of the other, then the circuit has greater sensitivity to the input with the stronger kinase, with accordingly more information transmitted through that input at the expense of information transmission through the weaker input. In order to extract the maximum information from dual inputs the circuit needs to give equal weight (equal kinase strength) to both input channels [37]. This QS system appears to use the parallel detection of chemically distinct autoinducers, through independent channels, to increase the amount of information that it can gather from the environment.

An interesting contrast is seen in the *lux* regulatory system that controls bioluminescence of *V. fischeri.* The LuxI/LuxR system of *V. fischeri* resembles that of *V. harveyi* in the sense that it also integrates three different autoinducer signals. These include two AHLs, i.e. the *N*-3-oxohexanoyl L-homoserine lactone (3OC6HSL) that is detected by the LuxR receptor and the *N*-octanoyl L-homoserine lactone (C8HSL) that interacts with the receptor AinR. The 3OC6HSL stimulates the *lux* operon while the effect of C8HSL is more complex. C8HSL interacts not only with AinR but also directly with LuxR, in competition with 3OC6HSL. In the absence of 3OC6HSL, the C8HSL may weakly activate *lux,* while in the presence of 3OC6HSL the addition of C8HSL may suppress *lux*. Therefore unlike the autoinducers of *V. harveyi*, the *V. fischeri* autoinducers act antagonistically, rather than additively, in their activation of *lux*.

Pérez et al. [31] studied the response of individual *V. fischeri* (containing a *gfp* reporter for the *lux* operon) to combinations of the C8HSL and 3OC6HSL inputs.

The study showed, first, that the use of two autoinducers does not reduce the noise in *lux* regulation. In *V. fischeri* the noise in *lux* output is a function only of the total activation level, and not the particular combination of signal inputs that produce that activation. Consequently the mutual information between the input signal combination ([C8HSL], [OC6HSL]) and the output (*lux* activation) was estimated at only about 0.53 bits, significantly less than the roughly 1.5 bits estimated by Mehta et al. for *V. harveyi*. As the bioluminescence is noisy with a coefficient of variation (= standard deviation/mean) cv $\simeq 1$, the *lux* system of *V. fischeri* is much noisier than that of *V. harveyi,* for which cv $\simeq 0.15$–0.4. In short, the mutual information in the QS circuit of *V. fischeri* is not enhanced through its use of two autoinducers.

Given that the *V. fischeri* AHLs have opposite effects on the activation of the circuit, these considerations of mutual information suggests that multiple autoinducers play a different role in *V. fischeri* than in *V. harveyi*. Rather than reducing noise in the circuit, the two signals may work antagonistically to minimize noise-driven activation of the QS circuit early in growth, when population densities are low [31]. Because even modest 3OC6HSL-induced activation of the *lux* circuit causes a few individual cells to emit bright bioluminescence [30], the production of small amounts of C8HSL may serve to suppress that energy-wasting response early in colony growth. This has no negative consequence at the higher 3OC6HSL levels that are found late in growth, as C8HSL has little effect on bioluminescence output under these conditions.

Using equation Eq. (7.5) to calculate $I(X, Y)$ from experimental data requires knowledge of the "prior distribution," or probability distribution $P_X(x)$ for the input variable X. It is unlikely that $P_X(x)$ is actually known for the organism in its natural environment(s). Therefore, the above calculations of $I(X, Y)$ for real bacteria depend on assumptions or estimates of the shape of $P_X(x)$. Both of the *Vibrio* analyses above were based in part on an assumption of a flat prior distribution for the activating inputs. Specifically, they assumed a flat distribution $P_X(x)$ such that all values $0 \leq x \leq 1$ are equally likely, where X represents the saturation of an underlying binding process involving the autoinducer concentration AI:

$$y = cx + (\text{noise}) \tag{7.7}$$

$$x = \frac{[\text{AI}]^n}{[\text{AI}]^n + K^n}$$

However, if the QS circuit is optimized to gather information from its environment, we may expect that n, K are tuned to maximize $I(X, Y)$ with respect to the true $P_X(x)$. This suggests in turn that the true $P_X(x)$—and also the true $P_Y(y)$—is the one that maximizes $I(X, Y)$, given the input–output relation and noise of the QS circuit [34, 38]. If the QS circuit adds only small, gaussian noise, then the optimal $P_Y(y)$ is a flat distribution, independent of y, with $P_Y(y)\mathrm{d}y = P_X(x)\mathrm{d}x$. Then regardless of how the input X is defined mathematically (whether X represents the autoinducer concentration as in Eq. (7.6) or the saturation of its binding as in Eq. 7.7), then the mutual information is optimal for $P_X(x) = P_Y(y)\ |\mathrm{d}y/\mathrm{d}x|$.

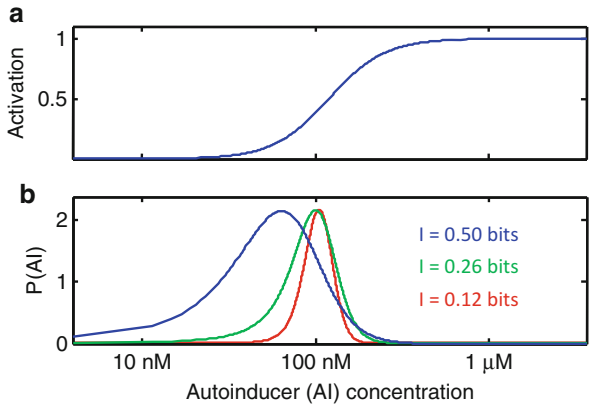

Fig. 7.4 (**a**) Activation profile for the *V. fischeri* bioluminescence QS circuit in response to 3OC6HSL autoinducer (AI) concentration. The sketch is based on experimental data that indicate a Hill function response with $n = 2.7$ and $K = 120$ nM [30]. The mutual information between the 3OC6HSL input and bioluminescence output can be calculated from this curve, the probability distribution $P(\mathrm{AI})$ for the signal input, and the experimental observation that the noise coefficient of variation (standard deviation/mean) is roughly unity at all levels of activation; (**b**) Shifts in $P(\mathrm{AI})$ significantly affect the mutual information between the circuit response and the signal input [AI]. The distributions $P(\mathrm{AI})$ have been scaled to same maximum for plotting

This hypothesis of optimal signal input has found experimental support in some other chemical signaling problems in biology, such as in morphogenesis [38]. For QS systems with Hill function response to autoinducers it sensibly implies that the natural range of autoinducer concentrations is most likely near the middle of the Hill function, where $[\mathrm{AI}] \sim K$.

In the LuxR/LuxI circuit of *V. fischeri* the noise is neither small nor Gaussian and so the true optimal probability distribution for the autoinducer signal concentration is not readily found. However Fig. 7.4 shows how the mutual information for that system would depend on different probability distributions for the signal concentration. Even in the presence of significant noise ($\mathrm{cv} \simeq 1.0$) modest shifts in the probability distribution $P(\mathrm{AI})$ can induce large (e.g., twofold or greater) shifts in the mutual information between input and output. It is interesting that strain differences and single-residue mutations of LuxR are known that significantly modulate the interaction between the two AHLs 3OC6HSL and C8HSL [39–41] in their effect on the *lux* genes. One route toward interpreting such bacterial strain differences in the sensitivity of QS networks may lie in interpreting the sensitivity parameters (n, K) for the different strains and autoinducers as providing the maximum information to the organism in the particular environments that those strains inhabit.

7.5 Spatial Range and Sensing

A lone microbe in solitary confinement represents one extreme scenario for studying QS. A large population of microbes in a perfectly mixed culture represents an opposite extreme. Between those two extremes are scenarios where many cells are present, mixing is imperfect, and the diffusion of autoinducer is neither fast nor slow on the time scale of gene expression. In biofilms or soils for example, AHL may be transported primarily by diffusion, leading to slow signaling over long distances. In such cases we anticipate that long range QS communication may face significant physical and chemical obstacles. The response of a population of bacteria is likely to be spatially and temporally heterogeneous. Studying these systems may tell us how effectively quorum sensing can synchronize gene expression in such environments. It may also tell us what kind of information a single cell can gather about its location with respect to other cells by detecting the QS signals that move through its environment.

In any environment the diffusive transport of autoinducer is limited at least by its diffusion coefficient D, its solubility, and its chemical stability [42]. The diffusion constants of AHLs are roughly estimated in the range of $\sim 5 \times 10^{-6}$ cm^2/s [43]. However, typical bacterial environments such as biofilms, the plant root zone, and flocculent materials have complex physical and chemical structure at micron length scales. Flow or advection may be nonexistent, so that AHL signals must travel almost entirely by diffusion. Physical diffusion may be restricted by poor spatial connectivity (tortuosity). Chemical interference from signaling by other bacterial and eukaryotic species is rampant [44]. AHL signals in such environments are also subject to degradation by enzymes (e.g., lactonases and acylases), alkaline pH, or high temperature [2, 42, 45, 46]. Clusters of confined bacteria may generate intense local gradients in chemical variables such as pH or oxygen concentration [47, 48]. Furthermore, the longer chain AHLs are hydrophobic and therefore are anticipated to have solubilities below 100 μM; they will therefore partition preferentially into hydrophobic phases, possibly including the lipid membrane of the cells [42]. While some smaller AHLs diffuse passively across the cell membrane, other long chain AHLs are known to require active transport out of the cell [49].

In short, there are many reasons to be pessimistic about the possibility that simple diffusion of an AHL can lead to effective communication over macroscopic distances. The final hindrance, however, is usually expected to be the slow speed of diffusive transport. If $D \sim 5 \times 10^{-6}$ cm^2/s, the signal requires $t \sim 1$ h to travel roughly 2 mm. Therefore the microbiology literature often asserts that, given (e.g.) soil/rhizosphere conditions and relevant time scales, true chemical communication over distances beyond 10–100 μm is unlikely [2, 42, 43, 50].

Nevertheless there have been some experiments aimed at measuring the distance or range over which a diffusing AHL signal can trigger gene expression. Gantner et al. [51] explored this idea of "calling distance" in quorum sensing *Pseudomonas putida* growing on plant root surfaces. They used a two-color fluorescent-protein reporting scheme, in which AHL-synthesizing cells produced red fluorescent protein

and AHL-sensing cells produced green fluorescent protein. They found that the in situ distance between a green AHL-sensing cell and the nearest red AHL-synthesizing cell was typically 2–20 μm in the root hair zone, although it was occasionally as large as 40–78 μm, or roughly 40× the 1–2 μm dimension of the cells themselves. While neither the amount of AHL synthesis nor the geometry of its diffusion were controlled in that experiment, the maximum calling distances were certainly larger than expected.

However a "large" distance of many microns corresponds to a brief time scale for diffusion: An AHL can diffuse over a calling distance of $L = 80$ μm in a time of only $t \simeq L^2/2D = 6$ s. Nevertheless the experiment does raise the question of whether bacteria can respond to AHL signals that are diffusing over longer distances, over periods of minutes or hours.

A subsequent study using a microfabricated array found a substantially greater length scale for signaling [52]. Those authors found that simple diffusion of the AHL secreted from a *P. aeruginosa* biofilm was sufficient to induce a response in cells growing up to 8 mm away. This result corresponds to a diffusion time $t \geq 10$ h, drastically longer than in the Gantner et al. study. It raises the question of whether we can quantify the effectiveness of QS communication on longer, macroscopic scales.

Dilanji and coworkers [20] addressed this question by studying the spatial and temporal patterns of gene regulation that are induced by the diffusion of a known quantity of AHL through a colony of bacteria. The bacteria contained the LuxR intracellular receptor of the *V. fischeri* LuxR/LuxI system, where LuxR activated a *gfp* reporter in response to the 3OC6HSL autoinducer. (The LuxI synthase of the autoinducer was absent.) The experiment imposes a near-ideal, one-dimensional geometry by introducing a droplet of AHL (3OC6HSL) at one terminus of a long agar lane. As the autoinducer slowly diffuses along the lane it activates the *gfp* reporter in the bacteria embedded in the agar, producing spatial and temporal patterns of fluorescence emission. Figure 7.5 shows the activation pattern as a function of time t (from introduction of the AHL) and distance x (from the point where the AHL was introduced). Remarkably, in both *V. fischeri* (*luxI* deficient) and in *E. coli* harboring the LuxR receptor, a response is observed over distances as large as $\simeq$10 mm from the site of AHL introduction, roughly 10–12 h after the AHL was introduced. The diffusible signal is capable of synchronizing regulation over distances far greater than 100 μm.

We might have anticipated that the temporal profile of the QS circuit's response as a function of distance would have the simple diffusion property of $t \propto L^2/2D$, seen in Fig. 7.5a: i.e., the signal spreads quickly at early times, but much more slowly as it moves farther away. If that were the case, the bacterium in a biofilm could gain some information about its distance from an AHL source by the time scale of its own QS activation. However the kinetics of the QS response in Fig. 7.5d have different properties. First, at a distance of 10 mm the response time scale of 10–12 h is noticeably faster than the time scale $t \simeq L^2/2D = 28$ h that one would estimate simply from diffusion of the AHL. Second, bacteria at all spatial locations $\leq$10 mm from the AHL source respond at essentially the same time. They also respond with an amplitude that is not especially sensitive to their distance from the

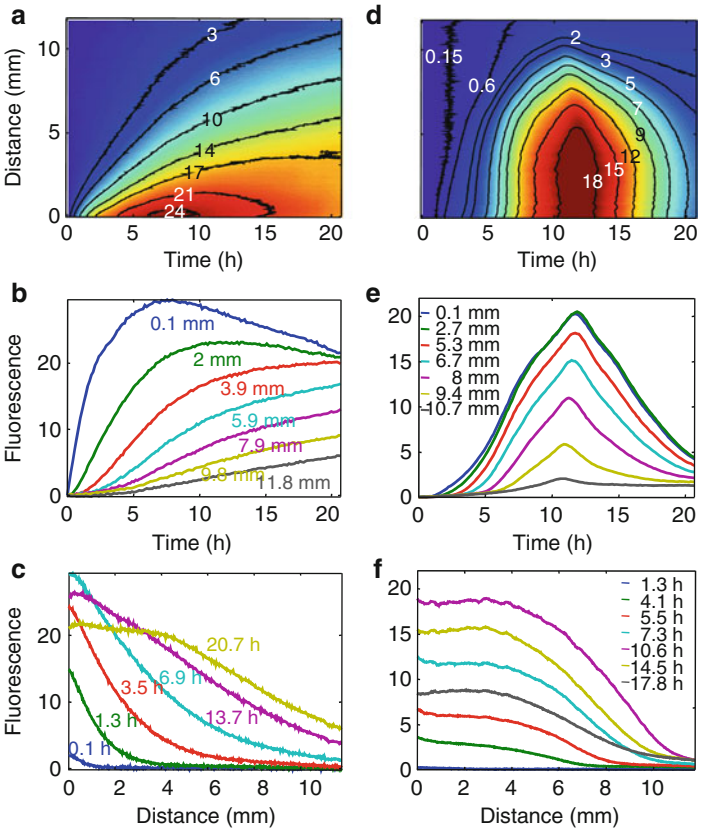

Fig. 7.5 Spatial and temporal pattern resulting from (**a**–**c**) simple diffusion of a fluorescent dye in one dimension, and (**d**–**f**) activation of a QS circuit by an autoinducer diffusing through a one-dimensional colony. In (**a**–**c**) a droplet of fluorescent dye is deposited at $x = 0$ at $t = 0$, and diffuses to larger x, leading to the resulting patterns of fluorescence in space and time (**a**), which are also shown in temporal (**b**) and spatial (**c**) cross sections. In (**d**–**f**) a droplet of 3OC6HSL is introduced at one terminus of a lane containing *AHL*-sensing bacteria (with LuxR controlling a *gfp* reporter, and lacking LuxI AHL synthase). The resulting pattern of GFP fluorescence (**d**), which is also shown in spatial and temporal sections (**e** and **f**), is qualitatively unlike the simple diffusion pattern of (**a**) [20]

source. In fact, the response throughout the agar lane is so well synchronized in time that it has an interesting mathematical property: If a droplet of AHL is introduced at $x = 0$, $t = 0$ and begins diffusing outward, then we can say that $F(x, t)$ is the degree of subsequent activation of the *lux* reporter at location x and time t. Formally, $F(x, t)$ can be represented as a series of terms containing separate spatial and temporal components

$$F(x,t) \simeq u_1(x)sv_1(t) + u_2(x)sv_2(t) + \cdots$$

The experimental data of Fig. 7.5d–f shows that the first term completely dominates this sum. All the spatial cross sections in Fig. 7.5e–f are similar ($\propto u_1(x)$) except in scale, and all of the temporal cross sections ($\propto sv_1(t)$) are similar except in scale. The activation profile $F(x, t)$ is primarily just the product of a spatial function $u_1(x)$ and a temporal function $sv_1(t)$.

This curious property is uncharacteristic of the solutions $C(x, t)$ of the diffusion equation which are shown in Fig. 7.5a–c. It owes something to the nonlinear character of the QS circuit's response to AHL concentration, and also to one of the less appreciated properties of simple diffusion. While a very long time is required for the overall AHL concentration in a large volume to become fully equilibrated by diffusion, a very small number of the particles that are introduced at one location will travel a long distance within a short period of time. Shortly after the AHL is introduced at one terminus of the lane, a few molecules have traveled a macroscopic distance through the agar. Owing to the very nonlinear (Hill function), nearly all-or-nothing character of the QS circuit's AHL response, the quick arrival of a small concentration of signal is sufficient to induce a fairly complete switching of the QS circuit throughout a substantial part of the colony.

Therefore, from the perspective of control, Fig. 7.5 shows that a signal traveling purely by diffusion can be surprisingly effective in synchronizing gene expression over a macroscopic distance.

However, such effective synchrony represents a problem for spatial information gathering by the population. The spatial profile of the maximum response (at $t \sim 10$–12 h) is fairly independent of x up to about 5 mm, and then it drops off quickly at larger x. Cells near ($x \leq 5$ mm) the source are maximally activated at the same time, while more distant cells are never activated. The same temporal profile is observed at all locations x, and the same (mostly flat) spatial profile $u_1(x)$ is observed at all times t. Therefore the probability distribution for the activation time $P(t_a)$ is sharply peaked at $t_a \sim 10$ h, indicating that a cell gains little information about its physical location by "measuring" its activation time t_a: there is little or no mutual information between the activation timescale and the cell's physical location in the colony. More broadly, because the individual cell responds to the AHL concentration in a mostly binary on/off fashion, a sensing bacterium—or a cluster of bacteria—can at best distinguish two locations—i.e., near and far—with respect to the source of the AHL. It cannot use the AHL's concentration profile $C(x, t)$ to implement a complex, spatial–temporal pattern of QS response. This is quite unlike the very precise spatial sensing that is accomplished through chemical signaling in morphogenesis, for example, where individual cells decode the concentration of a single diffusing morphogen to high precision and respond by implementing a complex program of gene activation [53, 54].

7.6 Conclusions

Quorum sensing is a remarkable behavior that regulates many functions in different types of bacterial populations inhabiting different social and physical environments. In interpreting QS systems as information-gathering devices it is important to think about what physically can and cannot be accomplished through the exchange of diffusible signals. The physics of diffusion are somewhat limiting unfortunately, and tend to suggest that detailed spatial information is difficult to gather with diffusible probes. Experimental evidence further indicates that noise in QS sensing circuits sharply limits the ability of an individual cell to gather and respond reliably to information received from these signals. Although collectively a cluster or a larger population of cells can benefit by averaging over the noise, there is little evidence that QS circuits are optimized for the benefit of the individual cell. In fact the observation that some quorum sensing regulated behaviors, such as genetic competence, directly exploit stochasticity in gene expression suggests that poor information throughput can be more a design feature than a shortcoming in quorum sensing systems.

On the other hand, the prevalence of QS is proof of its usefulness at the group-averaged level of clusters and cultures of cells. Despite the problems associated with diffusing signals, QS can provide surprisingly good spatial synchronization of gene regulation over macroscopic distances. Somewhat paradoxically, this is equivalent to saying that the state of its gene activation provides the cell with virtually no information about its spatial or temporal situation with respect to other cells.

It is perhaps surprising that the diffusing signal delivers so little spatial information to the cell, as there are certainly environments where the cell could benefit from information about its location with respect to the rest of the colony. The production and detection of multiple autoinducers could help QS bacteria in these situations gain spatial information. Additional spatial information may be available if the different autoinducers diffuse with significantly different coefficients D. Another interesting possibility arises if the autoinducer concentration provides regulatory input to more than one QS system, activating or repressing different combinations of independent genes to different extents as the autoinducer concentration evolves in time. Thus, even if the state of each gene provides ≤ 1 bit of information about the signal, the state of all the genes together could allow a higher precision readout of the local signal concentration, possibly permitting the organism to interpret its physical location with respect to other AHL sources. The soil microbe *Sinorhizobium meliloti* is an appealing candidate for such mechanism, as its SinI/SinR/ExpR QS circuit produces and detects multiple distinct AHL species with C12–C18 side chains [55, 56]. Many of these AHLs are poorly soluble and presumably vary in their diffusive mobility. Further *S. meliloti* AHL receptor ExpR was recently found to interact with multiple binding sites with different AHL sensitivity [57]. Consequently multiple regulated genes have the capability to respond at different AHL concentrations. We may anticipate that substantially greater mutual information between the overall output state and the position is

possible in such cases. Whether the organism can actually use such mechanisms to extract more information from the diffusing signal is an intriguing question that remains to be explored.

Acknowledgments This work was supported in part by an award from the National Science Foundation, MCB 0347124. The author also gratefully acknowledges current and former members and associates of the laboratory, including Patrick De Leenheer, Gabriel Dilanji, Minjun Son, Jessica Langebrake, Rupika Madhavan, Lauren McLeod, Pablo Pérez, Max Teplitski, and Joel Weiss.

References

1. Waters CM, Bassler BL (2005) Quorum sensing: cell-to-cell communication in bacteria. Annu Rev Cell Dev Biol 21:319–346
2. Boyer M, Wisniewski-Dye F (2009) Cell–cell signalling in bacteria: not simply a matter of quorum. FEMS Microbiol Ecol 70:1–19
3. Dunn AK, Stabb EV (2007) Beyond quorum sensing: the complexities of prokaryotic parliamentary procedures. Anal Bioanal Chem 387:391–398
4. Ng WL, Bassler BL (2009) Bacterial quorum-sensing network architectures. Annu Rev Genet 43:197–222
5. Alberghini S, Polone E, Corich V, Carlot M, Seno F, Trovato A, Squartini A (2009) Consequences of relative cellular positioning on quorum sensing and bacterial cell-to-cell communication. FEMS Microbiol Lett 292:149–161
6. Hense BA, Kuttler C, Mueller J, Rothballer M, Hartmann A, Kreft J (2007) Opinion – does efficiency sensing unify diffusion and quorum sensing? Nat Rev Microbiol 5:230–239
7. Platt TG, Fuqua C (2010) What's in a name? The semantics of quorum sensing. Trends Microbiol 18:383–387
8. Redfield RJ (2002) Is quorum sensing a side effect of diffusion sensing? Trends Microbiol 10:365–370
9. Melke P, Sahlin P, Levchenko A, JÃnsson H (2010) A cell-based model for quorum sensing in heterogeneous bacterial colonies. PLoS Comput Biol 6:e1000819
10. Boedicker JQ, Vincent ME, Ismagilov RF (2009) Microfluidic confinement of single cells of bacteria in small volumes initiates high-density behavior of quorum sensing and growth and reveals its variability. Angew Chem Int Ed Engl 48:5908–5911
11. Carnes EC, Lopez DM, Donegan NP, Cheung A, Gresham H, Timmins GS, Brinker CJ (2010) Confinement-induced quorum sensing of individual *Staphylococcus aureus* bacteria. Nat Chem Biol 6:41–45
12. Hagen S, Son M, Weiss J, Young J (2010) Bacterium in a box: sensing of quorum and environment by the LuxI/LuxR gene regulatory circuit. J Biol Phys 36:317–327
13. Connell JL, Wessel AK, Parsek MR, Ellington AD, Whiteley M, Shear JB (2010) Probing prokaryotic social behaviors with bacterial "Lobster traps". MBio 1:e00202-10
14. Connell JL, Whiteley M, Shear JB (2012) Sociomicrobiology in engineered landscapes. Nat Chem Biol 8:10–13
15. West SA, Winzer K, Gardner A, Diggle SP (2012) Quorum sensing and the confusion about diffusion. Trends Microbiol 20:586–594
16. Mashburn LM, Whiteley M (2005) Membrane vesicles traffic signals and facilitate group activities in a prokaryote. Nature 437:422–425
17. Langebrake JB (2013) Examples of reaction–diffusion equations in biological systems: marine protected areas and quorum sensing. PhD Dissertation, University of Florida

18. Ward JP, King JR, Koerber AJ, Croft JM, Sockett RE, Williams P (2003) Early development and quorum sensing in bacterial biofilms. J Math Biol 47:23–55
19. Danino T, Mondragon-Palomino O, Tsimring L, Hasty J (2010) A synchronized quorum of genetic clocks. Nature 463:326–330
20. Dilanji GE, Langebrake JB, De Leenheer P, Hagen SJ (2012) Quorum activation at a distance: spatiotemporal patterns of gene regulation from diffusion of an autoinducer signal. J Am Chem Soc 134:5618–5626
21. Williams JW, Cui X, Levchenko A, Stevens AM (2008) Robust and sensitive control of a quorum-sensing circuit by two interlocked feedback loops. Mol Syst Biol 4:234
22. Berg HC, Purcell EM (1977) Physics of chemoreception. Biophys J 20:193–219
23. Raj A, van Oudenaarden A (2008) Nature, nurture, or chance: stochastic gene expression and its consequences. Cell 135:216–226
24. Teng S, Wang Y, Tu KC, Long T, Mehta P, Wingreen NS, Bassler B, Ong NP (2010) Measurement of the copy number of the master quorum-sensing regulator of a bacterial cell. Biophys J 98:2024–2031
25. Cox CD, Peterson GD, Allen MS, Lancaster JM, McCollum JM, Austin D, Yan L, Sayler GS, Simpson ML (2003) Analysis of noise in quorum sensing. OMICS 7:317–334
26. Weber M, Buceta J (2011) Noise regulation by quorum sensing in low mRNA copy number systems. BMC Syst Biol 5:11
27. Weber M, Buceta J (2013) Dynamics of the quorum sensing switch: stochastic and non-stationary effects. BMC Syst Biol 7:6
28. Anetzberger C, Pirch T, Jung K (2009) Heterogeneity in quorum sensing-regulated bioluminescence of *Vibrio harveyi*. Mol Microbiol 73:267–277
29. Long T, Tu KC, Wang Y, Mehta P, Ong NP, Bassler BL, Wingreen NS (2009) Quantifying the integration of quorum-sensing signals with single-cell resolution. PLoS Biol 7:640–649
30. Pérez PD, Hagen SJ (2010) Heterogeneous response to a quorum-sensing signal in the luminescence of individual *Vibrio fischeri*. PLoS One 5:e15473
31. Pérez PD, Weiss JT, Hagen SJ (2011) Noise and crosstalk in two quorum-sensing inputs of *Vibrio fischeri*. BMC Syst Biol 5:153
32. Cai L, Friedman N, Xie XS (2006) Stochastic protein expression in individual cells at the single molecule level. Nature 440:358–362
33. Einolghozati A, Sardari M, Fekri F (2013) Design and analysis of wireless communication systems using diffusion-based molecular communication among bacteria. IEEE Trans Wirel Commun 12:6096–6105
34. Bialek W (2012) Biophysics: searching for principles. Princeton University Press, Princeton
35. Waltermann C, Klipp E (2011) Information theory based approaches to cellular signaling. Biochim Biophys Acta 1810:924–932
36. Phillips R, Kondev J, Theriot J, Garcia H (2012) Physical biology of the cell. Garland Science, New York
37. Mehta P, Goyal S, Long T, Bassler BL, Wingreen NS (2009) Information processing and signal integration in bacterial quorum sensing. Mol Syst Biol 5:325
38. Tkacik G, Callan CG Jr, Bialek W (2008) Information flow and optimization in transcriptional regulation. Proc Natl Acad Sci U S A 105:12265–12270
39. Collins CH, Arnold FH, Leadbetter JR (2005) Directed evolution of *Vibrio fischeri* LuxR for increased sensitivity to a broad spectrum of acyl-homoserine lactones. Mol Microbiol 55:712–723
40. Kuo A, Blough NV, Dunlap PV (1994) Multiple N-acyl-*L*-homoserine lactone autoinducers of luminescence in the marine symbiotic bacterium *Vibrio-fischeri*. J Bacteriol 176:7558–7565
41. Kuttler C, Hense BA (2008) Interplay of two quorum sensing regulation systems of *Vibrio fischeri*. J Theor Biol 251:167–180
42. Decho AW, Frey RL, Ferry JL (2011) Chemical challenges to bacterial AHL signaling in the environment. Chem Rev 111:86–99
43. Stewart PS (2003) Diffusion in biofilms. J Bacteriol 185:1485–1491

44. Teplitski M, Mathesius U, Rumbaugh KP (2011) Perception and degradation of N-acyl homoserine lactone quorum sensing signals by mammalian and plant cells. Chem Rev 111:100–116
45. Horswill A, Stoodley P, Stewart P, Parsek M (2007) The effect of the chemical, biological, and physical environment on quorum sensing in structured microbial communities. Anal Bioanal Chem 387:371–380
46. Wang Y, Leadbetter JR (2005) Rapid acyl-homoserine lactone quorum signal biodegradation in diverse soils. Appl Environ Microbiol 71:1291–1299
47. Flemming H, Wingender J (2010) The biofilm matrix. Nat Rev Microbiol 8:623–633
48. Stewart PS, Franklin MJ (2008) Physiological heterogeneity in biofilms. Nat Rev Microbiol 6:199–210
49. Pearson JP, Van Delden C, Iglewski BH (1999) Active efflux and diffusion are involved in transport of *Pseudomonas aeruginosa* cell-to-cell signals. J Bacteriol 181:1203–1210
50. Prosser JI (2012) Ecosystem processes and interactions in a morass of diversity. FEMS Microbiol Ecol 81:507–519
51. Gantner S, Schmid M, Dürr C, Schuhegger R, Steidle A, Hutzler P, Langebartels C, Eberl L, Hartmann A, Dazzo FB (2006) In situ quantitation of the spatial scale of calling distances and population density-independent N-acylhomoserine lactone-mediated communication by rhizobacteria colonized on plant roots. FEMS Microbiol Ecol 56:188–194
52. Flickinger ST, Copeland MF, Downes EM, Braasch AT, Tuson HH, Eun Y, Weibel DB (2011) Quorum sensing between *Pseudomonas aeruginosa* biofilms accelerates cell growth. J Am Chem Soc 133:5966–5975
53. Alon U (2007) An introduction to systems biology: design principles of biological circuits. Chapman & Hall/CRC, London
54. Gregor T, Tank DW, Wieschaus EF, Bialek W (2007) Probing the limits to positional information. Cell 130:153–164
55. Marketon MM, Gronquist MR, Eberhard A, González JE (2002) Characterization of the *Sinorhizobium meliloti* sinR/sinI locus and the production of novel N-acyl homoserine lactones. J Bacteriol 184:5686–5695
56. Teplitski M, Eberhard A, Gronquist MR, Gao M, Robinson JB, Bauer WD (2003) Chemical identification of N-acyl homoserine lactone quorum-sensing signals produced by *Sinorhizobium meliloti* strains in defined medium. Arch Microbiol 180:494–497
57. Charoenpanich P, Meyer S, Becker A, McIntosh M (2013) Temporal expression program of quorum sensing-based transcription regulation in *Sinorhizobium meliloti*. J Bacteriol 195(14):3224–3236

Chapter 8
Interplay Between Sibling Bacterial Colonies

Avraham Be'er, Sivan Benisty, Gil Ariel, and Eshel Ben-Jacob

8.1 Introduction

8.1.1 Using Intelligence to Cope with Stress

Bacteria in the wild are frequently exposed to harsh conditions, the sources of which include, but are not limited to, a lack of available nutrients, overcrowding and space limitations, the presence of enemies, and extreme environmental conditions, such as high temperatures and dryness. Their responses to stress can consist of radical behaviors, such as the deadly competition often observed between individuals of the same species [1–5].

The first and most fundamental of all organisms, bacteria have evolved mechanisms to ensure their survivability when faced with harsh conditions [6, 13]. They lead rich social lives in complex hierarchical communities, collectively sense the environment to glean information, learn from past experience, and make decisions. To engage in such complex, cooperative behavior, bacteria utilize highly sophisticated chemical communication mechanisms whose chemical language includes semantic and even pragmatic aspects [7].

A. Be'er (✉) • S. Benisty
Zuckerberg Institute for Water Research, The Jacob Blaustein Institutes for Desert Research, Ben-Gurion University of the Negev, Sede Boqer Campus, 84990 Midreshet Ben-Gurion, Israel
e-mail: beera@bgu.ac.il

G. Ariel
Department of Mathematics, Bar-Ilan University, Ramat Gan 52000, Israel

E. Ben-Jacob
School of Physics and Astronomy, Raymond and Beverly Sackler Faculty of Exact Sciences, Tel Aviv University, Tel Aviv 69978, Israel

Center for Theoretical Biological Physics, Rice University, Houston, TX 77025, USA

S.J. Hagen (ed.), *The Physical Basis of Bacterial Quorum Communication*, Biological and Medical Physics, Biomedical Engineering, DOI 10.1007/978-1-4939-1402-9_8

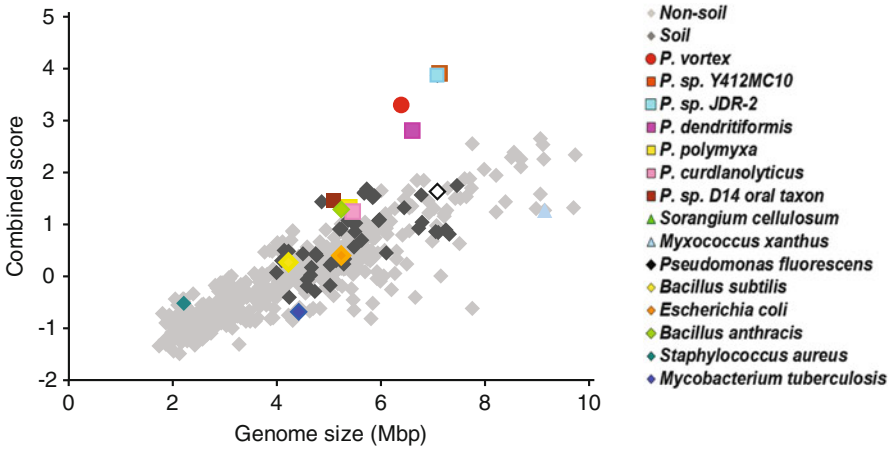

Fig. 8.1 The combined social IQ score as a function of genome size for 502 bacterial species. The *y*-axis represents the relative combined score (relative to the averaged score divided by the standard deviations). The social IQ scores of the "smart" *P. dendritiformis* are nearly three standard deviations above normal. Image was taken from [8] with minor modifications

The bacterial capacity to cope with stress is based on each species' distinctive abilities. While some bacteria are "goofs," others are "smart" and are able to survive a large variety of complex situations. Bacterial survivability is correlated with the microbial signal transduction system, which can be viewed as an information processing network comprising multiple sensory and transduction/output elements [8]. Comparative genomic studies revealed that, in general, microbial signal transduction system size increases as genome size grows [8]. Moreover, bacteria with elevated adaptability for survival in highly versatile and complex environments were found to have significantly larger, more sophisticated, and more diverse signal sensing and processing systems (Fig. 8.1). The relative numbers of the genes behind these systems can give a sense of "bacterial IQ," a measure that was found to be remarkably high for the *Paenibacilli* spp. (Fig. 8.1).

8.1.2 Paenibacillus dendritiformis

First identified in 1993, *Paenibacilli* spp. have been detected in a wide range of environments such as soil, water, the rhizosphere, vegetable matter, insect larvae, and in clinical samples. Recent years have witnessed increased interest in *Paenibacillus* spp., many of which were found to be important for industrial, agricultural, and medical applications. These bacteria produce extracellular substances, such as polysaccharide-degrading enzymes and proteases, which catalyze a wide variety of synthetic reactions in fields ranging from cosmetics to biofuel production. In addition, some *Paenibacillus* spp. also produce antimicrobial substances that affect

a wide spectrum of micro-organisms such as fungi, soil bacteria, plant pathogenic bacteria, and anaerobic pathogens such as *Clostridium botulinum*.

In line with the generally "high IQ" score obtained for members of *Paenibacillus* spp., extensive work on *P. dendritiformis* has revealed that they possess a large array of quorum communication mechanisms alternatingly capable of promoting fast colonization under growth-favorable conditions or of supporting survival strategies when confronted with a harsh environment. Five such mechanisms are listed below.

1. Differentiation: *P. dendritiformis* form and reshape large, intricately organized colonies comprising billions of cells [9–14]. Colony formation is enabled by differentiation, which confers on populations of otherwise identical, individual bacteria the capacity for cooperative self-organization. Once part of a colony, the bacteria can better compete for food resources and they enjoy greater protection against antibacterial assaults.
2. Lubrication: On hard surfaces, *P. dendritiformis* have the ability to secrete a lubricant that both reduces surface friction and that also facilitates rapid migration [13]. Such materials are secreted by the bacteria only when their cell count in a niche has become high enough, indicating that lubricant secretion is dependent on a quorum mechanism.
3. Swarming: Robust swarmers [15, 16], *P. dendritiformis* can swarm on a large variety of agar concentrations, including hard agar (2 %) and agar with limited nutrient levels. In fact, unlike *Escherichia coli* (require glucose for swarming), *Bacillus subtilis* (require high levels of moisture), and *Serratia marcescens* (unable to swarm at 37 ºC, i.e., mammalian body temperatures), *P. dendritiformis* swarm under most laboratory conditions. As in other species, however, the bacteria must reach sufficient cell density to swarm.
4. Sporulation: As with many other Gram-positive species, *P. dendritiformis* may enter sporulation mode if nutrient levels are insufficient for growth [2]. Dependent on population density, sporulation is enhanced by the self-secretion of subtilisin, which inhibits the growth of sibling *P. dendritiformis* colonies. Both the sporulation and swarming circuits of *P. dendritiformis* resemble those of *B. subtilis* and are dependent on the local bacteria concentrations.
5. Resistance: Another challenge bacteria often encounter is antibiotic stress. While some species are naturally resistant to specific types of antibiotics, others use persister cells [17] or small colony variants [18] to ensure their survival. These cells, which typically constitute very small fractions of bacterial populations, either do not reproduce or they reproduce very slowly. Phenotypically, however, they are considerably more resistant to the antibiotic than are regular cells from the same population, and as such, their survival ensures strain continuity. An additional *P. dendritiformis* survival mechanism that assists in fighting antibiotic attacks is the existence in this species of two well-characterized motile strains, or morphotypes, which are known as the *T* [19] and *C* [20, 21] morphotypes and which have the same 16S rRNA ribosome. While the two strains differ in terms of the corresponding survival strategy associated with each [13, 22], in most cases the two morphotypes will grow independently under the specific conditions

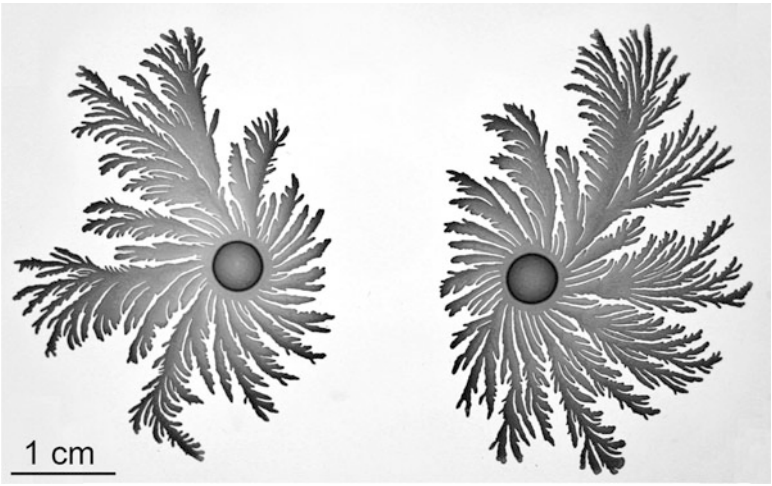

Fig. 8.2 Two neighboring *P. dendritiformis* colonies growing on 1.6 % agar with 1.5 g/L peptone

(temperature, humidity, agar rigidity, and food level) that are suitable for it. When subjected to antibiotic stress, however, a strain can switch to the other morphotype if it is better suited to survival in the antibiotic-tainted environment. Once favorable conditions return, cells can revert to the original morphotype. The majority of the work in this chapter focuses on the *T* morphotype.

Mechanisms that support the collective behavior of bacteria change the population of a single colony into a multi-cellular organism. Under such collective conditions, therefore, one expects that there may also be competition between sibling colonies (taken from the same culture), as suggested by the growth inhibition shown in Fig. 8.2.

8.2 Competition Between Sibling Colonies

8.2.1 Early Observations

In the early 1990s, Fujikawa and Matsushita [23] showed that sibling *B. subtilis* colonies grown on nutrient-poor agar in the same Petri dish did not merge. Each colony expanded in the direction of its neighboring colony but stopped short of making physical contact, leaving a gap of a few millimeters between the two colonies. Under rich growth conditions, however, the authors did not observe the phenomenon [24], and the colonies spread in homogenous patterns. The reason for the gap, they concluded, was nutrient depletion. Their observations illustrate a phenomenon similar to diffusion limited aggregation (DLA) processes [25], in

which the consumed nutrients diffuse through the medium, creating intricate branch patterns with gaps where nutrients were depleted.

About two decades later, a study by Gibbs et al. [26] on the interaction between *Proteus mirabilis* colonies showed that different *P. mirabilis* strains formed boundaries between colonies while those of sibling colonies of the same strain did not contain any boundaries. A fundamental requirement for boundary formation in the Gibbs et al. study is that bacteria exhibit the ability to discriminate between self and nonself. Swarms of mutants with deletions in the *ids* gene cluster did not merge with their parent. Thus, although Gibbs et al. suggested that the *ids* genes are involved in the ability of *P. mirabilis* to distinguish self from nonself, the specific mechanism of inhibition and its evolutionary advantage are still unclear.

The first study to show some sort of competition between **sibling** colonies that was not a result of food depletion focused on the *T* morphotype of *P. dendritiformis* [27–29]. Although simulations suggested that colonies were repelled due to some signaling factor secreted to the medium, the physical basis of that competition, its mode of action, and the chemicals involved in the process have still not been resolved.

8.2.2 Competition Between P. dendritiformis Colonies

Subsequent quantitative studies investigated the competition between *P. dendritiformis* colonies of the *T* morphotype [1–3]. In the first study [1], two sibling colonies were inoculated simultaneously on an agar plate, and their time development was monitored using an integrated incubation-imaging system to track bacterial colony growth over a period of a week (Fig. 8.3a). The initial development of each colony was virtually the same as that of a single, isolated colony: after a lag of 18 h, the two colonies began to expand outward, in the process developing intricate, branched patterns within well-defined, circular envelopes. The speed of envelope growth was isotropic and constant (Fig. 8.3b, c).

However, after a well-defined time that depended on the initial separation distance between the two colonies, the rates of growth of the colony growth fronts facing each other began to decelerate until growth there stopped altogether, leaving a gap between the pair of colonies (Fig. 8.3a). Other areas of the colonies, however, continued to grow unhindered. Surprisingly, the deceleration observed in the colony growth along the fronts that were opposite each other was independent of the initial separation distance, indicating a threshold mechanism. This suggested the presence of an inhibitory chemical. Indeed, colonies grown at different initial separation distances are affected the same way when they sense an inhibiting level above a threshold.

These results motivated us to investigate why the colonies stopped growing on their adjacent growth fronts while other areas of the colonies seemed unaffected. In contrast to what has been observed in studies of *B. subtilis* growth [23], food depletion can be ruled out as the primary cause since, given the length and time scales for colony growth, the diffusion constant of peptone in the agar was found to

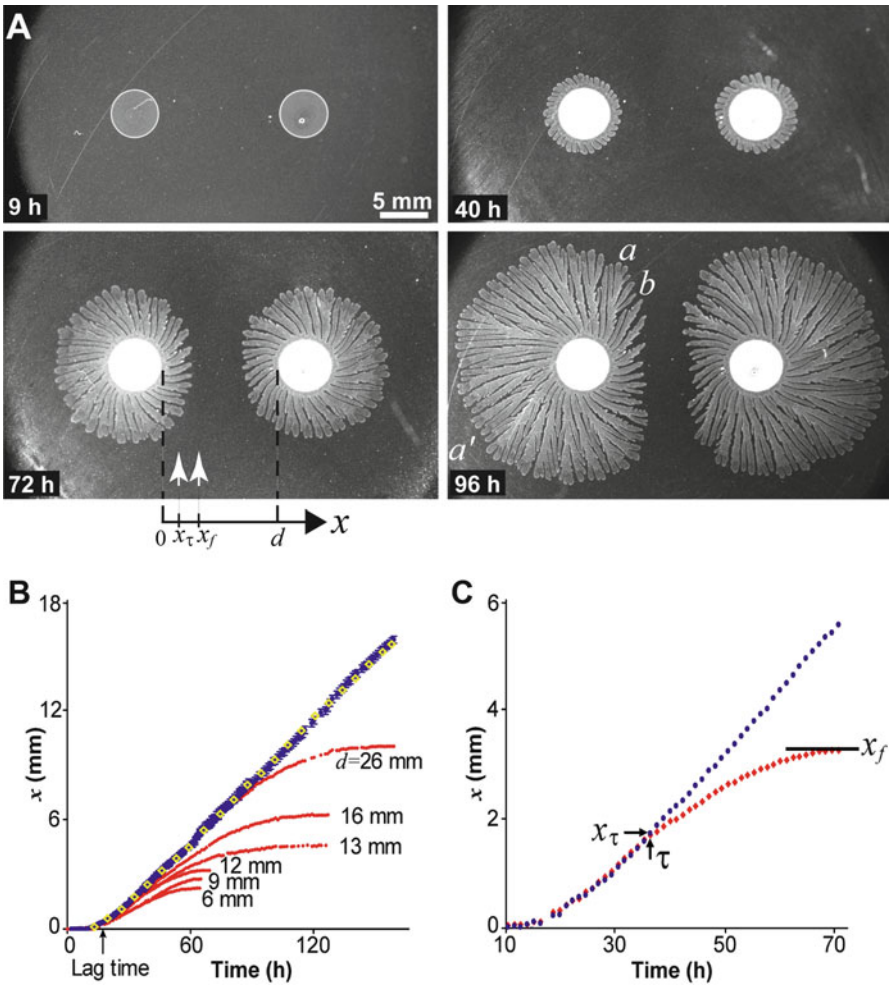

Fig. 8.3 Interaction between neighboring *P. dendritiformis* colonies growing on 1.5 % agar with 2 g/L peptone. (**a**) Images of adjacent growing colonies: 9 h after inoculation, no growth; 40 h, the onset of inhibition; 72 h, inhibited growth; 96 h, growth has stopped in region *b* but continues in regions *a* and a'. The labels on the *x*-axis (under panel **a**) indicate the initial distance *d* separating the two colonies (here 12 mm); the position $x_\tau(d)$ is where growth begins to decelerate, and the position $x_f(d)$ is where growth stops. (**b**) Position *x* of the growth front as a function of time for initial colony separation distances *d* of 6–26 mm; *blue* symbols aligned on a *straight line* correspond to the uninhibited growth in region a', whereas *red* symbols, aligned on the *curved lines* represent growth toward region *b* [see data for 72 h and for 96 h, (**a**)]. The *yellow diamonds* (on the *straight line*) represent the growth of a single colony for the same conditions. For both the single colony and for neighboring colonies with any separation *d*, there is the same lag time (18 h), followed by growth with a speed of 0.11 mm/h. (**c**) A well-defined transition (at $\tau = 36$ h, $x_\tau = 1.8$ mm) from uninhibited to inhibited growth for the colony in (**a**). Growth speed decelerates, and the growth front stops at x_f. Image was taken from [1] with minor modifications

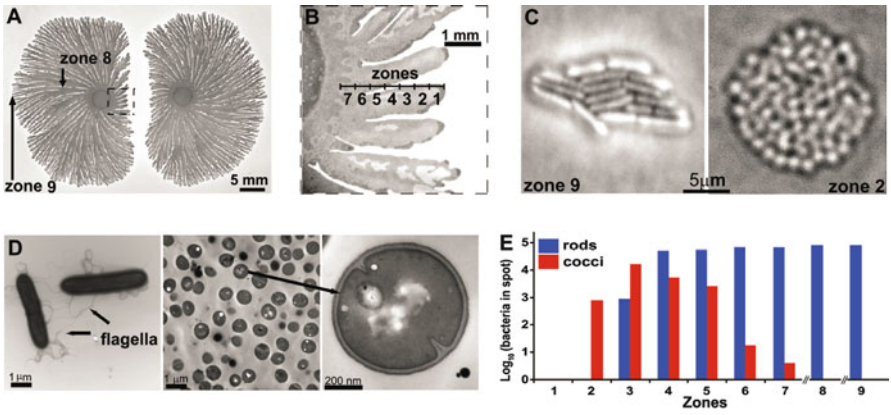

Fig. 8.4 Switch from rods to cocci. (**a** and **b**) Low (**a**) and high (**b**) magnifications of a competing colony. (**c**) Colonies formed from single bacteria taken from zone 9 (rods) and from zone 2 (cocci). (**d**) Transmission electron microscopy of rod-shaped, motile *P. dendritiformis* cells (*left*). Cocci (cross-section image) are shown at the same magnification as are the rods (*middle panel*) and at a higher magnification, revealing incipient cell division (*right*). (**e**) Number of bacteria recovered from each zone (250 × 250-μm area) are indicated in panels **a** and **b**. No bacteria were recovered from zone 1, and only cocci grew from zone 2. The number of rod-shaped bacteria increased with the distance from the inhibited interface, and only rods were recovered from zones 8 and 9. Image was taken from [3] with minor modifications

be too large (1.6×10^{-5} cm^2/s). Therefore, it was not clear why the bacteria simply stopped moving. Two possible explanations are that they entered the sporulation stage or that they died.

8.2.3 The Inhibited Region

To discover what caused the pattern of inhibited growth, bacteria were isolated from different regions of the two colonies and examined. These regions included the uninhibited area (zones 8 and 9), the colonies' centers (zone 7), and the area from the center to the inhibited tips (zone 1) (Fig. 8.4a, b). In zones 8 and 9, only rod-shaped motile bacteria were found, and in zone 8 some spores were also found, in line with what is expected from a single colony. Cells collected from the edges of the inhibited regions (zone 1) were dead, and no spores were found there, indicating an unexpected killing zone. However, microscopic examinations of cells from the inner regions within the zone of inhibition (zones 2–7) revealed small (0.7 μm in diameter), immotile but vegetative cocci in those zones that were not detected in zones 8 and 9 (Fig. 8.4c, d) [3]. The quantity of rods increased with increasing distance from the zones of inhibition of the competing colonies (Fig. 8.4e), and only cocci were recovered from the areas closest to the competing colonies (zone 2). No spores were found in zones 1–3.

A comparison of the DNA sequences of the 16S rRNA genes of the cocci and rods showed that they were identical, ruling out contamination. The cocci were thus considered to be a new phenotype of the *P. dendritiformis T* morphotype, but it was not clear what triggered their formation. To identify differences between rods and cocci to possibly shed light on what determines the formation of each form of *P. dendritiformis*, their growth and metabolism under different conditions were compared. Re-streaked multiple times for isolation and maintained as separate stocks, cocci and rods produced pure cultures in rich media and grew at the same rates during exponential phase.

The discovery of the new phenotype in the inhibited zones could not explain the deaths of cells at the tips (zone 1), but it suggested that cocci do not exist in a normal, vegetative colony and that they are the result of the competition between the colonies. Regardless of what the findings indicate about cocci, the zone of killing identified at the tips of the colonies dictated that we test for the existence of something more than a simple inhibitory element, i.e., for a killing factor. Material from the agar between two competing colonies was therefore extracted and re-introduced near a single, isolated, growing colony. The inhibitory influence of the extract on the colony and the changes in the colony's interior structure were found to be highly similar to those observed during colony–colony interaction. Moreover, bacteria collected from uninhibited regions grew normally in LB whereas that collected from the inhibited tips showed no growth, observations that are identical to those recorded with the two competing colonies.

8.2.4 The Role of Subtilisin

The extracted material was examined for its protein content [2]. Analyses by SDS-polyacrylamide gel and by Edman degradation sequencing revealed protein bands at 32, 30, and 12 kDa. In contrast, extracts from the agar surrounding single growing colonies showed only two protein bands, at 32 and 30 kDa.

BLASTP analysis revealed that the genes encoding the 32 and 30 kDa proteins were annotated in the *P. dendritiformis* genome as flagellin and subtilisin, respectively [2]. Flagellin had no effect on colony growth or morphology, but large amounts of subtilisin inhibited growth, and only dead cells were found in the inhibited area. Material extracted from agar near subtilisin-inhibited regions was found to contain the same 12 kDa protein detected in the region between two colonies. This suggested that high subtilisin levels trigger secretion of this third protein, which is involved in the inhibition process and cell death. The 12 kDa protein corresponded to a gene predicted to encode a larger, 173-amino-acid (20 kDa) protein that belongs to the DUF1706 family of conserved hypothetical proteins. The 20 kDa gene was named dfsB (dendritiformis sibling bacteriocin) and the 12 kDa protein was named Slf (sibling lethal factor).

To further characterize the effects of the proteins on *P. dendritiformis* colony growth, single growing colonies were exposed to different concentrations of

subtilisin. While low subtilisin levels promoted bacterial reproduction and colony expansion, at higher levels it initially promoted expansion. As exposure times grew, however, it eventually inhibited expansion. Moreover, very high subtilisin levels, as mentioned earlier, resulted in the death of cells at the inhibited interface. For the case of two competing colonies grown in a large Petri dish, the very early stages of growth were characterized by faster expansion (than in later stages) along the adjacent growth fronts, a finding that is likely because of the low levels of subtilisin secreted by both colonies.

In addition to the effect of subtilisin on cell growth, colony expansion is physically limited by surface tension—the colony cannot expand fast enough to create enough new space to accommodate the reproducing bacteria. When space and nutrients are in limited supply, therefore, increases in subtilisin help elevate bacterial density, thereby leading to nutrient stress. Further experiments [2] showed, however, that when space is not limited, subtilisin promotes reproduction independent of how much is added. But under space constraints, increases in bacterial density cause them to become overpopulated, which likely triggers their production of Slf to reduce the overall number of bacteria.

8.2.5 The Slf Toxin

The introduction of extracted Slf near a single growing colony inhibited that colony's growth. In fact, it was found to be an exclusively inhibitory protein, even at extremely low levels. In addition, when Slf was added to liquid cultures prior to their inoculation, no growth was detected. For grown liquid cultures, high levels of Slf lysed bacterial cells. More importantly, the evidence of cell lysis was visible at the edge of inhibited colonies (Fig. 8.5). Colony branches exposed to the lethal protein were destroyed within a few hours, indicating that Slf is the killing factor.

Based on its migration in polyacrylamide gels, Slf secreted into the medium has an approximate molecular weight of 12 kDa, but the predicted protein sequence of the gene dfsB is 173 amino acids, or 20 kDa (Fig. 8.6). The segment in amino acid positions 5–169 (larger letters in Fig. 8.6) is associated with a conserved Pfam family domain in many bacteria. The bold segment (Fig. 8.6), associated with the isolated protein, starts with the sequenced part of the detected peptide (underlined) and continues downstream to the end of the protein. The smaller size of the purified protein (12 kDa) indicates that the protein is processed or cleaved during secretion. The DNA encoding the 20 kDa DfsB protein was cloned into an expression vector, and the protein was synthesized and purified. After purification, the 20 kDa protein was treated with subtilisin, and the products were examined by SDS–PAGE gel electrophoresis. The subtilisin treatment resulted in conversion of the 20 kDa protein to a 12 kDa protein that comigrated with the 12 kDa protein isolated from the agar medium. Colonies were exposed to both the uncleaved 20 kDa species and the 12 kDa processed protein. The 20 kDa protein had no effect on *P. dendritiformis*

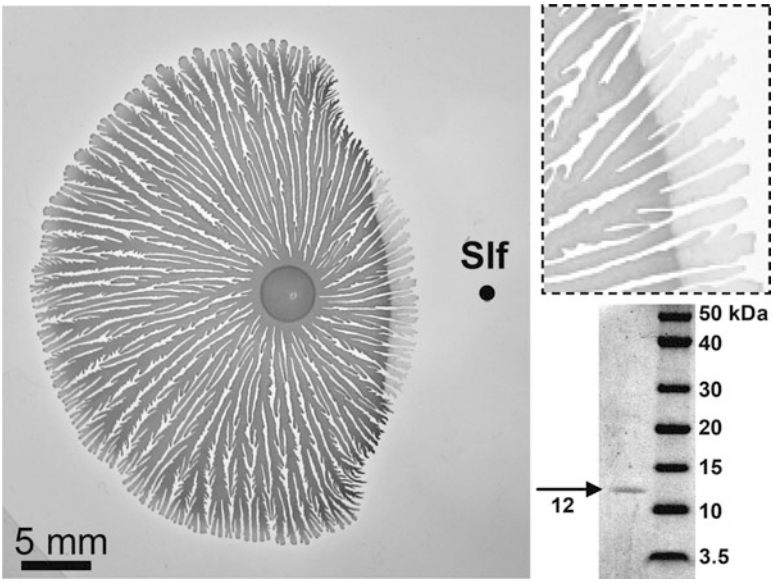

Fig. 8.5 Slf was introduced at the *black dot* near a single growing colony 4 days after inoculation. The faint region (shown at higher magnification in the inset) corresponds to lysed cells; growing branches were absent. Only a single band appeared in the gel electrophoresis results for the isolated Slf. Image was taken from [2] with minor modifications

MASYEYTSKEELKKTIHAAYLLLDGEFEGI
DDSQKDNRVPEVDRTPAEIIAYQLGWLHL
VMGWDRDELAGK**PVIMPAPGYKWNQLGGL**
YQSFYAAYADLSLTELRRLFRDTERQWLD
WIDTLSEEDLFTQSVRKWTGDKPNWPMAR
WIHINSAAPFKTFRAKIRKWKKHQRQA

Fig. 8.6 List of the 173 amino acids of the DfsB protein corresponding to the dfsB gene. *Large letters* indicate the segment at amino acid positions 5-169 that is associated with a conserved Pfam family domain. *Bold letters* indicate the segment of the isolated protein Slf. The detected peptide (Edman sequencing) is *underlined*. Image was taken from [2]

bacteria, but as was observed for the 12 kDa protein extracted from the area of inhibition between colonies, the processed 12 kDa fragment lysed growing colonies.

Tests of the toxic protein Slf on the *C* morphotype of *P. dendritiformis* showed that it is lethal, i.e., it lysed the cells. However, Slf had no effect on the closely related species *B. subtilis*. This suggests that similar to other bacteriocins, Slf has a narrow spectrum of activity.

8.2.6 *Reversible Phenotypic Switching Between Cocci and Rods*

The absence of cocci in areas of colonies not exposed to Slf suggested that the cocci were not preexisting in the population but were instead induced by exposure of the colony to Slf. Indeed, the addition of low levels of purified Slf to rod-like cultures resulted in phenotypic switching from rods to cocci, with the latter resistant to killing by Slf (Fig. 8.7). A more detailed metabolic profiling using Biolog Phenotype MicroArrays showed differences in carbon, nitrogen, phosphorus, and sulfur source utilization and in resistance to environmental stresses and antibiotics. In particular, cocci were much more resistant than rods were to osmotic stress and penicillin, indicating that there may be differences in the cell walls and membrane structures of the two morphologies. Thus, the cocci and rods exhibited striking differences in their abilities to survive and replicate under certain environmental and nutrient conditions.

Because the switch from rods to cocci was found to be an adaptive response to overcrowding [3], it seems likely that cocci could revert to the rod morphology under conditions that favor motile rods. Individual cocci inoculated on LB swarm plates (1 % agar) and monitored for the appearance of motile rods expanded slowly for the first 48 h, during which time only cocci were detected. After 50 h, rod-shaped, motile bacteria were observed at the colony edge. After an additional 6 h, rods multiplied and began to swarm in multiple layers in behavior similar to that observed in colonies initiated from single rods. At this stage cocci were not observed.

When multiple cocci colonies were present within a spot on the plate, the length of time required for cocci in each colony to switch to rods was proportional to the number of colonies initially present in the spot and to the proximity of those colonies to each other. This suggests that the transition from cocci to rods is not random but that it requires a secreted signal that is present in larger quantities when there are more colonies and when those colonies are situated closer to each other.

Such a signaling molecule may also be present in culture supernatants. To test for the presence of a secreted inducing signal, cocci were grown in LB broth for 18 h at 30 °C, and sterile supernatant from this culture was added to an equal volume of fresh medium prior to inoculation with cocci. In this culture, the shift to rods began at 18 h, whereas in culture without added supernatant, the transition did not occur until 22 h. This supports the hypothesis that a secreted factor, designated Ris (rod inducing signal), induces the switch from cocci to rods.

Rods grown in rich medium (LB) were also assessed for Ris production. Similar to the procedure followed with the coccus supernatant, the addition of rod supernatant to a culture of cocci also induced the shift from cocci to rods by 18 h. In contrast, however, exposure of the cocci culture to rod supernatant triggered the transition to the rod phenotype in more than 50 % of the cocci population by 18 h, compared to 3 % in the culture treated with coccus supernatant. The simplest explanation for this finding is that Ris is secreted in greater amounts by the rods, a scenario that may be part of a positive-feedback loop: cells that switch to the rod phenotype subsequently secrete the inducer in larger amounts, accelerating the

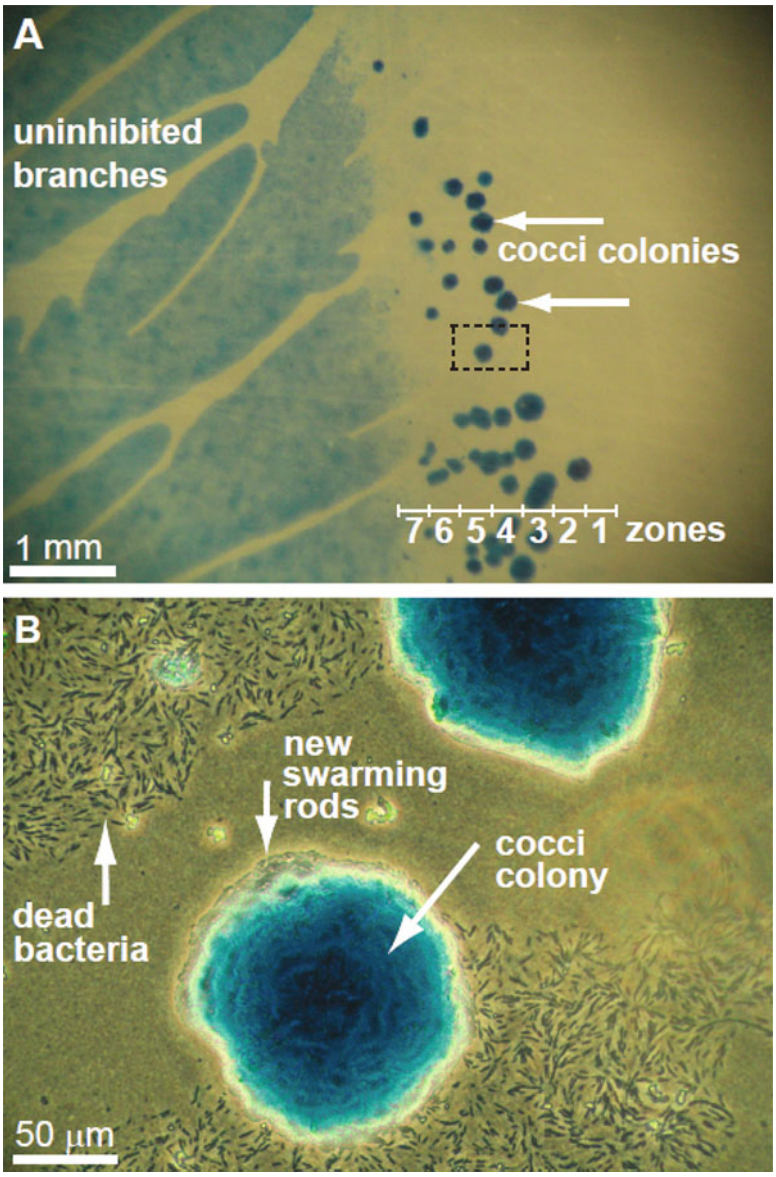

Fig. 8.7 Slf induces the switch from rods to cocci in a single growing colony. Purified Slf was placed 1 cm from the edge of the colony 4 days after inoculation. (**a**) Coccus colonies (*arrows*) in the inhibited regions 4 weeks after Slf introduction. (**b**) Higher magnification of the *marked rectangle* in panel **a**. Dead bacteria are visible in the inhibited region near coccus colonies. Rods are swarming from the edges of the coccus colonies. Image was taken from [3]

process of switching among the remaining cocci and ensuring that the transition is complete.

Ris was isolated from the culture supernatants of both rods and cocci by HPLC, individual fractions of which were tested for their ability to induce the phenotypic switch. Activity was associated with the fraction that eluted at 42 min from both rod and coccus supernatants. The fraction contained a single peak with maximum absorption at 214 nm. Placement of the isolated compound near a single coccus caused it to shift to the rod phenotype in less than 2 h, thus verifying that a specific secreted signal molecule induces the coccus to rod transition. However, Ris did not produce ninhydrin-positive spots on thin-layer chromatography (TLC) plates and did not absorb UV light at 280 nm, suggesting that it is not a peptide.

8.3 Mathematical Modeling: Self Regulation

The above results leave a key question unanswered: why is Slf produced by closely situated, neighboring colonies (or when subtilisin is added near single colonies) but not by single, isolated colonies?

To answer this question a mathematical model was developed. The model uses an approach in which bacteria, nutrients, prespores, subtilisin, and Slf are modeled as continuous fields, and the outer effective envelope of the colony is given by a smooth, time-dependent curve. The advantage of this approach is that the system is described as a free boundary problem, and the time evolutions of both the continuous fields and of the envelope can be modeled and simulated consistently and efficiently. This approach suits the problem at hand because it better describes the coarse-grained behavior of the colony rather than the exact shape of the edge of the lubrication layer. The envelope of growing neighboring colonies is depicted in Fig. 8.8a.

The main contribution of the model is the identification of a negative feedback loop that regulates the subtilisin concentration at the front of a growing colony. Figure 8.8b shows the profiles of the bacteria, nutrient, subtilisin, and Slf concentrations immediately after Slf was produced. One of the key features of the profile is that inside the colony, subtilisin concentration exceeds a critical threshold. However, this does not trigger Slf production because the motile bacterial concentration in this region is low. In line with the assumption that the exposure to subtilisin increases bacterial reproduction, it was found that high subtilisin levels at the front of a growing colony increase bacterial density. This, in turn, increases the colony expansion rate, and the bacteria at the front move farther away from the point of maximum subtilisin concentration. Subtilisin levels at the front subsequently decrease. In contrast, at low subtilisin concentrations, the opposite occurs, namely, decreases in bacterial reproduction and density and in colony expansion.

Combining the effects observed for high and low subtilisin concentrations, it was found that the subtilisin levels for a single colony reach a steady state in which the bacteria concentration is close to maximal, and therefore, the subtilisin

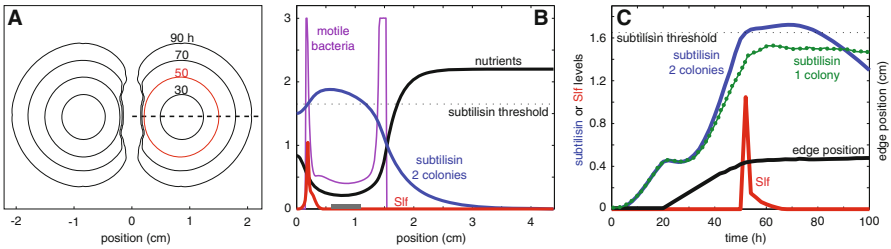

Fig. 8.8 Numerical simulation of colony competition. (**a**) The positions of the edges of competing colonies at 30, 50, 70, and 90 h. (**b**) Levels of motile bacteria (*purple*), subtilisin (*blue*), nutrients (*black*), and Slf (*red*) measured along the *horizontal dashed line* in A, 50 h after inoculation. The *gray rectangle* represents the initial inoculation droplet. For each panel, the model parameters and the initial conditions were the same; the initial distance between the colonies was 1.2 cm and the diameter of the dish was 8.8 cm, as in the experiments. (**c**) Subtilisin levels (in arbitrary units) at the moving edge of a colony as a function of time, both for a single colony (*green dots*) and for the inhibited interface in the case of two colonies (*blue line*). After 40 h, a competing colony senses its neighbor, and after 50 h the subtilisin level crosses a prefixed threshold (*horizontal dashed black line*). The *red curve* shows the level of Slf for the inhibited colony; no Slf is secreted in the single colony case. The *black line* shows the position of the edge of a colony growing toward a neighbor. The colony's edge starts to move after a lag time of 20 h, and then begins slowing down just before Slf is secreted. Image was taken from [2] with minor modifications

concentration at the front of the colony is regulated. This finding also accounts for the constant expansion rate of the colony. Likewise, an external source of subtilisin, such as a neighboring colony, can disrupt this regulatory mechanism (Fig. 8.8c). Simulations show that the disruption can happen via two routes: (1) added subtilisin from the neighboring colony and (2) nutrient depletion in the inhibited region between colonies, which increases the sporulation rate. The additional prespores, in turn, promote further increases in the subtilisin level. Another effect of nutrient depletion is the deceleration of colony expansion at its growth front. As explained previously, the bacteria at the front approach the area of maximum subtilisin concentration, and as a result, they reproduce faster than the colony can expand.

Bacterial stress under such conditions cannot be resolved through sporulation, as (1) sporulation requires additional nutrients, which may not be present, and (2) sporulating bacteria are assumed to secrete high levels of subtilisin, which would reduce the probability of colony survival. To ensure colony survival, therefore, it is suggested that the bacterial colony quickly reduce its population level. Indeed, the model predicts that the secretion of Slf will rapid lower the bacterial population, a finding that is consistent with laboratory observations.

8.4 Colonies of Closely Related Strains

The observations described so far summarize the results for the branching (*T*) morphotype of *P. dendritiformis*. Although its other morphotype, the chiral (*C*) morphotype [20, 21] has the same 16S rRNA ribosome, it differs in terms of several physical properties such as cell length, colony structure, and mode of migration [30]. We therefore decided to examine and compare the interactions between two *P. dendritiformis* sibling colonies of the *C* morphotype and between one each of the *T* and *C* morphotypes. In all cases the two colonies were inoculated simultaneously on the same plates. Compared with our results for the analyses of the interaction between two *T* morphotypes, our observations of interactions involving *C* morphotype (*C*–*C* or *T*–*C*) colonies indicated greater complexity, a finding rooted in the nature of the chiral morphotype and also due to the fact that we investigated the behavior of two distinct sub types of *C* (*C*+ and *C*−). Compared to the *C*− genome, that of *C*+ includes several additional segments. Bioinformatics analyses indicate that the extra segments are associated with a viral origin. Likewise, the *T* morphotype has *T*+ and *T*− sub types that correspond roughly to the +/− sub types of the *C* morphotype, and that undergo morphotype transitions to *C*+ and *C*−, respectively. Indeed, the sub types of the two morphotypes share many characteristics, but it is easier to induce morphotype transitions between the *T*− and *C*− sub types. Observations of colony–colony interactions described thus far (here, and in [1–3]) were of the *T*− sub type, but we are also working on interaction between *T*+ sub type sibling colonies (some preliminary work has already been done [27]).

Competition between two *C*− sub type colonies (Fig. 8.9a) showed results similar to those observed for the competition between two *T*− sub type colonies as well as between *T*− and *C*− sub type colonies. Also, Slf extracted from competing *T*− sub type [1] colonies lysed cells of a single growing *C*− sub type colony (see Fig. 8.5 in [2]). These competition results were, to an extent, expected because of the biological similarity between the two morphotypes (the genomes of the *T*− and *C*− morphotypes are very close).

C+ sub types, however, behaved differently. On the one hand, two *C*+ sub type colonies grown in the same Petri dish merged (Fig. 8.9b), suggesting that *C*+/*C*+ competition does not occur either because the *C*+ morphotype does not produce enough subtilisin to trigger the secretion of Slf or because it somehow blocks the regulation circuit. On the other hand, experiments in which *C*+ sub type colonies were grown near colonies of the *T*− sub type (Fig. 8.9c) or near *C*− sub type colonies did show the deadly competition observed in the previous tests of the *T* morphotype.

These results demonstrate that the regulatory process behind the competition behavior of *P. dendritiformis* is highly intricate, mainly due to the extra segments of viral origin present in the genome of the *C*+ morphotype. Therefore, *P. dendritiformis* should be researched further for its potential to provide important clues about the role of virus-mediated horizontal gene transfer between bacteria.

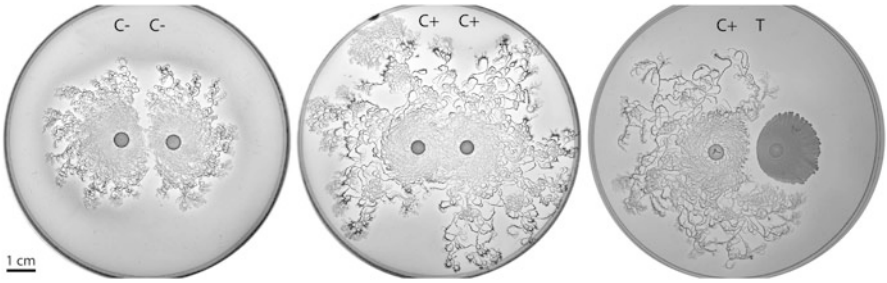

Fig. 8.9 Interaction between neighboring *P. dendritiformis* colonies growing on a 1.0 % agar with 2 g/L peptone. (**a**) Two *C*− colonies. A gap between the colonies is formed. (**b**) Two *C*+ colonies. No gap is formed. (**c**) Two colonies, one *C*+ and the other *T*, showing the gap that formed between them

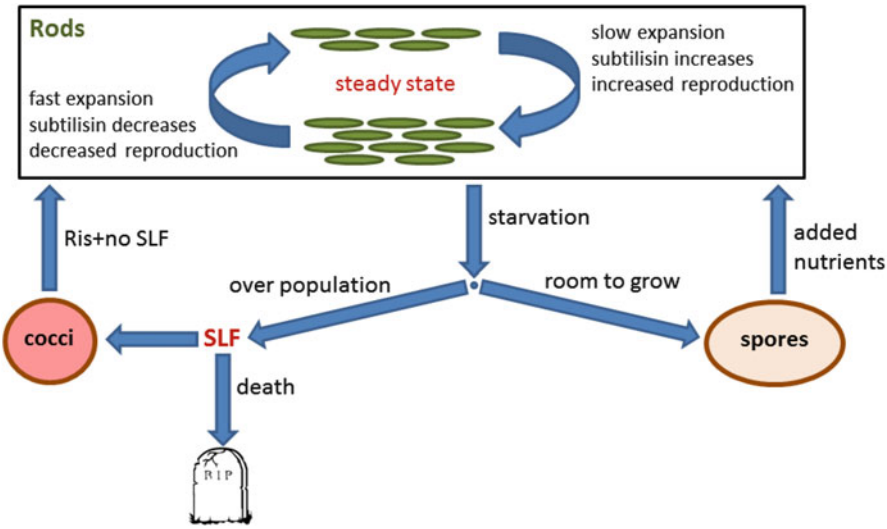

Fig. 8.10 A schematic diagram showing the different subtilisin-regulation stages of *P. dendritiformis*. At normal rich growth conditions, the cells are rods. The density at the tip of a growing colony is regulated by a negative feedback loop between the local concentration of subtilisin and the colony's expansion rate. Starvation or a close sibling colony disrupts this steady state, and as a result, bacteria either engage in sporulation or in the production of Slf. The presence of Slf in the growth medium quickly reduces the cell population and promotes the phenotypic transition of the bacteria into a more resilient cocci phenotype. When conditions are again favorable, cocci can switch back to the typical rod-shaped bacteria

8.5 Summary

The results indicate that *P. dendritiformis* has at least two mechanisms to deal with changing environmental conditions and to enable its long-term survival (Fig. 8.10). First, it has the ability to form spores that are highly resistant to harsh conditions.

The second mechanism is the formation of cocci—less resistant than spores but able to replicate even in the presence of Slf—which confers on cells near the leading edge of the colony the ability to continuously monitor the level of competition and the environment and to respond appropriately when sufficient nutrients are available for colony expansion. The shift between rods and cocci performed by *P. dendritiformis* requires the specific secreted bacterial signals Slf and Ris, which induce the relevant transition (rods to cocci or cocci to rods) in response to environmental cues. Thus, the population can be maintained as either rods or cocci under the appropriate conditions. For example, a culture consisting of all rods should contain high levels of Ris as the factor maintaining the population in the rod state. Under normal growth conditions, no Slf would be secreted and no transition to cocci would occur. In the event of sudden overcrowding, as in the case of encroaching colonies, Slf is produced, killing most of the rods at the leading edge. This killing of rods is essential to eliminate Ris production and enable the transition to cocci in response to low levels of Slf, a scenario that is apparent at the edges of the colonies on solid media, where cocci are found in areas that also contain dead rods (Fig. 8.7).

The ability to replicate and maintain the coccoid form in an inducible manner distinguishes this phenotype switching from other phenotypic changes—such as persistence cells, sporulation (which leads to a dormant state), or formation of cocci in stationary phase—as it allows *P. dendritiformis* to adapt to changing environmental conditions. Although this form of phenotypic switching has not been described previously, genes of unknown functions with homology to the *P. dendritiformis* Slf encoding gene are widespread in bacteria and yeast. Therefore, the lethal response to competition and associated phenotypic switching that have been observed in *P. dendritiformis* may be a common but previously unrecognized mechanism for regulation of population growth in nature.

References

1. Be'er A et al (2009) Deadly competition between sibling bacterial colonies. Proc Natl Acad Sci U S A 106:428–433
2. Be'er A et al (2010) Lethal protein produced in response to competition between sibling bacterial colonies. Proc Natl Acad Sci U S A 107:6258–6263
3. Be'er A et al (2011) Surviving bacterial sibling rivalry: inducible and reversible phenotypic switching in *Paenibacillus dendritiformis*. MBio 2:e00069-11. doi:10.1128/mBio.00069-11
4. González-Pastor JE et al (2003) Cannibalism by sporulating bacteria. Science 301:510–513
5. Hávarstein LS et al (2006) New insights into pneumococcal fratricide: relationship to clumping and identification of a novel immunity factor. Mol Microbiol 59:1297–1307
6. Vicsek T, Zafeiris A (2012) Collective motion. Phys Rep 517:71–140
7. Eldar A (2011) Social conflict drives the evolutionary divergence of quorum sensing. Proc Natl Acad Sci U S A 108:13635–13640
8. Sirota-Madi A et al (2010) Genome sequence of the pattern forming *Paenibacillus vortex* bacterium reveals potential for thriving in complex environments. BMC Genomics 11:1471–2164
9. Ben-Jacob E et al (1994) Generic modeling of cooperative growth patterns in bacterial colonies. Nature 368:46–49

10. Ben-Jacob E et al (1995) Complex bacterial patterns. Nature 373:566–567
11. Ben-Jacob E et al (1998) Cooperative organization of bacterial colonies: from genotype to morphotype. Annu Rev Microbiol 52:779–806
12. Ben-Jacob E (2003) Bacterial self-organization: co-enhancement of complexification and adaptability in a dynamic environment. Philos Trans A Math Phys Eng Sci 361:1283–1312
13. Ben-Jacob E et al (2000) Cooperative self-organization of microorganism. Adv Phys 49: 395–554
14. Ben-Jacob E, Levine H (2006) Self-engineering capabilities of bacteria. J R Soc Interface 3:197–214
15. Be'er A et al (2009) *Paenibacillus dendritiformis* bacterial colony growth depends on surfactant but not on bacterial motion. J Bacteriol 191:5758–5764
16. Zhang HP et al (2009) Swarming dynamics in bacterial colonies. Europhys Lett 87:1–5
17. Balaban NQ et al (2004) Bacterial persistence as a phenotypic switch. Science 305:1622–1625
18. Roth D et al (2013) Identification and characterization of a highly motile and antibiotic refractory subpopulation involved in the expansion of swarming colonies of *Paenibacillus vortex*. Environ Microbiol 15:2532–2544
19. Ben-Jacob E et al (2004) Bacterial linguistic communication and social intelligence. Trends Microbiol 12:366–372
20. Ben-Jacob E et al (1995) Cooperative formation of chiral patterns during growth of bacterial colonies. Phys Rev Lett 75:2899–2902
21. Sirota-Madi A et al (2012) Genome sequence of the pattern-forming social bacterium *Paenibacillus dendritiformis* C454 chiral morphotype. J Bacteriol 194:2127–2128
22. Ben-Jacob E et al (2001) Modeling branching and chiral colonial patterning of lubricating bacteria. In: Maini PK, Othmer HG (eds) Mathematical models for biological pattern formation. Springer Science Business Media, New York
23. Fujikawa H, Matsushita M (1991) Bacterial fractal growth in the concentration field of nutrient. J Phys Soc Jpn 60:88–94
24. Wakita J et al (1994) Experimental investigation on the validity of population dynamics approach to bacterial colony formation. J Phys Soc Jpn 63:1205–1211
25. Deepak N et al (2007) Segregation of fractal aggregates grown from two seeds. Phys Rev E 75:1–5
26. Gibbs KA et al (2008) Genetic determinants of self identity and social recognition in bacteria. Science 321:256–259
27. Ben-Jacob E et al (2000) Bacterial cooperative organization under antibiotic stress. Physica A 282:247–282
28. Golding I et al (1998) Studies of bacterial branching growth using reaction–diffusion models for colonial development. Physica A 260:510–554
29. Golding I, Ben-Jacob E (2001) The artistry of bacterial colonies and the antibiotic crisis. In: Reguera D, Bonilla LL, Rubi JM (eds) Coherent structures in complex systems, vol 567, Lecture notes in physics. Springer, Berlin
30. Be'er A et al (2013) Periodic reversals in *Paenibacillus dendritiformis* swarming. J Bacteriol 195:2709–2717

Chapter 9
Mathematical Insights into the Role of Feedback in Quorum-Sensing Architectures

Sara Jabbari and John R. King

9.1 Introduction

Cell-to-cell communication is now known to be a common phenomenon in the bacterial kingdom. Whether this signalling mechanism serves to unify the response of a population (from where the term quorum sensing first emerged), to detect the population density in the bacteria's immediate environment (diffusion sensing [1]), to combine the two (efficiency sensing [2]) or even to detect (and inhibit or promote) the presence of competitive or complementary species (cross-species or cross-kingdom signalling [3]), it is clear that it plays a crucial role in the lives of these organisms. Understanding these processes, therefore, is a key challenge in the quest to unravel bacterial behaviour and exploit or modify it for our own benefit. The applications for such understanding are far-reaching and include the development of novel compounds that suppress bacterial pathogenicity, forced production of useful chemicals and mimicry of existing (or creation of new) gene regulation networks in the emergent field of synthetic biology.

Though the range of known quorum-sensing systems is ever-expanding, they fall largely into two categories: homologues of the *luxIR* system in Gram-negative bacteria and Gram-positive homologues of the *agr* system.

The *luxIR* system is well documented, having been the first quorum-sensing system to be discovered [4]: it was shown to regulate bioluminescence by the

S. Jabbari (✉)
School of Mathematics and Institute of Microbiology and Infection, Edgbaston Campus, University of Birmingham, Birmingham, United Kingdom, B15 2TT
e-mail: s.jabbari@bham.ac.uk

J.R. King
School of Mathematical Sciences, University Park, University of Nottingham, Nottingham, United Kingdom, NG7 2RD
e-mail: john.king@nottingham.ac.uk

S.J. Hagen (ed.), *The Physical Basis of Bacterial Quorum Communication*, Biological and Medical Physics, Biomedical Engineering, DOI 10.1007/978-1-4939-1402-9_9

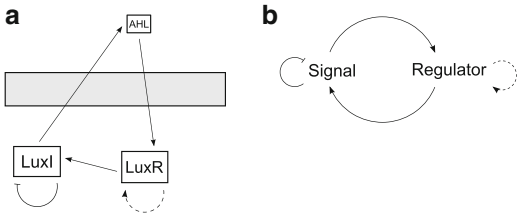

Fig. 9.1 The *luxIR* quorum sensing circuit is depicted in (**a**), with its reduced version in (**b**): in the latter, LuxI and AHL together correspond to the signal while LuxR serves as the regulator. We use (**b**) to build our generic (minimal) model of Gram-negative quorum sensing in Sect. 9.3.2.1. *Dashed lines* illustrate processes which do not necessarily occur in all *luxIR*-type systems. Note that auto-repression of the signal synthase LuxI occurs via an intermediary protein (RsaL) that we neglect from the model. The *shaded grey rectangle* represents the cell membrane

marine bacterium *Vibrio fischeri* in accordance with population size—at low cell density, light emission serves little purpose while at high cell density the bacteria are capable of producing enough light to be of use to the squid on which they live symbiotically. It is generally thought that the light, resembling moonlight on the water's surface, camouflages the squid, thus hiding it from potential predators. The process works through the production of a signal molecule from the *luxI* gene, see Fig. 9.1. For Gram-negative bacteria these are, more often than not, N-acyl homoserine lactones (AHLs). The AHL can diffuse in and out of the cell, through the cell wall, thus facilitating a means by which these signal molecules can transfer (and therefore communicate) between cells of the same species. Internal AHL activates the receptor protein, LuxR, through binding (in many cases this requires oligomerisation of the receptor protein and this will be discussed further in later sections). In addition to the target genes of the quorum-sensing system which require activation or inactivation in response to population size, activated LuxR can increase transcription of the *luxI* gene (resulting in more signal) and, in some cases, of its own *luxR* gene. In short, therefore, the larger the population of bacteria, the more signal molecule there will be and, in theory at least, the faster this process will occur. Equivalently, the cells might achieve quorum-sensing upregulation as a result of entering a particularly confined environment where signal molecules will accumulate much faster due to the lack of diffusion away from the cells.

In Gram-positive bacteria the general concept is much the same, except the difference in cell wall requires an alternative mechanism for signal secretion and detection. In this case, the quorum-sensing signal is most often a cyclic peptide, produced and secreted from the cell via the combined action of two proteins: AgrB (the exporter protein) and AgrD (the signal itself, converted into a peptide upon secretion), see Fig. 9.2. The externalised peptide, termed the autoinducing peptide (AIP), is detected by a receptor protein, AgrC, on the cell membrane. Binding of AIP to AgrC triggers a phosphorylation cascade between itself and the internal response regulator, AgrA. In its thus activated form, AgrA acts on transcription of its target

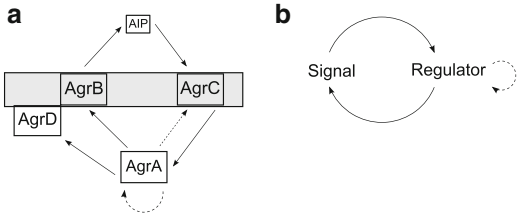

Fig. 9.2 A schematic representation of the *agr* quorum-sensing system. In (**a**) we illustrate the full network. *Dashed lines* illustrate processes which do not necessarily occur in all *agr*-type systems. The reduced network used for model building in Sect. 9.3.1.1 is given in (**b**), wherein the signal captures AgrB, AgrD and AIP and the regulator AgrA and AgrC. The *shaded grey rectangle* represents the cell membrane. We note that the abstract (minimal) version of the network, shown in (**b**), is a subcase of that in Fig. 9.1b, the negative feedback loop of which is missing

genes and on the *agr* genes themselves (in the case of *Staphylococcus aureus*, in which this system was first identified [5], this applies to all four of the *agr* genes; in other bacteria it can be fewer).

Homologues of these two systems form the majority of quorum-sensing mechanisms that have been discovered to this point (this widespread occurrence of the same network topologies itself being noteworthy), many of these interacting with additional gene regulation networks, including other quorum-sensing systems (as we shall note later, some bacteria are known to contain multiple quorum-sensing circuits). A small number of more complicated systems have also been uncovered, for instance in *V. harveyi* and *V. cholerae*. These will be discussed in more detail later in the chapter.

The target genes of the above quorum-sensing systems are widely varying in nature, as are their reasons for being regulated in a density-dependent manner. Common examples include pathogenicity, sporulation, bioluminescence and swarming motility [6,7]. What appears to be both common and central to all known systems is feedback in the governing gene-regulation-network architecture. Perhaps somewhat surprising, however, is the variety of feedback architectures employed, including a role for both negative and positive feedback in different systems.

Mathematical modelling is an obvious route by which to study and investigate these networks at a systems level, their complexity rendering their representation in a computational manner particularly useful. We next provide an overview of mathematical models of quorum sensing which have a focus on the role of feedback in each network, categorising the discussion into the hypothesised roles (rather than into the usual comparison of Gram-positive and Gram-negative systems). We complement this with some simple (but in some sense generic) examples of such models, based on the quorum-sensing architectures outlined in the biology review of [8] and being of a form suggested in Figs. 9.1b and 9.2b.

9.2 The Role of Feedback in Quorum Sensing

Since feedback plays such a central role in so many different gene regulation networks, we seek here to summarise the findings of a range of mathematical investigations into its function in relation to quorum sensing. The ever-expanding literature on this subject is already vast and we cannot hope to provide a comprehensive review. Instead, we have chosen a number of mathematical studies ranging across types of bacteria (both Gram-negative and Gram-positive—though Gram-negative models are far more prevalent in the literature—and both pathogenic and non-pathogenic) and quorum-sensing systems (*luxIR* and *agr* homologues, including a hybrid of these systems used by two particular Gram-negative bacteria). We divide the discussion into hypothesised roles for feedback, a surprising number of which overlap for both positive and negative loops.

9.2.1 Defining Response Shape

Generic models of feedback in gene regulation networks have often been used to demonstrate how different feedback architectures can give rise to varying classes of response. For instance in [9], a model of interacting gene regulation and metabolic networks, it is demonstrated that rewiring the feedback can alter a system response (typically in terms of the expression level of a particular gene to the level of a signal) from monotonically increasing or decreasing, to bi- (or multi-) stable-steady behaviour through to oscillations, illustrating the potential for the exploitation of gene regulation networks in synthetic biology. From a similar viewpoint, [10] provides a review of a number of papers (both theoretical and experimental) showing that feedback in combination with nonlinearities in the system (for example, co-operative binding of two proteins in the network or, similarly, dimerisation of one type of protein) can enforce multistability in a system. The authors argue that the ability to attain a given number of distinct stable steady states should allow a population to divide into this number of subpopulations, each with their own niche in a particular environment. Given that quorum sensing is generally assumed to enforce unified behaviour amongst one population of cells, this may seem counter-intuitive in the current context. However, we shall see in Sect. 9.2.2 that the simultaneous existence of phenotypically different subpopulations could indeed have relevance to quorum sensing.

In the most common cases, however, the goal of quorum sensing can be classified more straightforwardly, namely to transition a population of cells between two states, for example to switch on or off virulence-factor production (*S. aureus*) or bioluminescence (*V. fischeri*). The ability of a quorum-sensing system to exhibit bistability, therefore, could be extremely important and has been demonstrated in a large number of cases (at least theoretically) to take place in both Gram-negative

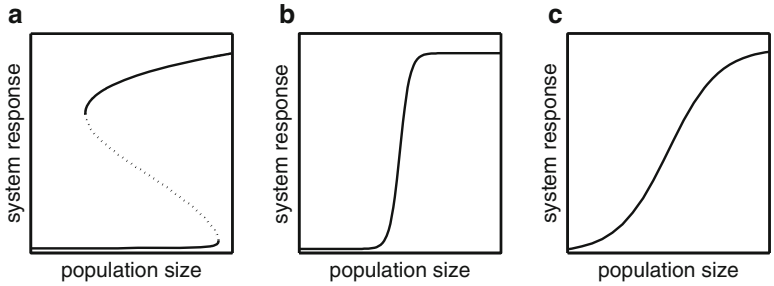

Fig. 9.3 A schematic illustrating the range of transition types discussed in Sect. 9.2.1. In (**a**) the system displays a bistable switch between responses (*solid lines* are stable, *dotted lines* unstable) and hysteresis, in (**b**) a monostable softer switch and in (**c**) a gradual transition between inactive and active (both (**b**) and (**c**) lacking hysteresis)

(for example, [11] and [12] concerning *Pseudomonas aeruginosa*) and Gram-positive ([13] and [14] on *S. aureus*) systems, but instances are more numerous than those listed here.

In general, low population numbers or density yield a quorum-sensing down-regulated steady state, with high numbers giving up-regulated responses. At intermediate levels three steady states may then exist: one stable and down-regulated, one stable and up-regulated, separated by one intermediary unstable state, see Fig. 9.3a. This facilitates a sharp and robust transition between the two states, alongside hysteresis when going in the opposite direction. Distinct critical population sizes switch the system from down- to up-regulated and vice versa. We shall see that this bistability has been shown to be caused directly by the presence of positive feedback onto the receptor protein (i.e., LuxR or its homologues) in Gram-negative systems, something that is not certain to occur in all bacteria possessing *luxIR* homologues.

In [11, 15] and [16], the existence of this particular feedback loop is considered explicitly. Haseltine and Arnold [16] compares three different versions of the quorum-sensing system in *V. fischeri*: one contains positive feedback onto both LuxR and LuxI, one onto LuxI alone and one with no feedback at all. It is demonstrated that the transition between the two states becomes sharper and stronger with the addition of each feedback loop: with both, bistability occurs (as in Fig. 9.3a), with only LuxI feedback a rapid but monostable switch is seen (Fig. 9.3b), while with no feedback at all the response is graded (Fig. 9.3c). Feedback onto LuxR alone is not considered as it is not thought biologically realistic. Through synthetic generation of each of these operons, the authors were able to verify these results experimentally and predict that their particular strain of *V. fischeri* is likely to contain feedback onto LuxI but little or none onto LuxR.

This lack of bistability is consistent with the model of [17] which, rather than representing each gene in the network, considers only the signal and subpopulations of down- and up-regulated *P. aeruginosa* cells, thus rendering the model more amenable to parametrisation from their experimental data. Any positive feedback therefore is included only implicitly and the model predicts a graded though fairly

sharp response from the system to increasing signal. It is possible that the implicit nature of the feedback in the model may be responsible for causing an intermediate response, i.e. most similar to Fig. 9.3b (representative of feedback only onto the signal in [16]).

Both [11] and [15] consider the *lasIR* quorum-sensing system of *P. aeruginosa* with and without feedback onto LasR. In this bacterium, quorum sensing plays a large role in the regulation of virulence and has accordingly been identified as a potential target for novel therapeutics. Due to the uncertainty of the presence of the LasR feedback loop, in these studies the effect of anti-quorum-sensing drugs on a circuit both with and without this loop is considered. The fact that LasR positive feedback induces bistability (as in [16]) has a knock-on effect on drug efficacy: the graded upregulation arising with no LasR feedback is best treated with a low steady dose of anti-LasR drug; conversely, the bistable switch implies one much larger dose of LasR is appropriate for successful downregulation of the quorum-sensing system.

The regulation of quorum-sensing systems by proteins that are not part of the quorum-sensing network itself is not uncommon: given that the purpose of the former is to translate a signal through a single cell or a population of cells, it is not surprising that its gene regulation network would be capable of interacting with other subcellular signalling networks. In some cases, bacteria even possess multiple interacting quorum-sensing networks. References [18] and [19] model the combined action of two quorum-sensing systems in *P. aeruginosa* and *V. fischeri*, respectively, the latter model having up to 21 steady states. Though not all of theses states will be both stable and biologically attainable, it is a fair assumption that the interaction of multiple feedback loops can cause a significant rise in the number of possible states the system can hold, in agreement with [10]. As implied above, we shall consider this further in Sect. 9.2.2.

In all of the above cases, mathematical bi- or multi-stability is caused by the presence of positive feedback loops, ensuring the cells' response is particularly strong. Interestingly, in [20] it is a negative feedback loop which forces the quorum-sensing system of *Agrobacterium tumefaciens* out of always (monotonically) attaining an up-regulated state and into a bistable system. The negative feedback occurs indirectly (via the TraM protein) on the receptor (TraR), in addition to the standard positive feedback on both TraR and the signal molecule. In the presence of the two positive loops, activation is too strong to prevent upregulation without self-regulated inhibition of the receptor protein.

The results of [16] and [20], therefore, contrast: in the second, two positive feedback loops give bistability, while in the first the result is monostability. Of course, the two theoretical studies consider different bacteria (*V. fischeri* and *A. tumefaciens*), meaning different mechanisms and parameters are used, but nevertheless it is clear that the role of feedback in defining the type of switch is not as clear-cut as one might expect. Indeed, bistability has been demonstrated in the model of the *agr* system of *S. aureus* even when feedback in the system is not considered [13]. Moreover, in a model of a generic Gram-negative system in [21], it is demonstrated that a nonlinear interaction in the network (here, dimerisation of LuxR being required for it to bind the signal) is sufficient to achieve bistability in

the network (though see Sect. 9.2.3 for further detail on this result). Thus, while feedback need not be the sole factor in determining the shape of the response-transition curve, it can evidently play a large part. Given the extra roles outlined below, perhaps it is the multi-tasking ability of feedback that has resulted in it being so prominent in quorum-sensing systems, with cells not relying on mechanisms like oligomerisation alone.

9.2.2 Tuning of Signal and Response Levels

We have discussed above how the presence of feedback loops can result in mixed subpopulations with varying phenotypes [10]. Such differences in phenotype might typically be explained by a difference in levels of the response regulator of a gene regulation network (in *agr*-homologues this is AgrA; in *luxIR*-homologues the response regulator is also the receptor protein, LuxR). In a model in [22] of the involvement of an *agr*-type quorum-sensing system in sporulation and solventogenesis by *Clostridium acetobutylicum*, it was shown that the *absence* of positive feedback into the receptor and response regulator enables a cell to tune its response more finely via response-regulator levels. Through comparisons with a model of the *agr* system in *S. aureus* [14] (where positive feedback occurs onto all elements of the *agr* system that controls virulence), it was clear that the reduced number of feedback loops could lower the quorum-sensing response. This ties in nicely with the purpose of quorum sensing in each of these organisms: sporulation is a survival mechanism (required in an acidic environment that is likely to occur when the population is dense) that is not needed by every cell in the population, whereas *S. aureus* gains no benefit by only a portion of the population becoming virulent. A population of sporulating cells can actually benefit from reserving a subpopulation in a vegetative state in case environmental conditions suddenly become more favourable to cell growth—the reversal of sporulation being both time and energy consuming.

In [22] a number of mechanisms of interaction between a quorum-sensing system and a sporulation-initiation gene regulation network were considered (either by direct phosphorylation of the response regulator of the latter, Spo0A, or via interference of the transcription of various different elements in the network). The ability of the network to tune response levels in the absence of feedback into *agrA* and *agrC* was seen only in the case of direct phosphorylation. For all other network topologies, the response was equivalent with or without these particular feedbacks, hence it was postulated that the feedback might be absent simply to prevent unnecessary overproduction of relevant elements in the network, thus saving the cells' energy.

Similarly, [23] discusses a range of ways of inhibiting quorum sensing (background inhibition of signal production, negative feedback onto the signal and the soaking up of signal molecules through competitive binding to some other constitutively produced molecule) in a generic model of quorum sensing in Gram-

negative bacteria (this work is an extension of [17], with the addition of repression producing a better model fit to their experimental data), finding that the second and third of these can result in a decreased proportion of up-regulated cells in the overall population. Furthermore, it is shown that this can prevent over-production of the signal molecule.

The level of signal molecule is a key focus of a number of studies of quorum sensing and it is often found that when the system does display bistability, moving between states unsurprisingly depends on the quantity of signal molecule. In [18], the first model to tackle two quorum-sensing systems in *P. aeruginosa* simultaneously, it is shown that the critical signal level required to induce this switch is dependent on the amount of RsaL protein, the protein responsible for mediating negative feedback on the LasI signal precursor: the more RsaL present, the more signal is required to induce the transition to a quorum-sensing up-regulated state. Thus feedback can be responsible for tuning both the level of response to quorum sensing within a population of cells and the quantities of signal molecule that are produced.

9.2.3 Noise Filtering

In modelling gene regulation networks, it is not uncommon to neglect certain aspects of the network to reduce its complexity and reduce the number of parameters that require estimating. In a number of quorum-sensing models this has been done by ignoring the feedback within the system. For example, [24] reduces the somewhat complicated quorum-sensing network of *V. harveyi* (which will be discussed further in Sect. 9.3.3) by omitting the multiple feedback loops involved. Despite the consequent lack of biological detail, the model fits luminescence data remarkably well, suggesting that perhaps the feedback is present to filter out noise and constrain the protein levels to those predicted by the model to give the observed experimental output.

In [20], the study of quorum sensing in *A. tumefaciens* mentioned in Sect. 9.2.1, it is postulated that the role of negative feedback in moving the system from being monostable (and always achieving upregulation) to bistable is manifested in the negative feedback dampening molecular noise in the system. Random fluctuations in receptor/regulator levels would otherwise disguise the system response, transforming the bistability into a smoother transition between states.

Interestingly, both negative and positive feedback loops appear capable of diluting the effects of noise. While we remarked that dimerisation was sufficient to induce bistability in a deterministic model of Gram-negative quorum sensing in [21], the authors also showed that bistability could be replaced with a graded response through the addition of noise, the same applying to positive feedback on LuxR without dimerisation. In combination, however, the system was shown to be able to produce bistability that was resistant to molecular noise.

The authors of [25] investigated alternative ways of dampening out noise. They hypothesised that the interaction of the *lux* and *ain* systems in *V. fischeri* (via the *ain* signal competitively binding LuxR but not activating it) could be responsible for controlling single cell variability (they had previously shown experimentally that the *luxIR* system alone could only maintain a stable response when averaged over the population [26]). However, even with *ain* in the model, a degree of variability between single cells remains. Hence it was concluded that the *ain* system may instead be involved in suppressing LuxR levels for as long as possible during growth and colonisation and is perhaps more likely to have a role in timing of the quorum-sensing response. Thus genetic feedback, rather than interacting systems, could be a simpler and more effective means to reduce noise within a quorum-sensing system.

9.2.4 Timing

Given that positive or negative feedback can adjust the levels of signal molecule in a system, it is natural to assume that feedback can have a role in the timing of the onset of quorum-sensing upregulation. Indeed, incorporating additional feedback into the receptor and response regulator of the quorum sensing system of *C. acetobutylicum* brings forward the onset of solventogenesis in [22]. However, surprisingly few mathematical models discuss the possible role for feedback in timing. While in some cases this is likely to be implicit (if feedback can, for instance, adjust the critical signal level at which a switch occurs, this ought to have a causal effect on timing of the switch in a given instance), in [23] it is actually found that, of the three types of repression investigated in the model (background inhibition, negative feedback and soaking up of signal molecule), negative feedback is the only one which does not noticeably affect timing of the quorum-sensing response.

9.3 Investigating Feedback with Mathematical Models

In order to illustrate how the role of feedback can be investigated with the aid of mathematical modelling, we now construct generic models of Gram-positive and Gram-negative circuits. These are much simplified (indeed, as simple as possible) and seek to capture, most importantly, the nature of the various feedback loops postulated; we omit details specific to individual networks as these will require more extensive work (as well as parameterisation), each being worthy of their own investigations. In the interests of being as comprehensive as possible within such a framework, we also consider the atypical quorum-sensing networks that have been proposed for *V. harveyi* and *V. cholerae*: these can be considered to be a hybrid of the generic Gram-positive and Gram-negative networks—more will be discussed on this in Sect. 9.3.3. Our approach builds on the quorum-sensing review of [8]

whereby we aim to mirror the biology-based characterisation of different quorum-sensing architectures therein with our own modelling results.

In each case we build a nonlinear ordinary differential equation model where variables represent the key components of the system and the kinetic terms describe in a simple way the interactions between these components (in reality these interactions may be indirect and governed in part by variables not considered here for brevity). We subsequently demonstrate how the role of feedback can be investigated by knocking out each loop from the models (either by setting a relevant parameter to zero or by altering a particular term) and comparing the resulting time-dependent solutions and steady-state curves to the wild-type model. This process is relatively straightforward and has been used in many of the more detailed studies discussed in Sect. 9.2; moreover, it illustrates the benefits of adopting a simple modelling approach.

We restrict our study within this chapter to deterministic models and therefore do not investigate the role of feedback in a noisy system explicitly. We do consider the three remaining hypothesised roles for feedback: defining transition type, tuning of key molecules and timing of the quorum-sensing response (though we shall see that, even in the absence of noise in the system, we can also gain some insight into the role of feedback in filtering noise).

9.3.1 Gram-Positive Quorum Sensing: The agr System

We begin with the less well-studied quorum-sensing system: *agr* homologues. As mentioned previously, this circuitry was first discovered in the pathogenic bacterium *S. aureus* (where it regulates virulence factor production) and has since been discovered in a variety of other Gram-positive bacteria: in *C. difficile* [27], *C. botulinum* [28, 29], *Enterococcus faecalis* [30] and *S. epidermidis* [31], *agr*-like systems also have a role to play in pathogenesis, while in non-pathogenic bacteria an *agr* system controls sporulation in *C. acetobutylicum* [32] and adherence in *Lactobacillus plantarum* [33].

As alluded to earlier, the majority of these species appear to adopt the feedback architecture of *S. aureus*, but some (notably *C. acetobutylicum*) have reduced levels of feedback. The reasons for this were investigated in [22] and as such we do not go into detail here. Instead we consider a simplified model and link the results to the putative roles for feedback discussed in Sect. 9.2.

9.3.1.1 Model Formulation

The general *agr* system is depicted in Fig. 9.2a and a simplified version in Fig. 9.2b; it is from Fig. 9.2b that we derive our model.

We assume the signal, s, and regulator, r, are each produced constitutively, at rates c_s and c_r, respectively. Regulator is activated irreversibly in response to the

Table 9.1 Descriptions of the variables and parameters used in the models for the *agr* and *luxIR* systems

Variable	Description	
s	Signal	
r	Regulator	
r^*	Active regulator	
Parameter	Rate of	Value
c_s	Basal signal production	0–1000
c_r	Basal regulator production	1
c_s^h	Increased signal production	10
c_r^h	Increased regulator production	10
α	Regulator activation	1
δ	Degradation	1
β, β_1	Ratio of regulator separation to binding on the operon	10
β_2	Ratio of regulator separation to binding on the operon	10

presence of signal at rate α. Rates of production of signal (c_s^h) and regulator (c_r^h) above the basal levels are induced by activated regulator, r^*. The ratio of separation to binding of the active regulator to the relevant operons is given by β; for simplicity we assume that this ratio is the same for both the signal and regulator (this is valid in *S. aureus*, where all the *agr* genes are contained within one operon, but may vary for species where this is not the case). Similarly, all molecules degrade at some rate δ (in reality this rate will vary between molecules).

The resulting (minimal) equations are

$$\frac{ds}{dt} = c_s + \frac{c_s^h r^*}{r^* + \beta} - \alpha s r - \delta s, \tag{9.1}$$

$$\frac{dr}{dt} = c_r + \frac{c_r^h r^*}{r^* + \beta} - \alpha s r - \delta r, \tag{9.2}$$

$$\frac{dr^*}{dt} = \alpha s r - \delta r^*. \tag{9.3}$$

Notice that the roles for s and r in this minimal model are symmetric when feedback is present onto both. To investigate how a cell may move from quorum-sensing down-regulated to up-regulated we use

$$s(0) = r(0) = r^*(0) = 0 \tag{9.4}$$

for the initial conditions.

For clarity, variable and parameter descriptions (including the default values for the latter) are given in Table 9.1. Note that we are using a specific parameter set merely to illustrate the type of behaviour that the above system can display (so that we do not even specify units). While biologically realistic parameter values are of course desirable in more detailed models, they vary between bacteria (and even

between strains of the same species); we seek here instead to examine qualitative behaviour of the quorum-sensing networks.

9.3.1.2 Numerical Investigations

The system (9.1)–(9.4) can easily be solved numerically; we do so using the `ode23` Runge–Kutta solver in Matlab R2013a. We also derive steady-state curves in XPPAUT Version 7.0. The simplified *agr* system modelled here contains two positive feedback loops (one onto the signal and one onto the regulator) and no negative feedback. The loops can be deleted from the model simply by setting $c_s^h = 0$ and/or $c_r^h = 0$.

We investigate the effect that these deletions have on the quorum-sensing behaviour by solving the system in response to various levels of signal: we can consider (9.1)–(9.4) to be representative of the quorum-sensing machinery in a single cell, hence varying c_s can be seen to be equivalent to varying the amount of signal molecule (produced also by neighbouring cells) in the environment (or equivalently to increasing population size or density). Steady-state curves in response to varying c_s are displayed in Fig. 9.4 and time-dependent solutions in Fig. 9.5.

In the wild-type model we see that the system is bistable, though much of the solution for one of the stable states lies in a biologically infeasible regime (variables should not be negative and we therefore do not plot these; we do, however, display $c_s < 0$ for visualisation of at least one of the bifurcation points). The inactive state arising when $c_s = 0$ is unstable and all positive values of c_s inevitably result in a quorum-sensing response being activated. We see from the results of removing either or both feedback loops that this is a combined effect of both loops.

Removing feedback into signal production ($c_s^h = 0$) alters the transition shape from a sharp jump (into a quorum-sensing up-regulated state) to a gradual transition as c_s increases (relating to Sect. 9.2.1). Removing feedback into the regulator (c_r^h) greatly lowers the overall response of the system (but retains the jump in activity) by lowering the amount of regulator which can be activated (see Sect. 9.2.2). We saw in [22] that altering the basal rate of regulator production has been found to modify (fine-tune) the response level appropriately, in agreement with results here.

Finally, if no feedback at all exists in the *agr* circuitry ($c_s^h = c_r^h = 0$), then the system, with increasing c_s, moves gradually to an active state but where the response is much lower. These results are reflected in the time-dependent solutions of Fig. 9.5 where we notice also that the time it takes for the quorum-sensing system to respond to signal is not noticeably affected by removal of either of the feedback loops.

9.3.1.3 Analytical Investigations

In addition to numerical solutions, we can also investigate the systems analytically for more insight into the system in general, though here is not the place to undertake

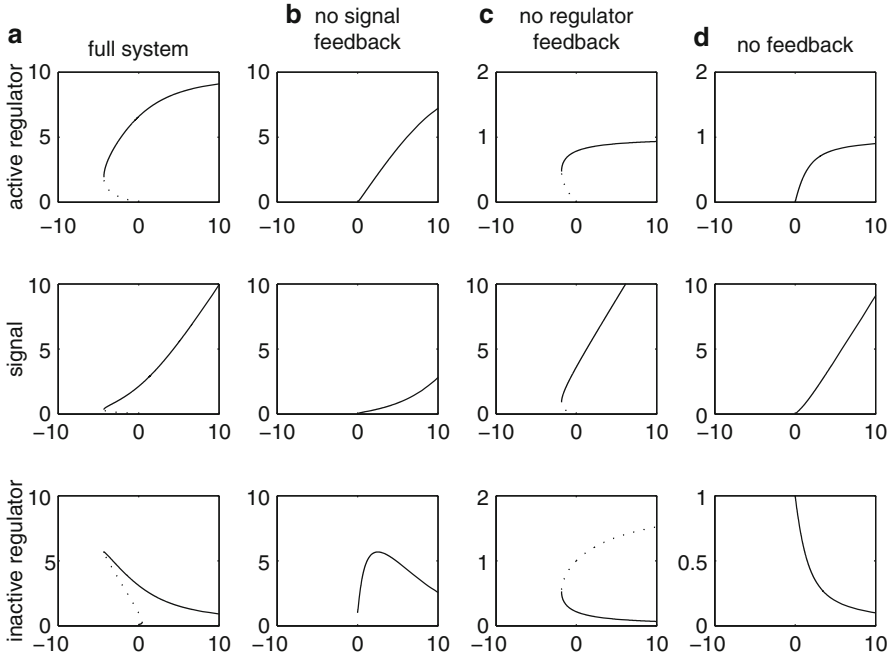

Fig. 9.4 Steady-state curves of the simplified *agr* circuitry (9.1)–(9.3) in response to changes in signal influx, c_s. Stable states are given with *solid lines* and unstable with *dotted*. The x-axis in each case is c_s. Column (**a**) represents the wild-type system, (**b**) when there is no feedback into signal production, (**c**) when there is no feedback into regulator production, and finally (**d**) when there is no feedback at all. The first, second and third rows represent active regulator, signal and inactive regulator levels respectively

extensive such investigations (those very limited ones that we do outline are in keeping with our goal of exploring models of minimal complexity). Here, we examine the case where the rate of activation is large. As $\alpha \to \infty$, two cases arise:

Case 1. $s \to 0$ (signal levels become negligible)
Case 2. $r \to 0$ (regulator levels become negligible)

Due to the symmetry in (9.1) and (9.2) noted above, we consider only Case 1. In this limit the equations become

$$\alpha s r \sim c_s + \frac{c_s^h r^*}{r^* + \beta}, \tag{9.5}$$

$$\frac{dr}{dt} \sim c_r - c_s + (c_r^h - c_s^h)\frac{r^*}{r^* + \beta} - \delta r, \tag{9.6}$$

$$\frac{dr^*}{dt} \sim c_s + \frac{c_s^h r^*}{r^* + \beta} - \delta r^*. \tag{9.7}$$

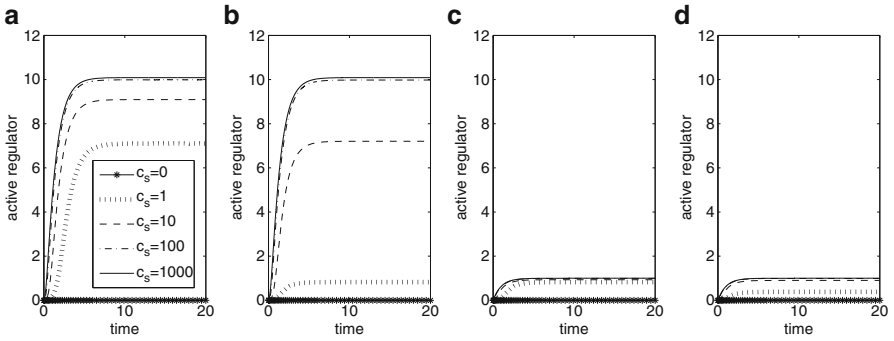

Fig. 9.5 Time-dependent solutions for the *agr* system (9.1)–(9.4) with (**a**) wild-type circuitry, (**b**) no positive feedback into signal production, (**c**) no positive feedback into regulator production and (**d**) no feedback at all. Population size is represented indirectly via the basal rate of signal production, c_s

Note that (9.7) and (9.6) can then be solved sequentially. For Case 1 to apply we require $c_r - c_s > 0$ to ensure the variables remain positive (else Case 2 arises).

In the limit as $\alpha \to \infty$, therefore, r^* (activated regulator) increases monotonically to its equilibrium state.

Case 1a. ($c_r^h - c_s^h > 0$), here the production rate of r will increase with r^* (as a natural result of the positive feedback loop).

Case 1b. ($-(c_r - c_s) < c_r^h - c_s^h < 0$) (the first inequality is needed for Case 1). This is unlikely since $c_r^h, c_s^h >> c_r, c_s$ but if $c_r^h \approx c_s^h$ we could have the counter intuitive behaviour that the increase in r^* leads to a decreasing production rate (and steady state value) of r.

9.3.2 *Gram-Negative Quorum Sensing: The luxIR System*

The *luxIR* system is the best characterised system and there is an abundance of literature available on the subject. In Sect. 9.2 we have already drawn attention to a number of examples of this system in a variety of bacteria and we do not echo this information here. Instead we move directly to model formulation.

9.3.2.1 Model Formulation

Figure 9.1a,b, respectively, illustrate the *luxIR* system and the schematic (abstract) version required for our model building in this study. Notice that when the systems are simplified, the only difference between the Gram-positive *agr* architecture and the *luxIR* one of Gram-negative species is the presence of negative feedback onto the signal in the latter. In both systems, positive feedback onto the regulator may

or may not occur depending upon the species (and strain) of interest. Note that in the interests of space, we do not consider the negative feedback onto regulator production as seen in *A. tumefaciens* since this seems not to be widely prevalent.

The model is built in the same manner as that in Sect. 9.3.1.1, but we now require the increased signal production to be both activated and inhibited by the presence of active regulator. The model becomes

$$\frac{ds}{dt} = c_s + \frac{c_s^h \beta_2 r^*}{(r^* + \beta_1)(r^* + \beta_2)} - \alpha s r - \delta s, \tag{9.8}$$

$$\frac{dr}{dt} = c_r + \frac{c_r^h r^*}{r^* + \beta_1} - \alpha s r - \delta r, \tag{9.9}$$

$$\frac{dr^*}{dt} = \alpha s r - \delta r^*. \tag{9.10}$$

To represent inhibition of signal production being weaker than activation (since the former occurs usually indirectly via homologues of the RsaL protein) we take $\beta_2 > \beta_1$ (parameters and variables for this model are also provided in Table 9.1). As before, we use

$$s(0) = r(0) = r^*(0) = 0. \tag{9.11}$$

9.3.2.2 Numerical Investigations

Given that when we consider only the minimal versions of the *agr* and *luxIR* networks the only difference between the two is negative feedback onto signal production, many of the results of Sect. 9.3.1 are also applicable here, see Figs. 9.6 and 9.7. Positive feedback onto signal production changes the shape of the system response from gradient to switch-like and positive feedback onto the regulator induces a much greater quorum-sensing response (that is more likely to coordinate behaviour of a whole population of cells than would a lower level of active regulator). Thus, the presence of the negative feedback loop does not appear to alter the roles of the two positive loops and the similarities between this and the *agr* architecture suggest that, despite the differences in mechanism between the two, any overall distinction between the two may be fairly subtle (though, naturally, a far more extensive parameter analysis than that provided here would be required to make more definitive statements).

Removal of the negative feedback onto signal production in fact makes little noticeable difference in our parameter regime. At lower values of c_s active regulator levels are higher in the absence of the loop while at higher values of c_s there is little to distinguish between the response, meaning that this negative feedback could be in place to prevent the cells from becoming quorum-sensing active prematurely. Thus the *luxIR* system may adopt this negative feedback loop to play a role in filtering noise from the system.

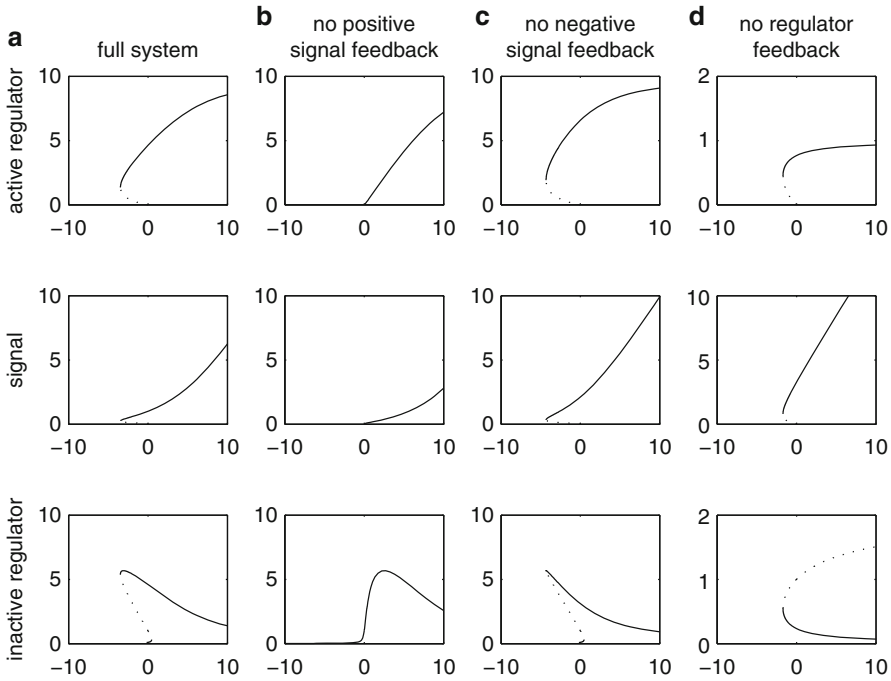

Fig. 9.6 Steady-state curves of the simplified *luxIR* circuitry (9.8)–(9.10) in response to changes in signal influx, c_s (the x-axis in each case is c_s). Stable states are given with *solid lines* and unstable with *dotted*. Column (**a**) represents the wild-type system, (**b**) no positive feedback into signal production, (**c**) no negative feedback into signal production, and finally (**d**) no positive feedback into regulator production. To achieve (**c**), Eq. (9.8) is replaced by (9.1). The first, second and third rows represent active regulator, signal and inactive regulator levels, respectively

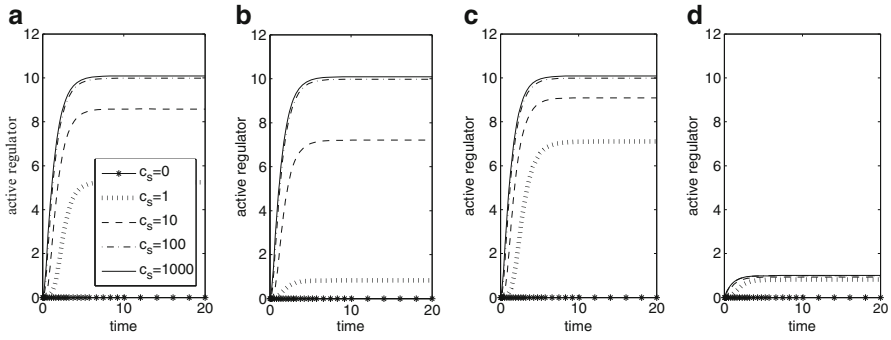

Fig. 9.7 Time-dependent solutions for the *luxIR* system (9.8)–(9.11) with (**a**) wild-type circuitry, (**b**) no positive feedback into signal production, (**c**) no negative feedback into signal production, and (**d**) no positive feedback into regulator production. Population size is represented indirectly via the basal rate of signal production, c_s

While we have to bear in mind that these results are parameter-dependent (and we have not sought a realistic parameter set), we again see no particular position for feedback in controlling the timing of the onset of a quorum-sensing response.

9.3.2.3 Analytical Investigations

We again consider the analytical effect on the system of taking $\alpha \to \infty$, i.e. a fast activation rate. Two cases emerge, as follows, that need separate description since the model is no longer symmetric between s and r.

Case 1. $s \to 0$ (signal level becomes negligible). The model becomes:

$$\alpha s r \sim c_s + \frac{c_s^h \beta_2 r^*}{(r^* + \beta_1)(r^* + \beta_2)}, \tag{9.12}$$

$$\frac{dr}{dt} \sim c_r - c_s + \left(c_r^h - c_s^h \frac{\beta_2}{r^* + \beta_2} \right) \frac{r^*}{r^* + \beta_1} - \delta r, \tag{9.13}$$

$$\frac{dr^*}{dt} \sim c_s + \frac{c_s^h \beta_2 r^*}{(r^* + \beta_1)(r^* + \beta_2)} - \delta r^*. \tag{9.14}$$

Hence r^* again increases monotonically and, since for $O(1)$ coefficients in (9.14) it never attains the regime in which the second term on the right-hand side of (9.14) $\sim c_s^h \beta_2 / r^*$, the behaviour is not qualitatively different from the previous case. If r^* does become sufficiently large, the c_s^h term becomes negligible (i.e. feedback onto the signal becomes insignificant) and the response of r becomes stronger in (9.13) relative to (9.6).

Case 2. $r \to 0$ (regulator levels becomes negligible). Here

$$\alpha s r \sim c_r + \frac{c_r^h r^*}{r^* + \beta_1}, \tag{9.15}$$

$$\frac{ds}{dt} \sim c_s - c_r + \left(\frac{c_s^h \beta_2}{r^* + \beta_2} - c_r^h \right) \frac{r^*}{r^* + \beta} - \delta s, \tag{9.16}$$

$$\frac{dr^*}{dt} \sim c_r + \frac{c_r^h r^*}{r^* + \beta} - \delta r^*. \tag{9.17}$$

In this case, the term in brackets in (9.16) becomes negative if r^* becomes sufficiently large, implying that signal production could effectively be switched off, giving a pulsed response rather than a sustained one.

9.3.3 The *V. harveyi* and *V. fischeri* Quorum-Sensing Systems

Though related to *V. fischeri*, the quorum-sensing systems of *V. harveyi* (a pathogen of marine organisms) and *V. cholerae* (the etiological agent of cholera) are somewhat different—[8] includes a review of these networks. These pathogens produce and secrete a signal molecule in much the same way as the *luxIR* system, but this signal is detected via a two-component system (akin to *agr*), i.e. the network is in some sense a hybrid of the two described above. Binding of the signal molecule to the receptor protein triggers a phosphorylation cascade between itself and the intracellular LuxO protein (note that in these systems, LuxO is considered active when it is in a dephosphorylated form, hence the bound receptor ultimately removes phosphates from LuxO). Activation of LuxO releases the production of multiple Qrr sRNAs that LuxO otherwise inhibits when inactive. Since Qrr sRNAs prevent production of the response regulator (LuxR) of the systems (via degradation of *luxR* mRNA), this releases production of LuxR, which is responsible for inducing a quorum-sensing response. We depict this process in Fig. 9.8 (including the feedback loops not addressed in the description above) but note that this is grossly simplified in several respects: intermediary molecules have been neglected where they do not have a direct role in feedback, in reality there are multiple types of Qrr sRNAs (which have different combined effects between *V. harveyi* and *V. cholerae*) and multiple signal–receptor pairs exist; see [8] for the full networks. For the purpose of this chapter, however, (i.e. to examine the role of feedback) it is satisfactory (and indeed desirable given the full system complexity) to ignore these components. In addition we neglect the receptor complex, LuxPQ, and assume LuxO dephosphorylation occurs in response to increased signal levels.

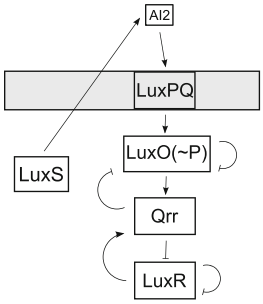

Fig. 9.8 A schematic representation of the simplified *V. harveyi* quorum-sensing network (due to the additional components required in this minimal network compared to the *agr* or *lux* systems, we do not illustrate a version in terms of only the "signal" and "regulator"). In reality, this system contains multiple signal–receptor pairings, Qrr species and intermediary molecules that we have neglected from the model. The full system (which we omit here in the interests of space due to its complexity) can be found in [8]. We depict here the LuxPQ receptor component but we do not include this in the modelling, assuming instead that phosphorylated LuxO levels relate directly to signal level (as we did for the *agr* model). The homologue of LuxR in *V. cholerae* is HapR

It is noteworthy that there is no positive feedback present in this network, meaning that, given the results of Sects. 9.3.1 and 9.3.2, one might expect a more graded response to increasing quorum-sensing signal (we shall see in Sect. 9.3.3.2 that this is indeed the case). On the other hand, there are four negative feedback loops (see Fig. 9.8). Possible explanations behind each of these loops are discussed in [8] and we shall revisit these here with our model.

9.3.3.1 Model Formulation

Very few models relevant to *V. harveyi* or *V. cholerae* quorum sensing exist in the literature and those that do focus mostly on specific aspects of either upstream elements (for example, [24]) or the action of the Qrr sRNAs (see [34] or [35]), for the large part neglecting feedback. We instead seek to formulate the simplest model that can account for all the feedback loops in this network.

Most terms in the equations are derived in the same manner as those for the *agr* and *luxIR* systems. In addition, we require autophosphorylation of LuxO in the absence of signal (at rate ϕ), dephosphorylation (and therefore activation) of LuxO∼P in the presence of signal (we recall that we omit the intermediary receptor proteins from the model) at rate α and degradation of LuxO and LuxR by Qrr sRNAs at rate κ_1 and κ_2, respectively (this also results in the degradation of Qrr sRNAs; note that, since we do not consider mRNA explicitly, we treat Qrr as acting directly on the relevant proteins). All variables and parameters are provided in Table 9.2. The model is given by

$$\frac{ds}{dt} = c_s - \alpha r_1^* s - \delta s, \tag{9.18}$$

$$\frac{dr_1}{dt} = \frac{c_{r_1}\beta}{r_1 + r_1^* + \beta} - \phi r_1 + \alpha r_1^* s - \kappa_1 q r_1 - \delta r_1, \tag{9.19}$$

$$\frac{dr_1^*}{dt} = \phi r_1 - \alpha r_1^* s - \delta r_1^*, \tag{9.20}$$

$$\frac{dq}{dt} = \frac{c_q r_1^* r_2}{(r_1^* + \beta)(r_2 + \beta)} - \kappa_1 q r_1 - \kappa_2 q r_2 - \delta q, \tag{9.21}$$

$$\frac{dr_2}{dt} = \frac{c_{r_2}\beta}{r_2 + \beta} - \kappa_2 q r_2 - \delta r_2. \tag{9.22}$$

Similarly to the previous sections, we take

$$s(0) = r_1(0) = r_1^*(0) = q(0) = r_2(0) = 0. \tag{9.23}$$

Note that, in contrast to the previous two models, there will always be regulator present in the model for $t > 0$ even when no signal is present.

Table 9.2 Descriptions of the variables and parameters used in the model for the quorum-sensing networks of *V. harveyi* and *V. cholerae*. As before, we use the simplest parameter set possible, though we find that δ must be small for any quorum-sensing response to be induced. Note that we have also made the simplification that Qrr sRNAs can be treated as acting on LuxO and LuxR proteins rather than the corresponding mRNAs

Variable	Description	
s	LuxS (signal)	
r_1	LuxO	
r_1^*	LuxO∼P	
q	Qrr	
r_2	LuxR (response regulator)	
Parameter	Rate of	Value
c_s	Basal signal production	0–100
c_{r_1}	LuxO production	1
c_{r_2}	LuxR production	1
c_q	Qrr production	1
α	Activation (dephosphorylation) of LuxO	1
ϕ	Auto-phosphorylation of LuxO	1
κ_1	Degradation of LuxO by Qrr	1
κ_2	Degradation of LuxR by Qrr	1
δ	Degradation	0.1
β	Ratio of regulator separation to binding on the operon	1

9.3.3.2 Numerical Investigations

We divide this section into discussion of the four different negative feedback loops, comparing our results with the postulated roles given in the microbiology review [8].

LuxO Autorepression

It is suggested in [8] that LuxO autorepresses in order to constrain its own levels and consequently those of the Qrr sRNAs that are produced in response to active LuxO levels. Removal of these loops in Fig. 9.9b does incur higher levels of LuxO and LuxO∼P, but does not significantly alter Qrr levels in our parameter regime (though this may be due to the influence of the remaining negative feedback loops operating). Removal of this loop has very little effect on final LuxR levels. Thus the results are in agreement with [8], suggesting that this autorepression loop may be responsible for avoiding undesirable effects of noise.

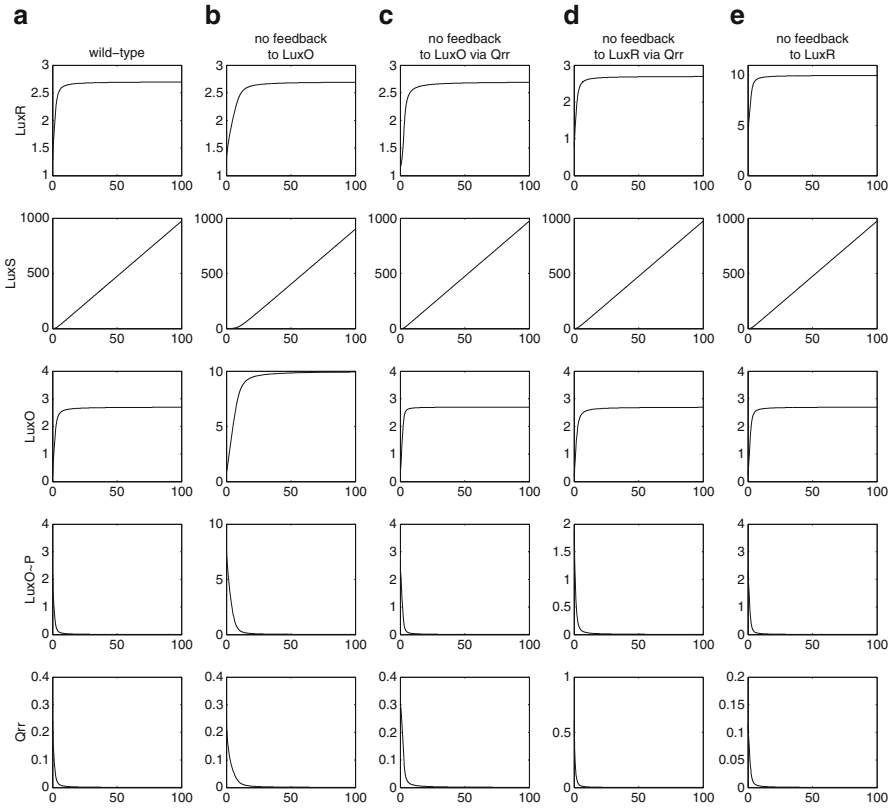

Fig. 9.9 Steady-state curves of the simplified *V. harveyi* and *V. cholerae* circuitry (9.18)–(9.22) in response to changes in signal influx, c_s (the x-axis in each case is c_s). All steady states depicted here are stable. Column (**a**) represents the wild-type system, (**b**) when there is no negative feedback into LuxO (the first term of (9.19) is replaced by c_{r_1}), (**c**) when there is no negative feedback into LuxO via Qrr ($\kappa_1 = 0$), (**d**) when there is no negative feedback into LuxR via Qrr (the first term of (9.21) is replaced by $c_q r_1^*/(r_1^* + \beta)$), and finally (**e**) no auto-repression by LuxR (the first term of (9.22) is replaced by c_{r_2}). The rows represent LuxR, signal (LuxS), active LuxO, inactive LuxO∼P and Qrr, respectively

LuxO Negative Feedback via Qrr

This feedback loop can be viewed in two ways: either to constrain the levels of LuxO or those of Qrr. We see in Fig. 9.9c that Qrr levels are increased slightly at low signal concentrations on removing this feedback loop, while LuxO concentrations remain largely the same. In agreement with [36], this does have a slight consequence on LuxR by lowering its levels (see Figs. 9.9c and 9.10c). Thus this loop may both filter out noise from Qrr levels and coordinate a greater "whole population" response at low signal levels.

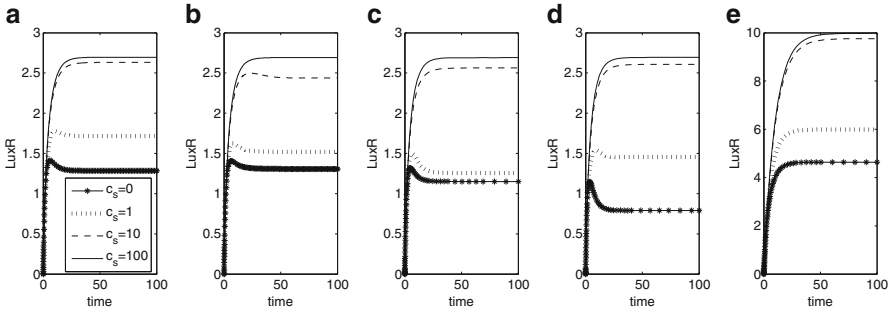

Fig. 9.10 Time-dependent solutions for the *V. harveyi* and *V. cholerae* quorum-sensing systems (9.18)–(9.23) with (**a**) wild-type circuitry, (**b**) no negative feedback into LuxO, (**c**) no negative feedback into LuxO via Qrr, (**d**) no negative feedback into LuxR via Qrr, and (**e**) no auto-repression of LuxR. Population size is represented indirectly via the basal rate of signal production, c_s

LuxR Negative Feedback via Qrr

It is hypothesised that this feedback loop should prolong the production of Qrr sRNAs and hence delay the cells attaining the levels of LuxR required for quorum-sensing activation. While it is difficult to see any difference between the wild-type steady-state curves and those where this loop has been removed (Fig. 9.9a, d) from the time-dependent solutions in Fig. 9.10d it is evident that in our parameter regime LuxR levels are actually lowered in the absence of this indirect LuxR negative feedback. This is likely to be a result of the interplay with the active loops and is worthy of further investigation to see whether this would be reproducible in reality or whether it is due to our specific parameter choice.

Timing of any quorum-sensing response again appears unaffected by this loop, but it is possible that this consequence could be lost from the model as a result of omission of intermediary species along the pathway, which would slow down the response.

LuxR Auto Repression

Removing LuxR autorepression has a similar effect to including positive autoinduction of the regulators in Sects. 9.3.1 and 9.3.2: LuxR levels significantly increase. This has little or no effect on the other variables in the model but the loop should prevent unnecessary production of LuxR (see Sect. 9.2.2). This agrees with the biological explanation in [8], where it is suggested that this loop will prevent runaway *luxR* transcription, minimising the chance of ill-timed commitment to quorum-sensing upregulation. Though it does not change the shape of the response (Sect. 9.2.1), it does alter the sensitivity of the overall system to signal levels. Furthermore, higher LuxR levels would make it trickier for the cells to switch *off* their quorum sensing response [36, 37].

Overall, therefore, this model implies that each individual negative feedback loop may prevent fluctuations in individual components of the network, constraining them to the desired level, whether this be to prevent unnecessary overproduction or to prevent inappropriate reactions to noisy inputs. This should ensure a coordinated response across a population of cells and matches neatly the evidence that both *V. harveyi* and *V. cholerae* are insensitive to small changes in signal level [8]. In addition, their mutual action maintains a graded response from the cells, preventing an on-off type switch [36] (though we note that in individual loop knock-outs, the response shape always remains largely the same (see Fig. 9.9), thus this may be as a result of their combined effects).

9.3.3.3 Analytical Investigations

For the *V. harveyi* and *V. cholerae* systems we consider the possibility that both the activation rate and the action of Qrr sRNAs are large: $\alpha, \kappa_1, \kappa_2 \to \infty$. This yields various possibilities and we focus on the case in which the signal and Qrr sRNA levels become negligible: $s, q \to 0$. This gives

$$\alpha r_1^* s \sim c_s, \tag{9.24}$$

$$q \sim \frac{c_q r_1^* r_2}{(r_1^* + \beta)(r_2 + \beta)(\kappa_1 r_1 + \kappa_2 r_2)}, \tag{9.25}$$

$$\frac{dr_1}{dt} \sim \frac{c_{r_1}\beta}{r_1 + r_1^* + \beta} - \phi r_1 + c_s - \frac{c_q \kappa_1 r_1^* r_2 r_1}{(r_1^* + \beta)(r_2 + \beta)(\kappa_1 r_1 + \kappa_2 r_2)} - \delta r_1, \tag{9.26}$$

$$\frac{dr_1^*}{dt} \sim \phi r_1 - c_s - \delta r_1^*, \tag{9.27}$$

$$\frac{dr_2}{dt} \sim \frac{c_{r_2}\beta}{r_2 + \beta} - \frac{c_q \kappa_2 r_1^* (r_2)^2}{(r_1^* + \beta)(r_2 + \beta)(\kappa_1 r_1 + \kappa_2 r_2)} - \delta r_2. \tag{9.28}$$

If, in addition, we take the small limit of the rate of LuxO autophosphorylation ($\phi \to 0$, so the cells are increasingly likely to become activated), then $r_1 \to 0$ and we have (we note that a number of limits are required in the current case to achieve the level of simplicity attained earlier in (9.5)–(9.7) and (9.12)–(9.17): the virtue of such an approach—and the reason for including the analysis—is that the properties of the resulting system, (9.29)–(9.31), are almost completely transparent)

$$\phi r_1 \sim c_s + \frac{c_{r_1}\beta}{r_1^* + \beta}, \tag{9.29}$$

$$\frac{dr_1^*}{dt} \sim \frac{c_{r_1}\beta}{r_1^* + \beta} - \delta r_1^*, \tag{9.30}$$

$$\frac{dr_2}{dt} \sim \frac{c_{r_2}\beta}{r_2 + \beta} - \frac{c_q r_1^* r_2}{(r_1^* + \beta)(r_2 + \beta)} - \delta r_2. \tag{9.31}$$

Note that at leading order in this scenario, response regulator levels (r_2) are governed by the negative feedback loops: the source term is monotonically decreasing in r_2 and the action of the Qrr sRNAs is present implicitly. Thus the negative feedback loops remain significant in this limit.

It is hoped that such comments indicate the potential scope and value of analytic (in particular, asymptotic) investigations.

9.4 Summary

We have provided a general review of mathematical models of quorum sensing that consider the role of feedback in bacterial cell communication. Drawing on this, four dominant roles were apparent: defining the shape of the system response (often controlled by the presence of a positive feedback loop inducing bistability), tuning of signal or regulator levels (usually either a positive feedback loop ensuring a coordinated response from a whole population of cells or the absence of a positive—or inclusion of a negative—loop either simply reducing unnecessary production of proteins or inducing population heterogeneity), filtering noise out from the system (largely via negative feedback) or in the timing of the onset of a quorum-sensing response.

Interestingly, the last of these does not frequently arise from the results of mathematical models but is often postulated in biological articles. It is possible therefore that feedback may not be as important in the timing of a quorum-sensing response as often assumed, but the modelling results could also be a consequence of the simplifying assumptions required to make a mathematical model tractable. For instance, considering transcription and translation separately (and therefore mRNA and proteins) could delay the signal transduction through a pathway in a numerical solution, providing more scope for feedback to affect timing, but would typically result in increased numbers of variables, parameters to estimate and complexity in the analysis.

The models presented of the *agr*, *luxIR* and *V. harveyi*/*V. cholerae* quorum-sensing systems were deliberately simplified for ease of analysis but were still able to identify the first three roles for feedback listed above. In the *agr* system, positive feedback influences the shape of the transition between quorum-sensing down- and up-regulated states and makes a coordinated response from the whole population more likely. The *lux* system, additionally, employs a negative feedback loop that is likely to play a role in filtering noise from the system. Similarly, the *V. harveyi* and *V. cholerae* systems adopt multiple negative feedback loops capable of constraining protein and signal levels and making the system robust to noise. Regarding this last network, it is possible to imagine that each loop dominates at the appropriate time as the signal is transmitted through the cell and this would likely best be studied using delay differential equations.

There is scope for an abundance of future work related to this review including more detailed models of specific networks (including such delay effects, as well

as stochastics) and, in particular, the inclusion of experimental data for better parameter estimation (genetic manipulation can be performed experimentally to reproduce the modified network architectures discussed in this study). It will be fascinating to see if different parameter regimes are capable of displaying different goals for identical feedback architectures. Moreover, as more quorum-sensing systems and their targets are identified, it will be enlightening to see how these targets tie in with the relevant feedback architecture.

Acknowledgements SJ thanks the MRC for funding in the form of a Biomedical Informatics Fellowship.

References

1. Redfield RJ (2002) Is quorum sensing a side effect of diffusion sensing? Trends Microbiol 10:365–370
2. Hense BA, Kuttler C, Müller J, Rothballer M, Hartmann A, Kreft J (2007) Does efficiency sensing unify diffusion and quorum sensing? Nature Rev Mirobiol 5:230–239
3. Williams P (2007) Quorum sensing, communication and cross-kingdom signalling in the bacterial world. Microbology 153:3923–3938
4. Nealson KH, Hastings JW (1979) Bacterial bioluminescence: its control and ecological significance. Microbiol Rev 43:496–518
5. Ji G, Beavis RC, Novick RP (1995) Cell density control of staphylococcal virulence mediated by an octapeptide pheromone. Proc Natl Acad Sci USA 92:12055–12059
6. Henke JM, Bassler BL (2004) Bacterial social engagements. Trends Cell Biol 14:648–656
7. Waters CM, Bassler BL (2005) Quorum sensing: cell-to-cell communication in bacteria. Annu Rev Cell Dev Biol 21:319–346
8. Ng W-L, Bassler BL (2009) Bacterial quorum-sensing network architectures. Annu Rev Genet 43:197–222
9. Oyarzún DA, Chaves M, Hoff-Hoffmeyer-Zlotnik M (2012) Multistability and oscillations in genetic control of metabolism. J Theor Biol 295:139–153
10. Smits WK, Kuipers OP, Veening JW (2006) Phenotypic variation in bacteria: the role of feedback regulation. Nat Rev Microbiol 4:259–271
11. Anguige K, King JR, Ward JP, Williams P (2004) Mathematical modelling of therapies targeted at bacterial quorum sensing. Math Biosci 192:39–83
12. Dockery JD, Keener JP (2001) A mathematical model for quorum sensing in *P. Aeruginosa*. Bull Math Biol 63:95–116
13. Gustafsson E, Nilsson P, Karlsson S, Arvidson S (2004) Characterizing the dynamics of the quorum-sensing system in *S. aureus*. J Mol Microbiol Biotechnol 8:232–242
14. Jabbari S, King JR, Koerber AJ, Williams P (2010) Mathematical modelling of the *agr* operon in *S. aureus*. J Math Biol 61:17–54
15. Anguige K, King JR, Ward JP (2005) Modelling antibiotic- and anti-quorum sensing treatment of a spatially-structured *P. aeruginosa* population. J Math Biol 51:557–594
16. Haseltine EL, Arnold FH (2008) Implications of rewiring bacterial quorum sensing. Appl Environ Microb 74:437–445
17. Ward JP, King JR, Koerber AJ, Williams P, Croft JM, Sockett RE (2001) Mathematical modelling of quorum sensing in bacteria. IMA J Math Appl Med 18:263–292
18. Fagerlind MG, Rice SA, Nilsson P, Harlén M, James S, Charlton T, Kjelleberg S (2003) The role of regulators in the expression of quorum-sensing signals in *P. aeruginosa*. J Mol Microbiol Biotechnol 6:88–100

19. Kuttler C, Hense BA (2008) Interplay of two quorum sensing regulation systems of *V. fischeri*. J Theor Biol 251:167–180
20. Goryachev AB, Toh D, Wee KB, Lee T, Zhang H, Zhang L (2005) Transition to quorum sensing in an *Agrobacterium* population: a stochastic model. PLoS Comp Biol 1:265–275
21. Goryachev AB, Toh D, Lee T (2006) Systems analysis of a quorum sensing network: design constraints imposed by the functional requirements, network topology and kinetic constants. Biosystems 83:178–187
22. Jabbari S, Steiner E, Heap JT, Winzer K, Minton NP, King JR (2013) The putative influence of the *agr* operon upon survival mechanisms used by *C. acetobutylicum*. Math Biosci 243: 223–239
23. Ward JP, King JR, Koerber AJ, Croft JM, Sockett RE, Williams P (2004) Cell-signalling repression in bacterial quorum sensing. Math Med Biol 21:169–204
24. Banik SK, Fenley AT, Kulkarni RV (2009) A model of signal transduction during quorum sensing in *V. harveryi*. Phys Biol 6:1–10
25. Pérez PD, Weiss JT, Hagen SJ (2011) Noise and crosstalk in two quorum-sensing inputs of *V. fischeri*. BMC Syst Biol 5:153
26. Pérez PD, Hagen SJ (2010) Heterogeneous response to a quorum-sensing signal in the luminescence of individual *V. fischeri*. PLoS ONE 5:e15473
27. Martin MJ, Clare S, Goulding D, Faulds-Pain A, Barquist L, Browne HP, Pettit L, Dougan G, Lawley TD, Wren BW (2013) The *agr* locus regulates virulence and colonization genes in *C. difficile* 027. J Bacteriol 195:3672–3681
28. Cooksley CM, Davis IJ, Winzer K, Chan WC, Peck MW, Minton NP (2010) Regulation of neurotoxin production and sporulation by a putative *agrBD* signaling system in proteolytic *C. botulinum*. Appl Environ Microb 76:4448–4460
29. Sebaihia M, Peck MW, Minton NP et al (2007) Genome sequence of a proteolytic (Group I) *C. botulinum* strain Hall A and comparative analysis of the clostridial genomes. Genome Res 17:1082–1092
30. Qin X, Singh KV, Weinstock GM, Murray BE (2001) Characterization of *fsr*, a regulator controlling expression of gelatinase and serine protease in *E. faecalis* OG1RF. J Bacteriol 183:3372–3382
31. Van Wamel WJB, van Rossum G, Verhoef J, Vandenbroucke-Grauls CMJE, Fluit AC (1998) Cloning and characterization of an accesory gene regulator (*agr*)-like locus from *S. epidermidis*. FEMS Microbiol Lett 163:1–9
32. Steiner E, Scott J, Minton NP, Winzer K (2012) An *agr* quorum sensing system that regulates granulose formation and sporulation in *C. acetobutylicum*. Appl Environ Microbiol 78: 1113–1122
33. Sturme MHJ, Nakayama J, Molenaar D, Murakami Y, Kunugi R, Fujii T, Vaughan EE, Kleerebezem M, de Vos WM (2005) An *agr*-like two-component regulatory system in *L. plantarum* is involved in production of a novel cyclic peptide and regulation of adherence. J Bacteriol 187:5224–5235
34. Fenley AT, Banik SK, Kulkarni RV (2011) Computational modeling of differences in the quorum sensing induced luminescence phenotypes of *V. harveyi* and *V. cholerae*. J. Theor. Bio. 274:145–153
35. Mehta P, Goyal S, Wingreen NS (2008) A quantitative comparison of sRNA-based and protein-based gene regulation. Mol Syst Biol 4:221
36. Teng SW, Schaffer JN, Tu KC, Menta P, Lu W, Ong NP, Bassler BL, Wingreen NS (2011) Active regulation of receptor ratios controls integration of quorum-sensing signals in *V. harveyi*. Mol Syst Biol 7:491
37. Svenningsen SL, Tu KC, Bassler BL (2009) Gene dosage compensation calibrates four regulatory RNAs to control *V. cholerae* quorum sensing. EMBO J 28:429–439

Chapter 10
The Role of Biosurfactants in Bacterial Systems

Raf De Dier, Maarten Fauvart, Jan Michiels, and Jan Vermant

10.1 Bacteria, Quorum Sensing, and Surfactant Production

The complex biochemistry inside bacterial systems results in the production of several species of molecules with complex composition and architecture. This architecture may have a specific biological role, but often also entails a significant surface activity of the molecules. For example, in the important process of quorum sensing, small chemical molecules are secreted by bacteria to achieve a basic form of communication between individual cells. Compounds such as peptides in Gram-positive bacteria and N-Acyl Homoserine Lactones (AHL) in Gram-negative bacteria [1] are continuously produced by these organisms. As the population grows, these signaling molecules reach a threshold concentration and trigger changes within a cell regarding gene expression, enzyme activity, secretion, and many other behaviors [2, 3]. However, among these secretion products are often surface active agents, or surfactants in short, as produced by bacterial systems such as *Bacillus subtilis*, *Escherichia coli*, *Rhizobium etli*, *Proteus mirabilis* and rhamnolipids in *Pseudomonas aeruginosa* [4, 5].

R. De Dier
Soft Matter, Rheology and Technology, KU Leuven - University of Leuven,
W. de Croylaan 46, B-3001 Heverlee, Belgium

M. Fauvart • J. Michiels
Centre of Microbial and Plant Genetics, KU Leuven - University of Leuven,
Kasteelpark Arenberg 20, B-3001 Heverlee, Belgium

J. Vermant (✉)
Soft Matter, Rheology and Technology, KU Leuven - University of Leuven,
W. de Croylaan 46, B-3001 Heverlee, Belgium

The laboratory of Soft Materials, Department of Materials at ETH Zürich,
Vladimir-Prelog-Weg 5, CH-8093, Zürich, Switzerland
e-mail: Jan.Vermant@cit.kuleuven.be

S.J. Hagen (ed.), *The Physical Basis of Bacterial Quorum Communication*, Biological and Medical Physics, Biomedical Engineering, DOI 10.1007/978-1-4939-1402-9_10

The most common usage of surfactants in biological sciences is for their bactericidal nature and their use in cell lysis. The addition of surfactants to a liquid suspension of bacterial cells causes these surface active molecules to adhere to the interface between the water phase and the cell wall where they disturb the surface interactions and subsequently may lead to rupture of the cell membrane [6]. In contrast, surfactants have also been shown to confer several biological advantages to the bacterial organism that can self-produce them, all related to the alteration of interfacial properties. One of these roles is to increase attachment of individual cells to hydrophobic surfaces, initiating the formation of biofilms [4, 7–9]. The same mechanism is also utilized to obtain emulsification of organic compounds, increasing the apparent solubility of carbon resources and so their availability to the bacterial community [10–12]. Additionally, molecules of the quorum sensing system may have a dual role as surfactant and the process of cell lysis can be used to rupture the cell membranes of neighboring competing organisms, such as viruses [13, 14], bacteria [4, 15], or fungi [16, 17]. Another important biological advantage of self-production of surfactants is the ability of rapid surface colonization. This process is referred to as swarming and describes a coordinated movement across solid or semi-solid surfaces at velocities that are much faster than any other type of motility such as swimming or gliding [18]. This will be discussed in more detail below.

The production of the surfactants that play a role in this variety of phenomena in bacterial systems seems often to be regulated by quorum sensing, and surfactant concentrations will be proportional to concentration. Only at high population densities, the concentration of the secreted signal molecules becomes significant. Processes such as improved adhesion, emulsification, and surface translocation can be seen as a built-in reaction to a high population density and accompanying low nutrient sources and brings forth a mechanism for attracting or seeking out new food sources.

10.2 Swarming as a Surfactant-Driven Fluid Flow

The main activity and challenge of bacterial communities is to survive. In order to achieve this, cells need sufficient amounts of nutrients and minerals to grow and reproduce. In an aqueous environment, this is an easy task, as diffusion of the available nutrients and the swimming movement of the cells lead to significant fluxes. However, colonies on solid or semi-solid surfaces have to cope with more difficult circumstances as both diffusion and cell movement are drastically reduced, which can lead to a depletion of nutrients for a large part of the cells within the community. One way to overcome these difficulties is the formation of a biofilm, a moist slime consisting of self-produced polysaccharides that encapsulates the cells in the colony, preventing dehydration and stimulating the partitioning of the accessible nutrients [19, 20].

When the population density within a colony exceeds a critical value for the resources to sustain, the cells need to undergo surface translocation in search for

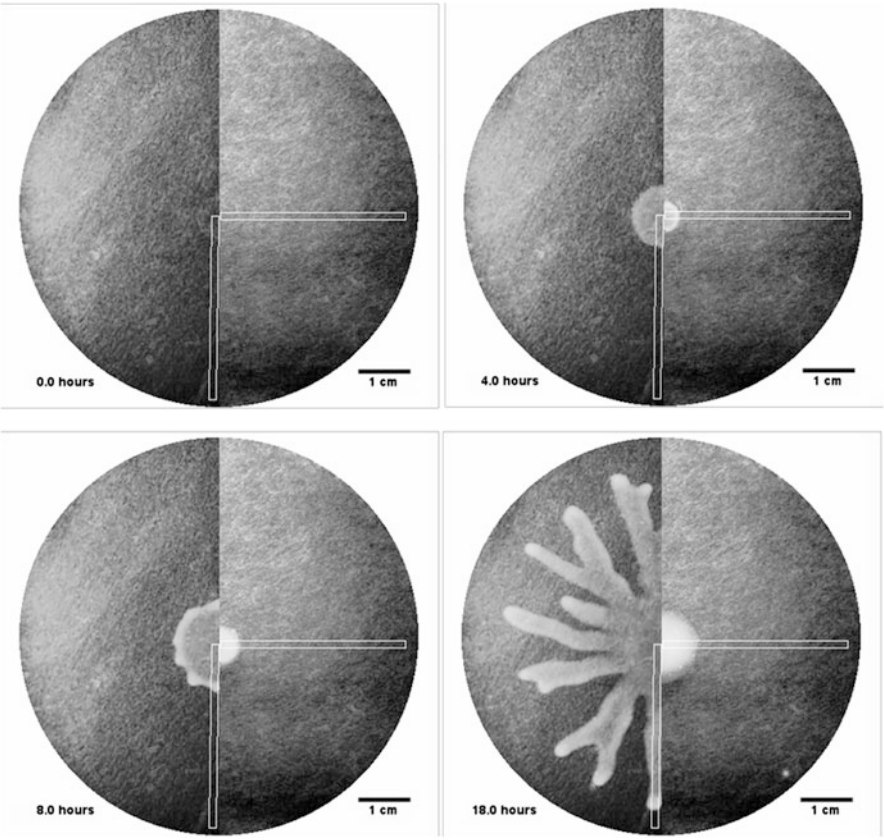

Fig. 10.1 Surface colonization of a swarming *P. aeruginosa* wild-type (*left*) and a non-swarming surfactant-deficient mutant (*right*) community [29]—Reproduced by permission of The Royal Society of Chemistry

new nutrient sources. Due to the high friction of the cell body with the solid or semi-solid substrate, this movement is significantly hampered. In response, some organisms have developed a mechanism where cells within the colony transform from vegetative to so-called *swarmer* cells, characterized by the presence of numerous flagella, in order to overcome the higher friction with the surface, and become strongly elongated by suppression of cell division [19, 21]. Although swarmer cells are mainly located at the colony edge, the process of swarming is found to be a strongly cooperative phenomenon between all participating cells in the biofilm. It has been suggested that the vegetative cells account for the supply of nutrients that are dispersed among all cells, while the swarmer cells, mostly situated at the edge, bundle their numerous flagella to form rafts, groups of side-by-side aligned cells [22] and expand the boundaries of the biofilm.

Numerous studies have shown that apart from cell differentiation also surfactants play an important role in swarming. However, often it was difficult to identify

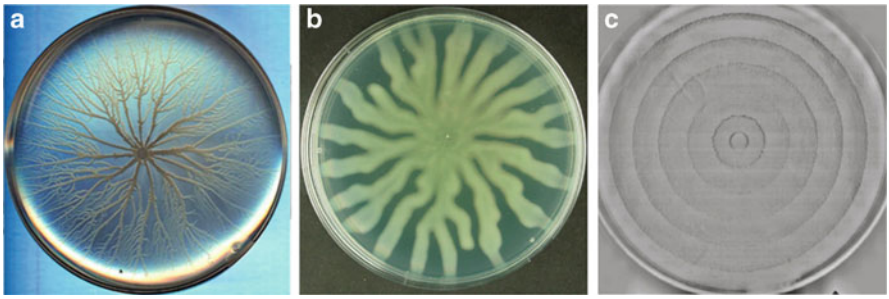

Fig. 10.2 A multitude of swarming patterns: Fractal-like patterns in *Bacillus subtilis* (**a**) [30] (Reprinted from Marrocco et al. [30] with permission from Cambridge University Press), dendritic shapes in *P. aeruginosa* (**b**) (Reprinted from Verstraeten et al. [20] with permission from Elsevier) and a "bulls eye pattern" *Proteus mirabilis* (**c**) (Reprinted figure with permission from Czirok et al. [31]. Copyright (2001) by the American Physical Society)

the exact role of these molecules [3, 19, 21–28]. An experiment, as illustrated in Fig. 10.1, shows a colony of *P. aeruginosa* on a semi-solid surface where the amount of nutrients is expected to decrease due to localized consumption. In the left part of the image, a wild-type strain undergoes a rapid surface colonization process upon reaching a high population density and accompanying depletion of the nutrients. In contrast, in the right-hand part, a mutant strain, in which only the gene that is responsible for the production of a bio-surfactant is knocked out, is not able to achieve a similar translocation, in spite of all other conditions being equal.

The swarming is often accompanied by striking and beautiful patterns (Fig. 10.2), such as the fractal-like patterns in *Bacillus subtilis* [32], the dendritic shapes in *P. aeruginosa* [33], or the concentric circles in *Proteus mirabilis* [31]. This way, it is often believed that the surfactant merely functions as a wetting agent in this process, lowering friction between cell and surface and it is surmised that differences in individual cell motility between the species are responsible for the variety of swarming patterns observed. Additionally, quantitative biological models are highly nonlinear and can produce a wide range of morphologies [34]. However, these models focus on matching the patterns with experimental observations and do not explain the velocities of swarming, nor the effect of different physical parameters. Despite the often biologically related mechanisms that are suggested, it may be that purely physico-chemical phenomena can account for these observations, where parameters such as the heterogeneity of the surface and the viscosity dependence on cell concentration all affect the action of swarming [29, 35]. Therefore, it has recently been suggested that all swarming observations, regardless of the differences in pattern formation, can be related to the same driving force that triggers the fast surface translocation, namely the surface active nature of the secreted molecules by the quorum sensing system and spatial variations in bacterial density. This surface tension gradient control is an a-specific mechanism, relying only on surface tension effects only, and hence it may be a generic mechanism in many bacterial systems [20, 29, 35–37].

To fully understand how differences in surface active molecules can activate a colony to cooperatively spread out over a surface, the properties of the surfactants need to considered. Surfactants locally modify the interfacial interactions with a change in the surface tension as a result, which strongly decreases for higher concentrations of surface active molecules. Concentration gradients of these surfactants that exist within the biofilm will result in gradients in surface tension, which can set up a liquid flow away from the zone of low surface tension, as liquid with a higher surface tension pulls onto the surrounding liquid. The result is that the biofilm starts to flow in a direction along the surface tension gradient towards the higher surfactant concentration, a phenomenon referred to as the Marangoni effect [38], mitigating the existing difference in surfactant concentration to even out the interface. If such surface tension gradients are observed to be present in bacterial systems, they can suggest a physico-chemical approach to understanding and controlling the swarming phenomenon.

10.3 Surfactant Concentration Gradients Induce Marangoni Flows

The occurrence of a Marangoni flow in bacterial systems is controlled by three factors: (i) a quorum sensing regulated or related production of the surface active species, (ii) strong concentration dependence of the interfacial properties, and (iii) the presence of a spatial or temporal gradient of the secreted surface active molecules. In only a few cases, swarming has been clearly related to the production of surfactants. Many other bacterial species that show swarming behavior have not been adequately screened for surfactant production or vice versa. Table 10.1 lists some of the known quorum sensing regulated surfactants that are secreted by diverse organisms. The concentrations that are encountered in the local environment are generally high and exceed the concentrations needed for Marangoni flows to occur. The surface active nature of these secreted molecules can easily be assessed by evaluating the change in surface tension with concentration, as illustrated in

Table 10.1 Quorum sensing-related surfactant molecules produced by diverse microorganisms. The relevant physico-chemical surfactant properties are: the surface tension value (σ), critical micelle concentration (CMC), and biologically relevant concentrations (c)

Microorganism	Surfactant	σ (mNm^{-1})	*CMC* (μM)	c (gL^{-1})	Reference
B. subtilis	Surfactin	27–32	0.02	2–3	[5, 39]
S. marcescens	Serrawettin	28–34	0.01	1	[40, 41]
P. aeruginosa	Rhamnolipid	28–30	0.04	2.5	[42, 43]
E. coli	α-haemolysin	47	0.002	–	[44]
R. etli	AHL	< 40	–	–	[36]

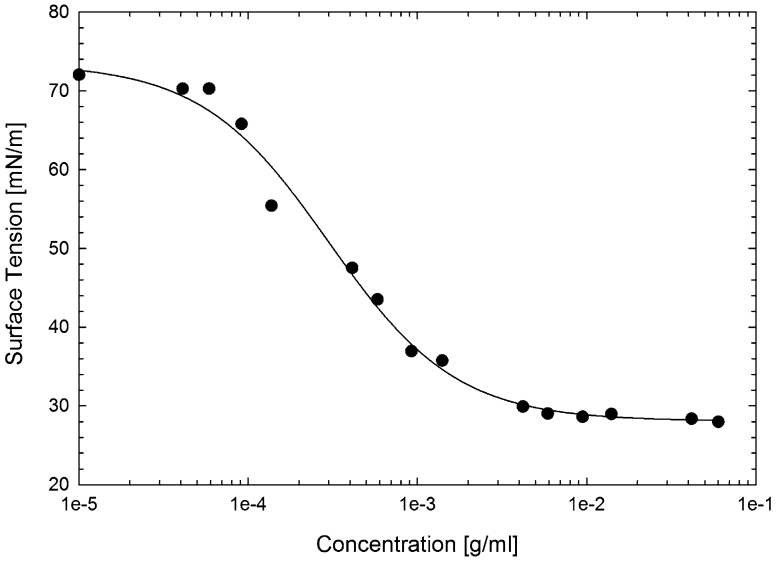

Fig. 10.3 Evolution of the surface tension as a function of concentration for rhamnolipids extracted from *P. aeruginosa* colonies

Fig. 10.3 for *P. aeruginosa* cells, measured using a Wilhelmy plate tensiometer. The surface tension drastically decreases in value starting at very low concentrations until it reaches a nearly constant value when the adsorption starts to compete with the formation of micelles in the bulk (as defined by the critical micelle concentration, CMC). As strong changes in surface tension can be achieved at small concentrations of surfactants, strong Marangoni flows can be generated within the bacterial community at biologically relevant concentrations.

The mechanism by which these local variations in surfactant concentration and surface tension emerge within the biofilm has not yet univocally been identified. Different hypotheses have emerged to explain the existence of such gradients. A first description brings into play the geometry of the entire bacterial biofilm [37], which can be described as a spherical cap. The height of the colony is the largest in the center and gradually decreases towards the edges, proportional to the number of cells present (Fig. 10.4a). Under the assumption that the surfactant production for each cell is identical, the concentration of surfactant at the colony edge is expected to be smaller than at the center of the cap, creating an outward gradient along the surface, in the same direction as the swarming phenomenon. This leads to a high surface tension in the liquid layer on top of the substrate pulling along the biofilm containing secreted surfactants.

Visualization of the actual geometrical shape of a biofilm shows that the spherical cap assumption is not valid for all microorganisms. Rather, a pancake-like geometry can be observed, where the height is approximately constant throughout the colony. A second explanation suggests a more localized distribution of surfactant molecules

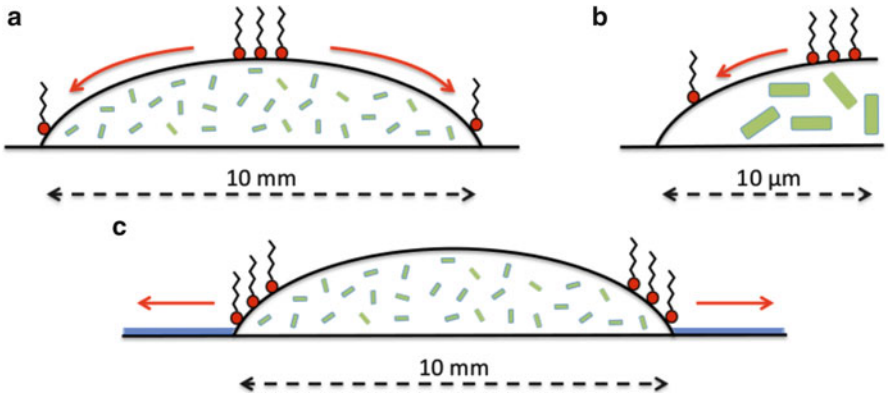

Fig. 10.4 Possible mechanisms for surfactant concentration gradients within bacterial biofilms: spherical cap geometry [37] (**a**), penetration depth theory [29] (**b**) and precursor film analysis [35] (**c**)

at the very edge of the biofilm [29], due to the impossibility of the bacteria to fully penetrate the outer layers of the biofilm leading to lower concentrations of bacteria near the edge (Fig. 10.4b). An additional effect may be the down-regulation of the surfactant production at the biofilm edges during the swarming process [45], creating a very local gradient in surface tension that drives the liquid flow.

A third interpretation states that the surfactant concentration gradient is not found within the biofilm itself, but between the colony and the underlying uncontaminated substrate [35] (Fig. 10.4c). In case the surface beneath the biofilm contains a sufficient amount of moisture, a continuous interface can be formed between the pristine substrate film and the concentrated surfactant solution of the biofilm.

10.4 Modeling the Swarming Process

A variety of models exist that characterize the swarming behavior of specific bacterial organisms. Three classes are routinely encountered in literature: (1) population growth (2) reaction-diffusion and (3) fluid mechanical-Marangoni models.

The basic population models are differential equation models solely based on the multiplication of cells using the nutrients that are available in the immediate environment, combined with an active, yet random movement of all cells in the colony during its growth. These actions are described using a system of partial differential equations and solved to obtain the evolution of all dependent parameters, such as cell concentration and nutrient levels in space and time. Additional effects such as chemotaxis, the increased mobility of cells located at the biofilm edge, and the bundled rafts of cells can be implemented to increase the directionality of the bacterial movement and to predict some of the experimentally observed patterns [31, 46–49].

Other authors describe swarming using reaction-diffusion models that contain a set of equations to represent the evolution in biofilm properties such as the cell density of "active" (motile) and "passive" (vegetative) cells and the local nutrient concentration by a range of processes including cell growth and division and nutrient diffusion and consumption. The cell movement is modeled as a random, diffusion-controlled operation that is initiated by the reaction on the property of interest, such as cell density, reaching a limit value [30, 50–52]. These reaction-diffusion models contain an excess of experimental parameters by which all observed swarming patterns can be represented. However, the association of these parameters with the underlying mechanisms that govern the process of swarming is limited such that no biological or physical explanations can be extracted from these models to describe the variations in the patterns of different bacterial species.

A third class of models uses a fluid mechanical approach, taking into account the effect of bacterial surfactant production and the accompanying Marangoni flows. A simple back-of-the-envelope calculation already allows to check if the Marangoni flows can possibly account for the mechanism during the swarming process by comparing the actual spreading velocities and the predicted velocities encountered in Marangoni flows [29,37]. Assuming the biofilm can be considered as a continuum (viscoelastic) liquid, the driving force for a Marangoni flow is the surface tension gradient, which creates a shear stress τ acting on the liquid:

$$\tau = \frac{\Delta\sigma}{L} \tag{10.1}$$

where L is the length scale over which a gradient in surface tension, $\Delta\sigma$ exists. Here, L can maximally be the radius of the bacterial colony. This spreading action is opposed by the process of viscous dissipation. Work against viscous forces is irreversibly converted into internal energy, proportional to the viscosity η and the velocity U of the moving fluid and inversely proportional to the biofilm height H:

$$\tau = \frac{\eta U}{H} \tag{10.2}$$

Taking experimental values for the biofilm height H and viscosity η and the size of the colony and realistic gradients of surface tension into the dimensionless analysis equations (10.1) and (10.2) and equating these lead to spreading velocities expected for Marangoni driven flows to be in the range of 0.5–5 μms^{-1}, which match the observed velocities in swarming colonies very well [29]. These velocities are an order of magnitude higher than what would be expected for other forms of surface translocation such as wetting and swimming.

More detailed descriptions and a full quantitative modeling exist that expand this simple dimensional analysis. These models bridge the phenomena occurring at the level of the individual cell with the effects at a macroscopic level. This way, processes such as cell growth and division, nutrient consumption, and production of quorum sensing signals and surfactants are correlated to their influence on a larger scale, the Marangoni effect [35, 53].

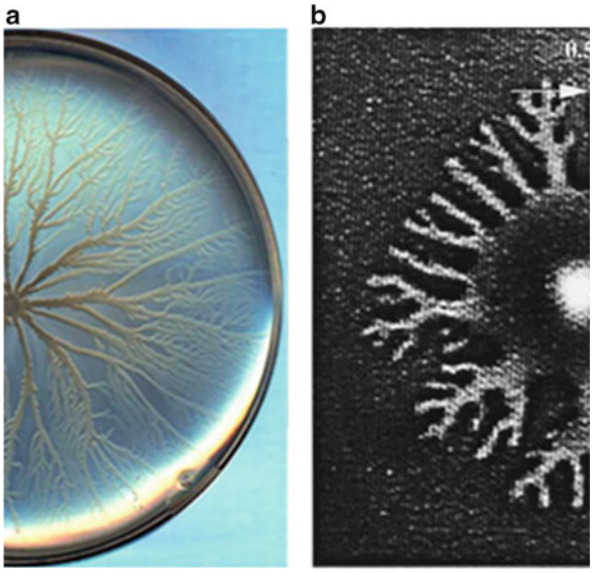

Fig. 10.5 Marangoni driven swarming: (**a**) Fractal-like swarming of *Bacillus subtilis* on a semi-solid agar surface [30] (Reprinted from Marrocco et al. [30] with permission from Cambridge University Press) and (**b**) patterns during spreading of an aqueous surfactant droplet on a thin water film (Reprinted with permission from Matar and Troian [54], Copyright 1999, AIP Publishing LLC)

Similar approaches as used in the basic differential equations or reaction-diffusion analysis models can be used to describe the biological processes on the single cell scale. To describe the physical process of the Marangoni forces, literature provides sufficient examples, such as the spreading of surfactant droplets on a thin water film [54–61]. The effects observed in these experiments, such as the spreading velocities, but more specifically the resulting patterns during the spreading action of the droplet uncover a strong similarity with the biofilm swarming observations, as illustrated in Fig. 10.5.

The evolution of the droplet (or biofilm) shape in presence of Marangoni stresses over time is represented by the change in height of the liquid layer, $H(x,t)$ as function of distance x and time t. Incorporated into this equation is the driving force of the Marangoni spreading, opposed by the action of creation of surface curvature, respectively:

$$\frac{\partial H}{\partial t} = -\frac{1}{2\eta}\frac{\partial}{\partial x}\left(\frac{\partial \sigma}{\partial x}H^2\right) - \frac{\sigma}{3\eta}\frac{\partial}{\partial x}\left(H^3\frac{\partial^3 H}{\partial x^3}\right) \tag{10.3}$$

The local surfactant concentration $\Gamma(x,t)$ allows to estimate the magnitude of the Marangoni forces, with an additional surface diffusivity (D_s) term:

$$\frac{\partial \Gamma}{\partial t} = -\frac{\partial}{\partial x}\left(\frac{1}{\eta}\frac{\partial \sigma}{\partial x}H\Gamma\right) - \frac{\partial}{\partial x}\left(\frac{\sigma}{2\eta}\Gamma H^2\frac{\partial^3 H}{\partial x^3}\right) + D_s\frac{\partial^2 \Gamma}{\partial x^2} \tag{10.4}$$

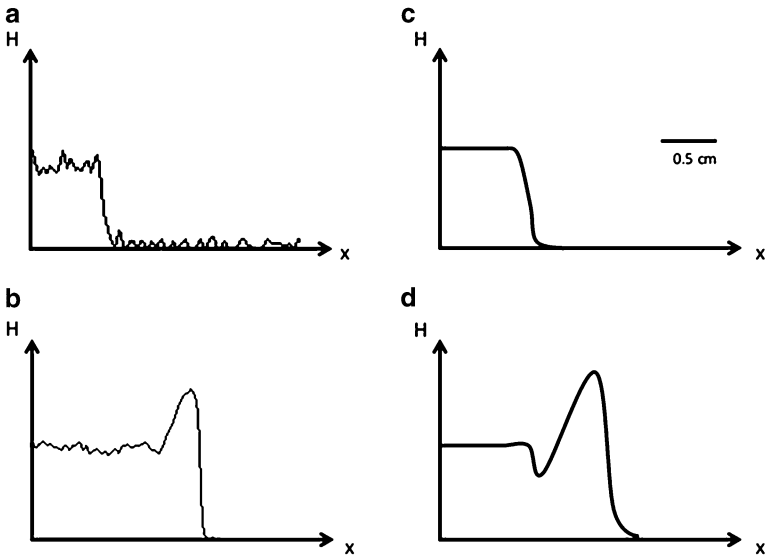

Fig. 10.6 Height profiles of swarming colonies (**a**-**b**) Experimental [29] biofilm and (**c**-**d**) predicted height profiles for Marangoni driven swarming, where (**a**) and (**c**) reflect the initial stage and (**b**) and (**d**) reflect the stage just before the pattern becomes unstable (Part a and b from [29]—Reproduced by permission of The Royal Society of Chemistry)

Both equations can be linked using an equation of state that relates the concentration of the surfactant to the surface tension property:

$$\frac{\sigma}{\sigma_0 - \sigma} = (\alpha - 1)\left(1 - \frac{\Gamma}{\Gamma_m}\left[\left(\frac{(\alpha + 1)}{\alpha}\right)^{1/3} - 1\right]\right)^{-3} \tag{10.5}$$

with σ_0 the surface tension of the pure liquid, $\alpha = \sigma/(\sigma_0 - \sigma)$ and Γ_m the maximum surfactant concentration at the interface [29, 37].

In each simulation step, both set of equations, on the local and macroscopic level, can be solved independently using suitable initial and boundary conditions. These results are subsequently used as an update for the starting solution in the next iteration step. In the initial stage, a droplet containing surfactant molecules is deposited onto a thin liquid film, representing a biofilm holding self-produced biosurfactants on top of a solid or semi-solid surface (Fig. 10.6a, c). Due to the low surface tension at the droplet interface and the higher surface tension at the pristine water film surrounding the droplet, Marangoni forces induce a radially outward flow from the center. Over time, a rim in the height of the spreading liquid, as shown in Fig. 10.6b,d, as the edge of the expanding droplet is not able to move as fast for the liquid that is pulled in from behind by Marangoni forces [57, 60]. These

steps occur in both the droplet spreading as in the biological swarming experiment and reveal a strong similarity between the experimental observations and theoretical simulations [35, 53], as emphasized in Fig. 10.6.

In a later stage, the rim becomes unstable by perturbations in surfactant concentration along the droplet's spreading edge, possibly created by inhomogeneities in the underlying substrate [55, 56]. These concentration differences destabilize the interface of the droplet and create local protrusions from the spreading colony at a velocity that is faster than the neighboring zones in the spreading rim, forming distinct fingering patterns as previously observed in Fig. 10.2.

The instabilities that occur along the edge of the rim have a dominant wavelength associated with the fingers. This wavelength is dependent on several parameters, such as temperature, substrate, and surfactant type, directly influencing the distance between the fingers that emerge from the spreading droplet. Given the highly nonlinear nature of the governing equations, it can be assumed that a change in one or more of these parameters can form the explanation why the swarming patterns in different bacterial organisms show variations, going from very thin, fractal-like patterns in *Bacillus subtilis* to thicker dendrites in *P. aeruginosa* to even no observable instabilities in *Proteus mirabilis* by surfactants that are not able to sufficiently destabilize the interface.

10.5 Drying of Bacterial Colonies

The presence of self-produced surfactants by bacteria has a strong effect on the swarming motility of the entire colony on a semi-solid or solid surface, which is a situation where the contact line of the colony is moving. In addition to this effect, surfactants also strongly affect the phenomena during the dehydration and drying of a biofilm, a situation where the contact line is pinned.

Figure 10.7 shows the difference between a dried colony of a *P. aeruginosa* colony for a wild-type and surfactant-production deficient mutant [62]. In the absence of surfactants, the dehydration leads to a ring-shaped pattern that is formed as the majority of all cells present in the biofilm are accumulated at the outer rim and only few are found in the center, as depicted in Fig. 10.7a. In contrast, for the surfactant-producing organism, observations show a uniform distribution of cells after complete evaporation of the colony (Fig. 10.7b). Moreover, the mutant does show a similar deposition pattern as the wild-type strain upon exogenous addition of surfactant. The presence of surfactant molecules appears to induce a completely different morphology during the drying of biofilms and will influence the viability of the colony once it rehydrates when environmental conditions improve. The uniform spreading of all cells encountered in the dehydration process can be seen as a natural strategy to prevent bacterial overlap and to maximize the chances to reach new food sources [63]. Interestingly, the surfactants can hence both cause height increases of a colony near the edge, when the colony is swarming and the contact line moves

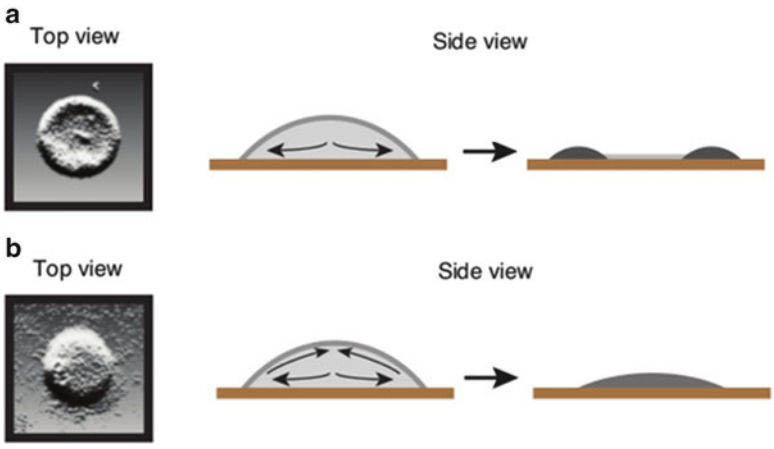

Fig. 10.7 The drying of a small bacterial colony for (**a**) surfactant-deficient mutant and (**b**) wild-type cells of *P. aeruginosa*—Reproduced from [62]

(as discussed in the previous section, when the colony is producing extra material), or do the opposite when the contact line of the colony is pinned (as during drying of the colony).

During the evaporation of water from a colony, or a droplet in general, a phenomenon commonly referred to as the "coffee ring effect" induces an internal flow from the center radially outwards [64–67]. This flow is strong enough to entrain all suspended matter, such as cells, and brings all this to the edge where they accumulate over time, leaving behind a ring-like deposit upon complete evaporation of all solvent.

When surfactants are self-produced by the colony, the dynamics change drastically. In addition to the accumulation of the bacterial cells, surfactant molecules are also convected from the center outwards by the internal flow and the concentration increases at the edge. As these molecules are advected from the center of the biofilm, a depletion of surfactants is created at the apex. These concentration differences along the free surface of the biofilm generate a mismatch in surface tension and create a Marangoni flow that is directed from the low surface tension at the edge to the higher surface tension at the quasi pristine interface in the center [62, 68]. The Marangoni flow acts together with the outward evaporative flow to create a swirling motion where cells that are convected outwards reach the edge and, once there, are pulled upwards and back inwards along the interface by the Marangoni flow. Over time, the swirling flow prevents accumulation and results in a homogeneous deposit of all cells after complete evaporation of the moisture in the colony.

10.6 Conclusion

In the process of quorum sensing, biosurfactants are often found to be among the secretion products in many bacterial species and they have proven to have a beneficial effect on the producing organism. In general, the presence of these molecules increases the chances of survival by an increase in the availability of food sources or the destruction of other, possibly harmful, cells. However, the biological advantage is visible the most in the phenomenon of swarming: a coordinated movement across solid or semi-solid surfaces at velocities much higher than gliding, twitching, swimming, or any other type of motility.

Simple experiments have shown the necessity of surfactants in this swarming process, which leads to the exploration of new resources when the population further grows. The main influence of surfactant molecules on this spreading behavior is, however, often misinterpreted and has generated an enormous amount of theories that only are applicable for the specific organism under study, resulting in a lack of a general perspective of a phenomenon that can universally be described by purely physico-chemical means. Apart from any possible role in communication, surfactants and the presence of local concentration gradients of these molecules and a resulting gradient in surface tension play a key role in swarming.

The pattern formation, height profiles, and swarming speeds can be rationalized and quantitatively predicted by considering the dependency of the different physico-chemical parameters and the surfactant activity. So far, only the fingering patterns have been investigated and an analysis of the set of nonlinear differential equations may require further investigations, in particular with respect to understanding the sensitivity of the different physico-chemical parameters that control the richness in experimentally observed patterns. Clearly, the questions of how the individual bacteria and their possible differentiation intervene in the phenomena remain highly relevant.

References

1. Miller MB, Bassler BL (2001) Quorum sensing in bacteria. Ann Rev Microbiol 55:165,199
2. Davey ME, Caiazza NC, O'Toole GA (2003) Rhamnolipid surfactant production affects biofilm architecture in pseudomonas aeruginosa pa01. J Bacteriol 185:1027–1036
3. Caiazza NC, Shanks RMQ, O'Toole GA (2005) Rhamnolipids modulate swarming motility patterns of pseudomonas aeruginosa. J Bacteriol 187(21):7351–7361
4. Fiechter A (1992) Biosurfactants: moving towards industrial application. Trends Biotechnol 10:208–217
5. Georgiou G, Lin S-C, Sharma MM (1992) Surface-active compounds from microorganisms. Biotechnology 10:60–65
6. Hotchkiss RD (1946) The nature of the bactericidal action of surface active agents. Ann New York Acad Sci 46:479–493
7. Ron EZ, Rosenberg E (2001) Natural roles of biosurfactants. Environ Microbiol 3(4):229–236

8. Raaijmakers JM, de Bruijn I, Nybroe O, Ongena M (2010) Natural functions of lipopeptides from bacillus and pseudomonas: more than surfactants and antibiotics. FEMS Microbiol Rev 34:1037–1062
9. Van Hamme JD, Singh A, Ward OP (2006) Physiological aspects part 1 in a series of papers devoted to surfactants in microbiology and biotechnology. Biotechnol Adv 24:604–620
10. Desai JD, Banat IM (1997) Microbial production of surfactants and their commercial potential. Microbiol Mol Biol Rev 61:47–64
11. Neu TR (1996) Significance of bacterial surface-active compounds in interaction of bacteria with interfaces. Microbiol Rev 60:151–166
12. Chrzanowski L, Lawniczak L (2012) Why do microorganisms produce rhamnolipids? World J Microbiol Biotechnol 28:401–419
13. Huang X, Lu Z, Zhao H, Bie X, Lü F, Yang S (2006) Antiviral activity of antimicrobial lipopeptide from bacillus subtilis fmbj against pseudorabies virus, porcine parvovirus, newcastle disease virus and infectious bursal disease virus in vitro. Int J Pept Res Therapeut 12(4):373–377
14. Vollenbroich D, Ozel M, Vater J, Kamp RM, Pauli G (1997) Mechanism of inactivation of enveloped viruses by the biosurfactant surfactin from bacillus subtilis. Biologicals 25:289–297
15. Bais HP, Fall R, Vivanco JM (2004) Biocontrol of bacillus subtilis against infection of arabidopsis roots by pseudomonas syringae is facilitated by biofilm formation and surfactin production. Plant Physiol 134:307–319
16. Touré Y, Ongena M, Jacques P, Guiro A, Thonart P (2004) Role of lipopeptides produced by bacillus subtilis ga1 in the reduction of grey mould disease caused by botrytis cinerea on apple. J Appl Microbiol 96:1151–1160
17. Wang J, Liu J, Chen H, Yao J (2007) Characterization of fusarium graminearum inhibitory lipopeptide from bacillus subtilis ib. Appl Microbiol Biotechnol 76:889–894
18. Henrichsen J (1972) Bacterial surface translocation: a survey and a classification. Bacteriol Rev 36(4):478–503
19. Harshey RM (2003) Bacterial motility on a surface: many ways to a common goal. Ann Rev Microbiol 57:249–273
20. Verstraeten N, Braeken K, Debkumari B, Fauvart M, Fransaer J, Vermant J, Michiels J (2008) Living on a surface: swarming and biofilm formation. Trends Microbiol 16:496–506
21. Kearns DB (2010) A field guide to bacterial swarming motility. Nat Rev Microbiol 8(9): 634–644
22. Copeland MF, Weibel DB (2009) Bacterial swarming: a model system for studying dynamic self-assembly. Soft Matter 5:1174–1187
23. Butler MT, Wang Q, Harshey RM (2010) Cell density and mobility protect swarming bacteria against antibiotics. Proc Natl Acad Sci 107(8):3776–3781
24. Niu C, Graves JD, Mokuolu FO, Gilbert SE, Gilbert ES (2005) Enhanced swarming of bacteria on agar plates containing the surfactant tween 80. J Microbiol Meth 62:129–132
25. Xu J, Platt TG, Fuqua C (2012) Regulatory linkages between flagella and surfactant during swarming behavior: lubricating the flagellar propeller. J Bacteriol 194(6):1283–1286
26. Kearns DB, Losick R (2003) Swarming motility in undomesticated bacillus subtilis. Mol Microbiol 49(3):581–590
27. Partridge JD, Harshey RM (2013) Swarming: flexible roaming plans. J Bacteriol 195(5): 909–918
28. Turner L, Zhang R, Darnton NC, Berg HC (2010) Visualization of flagella during bacterial swarming. J Bacteriol 192(13):3259–3267
29. Fauvart M, Phillips P, Bachaspatimayum D, Verstraeten N, Fransaer J, Michiels J, Vermant J (2012) Surface tension gradient control of bacterial swarming in colonies of pseudomonas aeruginosa. Soft Matter 8:70–76
30. Marrocco A, Henry H, Holland IB, Plapp M, Sé ror SJ, Perthame B (2010) Models of self-organizing bacterial communities and comparisons with experimental observations. Math Modell Nat Phenom 5:148–162

31. Czirok A, Matsushita M, Vicsek T (2001) Theory of periodic swarming of bacteria: application to proteus mirabilis. Phys Rev E Stat Phys Plasma Fluids Relat Interdiscipl Top 63:031915
32. Julkowska D, Obuchowski M, Holland IB, Sé ror SJ (2005) Comparative analysis of the development of swarming communities of bacillus subtilis 168 and a natural wild type: critical effects of surfactin and the composition of the medium. J Bacteriol 187:65–76
33. Tremblay J, Richardson AP, Lé pine F, Dé ziel E (2007) Self-produced extracellular stimuli modulate the pseudomonas aeruginosa swarming motility behaviour. Environ Microbiol 9:2622–2630
34. Ben-Jacob E, Cohen I, Levine H (2000) Cooperative self-organization of microorganisms. Adv Phys 49:395–554
35. Du H, Xu Z, Anyan M, Kim O, Leevy WM, Shrout JD, Alber M (2012) High density waves of the bacterium pseudomonas aeruginosa in propagating swarms result in efficient colonization of surfaces. Biophys J 103:601–609
36. Daniels R, Reynaert S, Hoekstra H, Verreth C, Janssens J, Braeken K, Fauvart M, Beullens S, Heusdens C, Lambrichts I, De Vos DE, Vanderleyden J, Vermant J, Michiels J (2006) Quorum signal molecules as biosurfactants affecting swarming in rhizobium etli. Proc Natl Acad Sci 103(40):14965–14970
37. Angelini TE, Roper M, Kolter R, Weitz DA, Brenner MP (2009) Bacillus subtilis spreads by surfing on waves of surfactant. Proc Natl Acad Sci 106(43):18109–18113
38. Marangoni C (1871) über die ausbreitung der tropfen einer flüssigkeit auf der oberfläche einer anderen. Annalen der Physik (Leipzig) 143:337–354
39. Yeh M-S, Wei Y-H, Chang J-S (2005) Enhanced production of surfactin from bacillus subtilis by addition of solid carriers. Biotechnol Progr 21:1329–1334
40. Matsuyama T, Tanikawa T, Nakagawa Y (2011) Serrawettins and other surfactants produced by serratia. Microbiol Monogr 20:93–120
41. Satyanarayana T, Johri BN, Prakash A (2012) Microorganisms in environmental management: microbes and environment. Springer, New York pp 638–640
42. Gunther NW, Nunez A, Fett W, Solaiman DKY (2005) Production of rhamnolipids by Pseudomonas chlororaphis, a nonpathogenic bacterium. Appl Environ Microbiol 71: 2288–2293
43. Raza ZA, Khalid ZM, Khan MS, Banat IM, Rehman A, Naeem A, Saddique MT (2010) Surface properties and sub-surface aggregate assimilation of rhamnolipid surfactants in different aqueous systems. Biotechnol Lett 32:811–816
44. Sanchez-Magraner L, Cortajarena AL, Goni FM, Ostolaza H (2006) Membrane insertion of escherichia coli /$alpha$-hemolysin is independent from mebrane lysis. J Biol Chem 281: 5461–5467
45. Tremblay J, Dé ziel E (2010) Gene expression in pseudomonas aeruginosa swarming motility. BioMed Central Genom 11:587
46. Kawasaki K, Mochizuki M, Matsushita A, Umeda T, Shigesada N (1997) Modeling spatio-temporal patterns created by bacillus subtilis. J Theor Biol 188:177–185
47. Esipov SE, Shapiro JA (1998) Kinetic model of proteus mirabilis swarm colony development. J Math Biol 36:249–268
48. Daniels R, Vanderleyden J, Michiels J (2004) Quorum sensing and swarming migration in bacteria. FEMS Microbiol Rev 28:261–289
49. Davies DG, Parsek MR, Pearson JP, Iglewski BH, Costerton JW, Greenberg EP (1998) The involvement of cell-to-cell signals in the development of a bacterial biofilm. Science 280: 295–298
50. Zorzano MP, Hochberg D, Cuevas MT, Gomez-Gomez JM (2005) Reaction-diffusion model for pattern formation in e. coli swarming colonies with slime. Phys Rev E 71:031908
51. Mimura M, Sakaguchi H, Matsushita M (2000) Reaction-diffusion modelling of bacterial colony patterns. Phys A 282:283–303
52. Golding I, Kozlovsky Y, Cohen I, Ben-Jacob E (1998) Studies of bacterial branching growth using reaction-diffusion models for colonial development. Phys A 260:510–554

53. Du H, Xu Z, Shrout M, Alber JD (2011) Multiscale modeling of pseudomonas aeruginosa swarming. Math Model Meth Appl Sci 21:939–954
54. Matar OK, Troian SM (1999) Spreading of a surfactant monolayer on a thin liquid film: onset and evolution of digitated structures. Chaos 9:141–153
55. Matar OK, Troian SM (1999) The development of transient fingering patterns during the spreading of surfactant coated films. Phys Fluid 11(11):3232–3246
56. Warner MRE, Craster RV, Matar OK (2004) Fingering phenomena associated with insoluble surfactant spreading on thin liquid films. J Fluid Mech 510:169–200
57. Troian SM, Herbolzheimer E, Safran SA (1990) Model for the fingering instability of spreading surfactant drops. Phys Rev Lett 65(3):333–336
58. Fischer BJ, Troian SM (2003) Growth and decay of localized disturbances on a surfactant-coated spreading film. Phys Rev E 67:016309
59. Fanton X, Cazabat AM, Qué ré D (1996) Thickness and shape of films driven by a marangoni flow. Langmuir 12:5875–5880
60. Cazabat AM, Heslot F, Troian SM, Carles P (1990) Fingering instability of thin spreading films driven by temperature gradients. Nature 346:824–826
61. Bertozzi AL, Münch A, Fanton X, Cazabat AM (1998) Contact line stability and 'undercompressive shocks' in driven thin film flow. Phys Rev Lett 81(23):5169–5172
62. Sempels W, De Dier R, Mizuno H, Hofkens J, Vermant J (2013) Auto-production of biosurfactants reverses the coffee ring effect in a bacterial system. Nat Comm 4:1757
63. Ben-Jacob E, Schochet O, Tenenbaum A, Cohen I, Czirok A, Vicsek T (1994) Generic modelling of cooperative growth patterns in bacterial colonies. Nature 368:46–49
64. Deegan RD, Bakajin O, Dupont TF, Huber G, Nagel SR, Witten TA (1997) Capillary flow as the cause of ring stains from dried liquid drops. Nature 389:827–829
65. Deegan RD, Bakajin O, Dupont TF, Huber G, Nagel SR, Witten TA (2000) Contact line deposits in an evaporating drop. Phys Rev E 62:756–765
66. Hu H, Larson RG (2002) Evaporation of a sessile droplet on a substrate. J Phys Chem B 106:1334–1344
67. Hu H, Larson RG (2005) Analysis of the microfluid flow in an evaporating sessile droplet. Langmuir 21:3963–3971
68. Still T, Yunker PJ, Yodh AG (2012) Surfactant-induced marangoni eddies alter the coffee-rings of evaporating colloidal drops. Langmuir 28:4984–4988

Chapter 11
Ecology of a Simple Synthetic Biofilm

Edward M. Nelson, Utkur Mirsaidov, Koshala Sarveswaran, Nicolas Perry, Volker Kurz, Winston Timp, and Gregory Timp

11.1 Introduction

Most bacteria are found in dense communities within biofilms [1, 2]. A biofilm comprises microcolonies of live bacteria with intervening water channels and layers of dead cells encapsulated in a hydrated matrix of polysaccharides, proteins, and other extracellular polymeric substances (EPS). A biofilm confers a competitive advantage on the community over a free-swimming planktonic bacterium as it affords protection against environmental stresses like oxidants, antibiotics, extreme pH shifts, or macrophages [3]. Because they are so prevalent—biofilms can be found in everything from water distribution systems to catheter tubes [4, 5] and troublesome—biofilms have been implicated in 65 % of all infections [6, 7]—their development, architecture, and population dynamics have been the subjects of intense scrutiny. However, the creation of relevant models remains a vexing problem because native biofilms are so complex. Methods have been developed to synthesize model biofilms based on passing a bacterial suspension through a flow-cell [8] or

E.M. Nelson • K. Sarveswaran • N. Perry • V. Kurz
Electrical Engineering, University of Notre Dame, Notre Dame, IN 46556, USA
e-mail: enelson6@nd.edu; ksarvesw@nd.edu; Nicholas.Perry.78@nd.edu; vkurz@nd.edu

U. Mirsaidov
Department of Physics, National University of Singapore, Singapore 117551, Singapore
e-mail: phyumm@nus.edu.sg

W. Timp
Department of Biomedical Engineering, Johns Hopkins University, Baltimore, MD, USA
e-mail: wtimp@jhu.edu

G. Timp (✉)
Electrical Engineering and Biological Sciences Departments, University of Notre Dame, Notre Dame, IN 46556, USA
e-mail: gtimp@nd.edu

S.J. Hagen (ed.), *The Physical Basis of Bacterial Quorum Communication*, Biological and Medical Physics, Biomedical Engineering, DOI 10.1007/978-1-4939-1402-9_11

parallel plate reactors [9, 10], but they do not generally afford control over the biofilm architecture with single cell specificity, while concurrently allowing for testing dynamics—and a lot of this work is accomplished in single species biofilms.

The complex heterogeneous community of microbes comprising a native biofilm reflects different epigenetic and genetic constituencies, and environmental gradients in nutrient and flow conditions. The EPS encapsulates the cells, placing them in close proximity within the biofilm, and enabling genetic exchange, cell-to-cell communications and the formation of symbiotic microconsortia [2]. Intraspecies and interkingdom communications occur within a biofilm all at the same time, which can affect the formation, structure, and fitness in an ecological niche [11]. For example, some bacteria within a biofilm have been observed to coordinate their response to an environmental stimulus through quorum-sensing (QS) signals [12–16]. According to the QS hypothesis, bacteria count their numbers by producing, releasing, and detecting small, diffusible, signaling molecules. QS can coordinate differentiation in a biofilm, producing phenotype diversity that allows adaptation to the environment, and has been implicated in bacterial surface motility [15] and biofilm architecture, and may play a role in the exchange of genetic materials [13, 16]. However, the information communicated by the QS signals can depend on environmental conditions—mixing and flow, and the density, distribution and type of cells producing the signals and their antagonists [17–20]. This observation has prompted an alternative view, which posits that the QS signal acts simply as a probe measuring mass transport in the microenvironment of otherwise autonomous cells [12, 13]. Finally, noise in the QS communication channel can compromise the coordination of the cellular response to environmental changes [21–25]. In part, the origins of the noise can be traced to the stochasticity associated with a few copies of genes and low concentrations of protein and ligands either in the QS signal transmitter, the receiver or the medium connecting the two. To mitigate the noise, some QS systems rely on stochastic, bistable switching elements to coordinate behaviors and produce predictable biological functions [21].

In the chapter that follows, we review our efforts to develop a model that captures some aspects of the ecology in a biofilm [17, 21, 26–28]. To explore the ecology, live-cell lithography was used to create two-dimensional (2D) and three-dimensional (3D) synthetic biofilms from genetically engineered bacteria [26, 28]. Live-cell lithography described in the next Sect. 11.2 uses laminar flows in a microfluidic device to convey cells within the capture range of multiple, time-shared holographic optical tweezers formed from a laser using a high numerical aperture objective along with acousto-optical deflectors (AODs) and a spatial light modulator (SLM) that are used to precisely manipulate the 3D positions of multiple cells into arrays. Subsequently, the cells in the arrays were encapsulated in a photopolymerized hydrogel—creating a living "voxel". The bacteria forming the voxels in a synthetic biofilm were transformed with plasmids that separately transmit and receive acyl-homoserine lactone (AHL) signaling molecules used in QS [24–27] to create communication links (com-links).

Generally, in QS, each cell is both a transmitter and receiver, and requires two proteins: (1) an AHL-synthase (I); and (2) an AHL-binding protein (R), which acts

as a signal receptor and transcriptional activator [12, 29, 30]. The AHL-synthase produces AHL that, in combination with the AHL-binding protein, positively regulates the production of the synthase creating a positive feedback loop. In many gram-negative bacteria, QS is accomplished by a signaling circuit comprised of a protein homologous to LuxI of *Vibrio fischeri*, which produces a diffusible AHL signal, as well as a receptor protein that is homologous to LuxR of *Vibrio fischeri*. Thus, in QS, there is no distinction between transmitting and receiving cells since each cell is both a transmitter and receiver. However, in this work, the QS circuitry was separated into two cell types, a transmitter and receiver, to form a com-link that can be spatially distributed. The transmitter can signal only—and the receiver transmits no signal at all. Thus, native QS circuits were separated into two parts: one gene that co-expresses the AHL-synthase with a fluorescence reporter and another that produces the AHL-binding protein that activates a fluorescent reporter in the presence of AHL. Subsequently, separate bacteria were transformed with these sub-circuits. In the second Sect. 11.3, we describe tests of cell-to-cell signaling. The *lux* quorum sensing (QS) system of *Vibrio fischeri* and the *lac* induction system in *E. coli* were chosen for testing cell signaling in a biofilm because many of the parameters that govern the reaction kinetics are already known, enabling quantitative simulations of the experiments for prediction of the outcomes from an environmental stimulus [21, 27, 31, 32]. Moreover, due to live-cell lithography it was possible, in principle, to address each cell of each voxel to assess the effect of the environment on gene expression.

Noise is inherent to single-cell behavior; it results from the small cell volume and stochasticity associated with a few copies of genes and dilute concentrations of molecules. Moreover, cascading variable elements can amplify noise [22–24, 33–35]. Each step in a cascade receives a stochastic signal from its upstream transmitter and adds variability to it. Interestingly, in the third Sect. 11.4 we show that, despite the noise in the transmitted signal, the receiver response was found to be tightly coordinated after the initial pulse of inducer in these synthetic biofilms—a stochastic switch in the receiver gene circuit actually provides noise abatement—and the noise is suppressed compared to the transmitter [21].

Thus, the gene circuitry in these simple biofilms reflects an integrated design approach [36] that promotes coordinated activity by leveraging noisy signaling systems that are responsive to the environment. We pursued this route in an attempt to produce a predictable biological function, which is the primary goal of all synthetic biology. Whereas native QS systems are supposed to rely on stochastic, bistable switching elements to coordinate behaviors [37] prior to this effort, it was problematic to study the behavior of these feedback mechanisms directly in single cells due to the difficulty in controlling the microenvironment and probing the resulting behavior at the same time. These models provide an opportunity to follow the coordination of single-cell behavior. Moreover, these efforts represent a launch point for the study of more complex models described in the final Sect. 11.5 that can be accessed through live-cell lithography.

11.2 Creating Synthetic Biofilms with Live-Cell Lithography

There are a number of ways to co-culture two or more cell types and control the cell positions [38–48] and each has advantages and limitations, but none of these techniques has shown the ability to assemble individual cells with single cell precision into heterotypic 3D configurations like that found in vivo as live-cell lithography can. At the core of the live-cell lithographic approach is the ability to create heterotypic microarrays of cells using optical tweezers in conjunction with a microfluidic device to control with submicron-scale precision the cell-type and position within the tissue [26, 28]. The optical tweezers are formed from a laser using a high numerical aperture objective along with AODs and an SLM that are used to manipulate the 3D positions of multiple cells into arrays. Cells are conveyed to the tweezers using laminar flows in a multi-port microfluidic device, tweezed into position, and subsequently encapsulated in a photopolymerizable hydrogel—creating a living voxel. As illustrated in Fig. 11.1a, a single living voxel, consisting

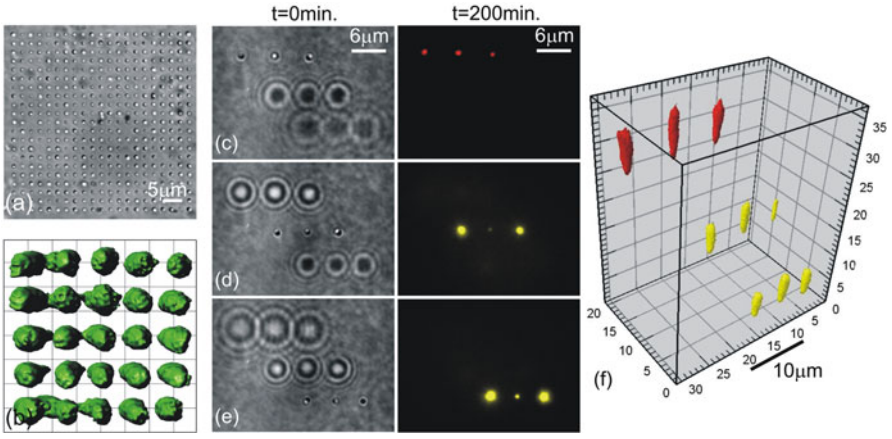

Fig. 11.1 Optical micrographs showing living voxels containing bacteria. (**a**) A transmission micrograph of a 21×21—2D microarray of *P. aeruginosa* formed with a 100×, 1.25NA oil immersion (Zeiss Plan-Apo) objective at $\lambda = 900$ nm using <2 mW per trap. (**b**) A false-color iso-surface generated from volumetric data obtained from deconvolved confocal images of a single voxel consisting of a 5×5 array of *P. aeruginosa*. The average center-to-center distance is 1.52 ± 0.06 μm and average space between each bacterium is 354 ± 134 nm. (**c**–**e**) Transmission and fluorescent micrographs of a single heterologous 3D voxel of *E. coli* with the focus at $z = 18$, 9, and 0 μm, respectively. The first images in (**c**–**e**) are transmission micrographs taken at $t = 0$, just prior to induction. The *second column* shows fluorescent images obtained 200 min later. A 3×1 array of cells expressing mRFP is located in the top plane at $z = 18$ μm, while 3×1 arrays expressing YFP are located at $z = 9$ and 0 μm. When 2 mM IPTG in M9 media is broadcast to the array at 0.03 μl/min flow, the cells detect the inducer in their microenvironment above threshold and begin to produce mRFP1 (*red fluorescence*) and YFP (*yellow fluorescence*). (**f**) A false-color perspective iso-surface, reconstructed from volumetric data obtained from a series of confocal images, showing the same voxel as in (**c**–**e**). Adapted from [26, 28]

of hundreds of bacteria, can be assembled in a microfluidic channel and the spacing between the bacteria can be precisely controlled (Fig. 11.1b). The voxels are not limited to planar cell configurations either. If the beam entering the objective lens is slightly divergent, then the entire pattern of traps comes to focus at a different point along the optical axis. This divergence can be introduced dynamically using a Fresnel lens encoded into the liquid crystal array of an SLM with a time-shared focus. Figures 11.1c–e show 3D voxels formed using time-shared holographic optical traps (HOTs) comprised of three 2D—3×1 heterologous sub-arrays of genetically engineered *E. coli* incorporating YFP-LVA and mRFP-LVA functionally linked to *lac*. The fluorescence images, illustrating the heterologous character of the array and viability, were taken 200 min. after broadcasting the ligand isopropyl-β-D thiogalactopyranoside (IPTG) into the array. Genetically engineered bacteria like these represent an especially stringent test of this strategy for tissue engineering because, aside from the plasmids used to transform them, the cells are otherwise morphologically identical.

While optical trapping can be used to create vast networks of cells resembling tissue, the trapping beam still has to be held on the cells to maintain the array. To minimize exposure to the laser beam, the position of the cells was fixed in a bio-compatible scaffold made from a photopolymerizable poly(ethylene glycol) diacrylate (PEGDA) hydrogel. After assembling the array with tweezers, the pre-polymer solution in the microfluidic channel was exposed to UV light to form the gel. PEGDA hydrogel is an efficacious scaffold because UV exposure for photopolymerization can be relatively minimal ($\sim$0.1–1 s at $<$100 mW/cm^2) [28, 41] and it is porous [21, 49, 50], allowing for transport of nutrients to the cell and waste away from it. Hydrogels have been shown to maintain viability and activity of bioluminescent *E. coli* for up to two weeks without a change in the dose-dependent induction [51]. Finally, employing a step-and-repeat strategy [26], the live-cell lithography tool can step to an adjacent location in any direction while maintaining registration with a reference voxel, and repeat the process. By stitching together living voxels this way, it is possible to create cytoarchitectures of any size, shape, and constituency that mimic in vivo tissue.

11.3 Forming a Com-Link in a Synthetic Biofilm

Using the step-and-repeat method, heterologous networks can be precisely assembled consisting of thousands of living cells without loss of viability [26]. Using this method to capture one of the more essential aspects of biofilm biology, a communication link was formed in a synthetic biofilm by first splitting the *lux* QS system into gene circuits consisting of separate sets of transmitters and receivers, transforming *E. coli* (*DH5*α) with them, and subsequently stitching together voxels of transmitters and receivers. Two of the com-links that have been implemented are represented schematically in Fig. 11.2a, b [17, 21]. These *lux* com-links incorporate transmitter cells that harbor either: (a) the plasmid 111 (4,640 bp), which has

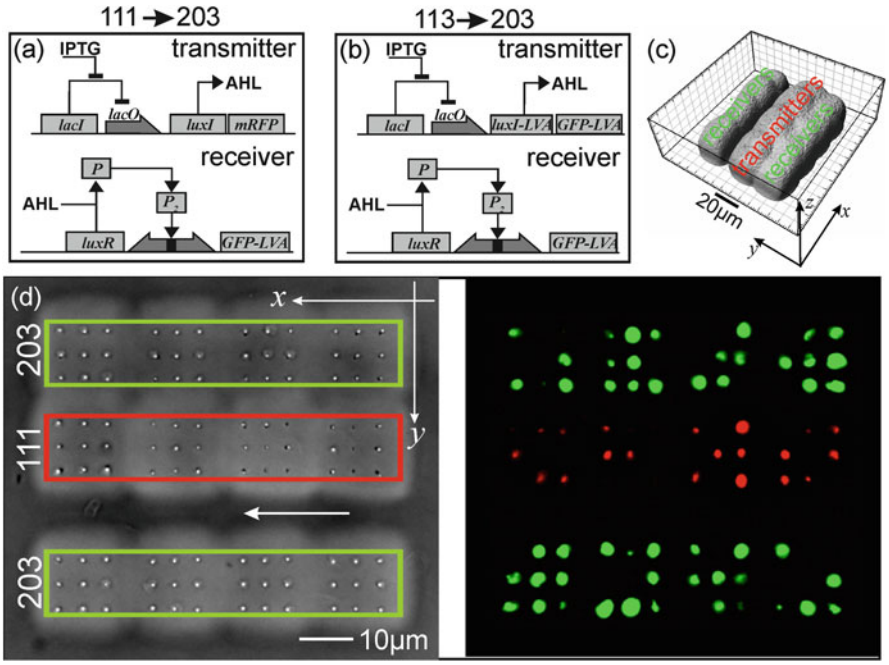

Fig. 11.2 A biofilm model. (**a**) (111) Transmitter bacteria produce luxI (AHL producing enzyme) as well as mRFP under control of the *lac* operon induced with IPTG. (203) Receiver bacteria produce LuxR (AHL-binding protein) constitutively under the *luxP(L)* promoter. LuxR binds to AHL, then dimerizes and binds to the lux operon, upregulating *luxP(R)* and downregulating *luxP(L)*. Upon receipt of AHL, receivers produce GFP-LVA, a rapidly degradable form of GFP. (**b**) Like (**a**), but the (113) transmitter bacteria produces luxI-LVA and GFP-LVA instead of mRFP. (**c**) A volume reconstruction obtained from confocal images of an array of 111-transmitter and 203-receiver voxels stitched together to form a com-link. The hydrogel was stained with rhodamine to form a confocal image. (**d**, *left*) Top-down transmission optical micrograph of a 3×4 array of 3×3 homologous microarrays of transmitters (highlighted in *red*) and receivers (highlighted in *green*) encapsulated inside a hydrogel. The architecture was formed from voxels each encapsulated in a hydrogel microstructure of size $27 \times 27 \times 40$ μm using a step-and-repeat methodology. The 1×4 voxel of receivers on the top is separated from the 1×4 voxel of transmitters by a microchannel 10 μm wide and 120 μm long. The arrow indicates the flow direction. (**d**, *right*) Fluorescent image of the same array 600 min after induction with IPTG

an IPTG-inducible luxI gene, co-expressed with red fluorescent protein (mRFP) (Fig. 11.2a); or (b) the plasmid 113 (4,854 bp), which has an IPTG-inducible luxI-LVA (degradable LuxI) gene, co-expressed with a degradable version of the green fluorescent protein (GFP-LVA) (Fig. 11.2b). Lux-LVA and GFP-LVA are unstable and degrade by proteolytic digestion with a half-life of 40 min [52]. The expression of LuxI in the 111 transmitter facilitates the synthesis of *N*-(β-ketocaproyl)-L-homoserine lactone ($3OC_6HSL$ or AHL) by leveraging the cell metabolism [17]. From normal metabolic products (S-adenosyl methionine and an acyl-ACP carrier protein used in fatty acid synthesis) LuxI catalyzes the production of AHL that

then diffuses across the cell membrane out into the environment. Likewise, the 113 transmitters co-expressed degradable forms of LuxI (LuxI-LVA) and a GFP (GFP-LVA) reporter under a *lac* promoter [21]. Upon induction with IPTG, AHL is produced transiently by LuxI-LVA and diffuses across the 113 cell membrane, until it degrades.

The *lux*-receivers harbor the plasmid 203 (3,739 bp) that expresses GFP-LVA when *LuxR* is complexed with AHL (*P*), and the dimer (P_2) binds the *luxP(L)* promoter. The receiver plasmid consists of a bidirectional promoter *luxP*; the *luxP(L)* promoter controls LuxR production and the *luxP(R)* promoter controls GFP-LVA production. It has been shown that LuxR in combination with this promoter positively auto-regulates the QS response by modulating its own expression [21, 27, 53]. While *luxP(R)* has only a low-level basal expression, it is strongly up-regulated in the presence of the LuxR-3OC_6HSL (P_2) dimer and produces GFP-LVA. This gene component is derived from one of the two interlocked feedback loops found in the *lux* QS circuitry found in *V. fischeri*. The bistability of this switch is a hallmark of the positive autoregulation associated with the feedback loop, which modulates the expression of LuxR as part of the QS response. Subsequently, we tested for coordination in the response to changes in the gene environment.

As a preliminary test of the com-links, networks of transmitters and receiver voxels were created on a hydrogel scaffold embedded in a microfluidic device that allows for control of fluid flow and the broadcasting of exogenous inducers. Figure 11.2c is a perspective iso-surface, reconstructed from volumetric data obtained from a series of confocal images, showing the 3D aspects of the hydrogel microstructure containing a 2D 3×4 array of voxels, each containing 3×3 *E. coli* transformed to be either transmitters or receivers. Interposed between two 1×4 arrays of *lux*-receivers (203) voxels, there is a 1×4 array of *lux* transmitter (111) voxels; one of the receiver arrays is separated from the transmitters by an open channel whereas the other is in intimate contact. Figure 11.2d shows a transmission image of the same array of voxels at $t = 0$ h, just prior to induction with IPTG. Whereas the 1×4 receiver (green highlight) and transmitter (red highlight) voxels at the top of the image are stitched together into what amounts to one hydrogel microstructure—the adjacent voxels are spaced ~30 μm apart (in *x* and/or *y*) using a motorized *x*-*y* stage (Zeiss DC) with 0.25 μm step resolution, the array of receiver voxels at the bottom of the image (highlighted in green) was separated from the arrays at the top by a microchannel that is ~10 μm-wide and 120 μm-long. The microchannel was created by increasing the spacing between hydrogel microstructures to 35 μm in the *y*-direction.

To test the $111 \rightarrow 203$ com-link, 2 mM of IPTG in M9 media was broadcast into the microfluidic device containing the network of transmitters and receivers shown in Fig. 11.2d at $t = 0$ min with a quasi-static flow rate of 50 nL/min. The diffusion coefficients of the inducer and AHL in the hydrogel were estimated using a fluorescent surrogate (rhodamine) with a similar molecular weight, to be $D^{\text{hydrogel}}_{\text{rhodamine}} = 17 \pm 10\ \mu\text{m}^2/\text{s}$, which is less than 5 % of the value measured for free diffusion of the same ligand in water, but consistent with a high cross-linking

density in the PEGDA hydrogel [21, 54]. As a result, the inducer concentration was estimated to be practically uniform after broadcasting into the biofilm from the microfluidic device, varying <1 % throughout the array within 90 s. After about 1 h, (red) fluorescence was observed with continuously increasing intensity so that it could be seen clearly at 2 h, indicating the co-expression of LuxI and therefore the production of AHL. When the AHL concentration in the hydrogel exceeded ~2 nM [17, 21, 27]—near $t = 3.7$ h—the receivers produce sufficient GFP-LVA to observe fluorescence above the background. Figure 11.2d (right) shows the corresponding fluorescence observed in the same array at $t = 10$ h after induction. Clearly, the *lux*-transmitters (111) are linked to the receivers (203) as evident from the fluorescence.

Figure 11.3 illustrates the cell signaling dynamics of a similar network comprising the $111 \rightarrow 203$ com-link, formed in a hydrogel scaffold by juxtaposing 2×4 arrays of (3×3) 203-receiver voxels (72 total) next to a 1×4 array of (3×3) 111-transmitter voxels (36 total), where the receivers are separated from the transmitters by a 10 μm-wide open microchannel as illustrated in the transmission image. Starting at time $t = 0$, the microfluidic was used to broadcast 2 mM of IPTG to the array at a quasi-static flow rate (30 nL/min) to induce production of AHL in the transmitters. After 2 h, (red) fluorescence was observed in the transmitter array (fluorescence image in Fig. 11.3a) indicating the production of AHL that, in turn, diffused out of the cell and into the environment. Accumulation of the AHL in the environment eventually initiated GFP-LVA production and fluorescence in the receivers at 2.5 h establishing the connection to the transmitter. After about 3.7 h (Fig. 11.3a) the flow rate was increased to 10 μL/min for 40 min, flushing the array of any residual AHL and subsequently the receiver fluorescence diminished whereas the transmitter fluorescence continued to grow, as there has been no change in the IPTG inducer concentration. The network was then allowed to recover in quasi-static flow conditions and the receiver fluorescence returns as before. This procedure was repeated again at $t = 7.3$ and 10.2 h with similar results.

The fluorescence responses measured over each element in each of the *lux* transmitter and receiver voxels are summarized in the kymographs of Fig. 11.3b–d (left), respectively. The kymographs track the logarithm of the fluorescence of each region-of-interest (ROI) in the array, illustrating the timing of the response relative to the IPTG pulses. The green and red lines in the kymographs demarcate the intervals in which the flow rate in the overlying microfluidic channel was increased from quasi-static (50 nL/min) to 10 μL/min (green) and vice versa (red). Each ROI was defined to be 5 μm on edge so that initially it encompassed the length and breadth of a single bacterium in the super-array. However, as the measured doubling time in the film was 185 ± 10 min, cell proliferation eventually led to multiple bacteria within each ROI. Still, it was possible to follow the dynamics associated with a single cell using confocal microscopy and a comparison shows the same trends were observed with a 5 μm ROI [21]. Thus, due to the length and width of the bacteria, the difficulties in tracking a single cell through proliferation, and economy in the analysis, the scope of an ROI 5 μm on edge was used to define the volume of the stochastic response [21].

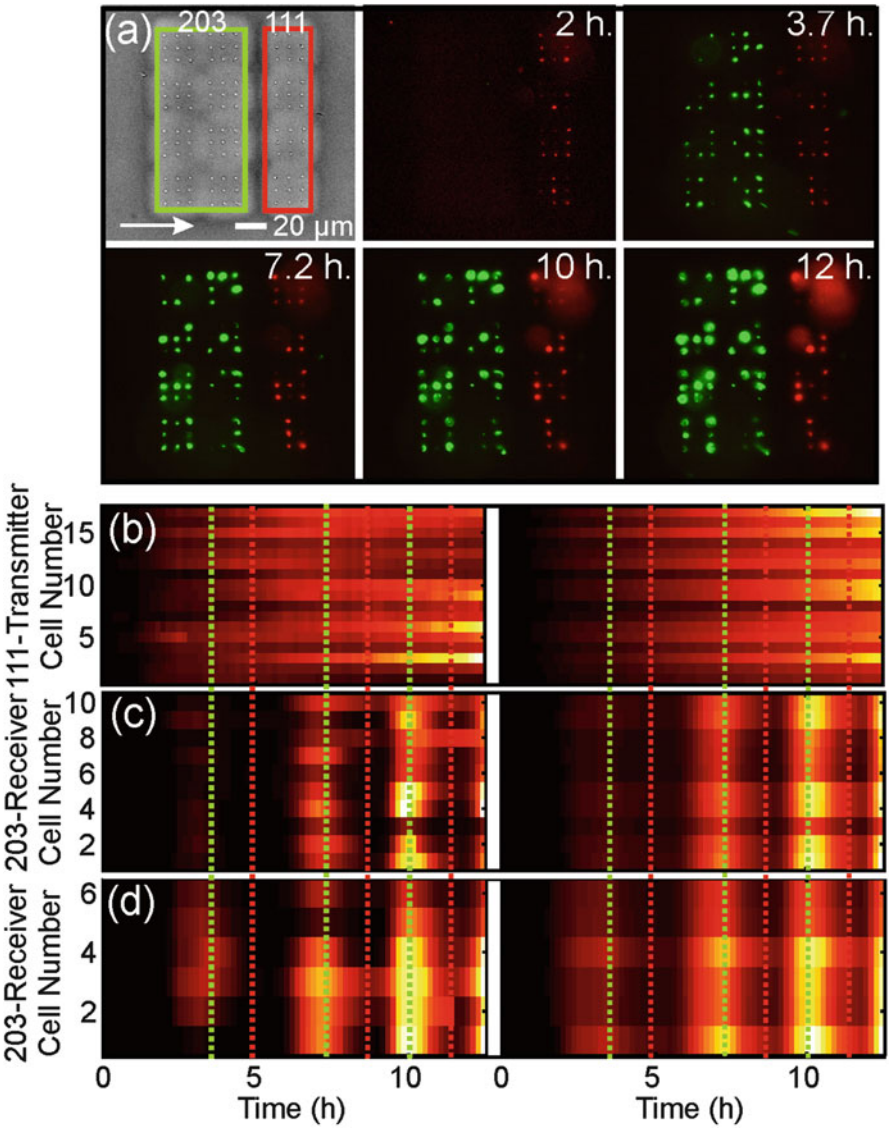

Fig. 11.3 Voxels of 111 transmitters juxtaposed with a 203 receivers separated by a 10 μm wide open microchannel. (**a**) Transmission ($t = 0$ h) and fluorescence images taken at $t = 2$, 3.7, 7.2, 10, and 12 h of a 3×4 array of voxels, consisting of one column of transmitter cells (*right most column*) downstream of two columns of receiver cells. The transmitter array was separated from the receivers by a 10 μm wide and 120 μm long channel oriented perpendicular to the flow. The arrow indicates the flow direction. Signaling was initiated at $t = 0$ by broadcasting 2 mM IPTG into the microfluidic under quasi-static flow (50 nL/min). After 2.5 h, fluorescence is observed in the receiver arrays. At 3.7 h, the flow rate was increased to 10 μL/min for 0.7 h, and subsequently the system was allowed to recover in quasi-static flow. Similarly, the system was flushed again at 7.3 and 10.2 h and allowed to recover. (**b**–**d**) Kymographs of the log of the fluorescent intensity

It is apparent from the kymographs that the integrity of the com-link between the transmitters and receivers can be compromised, depending on the flow rate [17]. Even though the 111 transmitters produce a signal continuously, the 203 receivers detect it only intermittently. To account for the disruption in the com-link, these experiments were simulated stochastically using the models depicted schematically in Fig. 11.2a with parameters that are tightly constrained by the literature [31, 32]. Stochastic simulations of the *lux* com-link that account for the bistable switching element, the promoter *luxP* used in the receiver, have already been successfully and extensively tested [17, 21, 27]. The results (Fig. 11.3b–d (right)) capture the fluorescent response to changes in mass transport conditions perfectly. The close correspondence with the experimental outcomes related to the timing, spatial dependence and strength of the fluorescent signals implies further that the inducer and signal gradients were represented accurately.

The simulated AHL concentration gradient, corresponding to $t = 3.7$ h expected at the fluorescent peak in the first pulse is delineated in Fig. 11.4a–c. Apparently, judging from Fig. 11.4a, the velocity of the flow above and throughout the open channel in the same plane as the cell array has little effect on the concentration profile since the contours of uniform concentration (Fig. 11.4c) are hardly disrupted by flow in the channel. Whereas the velocity in the plane of the bacteria is low (<20 nm/s), the majority of signal flux is conveyed convectively over the top of the arrays. This argument is supported by the observation that, despite the low velocity, a change to high flow completely disrupts the com-link and extinguishes the receiver fluorescence.

The gradient in AHL subtly affects the coordination of the receiver responses. Corresponding to AHL concentrations that differ by 0.5 nM from each other (Fig. 11.4c), three galleries were identified in the receiver array. In each gallery, the mean fluorescence response measured during the first IPTG pulse was subsequently calculated and plotted in Fig. 11.4d, e. The plot in Fig. 11.4d indicates that the receivers closest to the transmitter array showed the largest receiver fluorescent response. If the receiver arrays closest to the transmitters are induced sooner than those on the opposite side were, it seems that the total amount of fluorescent protein measured by the fluorescence produced by the former was greater. However, Fig. 11.4e indicates that cells in different galleries begin to express GFP at nearly the same time in relation to external stimuli (i.e., $\tau \neq 0$). To quantify the coordination of responses between ROIs in these regions, the similarity function [21]:

Fig. 11.3 (continued) corresponding to individual cells in (**a**) as a function of time. The fluorescence observed in the left and right column of receivers is shown in (**b**, *left*) and (**c**, *left*), respectively; the fluorescence of the transmitter array is shown in (**d**, *left*). Simulations of conditions similar to the experiment reveal the same behavior as a function of the flow conditions and time. The timing of the flows is demarcated by the *green dotted lines* where 50 nL/min ceased and 10 μL/min commenced, and the *red dotted lines* where the 10 μL/min ceased and the 50 nL/min flow resumed

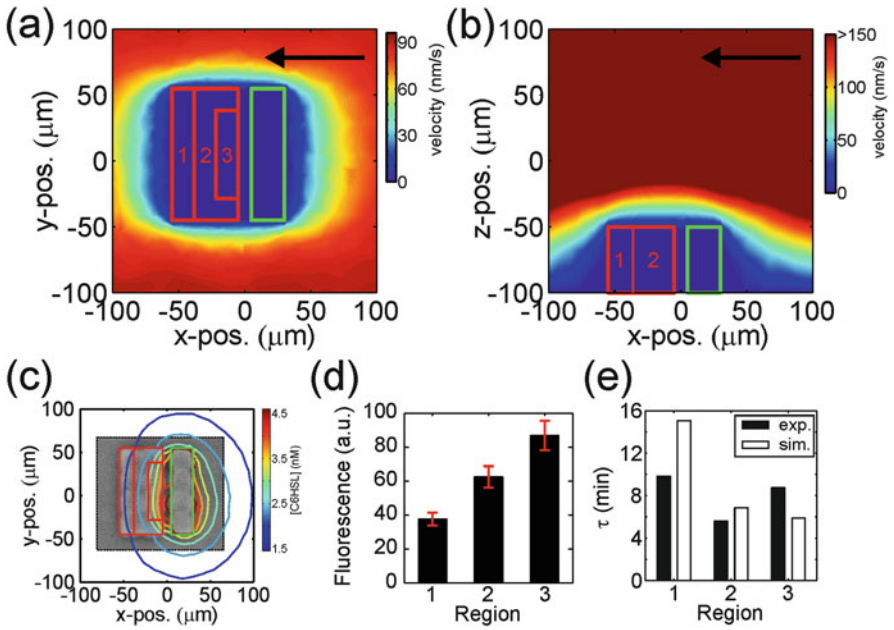

Fig. 11.4 (**a**) A finite element simulation of the fluid velocity in the microfluidic in the plane of the arrays. The *solid lines* denote the edges of the hydrogel arrays and the numbered galleries. The *arrow* indicates the direction of flow. (**b**) Velocity profile through the center of the array showing quasi-static flow. The *solid lines* depict the edges of hydrogel array and the selected numbered galleries. The *arrow* indicates the direction of flow. (**c**) Contour plot of the simulated $3OC_6HSL$ concentration superimposed over a transmission image of the array. (**d**) Mean and standard deviation of the fluorescence in the three regions delineated in (a) where the simulated concentration is nearly uniform. (**e**) The *bar graph* summarizing the synchronicity measured by the corresponding τ of the fluorescence data (*filled*) and simulation (*empty*)

$$S_{ij}(\Delta t) = \sqrt{\frac{\left\langle \left[x_i(t+\Delta t) - x_j(t) \right]^2 \right\rangle}{\left[\left\langle x_i^2(t) \right\rangle \left\langle x_j^2(t) \right\rangle \right]^{1/2}}} \quad \text{with} \quad \tau \equiv \left| \Delta t|_{S_{ij}=\text{Min}} \right|. \tag{11.1}$$

was used and the value of τ was plotted for the same three regions. Here, $x_i(t)$ was a measure of the fluorescence of cell i at time t, and Δt was the time differential between the signal responses. For our purposes, the logarithmic derivative of the fluorescence was used as a measure of the fluorescence to improve sensitivity to weak signals. Taken together, the data of Fig. 11.4 implies that the position within the array affects the strength of the fluorescent response, but not necessarily the timing, and so it is possible to differentiate the expression profile by choosing the relative position of the transmitter and receiver. Here, the differences were subtle, however. It has been shown [27] that when the receivers are separated by greater distances in a sharper chemical gradient, patterns emerge among phenotypes that

could bestow a fitness advantage affecting, for example, the evolution of antibiotic resistance [55] or even bacterial-induced regulation of host cell function in bacterial infections [56]. For subsequent IPTG pulses in the flow rate, the advantage derived from proximity is lost entirely and the fluorescence across the three regions becomes nearly uniform and tightly synchronized. This occurs because the signal sensitivity in the receiver improves dramatically due to the up-regulation of the bistable element in the lux receiver gene, and the associated memory invested in the number of LuxR molecules [21, 27].

11.4 Noise, Epigenetic Memory, and Synchronization

The 111 transmitters in the $111 \rightarrow 203$ com-link produced AHL unremittingly. The concentrations of LuxI and mRFP do not degrade even in the absence of IPTG and so once it is induced, the production of AHL continued unabated. The data demonstrates unequivocally that under these conditions there is not a single cell density for which QS-regulated genes are induced or repressed, but rather the signaling is acutely sensitive to mass transport [17]. On the other hand, it is difficult to assess the effect of noise on the com-link due to the prevalence of AHL. Despite the gradients that develop, the concentration of AHL was found to be above the bifurcation threshold everywhere within the array and the corresponding responses of the 203 receivers were at least partially entrained ($\tau < 15$ min) within the measurement frequency and improved with subsequent broadcasts.

It was hypothesized that the response of the receivers in a synthetic biofilm like this could be entrained to fluctuations in the environment by using the bistable element like that found in 203 and the resulting epigenetic memory that emerges from integrated bursts of LuxR transcription [21, 27]. Memory is a property of biochemical systems with bistability. Under identical chemical conditions, the system can be in either one of the two alternative states HIGH or LOW; the state the system occupies depends on its recent history. The memory in 203 receivers was invested in the concentration of LuxR. The concentration of LuxR affects the sensitivity of the bacteria to AHL exposure; high levels of LuxR allow the bacteria to respond to lower levels of AHL with up-regulation (HIGH state), while cells with low levels of LuxR are unresponsive without higher levels of AHL (LOW state). Changes in the memory status can occur either through production of LuxR via induction with AHL (LOW $\rightarrow$ HIGH), or via dilution of the LuxR concentration over time through cell division (HIGH $\rightarrow$ LOW) [21].

To estimate the number of molecules required to establish a persistent epigenetic memory, the time evolution of fluorescent GFP expression was tracked in single cells and the results were simulated using the same conditions to infer the number of molecules in play. The concentration of AHL was uniform with less than 1 % variation throughout the array within about 1.5 min after a 100 μL/min flush, yet the cells in Fig. 11.5a, b appeared to "blink" repeatedly on-and-off again over ∼120 min [27]. Out of the 81 cells in the array, 27 (33 %) demonstrated this behavior, while

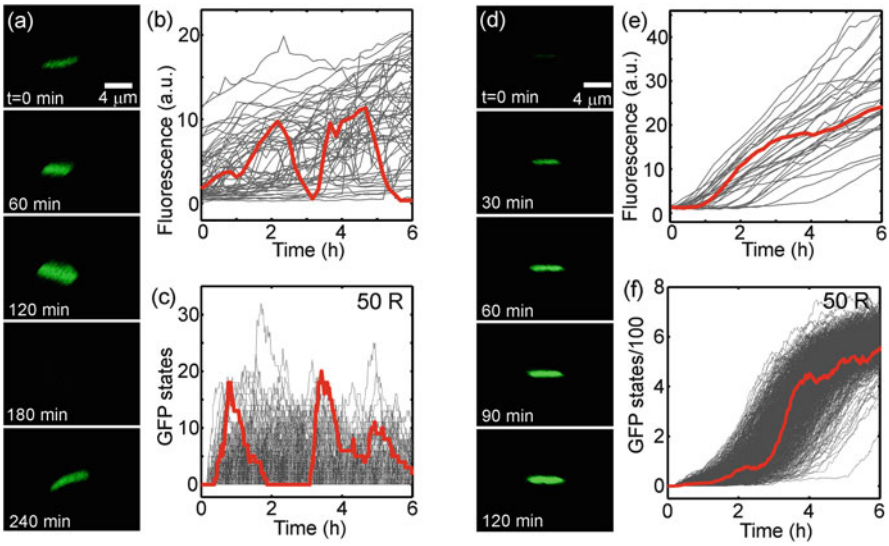

Fig. 11.5 (**a**) Fluorescent confocal microscopy illustrating transcriptional bursting at 3 nM AHL. GFP-LVA is expressed, making the receiver bacteria fluorescent, and then degraded due to the LVA tag, resulting in a loss of fluorescence. Two blinks are shown. (**b**) Time evolution of the fluorescence associated with the cell in (**a**) is highlighted in *red*, while the response of 60 others to the same experimental conditions are in *gray*. A typical response from one cell is highlighted in *red*. (**c**) Stochastic simulations showing the evolution of GFP-LVA with three molecules of extracellular AHL. The cells are initialized with 50 LuxR (R) molecules. A typical response from one cell out of 1,000 is highlighted in *red*. (**d**) Like (**a**), but for 100 nM AHL. (**e**) Like (**b**), the evolution of the fluorescence associated with a single cell represented in (**d**) is highlighted in *red*, while the response of 30 cells to the same conditions are in *gray*. (**f**) Like (**c**), stochastic simulations showing the time evolution of GFP-LVA at 50 molecules of extracellular AHL. Adapted from [27]

33 (41 %) were in the HIGH state and 21 (26 %) were in the LOW state. In contrast, at 100 nM AHL, the fluorescence increased monotonically (Fig. 11.5d, e), which is consistent with cells in either a HIGH or LOW state responding to this saturating condition by inducing the HIGH expression state in the population. It was proposed that this blinking is a result of transcriptional bursting, the subsequent degradation of GFP-LVA, and the resulting fluctuations in the number of GFP-LVA molecules [27], and the characteristics of the transcription bursts were used to infer information about the LuxR concentration through stochastic simulations. Drawing the parameters that govern the reaction kinetics of LuxR from current literature [31], the single-cell fluorescence data was simulated using the receiver model in Fig. 11.2a, b [27]. This model accurately captures the transcription and translation of both LuxR and GFP-LVA in each cell—e.g., independent stochastic simulations of an ensemble of 1,000 cells, initialized with 50 LuxR molecules per cell, indicates a bifurcation threshold for AHL concentrations between 1 and 2 molecules per cell (2 nM). For extracellular concentrations of AHL > 2 molecules, the cells switch to the HIGH expression state based on the number of fluorescent GFP molecules

in the system, in agreement with cytometry measurements [21]. According to the simulation, positive autoregulation produces bistability at an AHL concentration near two molecules of extracellular AHL per cell or about 3 nM.

Figure 11.5c shows the simulated time evolution of GFP-LVA for 100 cells out of an ensemble of 1,000 cells with 50 initial LuxR molecules per cell and 3 molecules of extracellular AHL per cell. A single representative cell was selected and plotted in red for clarity. If the initial number of LuxR molecules was 50 per cell, then 22.4 % of the cells would blink, while 25.4 % would remain in the LOW state, which compares favorably to the experimental data. Thus, by comparing the fractional population that blinks, switched to HIGH or remained LOW, simulated over a range of initial molecule numbers with the experimental data, it was concluded that each cell had approximately 50 LuxR initially. Finally, for cells with a starting concentration of 50 ± 10 LuxR molecules, it was estimated that the mean number of LuxR molecules in a cell is about 140 after 6 h of exposure to 3 nM AHL. Thus, LuxR accumulates in the cell with continuous exposure to AHL and the memory improves, even if GFP-LVA degrades.

The delicate balance between GFP-LVA production and proteolytic digestion produced bursts of fluorescence. From the model, it was inferred that LuxR is also produced in bursts, but unlike GFP-LVA, it accumulated in the cells as it degraded only by dilution through cell proliferation. In contrast with the 3 nM exposure, in 100 nM AHL, GFP-LVA (and by inference, LuxR) was produced at so high a rate as to be practically continuous, thus leading to the monotonic increase in fluorescence shown in Fig. 11.5e. The simulation in Fig. 11.5f with 50 initial LuxR molecules was consistent with this behavior. All the simulations indicate the mean number of LuxR in each microcolony grows to >970 molecules (in each cell the number grows to >485 molecules) after the initial 6 h exposure to 100 nM AHL, which gives rise to persistent memory as the mean doubling time for the 203 bacteria is 190 min [27]. Taken together, the data supports the idea that the *luxP* promoter is a stochastic bistable element that is sensitive to the current environment and its history and that an epigenetic memory develops when the number of LuxR molecules exceeds about 500 in a receiver [21, 27].

To elicit the effect of noise on the signaling cascade and the corresponding response of the bistable switch in the receiver, another com-link consisting of 113 transmitter and 203 receiver voxels was created; the transmitters are highlighted in red and the receivers in green in Fig. 11.6a. The kymograph in Fig. 11.6b shows the time development of the logarithm of the fluorescence of each transmitter ROI, illustrating explicitly the asynchrony in the timing associated with the first three 0.75 mM IPTG pulses broadcast into the array. The first IPTG pulse is broadcast into the array at $t = 0$, but the onset of fluorescence is not observed until 2 h later. Then at $t = 5$ h, the IPTG concentration is reduced to zero for 2 h. Starting at $t = 7$ h, the IPTG induction cycle is repeated twice more: broadcasting IPTG for 2 h, flushing to zero for 2 h and then broadcasting IPTG again at 11 h for 2 h. Corresponding to the three IPTG pulses broadcast into the array, the mean time differential among all the cells is $\tau_0 = 15$ min for the first pulse, whereas $\tau_1 = 5$, and $\tau_2 = 6$ min, for the

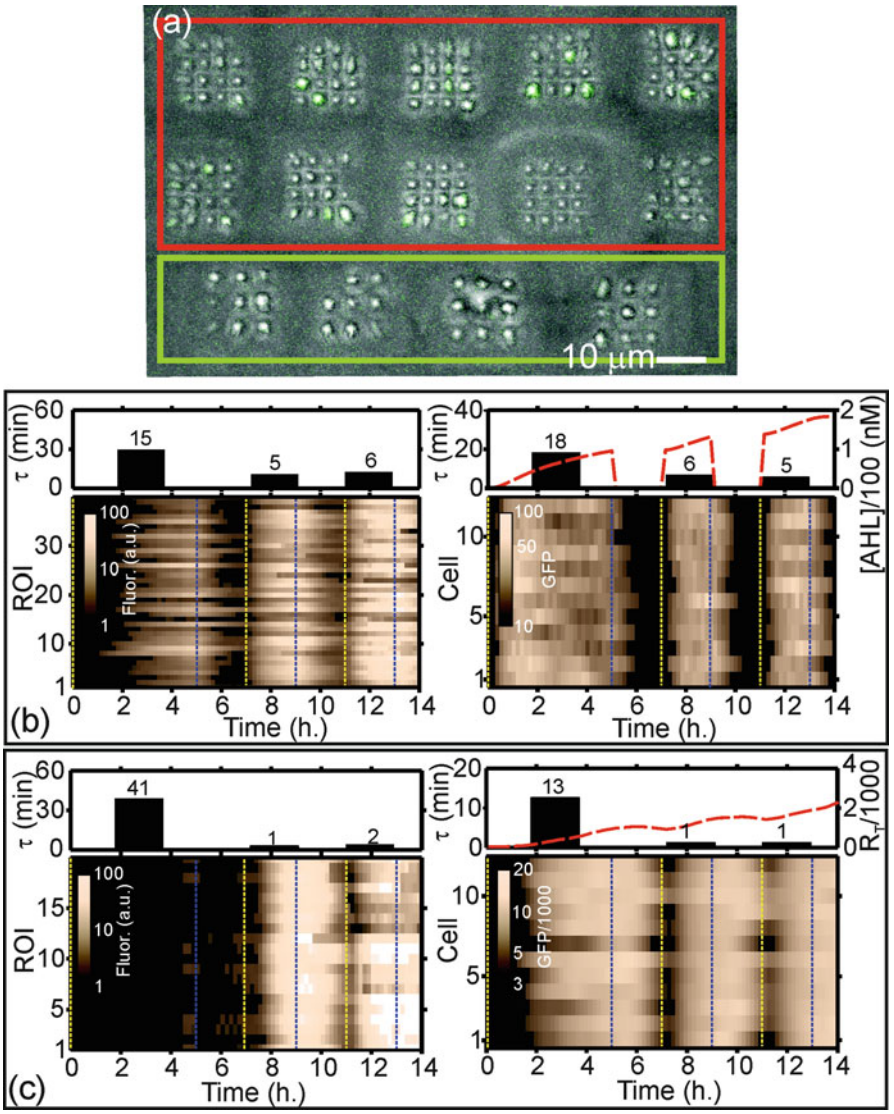

Fig. 11.6 The coordinated response of 203 receivers to noisy 113 transmitters. (**a**) Transmission image of a 2×5 array of (4×4 arrays of) 113 transmitter voxels (160 cells) highlighted in *red*, alongside a 1×4 array of (3×3 arrays of) 203 receiver voxels highlighted in *green* in a microfluidic at $t = 0$. A concentration of 0.75 mM of IPTG was broadcast into the array at $t = 0$ h, ending 5 h later; and subsequently at $t = 7$ and 11 h, each lasting 2 h. The beginning and end of each IPTG broadcast are represented by *blue* and *yellow* lines, respectively. The mean time differential between the signals, τ, is shown in the bar graph above the kymograph. (**b**, *right*) Stochastic simulation of the production of fluorescent GFP-LVA in 12 cells under conditions identical to the experiment represented in (**b**, *left*) with an initial 40 LacI molecules/cell and 10 DNA operators/cell. The *bar graph* above the kymograph summarizes the corresponding τ and AHL concentration at the receivers, inferred from the simulation. (**c**, *left*) A kymograph of the time

subsequent two pulses, respectively, as shown in the bar graph above the kymograph. Therefore, the transmitter cells, which were initially uncoordinated, become only weakly entrained to the IPTG in the environment.

On the other hand, Fig. 11.6c illustrates the tightly coordinated response of the receivers in the same super-array after the initial pulse from the transmitters. The relatively noisy transmitters conveying AHL into the super-array initially produce an uncoordinated response among the receivers measured by the time differential $\tau_0 = 41$ min, corresponding to the first IPTG pulse. However, after the second and third broadcasts of IPTG, the time differential falls below 3 min to $\tau_1 = 1$ and $\tau_2 = 2$ min, respectively. Thus, the noise in the receivers was substantially reduced after the initial pulse measured relative to the noise in the transmitters.

To discover the relationships between the number of LacI, LuxI-LVA, GFP-LVA, and AHL molecules produced in the transmitters and the LuxR and GFP-LVA produced in the receivers, the dynamics were simulated stochastically under the conditions of the experiments described in Fig. 11.6b, c [21]. The simulation results, which are summarized by corresponding kymographs Fig. 11.6b, c (right) for the transmitters and receivers, respectively, capture the entrainment observed in the experiment. In particular, except for the first pulse, the τ bar graphs above each kymograph agree quantitatively with the time differentials measured in the transmitters and receivers. (The difference between simulation and experiment in the first pulse was attributed to the very weak fluorescence and instrumental noise, and other sources of stochastic variations that are not included in the model.) From the correspondence observed after the first pulse, it is inferred that there are ~40 LacI molecules in each transmitter, whereas the number of LuxR molecules in the receivers exceeds the critical value for a persistent memory of ~500 just after the first IPTG cycle ends, as evident from the plot in Fig. 11.6c, at which time the concentration of AHL in the receiver array (located 25 μm from the transmitters) exceeds 95 nM. (By the end of the second cycle, the concentration exceeds 130 nM AHL.) Since the concentration of IPTG $>4.4 \times 10^5$ molecules/cell (0.75 mM), while the number of LacI that is expressed constitutively is only ~40 molecules/cell, the number of LacI molecules (and the plasmid copy number) are critical factors limiting entrainment of the transmitter to $\tau \sim 5$ min. On the other hand, with the transmitters exuding an AHL concentration in excess of the bifurcation threshold (2 nM), the memory held in LuxR is established after the first IPTG pulse so that the time differential in the receiver array collapses to $\tau \sim 2$ min and the response becomes tightly coordinated.

Fig. 11.6 (continued) evolution of the logarithm of the fluorescent intensity of 20 ROIs in the receiver 203 portion of the array shown in (**a**). The beginning and end of each IPTG broadcast are represented by *blue* and *yellow* lines, respectively. (**c**, *right*) Stochastic simulation of the production of fluorescent GFP-LVA in 12 cells under conditions identical to the experiment represent in (**d**, *left*) with an initial 50 LuxR molecules/cell and 10 DNA operators/cell. The *bar graph* above the kymograph summarizes the corresponding τ and the number of LuxR molecules inferred from the simulation. Adapted from [21]

Thus, by exercising precise control over the gene's microenvironment, it was established that the autoregulation of the Lux receptor provides a memory for the system, increasing the sensitivity and removing variability via accumulation of the receptor protein [21, 27]. The memory that is invested in LuxR depends on the initial exposure and degrades only by cell proliferation. It persists for several generations, even in the absence of the QS signal [21], and so it represents an epigenetic inheritance. This retained epigenetic memory allows for phenotypic inheritance, while providing a minimal level of signal response. Feedback is necessary for this behavior, as it is not present in the *lac* repressor system alone. Owing to the memory of fluctuations in a precisely controlled environment, heritable variations in gene expression create phenotype diversity within an isogenic population of bacteria. The phenotype diversity in the population was manifested in exposure to a short-term stimulus (such as a pulse of AHL at low concentration), which promoted a maximally fit population. On the other hand, persistent exposure to AHL removes phenotype diversity with the majority of the cells transforming to the HIGH state. The memory allows both adaptation to persistent changes in environment and the ability to respond to short-term changes via diversity of phenotype [21]. Thus, the stringent control over the cell's genes and its microenvironment offered by this simple model allows for unequivocal tests of hypotheses, especially those related to gradients in nutrients or environmental signals that might affect phenotype development.

11.5 Further Development of the Biofilm Model

A simple model for a biofilm consists of microorganisms forming microcolonies surrounded by EPS with open, water-filled channels between the colonies that promote the influx of nutrients and the efflux of waste [57]. However, this simple model does not capture the complexity found in nature. The principals of systems biology have been used to unravel some aspects of the complexity of biofilms with the aim of identifying and disrupting the interspecies associations. For example, correlation network analysis has revealed two salient aspects of dental plaque (one of the more complex biofilms): network centralities and hubs [58], which are doubtless affected by both the constituencies and the architecture. More than 500 bacterial taxa have been isolated from oral surfaces [59]. Recently, more insight into the microbial diversity in a biofilm was gleaned by using 454 pyrosequencing technology [60] to obtain preliminary data on a hyper-variable region of the 16S rRNA gene extracted from samples taken from two water meters (of private households in a city in the United States) [61]. As many as 400 operational taxonomy units or bacterial phylogenetic types (at 97.5 % similarity in 16S RNA sequence) were found in two water meters located at different regions of a drinking water distribution system. The results support the assertion that polymicrobial biofilm models are needed.

Biofilm morphology varies widely. Oral biofilms can be up to 1 mm thick, whereas biofilms on catheters vary in thickness from 3 to 490 μm [62]. The microstructure exhibited in a biofilm depends on the cellular constituencies and the environmental niche. The morphology can be flat, rough, or filamentous, and the porosity can vary dramatically, depending on open channels and water-filled voids. For example, according to Baum et al. [63], chemotaxis and water currents have been used to explain large (300–500 μm in diameter) periodic bacterial patterns on mucus veils suspended over sulfidic marine sediments [64], whereas mushroom-shaped cell clusters and pillars are produced by *Pseudomonas aeruginosa* [65].

Live-cell lithography can be used to tackle some of the challenges currently confronting synthetic biofilm engineering; specifically: open channel formation, encapsulation, and polymicrobial cytoarchitectures. The open channels that are evident in biofilms found in potable water systems, for example, compound the spatial complexity because they facilitate mass transfer. Higher nutrient concentrations in the channel translate to more concentrated cellular metabolites and by-products under cell clusters [66]. To mimic these structures, arrays of voxels can easily be interlaced with open microchannels to form a vascular network by simply offsetting the position of the living voxels in 3D by distances as small as 1 μm, leaving a void between them (Fig. 11.7) [67]. Figure 11.7 illustrates this capability using stacked voxels consisting of two different types of bacteria 113 transmitters, (highlighted in red) sandwiched between 203 receivers. Staining the hydrogel reveals the open channel in the center of the microstructure (Fig. 11.7c). Advection through the open channel predominates over the mass transfer due to diffusion in the hydrogel. Moreover, while the encapsulation of living cells in hydrogel remains one of the main challenges in tissue engineering, because each cell-type can demand a specific encapsulating microenvironment [68], by using photopolymerizable hydrogels in combination with cyto-compatible chemistries, it is possible to tailor the microenvironment within each voxel to a specific cell-type.

In summary, although the challenges to recapitulating the complexity found in a biofilm are daunting, the problem may yet yield to live-cell lithography used in conjunction with gene engineering. Because biofilms are so prevalent and troublesome in human health, the need is urgent. For example, *Pseudomonas aeruginosa* in biofilms show extraordinary resistance to antibiotics (1,000–1,500× less susceptible). Several mechanisms have been proposed to explain the resistance: (1) the extracellular matrix where the bacterial cells are embedded presents a diffusion barrier to penetration of antimicrobial agents; (2) the majority of the cells in a biofilm are in a slow growing, nutrient-starved state that is not so susceptible to antibiotics; and (3) the cells in a biofilm adopt a protected biofilm phenotype (*i.e.* persister cells), with elevated expression of drug-efflux pumps [12]. The problem remains unresolved for two reasons: lack of relevant models and testing protocols.

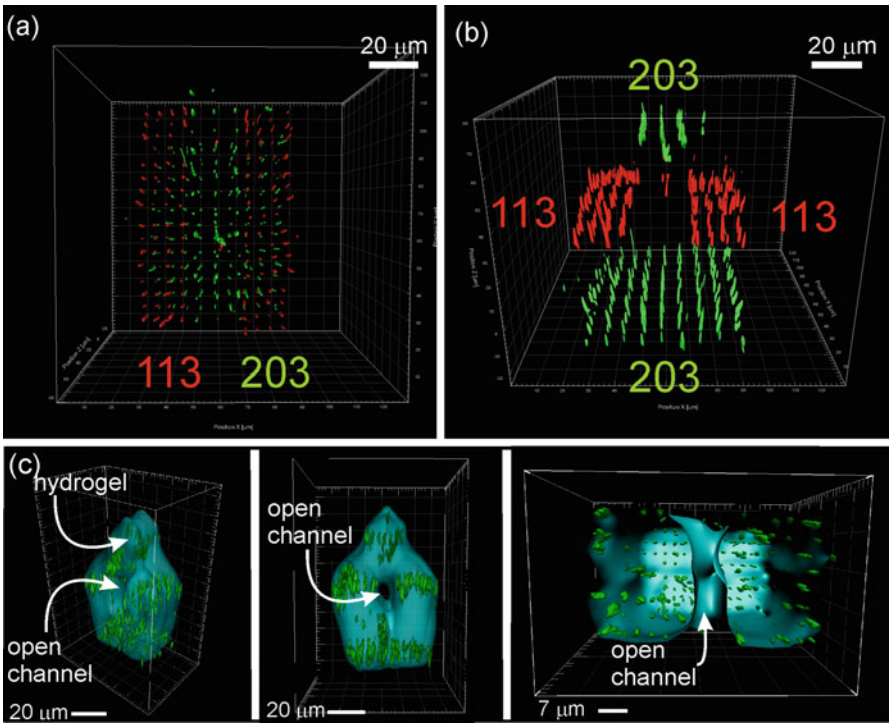

Fig. 11.7 (**a**, **b**) Confocal transmission images obtained from a 3D array of homologous voxels of 113 transmitters (*red*) and 203 receivers (*green*) top-down and in perspective from the front, respectively. The transmitters in the middle layer were sandwiched between 203 receivers on the top and bottom layers (**c**) False-color perspective iso-surfaces reconstructed from confocal images showing 3D arrays of 111 transmitters and 203 receivers surrounding a lumen: (**c**, *left*) is a perspective; (**c**, *middle*) is a side view and (**c**, *right*) is a top view

Acknowledgments We gratefully acknowledge support from NSF CCF-1129098. We are also grateful to R. Weiss for the donation of receiver plasmids and W-T Liu for sharing his preliminary sequencing data.

References

1. Hall-Stoodley L, Costerton J, Stoodley P (2004) Bacterial biofilms: from the natural environment to infectious diseases. Nat Rev Microbiol 2:95
2. Flemming H-C, Wingender J (2010) The biofilm matrix. Nat Rev Microbiol 8:623
3. Costerton JW, Lappin-Scott HM (1989) Behavior of bacteria in biofilms. Am Soc Microbiol News 55:650
4. Chauret C, Volk C, Creason R, Jarosh L, Robinson J, Warnes C (2001) Detection of Aeromonas hydrophila in a drinking-water distribution system: a field and pilot study. Can J Microbiol 47:782

5. Stickler DJ (2008) Bacterial biofilms in patients with indwelling urinary catheters. Nat Clin Pract Urol 5:598
6. Ramage G, Martinez JP, Lopez-Ribot JL (2006) Candida biofilms on implanted biomaterials: a clinically significant problem. FEMS Yeast Res 6:979
7. Lewis K (2001) Riddle of biofilm resistance. Antimicrob Agents Chemother 45:999
8. Kharazmi A, Giwercman B, Høiby N (1999) Robbins device in biofilm research. Methods Enzymol 310:207
9. Stoodley P, Dodds I, De Beer D, Scott H, Boyle J (2005) Flowing biofilms as a transport mechanism for biomass through porous media under laminar and turbulent conditions in a laboratory reactor system. Biofouling 21:161
10. Augspurger C, Karwautz C, Mussmann M, Daims H, Battin T (2010) Drivers of bacterial colonization patterns in stream biofilms. FEMS Microbiol Ecol 72:47
11. Dufour D, Leung V, Lévesque CM (2012) Bacterial biofilm: structure, function, and antimicrobial resistance. Endo Topics 22:2
12. Fuqua C, Parsek MR, Greenberg EP (2001) Regulation of gene expression by cell-to-cell communication: acyl-homoserine lactone quorum sensing. Annu Rev Genet 35:439
13. Hentzer M, Givskov M, Eberl L (2004) Microbial biofilms. In: Mahmoud G (ed) ASM, Washington, DC, p 118
14. Pappas KM, Weingart CL, Winans SC (2004) Chemical communication in proteobacteria: biochemical and structural studies of signal synthases and receptors required for intercellular signalling. Mol Microbiol 53:755
15. Shirtliff ME, Mader JT, Camper AK (2002) Molecular interactions in biofilms. Chem Biol 9:859
16. De Kievit TR, Iglewski BH (2000) Bacterial quorum sensing in pathogenic relationships. Infect Immun 68:4839
17. Timp W, Mirsaidov U, Matsudaira P, Timp G (2009) Jamming prokaryotic cell-to-cell communications in a model biofilm. Lab Chip 9:925
18. Redfield R (2002) Is quorum sensing a side effect of diffusion sensing? Trends Microbiol 10:365
19. Hense BA, Kuttler C, Müller J, Rothballer M, Hartmann A, Kreft J-U (2007) Does efficiency sensing unify diffusion and quorum sensing? Nat Rev Microbiol 5:230
20. Horswill AR, Stoodley P, Stewart PS, Parsek MR (2007) The effect of the chemical, biological, and physical environment on quorum sensing in structured microbial communities. Anal Bioanal Chem 387:371
21. Nelson EM, Kurz V, Perry N, Kyrouac D, Timp G (2014) Biological noise abatement: coordinating the responses of autonomous bacteria in a synthetic biofilm to a fluctuating environment using a stochastic bistable switch. ACS Synth Biol 3:286
22. Pedraza JM, van Oudenaarden A (2005) Noise propagation in gene networks. Science 307:1965
23. Raser JM, O'Shea EK (2005) Noise in gene expression: origins, consequences, and control. Science 309:2010
24. Samoilov MS, Price G, Arkin AP (2006) From fluctuations to phenotypes: the physiology of noise. Sci STKE 2006:re17
25. Thattai M, van Oudenaarden A (2004) Stochastic gene expression in fluctuating environments. Genetics 167:523
26. Mirsaidov U, Scrimgeour J, Timp W, Beck K, Mir M, Matsudaira P, Timp G (2008) Live cell lithography: using optical tweezers to create synthetic tissue. Lab Chip 8:2174
27. Kurz V, Nelson E, Perry N, Timp W, Timp G (2013) Epigenetic memory emerging from integrated transcription bursts. Biophys J 105:1526
28. Akselrod G, Timp W, Mirsaidov U, Zhao Q, Li C, Timp R, Timp K, Matsudaira P, Timp G (2006) Laser-guided assembly of heterotypic three-dimensional living cell microarrays. Biophys J 91:3465
29. Miller MB, Bassler BL (2001) Quorum sensing in bacteria. Annu Rev Microbiol 55:165
30. Bassler BL, Losick R (2006) Bacterially speaking. Cell 125:237

31. Goryachev AB, Toh DJ, Lee T (2006) Systems analysis of a quorum sensing network: design constraints imposed by the functional requirements, network topology and kinetic constants. Biosystems 83:178
32. Stamatakis M, Mantzaris NV (2009) Comparison of deterministic and stochastic models of the lac operon genetic network. Biophys J 96:887
33. Blake WJ, Balázsi G, Kohanski MA, Isaacs FJ, Murphy KF, Kuang Y, Cantor CR, Walt DR, Collins JJ (2006) Phenotypic consequences of promoter-mediated transcriptional noise. Mol Cell 24:853–865
34. Ozbudak EM, Thattai M, Kurtser I, Grossman AD, van Oudenaarden A (2002) Regulation of noise in the expression of a single gene. Nat Genet 31:69–73
35. McAdams HH, Arkin A (1997) Stochastic mechanisms in gene expression. Proc Natl Acad Sci U S A 94:814–819
36. Danino T, Mondragón-Palomino O, Tsimring L, Hasty J (2010) A synchronized quorum of genetic clocks. Nature 463:326
37. Rao CV, Wolf DM, Arkin AP (2002) Control, exploitation and tolerance of intracellular noise. Nature 420:231–237
38. Hui EE, Bhatia SN (2007) Micromechanical control of cell–cell interactions. Proc Natl Acad Sci U S A 104:5722
39. Chen C, Mrksich M, Huang S, Whitesides G, Ingber D (1997) Geometric control of cell life and death. Science 276:1425
40. Ozkan M, Pisanic T, Scheel J, Barlow C, Esener S, Bhatia SN (2003) Electrooptical platform for the manipulation of live cells. Langmuir 19:1532
41. Albrecht DR, Underhill GH, Wassermann TB, Sah RL, Bhatia SN (2006) Probing the role of multicellular organization in three-dimensional microenvironments. Nat Methods 3:369
42. Golden AP, Tien J (2007) Fabrication of microfluidic hydrogels using molded gelatin as a sacrificial element. Lab Chip 7:720
43. Ling Y, Rubin J, Deng Y, Huang C, Demirici U, Karp JM, Khademhosseini A (2007) A cell-laden microfluidic hydrogel. Lab Chip 7:756
44. Visconti RP, Kasyanov V, Gentile C, Zhang J, Markwald RR, Mironov V (2010) Towards organ printing: engineering an intra-organ branched vascular tree. Expert Opin Biol Ther 10:409
45. Jakab K, Norotte C, Marga F, Murphy K, Vunjak-Novakovic G, Forgacs G (2010) Tissue engineering by self-assembly and bio-printing of living cells. Biofabrication 2:022001
46. Rezende RA, de Souza Azevedo F, Pereira FD, Kasyanov V, Wen X, de Silva JVL, Mironov V (2012) Nanotechnological strategies for biofabrication of human organs. J Nanotechnol 2012:149264
47. Miller JS, Steven KR, Yang MT, Baker BM, Nguyen D-HT, Cohen DM, Toro E, Chen AA, Galie PA, Yu X, Chaturvedi R, Bhatia SN, Chen CS (2012) Rapid casting of patterned vascular networks for perfusable engineered three-dimensional tissues. Nat Mater 11:768
48. Nahmias Y, Schwartz RE, Verfaillie CM, Odde D (2005) Laser-guided direct writing for three-dimensional tissue engineering. Biotechnol Bioeng 92:129
49. Cruise GM, Scharp DS, Hubbell JA (1998) Characterization of permeability and network structure of interfacially photopolymerized poly(ethylene glycol) diacrylate hydrogels. Biomaterials 19:1287
50. Nguyen KT, West JL (2002) Photopolymerizable hydrogels for tissue engineering applications. Biomaterials 23:4307
51. Kim BC, Gu MB (2003) A bioluminescent sensor for high throughput toxicity classification. Biosens Bioelectron 18:1015
52. Andersen JB, Sternberg C, Poulsen L, Bjorn S, Givskov M, Molin S (1998) New unstable variants of green fluorescent protein for studies of transient gene expression in bacteria. Appl Environ Microbiol 64:2240
53. Williams W, Cui W, Levchenko A, Stevens AM (2008) Robust and sensitive control of a quorum-sensing circuit by two interlocked feedback loops. Mol Syst Biol 4:234
54. Wu Y, Joseph S, Aluru NR (2009) Effect of cross-linking on the diffusion of water, ions, and small molecules in hydrogels. J Phys Chem B 113:3512

55. Adam M, Murali B, Glenn NO, Potter SS (2008) Epigenetic inheritance based evolution of antibiotic resistance in bacteria. BMC Evol Biol 8:52
56. Bierne H, Hamon M, Cossart P (2012) Epigenetics and bacterial infections. Cold Spring Harb Perspect Med 2:a010272
57. Costerton JW, Lewandowski Z, Caldwell DE, Korber DR, Lappin-Scott HM (1995) Microbial biofilms. Annu Rev Microbiol 49:711
58. Duran-Pinedo AE, Paster B, Teles R, Frias-Lopez J (2011) Correlation network analysis applied to complex biofilm communities. PLoS One 6:e28438
59. Kolenbrander PE (2000) Oral microbial communities: biofilms, interactions, and genetic systems. Annu Rev Microbiol 54:413
60. Margulies M, Eqholm M, Altman WE, Attaya S et al (2005) Genome sequencing in microfabricated high-density picolitre reactors. Nature 437:376
61. Hong P-Y, Hwang C, Ling F, Anderson GL, LeChevallier MW, Liu W-T (2010) Pyrosequencing analysis of bacterial biofilm communities in water meters of a drinking water distribution system. Appl Environ Microbiol 76:5631
62. Percival SL, Malic S, Cruz H, Williams DW (2011) Biofilms and veterinary medicine, vol 6, Springer series on biofilms. Springer, Berlin, pp 41–48
63. Baum MM, Kainović A, O'Keeffe T, Pandita R, McDonald K, Wu S, Webster P (2009) Characterization of structures in biofilms formed by a Pseudomonas fluorescens isolated from soil. BMC Microbiol 9:103
64. Thar R, Kühil M (2002) Conspicuous veils formed by vibrioid bacteria on sulfidic marine sediment. Appl Environ Microbiol 68:6310
65. Davies DG, Parsek MR, Pearson JP, Iglewski BH, Costerton JW, Greenberg EP (1998) The involvement of cell-to-cell signals in the development of a bacterial biofilm. Science 280:295
66. Wimpenny JWT, Colasanti R (1997) A unifying hypothesis for the structure of microbial biofilms based on cellular automaton models. FEMS Microbiol Ecol 22:1
67. Perry N, Nelson EM, Sarveswaran K, Kurz V, Timp G (2013) Wiring a biological integrated circuit (unpublished manuscript)
68. Seliktar D (2005) Extracellular stimulation in tissue engineering. Ann N Y Acad Sci 1047:386

Chapter 12
Engineering Cell-to-Cell Communication to Explore Fundamental Questions in Ecology and Evolution

Robert Phillip Smith, Lauren Boudreau, and Lingchong You

Synthetic biology has created countless examples of gene circuits that lead to novel behavior in cells [1]. While the technological applications of these circuits, in terms of their use in medicine [2], industry [3, 4], and to study systems biology [5] has been acknowledged, synthetic biology is increasingly used to explore questions in evolution and ecology [6]. Traditionally, evolutionary and ecological studies have taken two separate approaches to address scientific questions. One traditional approach uses mathematical modeling to capture the essential aspects of the dynamic or relationship under study. Research is performed *in silico*, allowing the researcher to explore multiple parameters in a well-defined system, as compared to studying the relationship in its natural setting. However, predictions generated by mathematical models are often not verified experimentally, leading to questions regarding their validity [6]. On the other hand, studying a single dynamic in a natural setting offers its own set of challenges. Here, the single dynamic of interest may be subject to multiple interacting factors, which may obscure its true contribution to the relationship under study [7]. Synthetic biology thus offers a well-rounded intermediate between these two approaches; modeling predictions are verified in living, experimental systems [6, 7]. This dual approach has allowed for the study of ecological and evolutionary dynamics that would be nearly impossible to study in the natural environment. Indeed, the number of studies that have utilized synthetic biology to study such relationships is growing quickly (e.g., [8–10]).

R.P. Smith (✉) • L. Boudreau
Division of Math, Science and Technology, Nova Southeastern University,
Fort Lauderdale, FL 33314, USA
e-mail: rsmith@nova.edu

L. You
Department of Biomedical Engineering, Duke University, Durham, NC 27708, USA

Center for Systems Biology, Duke University, Durham, NC 27708, USA

S.J. Hagen (ed.), *The Physical Basis of Bacterial Quorum Communication*, Biological and Medical Physics, Biomedical Engineering, DOI 10.1007/978-1-4939-1402-9_12

A critical aspect in the vast majority of ecological settings is the interactions that occur between the individuals in the environment. Such interactions often dictate the dynamics of the ecosystem and have thus been extensively studied (e.g., [11]). The engineering of bacteria that can communicate with one another has been a fundamental step in implementing synthetic circuits to study interactions observed in ecological settings. One of the more widely used mechanisms to engineer cell-to-cell communication is through quorum sensing, which allows for the density-dependent regulation of gene expression. Quorum sensing allows cell-to-cell communication through acylhomoserine lactone (AHL) molecules. These small molecules diffuse quickly [12], do not require cellular machinery for export as they can readily pass through the cell membrane and cell wall [12], and require few genes in order to be implemented in a gene circuit. As such, this simple system has allowed the facile implementation of cell-to-cell communication in engineered bacteria, which has revolutionized our ability to understand ecological and evolutionary relationships. In the following chapter, we review studies that have taken advantage of quorum sensing to engineer gene circuits to study ecological and evolutionary dynamics. We touch upon circuit and experimental design and how the results have furthered our understanding of important natural processes.

12.1 Using Quorum Sensing Genetic Components to Engineer Cell-to-Cell Communication

The process of engineering gene circuits that allow for cell-to-cell communication via quorum sensing was first demonstrated by You et al. [13]. In this seminal study, the authors constructed a gene circuit to allow for the implementation of population density control in the bacterium *Escherichia coli* (Fig. 12.1a). The authors' circuit consists of the well-characterized LuxI/LuxR quorum sensing system from *Vibrio fischeri*. A $P_{lac/ara\text{-}1}$ promoter drives the expression of *luxI*, which synthesizes the AHL 3OC6HSL, the concentration of which increases proportional to cell density. Once a sufficiently high concentration of 3OC6HSL is reached, it binds to the LuxR receptor (driven by the $P_{lac/ara\text{-}1}$ promoter) and drives the expression of the toxic fusion protein, LacZalpha-CcdB, via the P_{lux} promoter. Once expressed, the LacZalpha-CcdB toxic fusion protein, which consists of the LacZ protein fused in frame to CcdB, a toxin protein that poisons the gyrase complex [14], leads to cell death. The overall circuit logic is as follows. As the engineered bacteria increase in cell density, 3OC6HSL accumulates in the medium. Once a sufficiently high concentration of 3OC6HSL is reached, it activates the expression of the toxic fusion protein, thus causing the cells to die. The author's model predicts that activation of the circuit in their engineered bacteria would cause the cell density to approach a steady state that was lower than the carrying capacity achieved without gene circuit activation. In addition, as the engineered bacteria approached this lower steady state, dampened oscillations were predicted to occur (Fig. 12.1b).

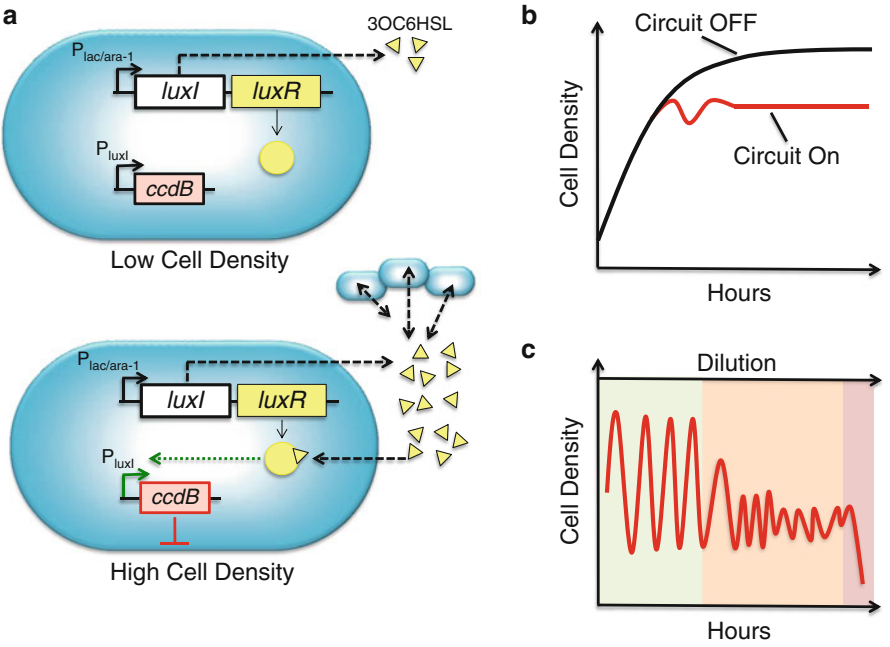

Fig. 12.1 Engineering cell-to-cell communication in *E. coli*. (**a**) Using AHL mediated cell-to-cell communication to implement a population control device. The $P_{lac/ara-1}$ promoter drives the expression of *luxI* (synthesizes the AHL 3OC6HSL, *yellow triangles*) and *luxR*, the 3OC6HSL receptor. The P_{luxI} promoter regulates expression of the *ccdB* fusion protien, which is a toxin and can kill the cell. At low cell density, *ccdB* is not expressed as insufficient 3OC6HSL is produced. At high cell density, the CcdB toxin protein is expressed, leading to cell death and programmed population control. (**b**) Programmed population control in *E. coli*. With the circuit OFF, the population of *E. coli* reaches the nutrient-controlled carrying capacity. With the circuit ON, the population reaches a circuit-controlled carrying capacity, which is lower than the nutrient-controlled carrying capacity. As the population approaches the circuit-controlled steady state, dampened oscillations occur. (**c**) When grown in a microchemostat, the amplitude and period of oscillations could be controlled by dilution. Increasing the dilution rate served to decrease the amplitude and period of the oscillations. A sufficiently high dilution rate resulted in the population being washed out of the microchemostat

Indeed, these predictions were confirmed through experimental analysis. Without gene circuit activation, the engineered bacteria grew exponentially until the nutrients in the medium were exhausted, after which additional growth was not observed. However, with circuit activation, the cells grew exponentially until a threshold point where the cell density underwent dampened oscillations before reaching a steady state that was lower than the carrying capacity of the medium (i.e., the final density of bacteria without gene circuit activation). The engineered bacteria were held at this circuit-controlled steady state for over 30 hours. Using a fluorescent assay that reported the activity of LacZ, and thus the concentration of the LacZalpha-CcdB toxic fusion protein, the authors observed tight dynamic coupling between

growth of the engineered bacteria and the concentration of the toxic fusion protein. Specifically, the population of engineered bacteria was able to grow as long as the expression of toxic fusion protein was below the steady state. A decline in population density was observed if excess (i.e., above the steady state) toxic fusion protein was expressed. As such, dampened oscillations of toxic fusion protein amount, both above and below the steady state, resulted in dampened oscillations in population density.

Interestingly, the authors' model predicts that cell density at the gene circuit-controlled steady state is tunable by modulating the degradation rate of 3OC6HSL. To modulate the degradation rate of 3OC6HSL experimentally, the authors increased the pH of the medium, which had been shown previously to destabilize various AHL molecules [15]. The authors observed a fourfold increase in the number of cells at the gene circuit-controlled steady state as the pH of the medium was increased from 6.2 to 7.8. This increase in steady state was independent of the levels of toxic fusion protein inside the cell as the levels were found to be consistent as pH was varied.

In a follow-up study, Balagadde et al. used the same engineered bacteria [13] to demonstrate controlled bacterial growth in a microchemostat; a microfluidic bioreactor that allows for the computer-regulated exchange of growth medium during long-term bacterial cell culture [16]. By growing the engineered bacteria in the microchemostat and monitoring bacterial growth at the single cell level, the authors were able to examine additional cycles of dampened oscillations that were not previously observed when the cells were grown in batch culture [13]. Furthermore, the authors were able to control the timing of circuit activation either by introducing exogenously added IPTG (activates the gene circuit via the $P_{lac/ara-1}$ promoter) to the medium or by removing it. The authors observed that cells that were initially grown with the circuit activated (i.e., IPTG in the medium) would return to normal wild-type growth (i.e., no dampened oscillations), with a wild-type steady state, shortly after the removal of IPTG from the medium. Concurrently, the addition of IPTG to the growth medium of cells previously grown without IPTG (circuit off) resulted in a near immediate decline in population density to the gene circuit-controlled steady state with dampened oscillations. Interestingly, by changing the dilution rate of the medium from the microchemostat, the authors could control the period and amplitude of the dampened oscillations. Specifically, with a low dilution rate, the dampened oscillations had a short period and large amplitude. Increasing the dilution rate served to decrease the period and the amplitude of the dampened oscillations until the dilution rate was sufficiently high and the cells were washed out of the microchemostat (Fig. 12.1c).

The results presented in these two papers were fundamental in establishing mechanisms to engineer cell-to-cell communication in bacteria. Not only did they serve as a proof-of-principle towards constructing more complex gene circuits allowing cell-to-cell communication, but they also demonstrated the tunability and simplicity of how such systems can be used in order to generate complex dynamics in a population of *E. coli*.

12.2 Engineering Cell-to-Cell Communication to Understand Competitive Dynamics in Ecology and Evolution

One of the first applications of synthetic gene circuits allowing cell-to-cell communication using quorum sensing to explore ecological dynamics was published in 2008. Balagadde et al. engineered two *E. coli* strains to communicate bi-directionally using two different quorum sensing systems (Fig. 12.2a) to study oscillatory predator–prey dynamics [17], which are often found in natural settings [18]. One strain, the predator, contains a circuit consisting of the $P_{LtetO-1}$ promoter driving the expression of *luxR* and *lasI* (produces the AHL 3OC12HSL). In addition,

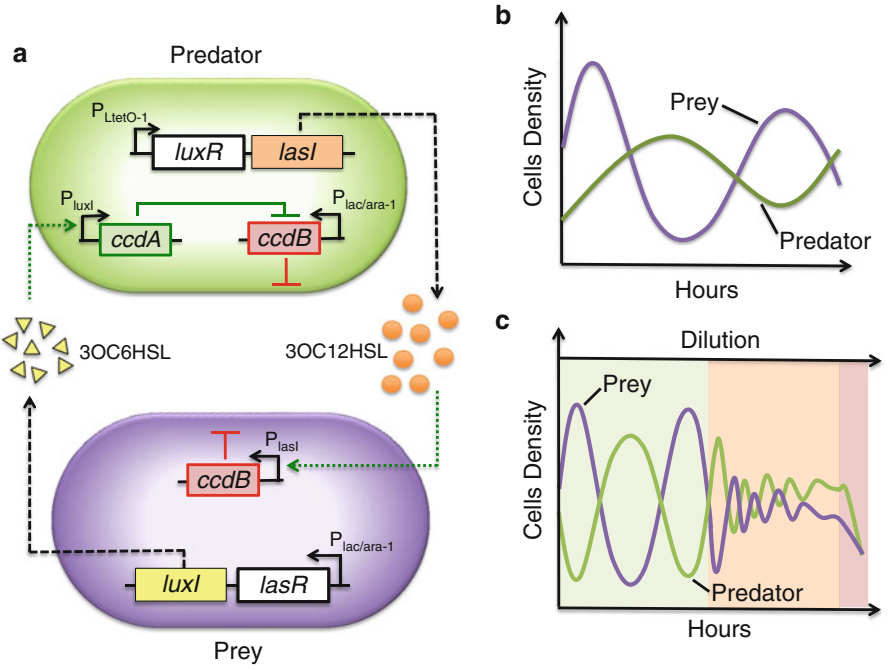

Fig. 12.2 A synthetic predator–prey system leads to canonical oscillatory dynamics. (**a**) Engineering gene circuits in *E. coli* to create predator and prey strains. In the predator strain, a $P_{LtetO-1}$ promoter drives the expression of *luxR* and *lasI* (synthesizes 3OC12HSL (*orange circles*)) while a $P_{lac/ara-1}$ promoter drives *ccdB*. In the prey strain, a $P_{lac/ara-1}$ promoter drives the expression of *ccdB*, *luxI* (synthesizes 3OC6HSL (*yellow triangles*)), and *lasR*. 3OC6HSL from the prey strain rescues the predator strain by activating the P_{luxI} promoter, which drives the expression of *ccdA*. 3OC12HSL from the predator strain kills the prey strain via a P_{lasI} promoter that drives the expression of *ccdB*. (**b**) When grown together in a microchemostat, the growth of the predator and prey strains followed canonical oscillatory dynamics. The *purple line* represents the prey population. The *green line* represents the predator population. (**c**) Modulating the dilution rate of the microchemostat altered the period and amplitude of the predator–prey oscillations. Increasing the dilution served to dampen the oscillations until the dilution rate was increased sufficiently as to remove both populations from the microchemostat

this strain contains a toxin/antitoxin circuit. The toxin, *ccdB*, is expressed via the $P_{lac/ara-1}$ promoter, while the antitoxin, *ccdA*, is regulated using the P_{luxI} promoter. The second strain, the prey, contains a circuit consisting of the $P_{lac/ara-1}$ promoter driving the expression of *lasR* (the receptor for 3OC12HSL) and *luxI*, as well as the P_{lasI} promoter driving expression of *ccdB*. The overall circuit logic is as follows. The production of 3OC12HSL from the predator strain activates the expression of CcdB is the prey strain, thus killing the prey. As the prey population decreases in density, so does the concentration of 3OC6HSL in the medium. An insufficient concentration of 3OC6HSL negatively affects the predator strain, as it can no longer activate the expression of CcdA (which binds to and inactivates CcdB). A sufficient decline in the prey population causes CcdB in the predator population to begin killing the predator strain. A reduction in the predator population simultaneously decreases the amount of 3OC12HSL being produced, which stops CcdB from being expressed in the prey strain, thus allowing the prey population to grow. Over time, the interplay between these two populations is predicted to result in canonical predator–prey dynamics (Fig.12.2b). Indeed, the authors verified that these engineered bacteria could interact and lead to predator–prey dynamics when grown in a microchemostat [16].

While the authors did not set out to explore a specific ecological question outside of engineering predator–prey dynamics in cells, they did, however, uncover a unique dynamic with respect to the rate at which the predator and prey populations are diluted from the microchemostat. In a sense, dilution may effectively represent dispersal away from a confined location where predator–prey dynamics are occurring. As predicted by a mathematical model, the authors demonstrated that at a low dilution rate, oscillations with long periods were produced (Fig. 12.2c). Increasing the dilution rate led to dampened oscillations while further increases led to the abolishment of predator–prey oscillations as the entire population was removed from the microchemostat. With these unexpected findings, the authors may have discovered a unique factor that modulates canonical predator prey dynamics in nature.

In 2009, the same predator and prey strains were used to examine how biodiversity was affected by motility [19]. Understanding the mechanisms that control biodiversity is paramount in maintaining microbial ecosystems, which often form the foundation of larger ecosystems [20]. Previous studies had indicated that reducing motility promoted biodiversity [9, 21]. However, it remained unclear as to how motility would affect biodiversity when individuals in the ecosystem communicated over long distances through small diffusible chemicals such as AHL. Indeed, examples of predator–prey interactions that occur via small diffusible chemicals are apparent in the environment [22].

To understand how motility affects biodiversity, the authors first grew both the predator and prey strains in two different well-mixed culture conditions: in liquid medium, which allowed the highest cellular motility, and in a well-mixed culture distributed on an agar plate, which allowed the lowest motility (Fig. 12.3a). Using a modified version of Simpson's biodiversity index ($\mathrm{BI} = 1 - \sum_{i=1}^{2} x_i^2 = 2x_1x_2$, where BI represents the biodiversity index, and x represents the ith population of

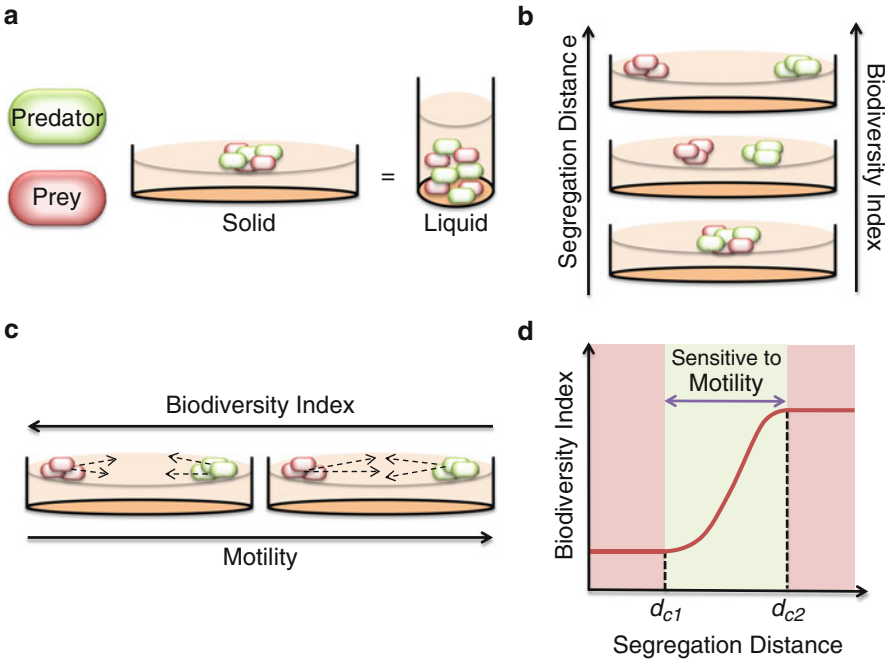

Fig. 12.3 Segregation distance and motility affects the biodiversity index in a predator–prey ecosystem. (**a**) Using a modified version of the predator–prey strains shown in Fig. 12.2 (predator strain modified to produce green fluorescent protein and prey strain modified to produce red fluorescent protein), the authors explored how motility alters the biodiversity index of a predator–prey ecosystem. When the predator and prey strains were well mixed and grown on either solid medium (an agar plate, low motility) or liquid medium (high motility), the biodiversity index was nearly identical between the two conditions. (**b**) When grown in spatially partitioned habitats, increasing the segregation distance between the predator and prey populations served to increase the biodiversity index. (**c**) For a given segregation distance, increasing the motility of the predator and prey populations served to decrease the biodiversity index. Arrows represent motility. (**d**) A general rule to describe the impact of segregation distance and motility on biodiversity index. Segregation distance has negligible impact on the biodiversity index until a critical segregation distance is reached (d_{c1}). Past this critical point, increasing segregation distance serves to increase the biodiversity index until a second, critical segregation (d_{c2}) distance is reached. Here, increasing the segregation distance had a negligible impact on biodiversity. Motility can affect the biodiversity index when the segregation distance is between d_{c1} and d_{c2}

the co-culture), and consistent with modeling predictions, the authors observed that motility had a negligible effect on biodiversity when both the predator and prey strains were well mixed. That is, the biodiversity index was the same in both conditions. Interestingly, this counterintuitive result conflicted with previous studies that had indicated a significant effect of motility on biodiversity [21]. Using their mathematical model, the authors suggested that while changing the motility of each bacterial strain changed its spatial distribution, it did not change the ratio of the

spatially averaged densities of the predator and prey strains and thus it did not change the biodiversity index.

Next, the authors sought to determine how biodiversity would be affected if both the predator and prey strains existed in spatially partitioned habitats, which have been previously suggested to affect the biodiversity index [23]. Using a mathematical model, the authors predicted that increasing the segregation distance between the two populations serves to increase biodiversity. Their model suggests that when the two populations are inoculated together at the same point (i.e., a segregation distances of zero), the predator strain would move away from its inoculation point rapidly, effectively trapping the prey population at its inoculation point. However, increasing the segregation distances between the two strains decreases the strength of the long-range chemical interactions (via AHLs), which serves to decrease the killing and rescuing rates, as well as competition for nutrients. Using their engineered bacteria, the authors seeded separate populations of the predator and prey strains at distances ranging from 0 to 2 cm apart on an agar plate. As determined by the amount of fluorescent protein produced by each engineered strain (the predator was modified to produce green fluorescent protein (GFP) and the prey was modified to produce red fluorescent protein), the biodiversity index increased as the segregation distance increased (Fig. 12.3b).

In addition, the authors' model predicts that decreasing motility in partitioned habitats increases biodiversity, which was confirmed through experimental analysis. Experimentally, the authors modulated the motility of the bacteria by changing the percentage of the agar in an agar plate where higher percentages of agar served to limit motility. Their model suggests that this change in biodiversity index is due to the ability of motility to control the spatiotemporal interaction strengths between the predator and prey populations. At high motility, the predator and prey strains approach each other quickly. Here, the increased local concentration of 3OC12HSL (secreted by the predator strain) causes rapid killing of the prey serving to decrease the biodiversity index of the system. At low motility, the populations approach each other less rapidly. The prey encounters less 3OC12HSL, allowing the population to grow, which increases the biodiversity index (Fig. 12.3c). Using this explanation, the authors developed a general rule to determine the impact that partitioned habitats would have on biodiversity and motility (Fig. 12.3d). Increasing the segregation distance between the two populations does not affect biodiversity until a critical segregation distance (d_{c1}) has been reached. Here, increasing the segregation distance increases the biodiversity index until a second, critical segregation distance (d_{c2}) is achieved, where any additional increase in the segregation distance does not affect the biodiversity index. Only within these two critical distances, motility impacts the biodiversity index. These results, and general rule, may impact the way in which species are managed in order to increase or maintain biodiversity in a natural setting. Moreover, this study revealed several, previously overlooked facets that complicate the dynamics between microbial populations that interact via small diffusible molecules.

12.3 Engineering Cell-to-Cell Communication as a Tool to Understand Cooperation

While gene circuits using quorum sensing have allowed us to understand the dynamics of ecological relationships where two populations interact and compete, it has also allowed us to examine several prominent behaviors observed when populations of bacteria cooperate. At its very foundation, quorum sensing represents a form of bacterial cooperation. Examples of bacteria that secrete and use public goods (such as AHL) are ubiquitous in nature (e.g., [24]). The production and excretion of the public good is a costly process for each cell as it requires an energy investment. However, once released, the public good itself has a benefit to the population as a whole, such as the ability to relieve stress (e.g., [25]). The production of public goods is often placed under the regulation of quorum sensing. Here, the public good is only produced once the population of bacteria has reached a sufficiently high density. Such regulation is thought to be advantageous to the cell as the production of certain public goods may only be beneficial when a sufficiently high density of cells is present and are thus capable of creating sufficient public good to relieve a stressor. While this advantage has been demonstrated previously using a natural biological system [26], the exact conditions under which quorum sensing regulated public good production becomes advantageous remain relatively unexplored (Fig. 12.4a). In 2012, Pai et al. used a synthetic biology approach to determine the conditions under which quorum sensing regulated public good production becomes advantageous [27]. Their circuit consists of IPTG inducible *luxI* and *luxR* genes (Fig. 12.4b). Sufficient production of 3OC6HSL (via LuxI) activates the production of the public good, a modified beta-galactosidase, BlaMs, which is secreted from the cell via an engineered HlyB–HlyD transport system. Once BlaMs is secreted out of the cell, it can degrade 6-APA, an antibiotic that causes stress to the cell by destroying the cell wall. Their circuit design allowed for three conditions of circuit activation; ON, in which the medium is supplemented with 3OC6HSL thus serving to activate continuous production of BlaMs, OFF, in which BlaMs and 3OC6HSL are not created and QS, in which 3OC6HSL is produced by LuxI and the production of BlaMs only occurs once a sufficiently high concentration of 3OC6HSL is produced.

The authors initially performed a cost–benefit analysis of quorum sensing mediated BlaMs production in the population. They first determined that BlaMs production is only beneficial when initiated at high cell density. As predicted by a mathematical model, when grown in the ON state, a culture initiated from a high cell density outgrew cells in the OFF condition (that were initiated from the same initial density). Here, the ON population initially grew at a rate slower than the OFF population due to the cost of producing BlaMs. However, due to 6-APA degradation by the secreted BlaMs, the growth rate of the ON culture eventually surpassed the growth rate of the OFF culture, thus demonstrating the advantageous nature of BlaMs production at high initial cell density. In contrast, when the cell cultures were initiated from a low initial cell density, cells in the OFF condition outgrew

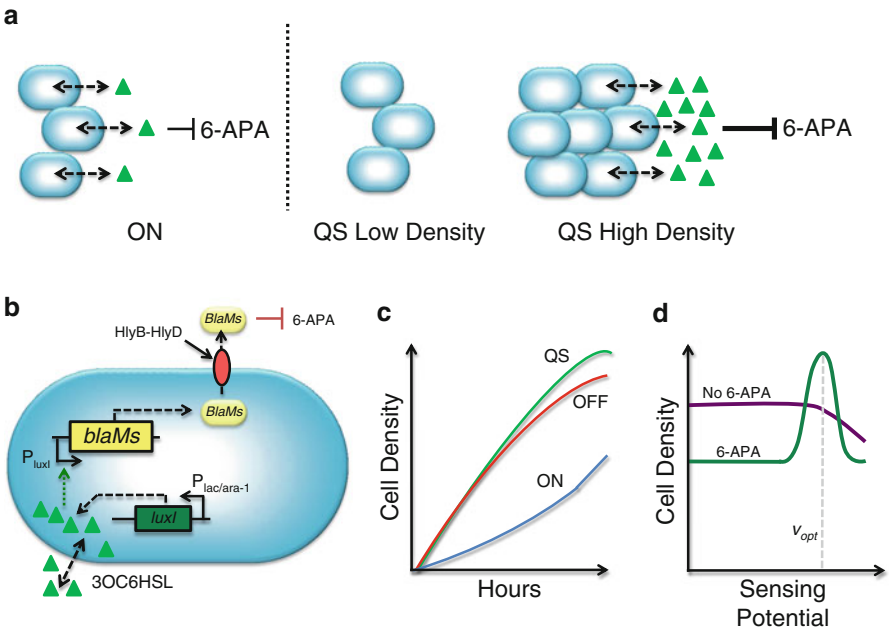

Fig. 12.4 Quorum sensing regulated production of a costly public good is beneficial to a population of bacteria in alleviating a stressor. (**a**) Two potential strategies to deal with an external stressor (6-APA). In one strategy (*left panel*), public good production (*green triangles*), which inhibits the stressor, is produced and excreted a constant rate regardless of the cell density. In a second strategy, production of the public good is regulated through quorum sensing. As such, the public good is only produced at a sufficiently high density. (**b**) A synthetic circuit to explore optimality in quorum sensing regulated public good production. An IPTG inducible $P_{lac/ara-1}$ promoter drives the expression of *luxI* (synthesizes the 3OC6HSL, *green triangles*) and the production of *luxR* (gene not shown). At a sufficient high concentration (i.e., a sufficiently high cell density), 3OC6HSL binds to LuxR, which activates the P_{luxI} promoter to trigger the production of BlaMs, a public good that can degrade the antibiotic 6-APA. An engineered HlyB–HlyD transporter moves BlaMs into the extracellular environment. (**c**) Growth of the ON, OFF, and QS populations in the presence of 6-APA initiated at low initial cell density. The ON population does not reach the same cell density as the QS and OFF populations due to the cost of BlaMs production. The QS population is able to exceed the growth of the OFF population due to the overall benefit of quorum sensing regulated BlaMs production. (**d**) Optimality in sensing potential, which is defined as the cell density at which public good production is initiated. For a given concentration of 6-APA (*green line*), an optimal cell density (v_{opt}, *gray dashed line*) to initiate BlaM production exists. Here, the greatest amount of growth is observed. In the absence of 6-APA (*purple line*), cell density decreases near monotonically with increasing sensing potential

those in the ON condition. As predicted by their model, cells in the ON condition continued to pay the cost of BlaMs production but could not take advantage of its production as the concentration of BlaMs in the medium was insufficient to relieve the stress caused by 6-APA. This resulted in a low growth rate as compared to cells grown in the OFF condition.

The authors then sought to determine the conditions under which quorum sensing mediated production of BlaMs was more advantageous. They grew their engineered bacteria initiated from low cell density under the three conditions, OFF, ON, and QS (Fig. 12.4c). As predicted by their model, the OFF culture vastly outpaced the growth of the ON culture. Initially the growth rates of the OFF and QS cultures were nearly identical but over time the QS population began to grow faster than the OFF condition due to the production of BlaMs. Further experimentation confirmed that QS was advantageous under several conditions (i.e., varying levels of 6-APA), the only exception being when 6-APA is not present in the culture. Here, the OFF culture prevailed.

While quorum sensing appeared to be a beneficial strategy for the cells when initiated from a defined initial density, the authors sought to determine if quorum sensing remained beneficial after a population of bacteria has undergone dispersal, which may lead to high variability in the number of initial individuals in a subpopulation [28]. Dispersal serves to restart the growth cycle from a low cell density after a population has reached a high cell density. Such dynamics are often observed in the dispersal and formation of biofilms, fruiting body development or sporulation [28]. Experimentally, the authors could simulate dispersal by diluting cells from a high cell density into separate wells of a 96 well plate. Each well represented a subpopulation initiated from an initial density of ∼2–3 cells/well, which was estimated experimentally. As predicted by their model, cells grown in the QS condition continued to outcompete those in the OFF condition even after dispersal, demonstrating that quorum sensing continued to be a robust mechanism to regulated public good production.

The amount of variability in the initial number of cells in each subpopulation may vary in the natural setting. As such, the authors repeated their experiment under two different conditions; a high spread condition, which had higher variability around a common central mean of initial number of cells, and a low spread condition. As predicted by their model, subpopulations initiated from the high spread (higher variability around the mean) condition significantly outgrew the low spread condition (lower variability around the mean). The authors hypothesized that this observation could be accounted for by the number of subpopulations initiated from both initial high and low cell density. Here, the high spread population has more subpopulations with both high and low initial cell densities, as compared to the low spread condition. As such, the high density subpopulations will be the first to reach the critical threshold to allow for BlaMs production, which in turn benefits the population allowing them to grow faster. The increased number of high initial density subpopulations observed in the high spread condition causes this condition to outcompete the low spread condition. These results demonstrate that enhanced variability during seeding of subpopulations serves to increase the benefit of placing public good production under the regulation of quorum sensing.

Finally, the authors used their engineered bacteria to explore the optimal cell density at which to activate quorum sensing regulated production of BlaMs. Initially, they explored this concept using a previously developed metric, sensing potential (ν) [29]. ν is a lumped metric that determines the density at which quorum sensing is

activated; the higher value of v, the lower the cell density at which quorum sensing is activated [29]. Without stress (i.e., 6-APA), their model predicts that overall growth increases with decreases in v. That is, the OFF condition (i.e., $v = 0$) leads to the highest growth in the absence of stress. However, with the inclusion of stress, overall growth is a biphasic function of v, which leads to an optimal value of v (called v_{opt}) where growth is highest (Fig. 12.4d). This relationship results from two opposing parameters; cost, which increases with activation at lower cell density (i.e., high values of v) and benefit, which decreases with activation at high cell density (i.e., low values of v). The authors verified the model predictions experimentally by varying the concentration of IPTG in the medium, which served to control the cell density at which the production of BlaMs was activated. They observed that the highest growth was achieved at an intermediate concentration of IPTG. The authors note that this finding has implications in the use of quorum sensing disrupters for the control of pathogens that use such systems to regulate pathogenicity, such as *Pseudomonas aeruginosa* [30] and *Vibrio cholera* [31]. The authors caution that $adhoc$ manipulation of the quorum sensing threshold may increase total bacterial growth, and could thus exacerbate a bacterial infection.

While quorum sensing regulated production of public goods appeared to be advantageous under several conditions, the mechanisms by which this cooperative behavior (such as the production of a public good) is maintained in a population remain relatively unexplored. In general, "cheating" individuals can infiltrate populations of cooperating cells. These "cheaters" take advantage of the cooperative behavior but do not pay the "cost" of cooperation. In microbial systems, a cost can be associated with the energy and building blocks required to produce a public good. As such, cheaters will often proliferate faster than the cooperating cells, and thus could dominate a population over time. Nevertheless, it is apparent that cooperators continue to be maintained within natural populations [32]. One particularly puzzling aspect of such maintenance is Simpson's paradox: the total proportion of cooperators in any subpopulation is lower than cheaters, however when the global population is considered (e.g., the summation of all subpopulations), the total proportion of cooperators is higher than cheaters (Fig. 12.5a, [33]).

To investigate how Simpson's paradox may arise in a microbial system, Chuang et al. engineered two strains of *E. coli*: a cooperator strain and a cheater strain (Fig. 12.5b, [34]). The cooperator strain contains a circuit that consists of the constitutive P_R promoter that drives the expression of *rhlI* (and a GFP for strain identification), the P_{lacI^q} promoter that drives the expression of the *rhlI* receptor (RhlR) and *rhlI*, which synthesizes the AHL C4HSL. The C4HSL responsive P_{rhl} promoter drives the expression of *catLVA*, which confers the ability to resist the antibiotic chloramphenicol. The cheater strain contains both the P_{lacI^q} promoter that drives *rhlR* and the P_{rhl} promoter that drives *catLVA* but it does not synthesize C4HSL. Therefore, the cheater strain does not cooperate (i.e., does not synthesize the public good C4HSL) but can take advantage of the C4HSL produced from the cooperator strain. In addition, the metabolic burden associated with producing C4HSL and GFP reduces the growth rate of the cooperator strain. The necessary

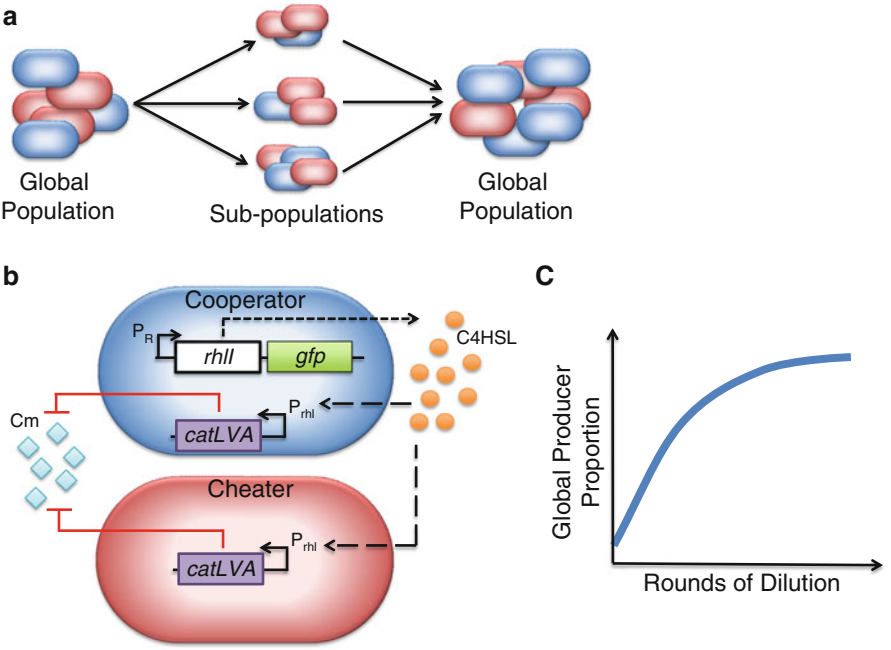

Fig. 12.5 A synthetic system realizes Simpson's paradox and reveals a unique effect of extreme dilution. (**a**) The overall logic of Simpson's paradox; the total proportion of cooperators (*blue cells*) is lower in all subpopulations [relative to cheaters (*red cells*)]. However, when the global population is considered, the global proportion of cooperators is higher than cheaters. (**b**) A synthetic system to realize Simpson's paradox. Cooperator cells contain a P_R promoter that drives the expression of *rhlI* (synthesizes C4HSL, *orange circles*) and a green fluorescent protein. This circuit causes the cooperator strain to pay the "cost" for cooperation. Both the cooperator and cheater cells contain a P_{rhl} promoter that drives the expression of *catLVA*, which degrades the antibiotic chloramphenicol (Cm, *blue diamonds*) and allows cells growth. (**c**) Multiple rounds of dilution (i.e., dispersal) and pooling served to increase the overall proportion of cooperator cells from 10 to 95 %. As such, extreme dilution may represent a mechanism by which cooperators are maintained within a population consisting of cooperators and cheaters

conditions for studying Simpson's paradox, reduced growth by cooperators and access to a public good by cheaters, are thus achieved using these two strains.

To determine if Simpson's paradox could be realized by these engineered bacterial strains, the authors examined the growth of ten different cultures, each initiated from a different proportion of cooperator and cheater populations. As predicted by a mathematical model and determined experimentally, the global proportion of cooperators increased relative to the global population of cheaters, despite the fact that the proportion of cooperators was lower than cheaters in each subpopulation. As such, these two strains could indeed realize Simpson's paradox.

Previous studies have indicated that an important mechanism by which Simpson's paradox can be maintained in natural populations is through repeated formation of new populations. This may be realized through dispersal of individuals

from an established population and may lead to a sufficiently large variance in subpopulation initial density. Here, the composition of each group follows a Poison distribution, which will result in stochastic fluctuations in the initial composition of each group. To test this hypothesis experimentally, the authors diluted a population containing equal proportions of cooperators and cheaters into 288 subpopulations. The number of initial bacteria in each population followed a Poison distribution with a value of λ, where a smaller value of λ indicated a smaller average number of initial bacteria. After growing all of the subpopulations for 12 h, the authors pooled the subpopulations and determined the proportion of cooperators. They observed that for a sufficiently low value of λ, Simpson's paradox could be maintained. However, if λ was sufficiently high, the global proportion of cooperators was lower than that of cheaters, thus failing to maintain Simpson's paradox. Interestingly, the authors performed the aforementioned dilution experiment starting with an initial population containing 10 % cooperators and a value of λ of $\sim$2 (average of two cells initiating each subpopulation) for several rounds. After five rounds of dilution, the authors observed that 95 % of global population consisted of cooperator cells (Fig. 12.5c). As such, the authors demonstrated that extreme dilution favors the maintenance of cooperation in their microbial population, which may explain how cooperation is maintained in the face of natural selection, which would favor cheaters.

One of the most widely studied relationships with respect to the maintenance of a cooperative behavior is Hamilton's rule [32], which has the general equation of $br > c$. Here, b represents the benefit associated with a public good, c represents the cost associated with the production of the public good, and r represents the relatedness between the individuals in the population. In essence, the equation predicts that cooperators will be maintained in a population if the benefit and/or relatedness of the population outweigh the cost of producing a public good [32].

Building on their 2009 study, Chuang et al. used their previously engineered cooperator and cheater strains to examine the interplay between the parameters in Hamilton's rule [35]. Modification of their experimental setup and gene circuit allowed them to individually modulate the parameters of Hamilton's rule. By changing the proportion of cooperators in a population consisting of both cooperators and cheaters, the authors could modulate the parameter r, where a higher proportion of cooperators would correspond to a higher value of r. To modulate c, the authors engineered the cooperator strain to lack the *argH* gene, thus rendering the strain auxotrophic with respect to arginine. As such, the authors could control the growth rate of this cooperator strain by tuning the concentration of arginine in the medium. Here, lower concentrations of arginine would lead to a slower growth rate, which was verified experimentally and represented an additional cost (c) of being a cooperator. Finally, to modulate b, the authors engineered the cooperator and cheater strains to contain an additional copy of the RhlR receptor gene. The extra copies of *rhlR* would cause the cells to respond more readily to any C4HSL in the medium, ultimately serving to increase the benefit for a given quantity of C4HSL.

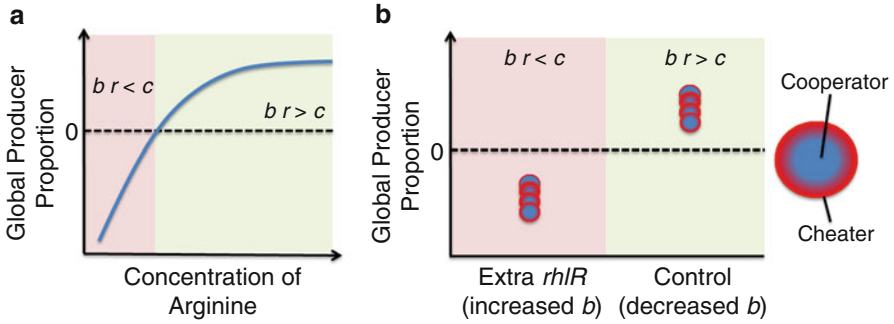

Fig. 12.6 Using synthetic cooperator and cheater strains to explore Hamilton's rule, $b\,r > c$, where b represents benefit of the public good, r represents the relatedness of the individuals, and c represents the cost of cooperation. (**a**) Using a modified cooperator strain shown in Fig. 12.5 (an arginine auxotroph), the authors explored the effect of modulating the cost parameter (c) in Hamilton's rule. When the cost of cooperation was sufficient high (low concentration or arginine in the medium, *red shaded area*), the proportion of cheaters was higher than that of cooperators. However, with a sufficiently low cost (high concentration of arginine in the medium, *green shaded areas*), the total proportion of cooperators was higher than cheaters. (**b**) Using a modified cooperator strain (extra copy of RhlR receptor protein, which served to increase b), the authors observed an unexpected consequence of Hamilton's rule. Here, increasing b (*red shaded area*) served to decrease the proportion of cooperator cells such that the cheater population dominated. The authors suggest that unexpected nonlinearities within Hamilton's rule resulted in this unexpected observation. *Red area* of the circle represents the proportion of cheaters. *Blue area* of the circle represents the proportion of cooperators

Using their newly engineered Δ*argH* auxotrophic strain, the authors modulated the c parameter in Hamilton's rule by manipulating the concentration of arginine in the growth medium. The authors grew several subpopulations of Δ*argH* cooperators and cheaters, where each subpopulation had a different initial proportion of cooperators ranging from 10 to 95 %. They observed that as the concentration of arginine in the medium was decreased (i.e., increasing c), the proportion of cooperators decreased in the culture. Therefore, below a critical amount of arginine, the proportion of cooperators decreased (Fig. 12.6a). The authors explained this result is based on Hamilton's rule. As arginine decreased, the cost associated with cooperation (c) increased. Eventually the value of c exceeds the value of br (i.e., $br - c$), thus causing the proportion of cooperators to decrease in the subpopulation. Next, the authors explored the consequences of modulating the b parameter of Hamilton's rule by growing subpopulations of cooperators and cheaters harboring the additional copy of the RhlR receptor. Interestingly, the authors observed that the additional copy of this receptor, which was intended to increase b, in fact reduced b and resulted in a decrease in the proportion of cooperator cells (irrespective of the initial proportion of cooperators in the subpopulation, Fig. 12.6b). The authors suggest that this counterintuitive result stems from the nonlinear relationship between growth and cooperator proportion when an additional copy of *rhlR* is present. This in turn caused b to be dependent on both the number of copies

of *rhlR* genes, as well as the initial proportion of cooperators. As such, the authors were able to uncover a unique relationship that could not be predicted simply from measuring *b*, *c*, and *r* alone. Instead, in order to truly understand the relationship between cooperators and cheaters in a microbial system, one must consider multiple scenarios or parameters that can be varied, such as the initial proportion of cooperators in a population or the specific biochemistry of each of the individuals in the population.

While the secretion of a public good represents a form of altruism, the evolutionary constraints that lead to more extreme forms of cooperation, such as altruistic cell death, remain relatively unexplored. Altruistic cell death is particularly puzzling as there is no direct benefit to the cells that undergo death. In 2012, Tanouchi et al. aimed to unravel the conditions that made altruistic death advantageous for a population of bacteria (Fig. 12.7a, [36]). The authors implemented a gene circuit in *E. coli* consisting of two modules: a suicide module and a public good module (Fig. 12.7b). The suicide module is activated via 6-APA, a beta-lactam antibiotic that causes murein, a component of the cell wall, to break down and generate the cell wall intermediate aMur-Tp inside of the cell. aMur-Tp activates the P_{ampC} promoter through its transcriptional regulator AmpR. In their circuit, activation of the P_{ampC} promoter causes transcription of the E lysis gene, originally isolated from bacteriophage ΦX174. In the public good module, the $P_{lac/ara-1}$ promoter drives the expression of a non-secreted form of BlaM. The overall circuit logic is as follows: sufficient murein degradation by 6-APA activates the expression of the E lysis gene, which leads to cell lysis. This, in turn, releases the public good BlaM, which degrades 6-APA and serves to counteract the negative effects of this antibiotic and thus benefitting the remaining population of cells. Initially, the authors sought to determine if their circuit design could function to create altruistic cell death. The authors grew bacteria containing their synthetic circuit (termed PAD for "programmed altruistic death") in the presence of 6-APA. In addition, the authors used a control strain (termed NPD for no programmed death), which lacked the E lysis gene. As such, NPD could not undergo lysis, but continued to produce non-secreted BlaM. When both strains were grown in the presence of 6-APA, there was an initial significant decrease in cell density of the PAD strain (as compared to the NPD strain), owing to E lysis gene mediated cell lysis. However, after 18 h of growth, the cell density of the PAD strain surpassed that of the NPD strain (Fig. 12.7c). This experiment served as a proof-of-principle that altruistic death can be advantageous to a population of single-celled organisms.

Guided by mathematical modeling, the authors then explored the conditions that would lead to optimality in altruistic cell death. Initially, the authors explored the effects of modulating two key parameters, the rate of cell death (which could be increased by increasing the rate of E lysis gene synthesis via changes in the ribosomal binding sequence) and the rate of public good production (which could be increased by increasing the concentration of IPTG in the medium). Their model predicts a key tradeoff with respect to the rate of cell death. For a given rate of public good production, a low rate of cell death leads to insufficient release of BlaM, which causes total population extinction as insufficient 6-APA is degraded.

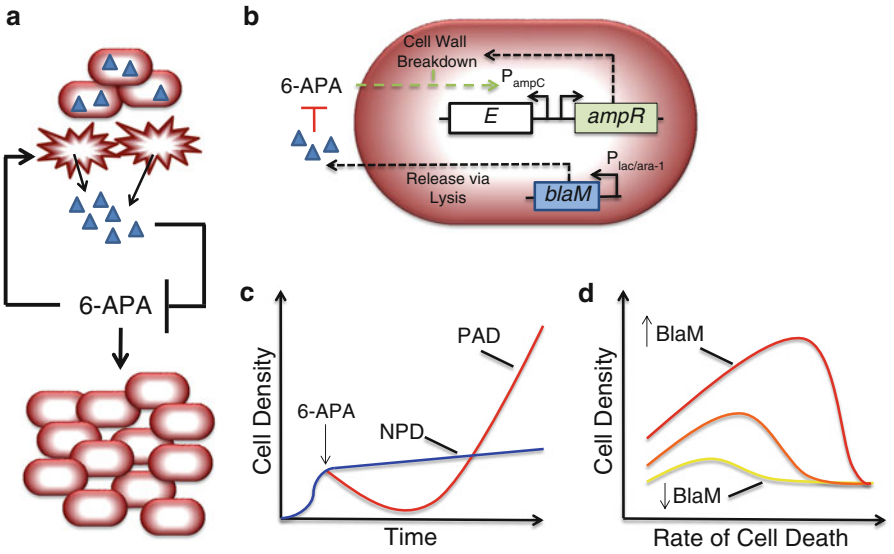

Fig. 12.7 A synthetic system to explore optimality in altruistic cell death. (**a**) The overall logic of the synthetic system. Engineered bacteria (*red ovals*) produce a public good (BlaM, *blue triangles*) that can only be released from the cells via cell lysis (i.e., altruistic death). The public good can degrade the antibiotic 6-APA, which can cause cell death by activating the E lysis gene. Cell lysis via 6-APA results in the release of public good, which causes degradation of 6-APA. This causes the remaining unlysed cells to grow. (**b**) The growth advantage produced by altruistic cell death. Without altruistic cell death (NPD strain, *blue line*), the increase in cell density was negligible following the addition of 6-APA. However, with altruistic cell death (PAD strain, *red line*), growth initially decreased after the addition of 6-APA due to altruistic cell death via the E lysis gene. However, after a given time, the remaining cells increased in density (over that of the NPD strain) owing to the release of BlaM and the degradation of 6-APA. (**c**) Optimality in altruistic cell death depends upon two key variables; the rate of cell death and the rate of public good production (BlaM). As the rate of cell death increases, the rate of public good production that leads to the greatest increase in cell density also increases

However, a high rate of cell death does not allow for a sufficiently high population of bacteria to benefit from the release of BlaM, thus leading to lower growth rates of the surviving bacteria. Interplay between these two parameters leads to an optimal level of altruistic death, where the remaining population would grow the most. Using variations of the PAD strain (each strain produced the E lysis gene at different rates), the authors observed that increasing the rate of BlaM production caused the rate of E lysis gene production, that leads to the highest amount of growth due to altruistic cell death, to shift to higher levels (Fig. 12.7d). The authors suggested that these dynamics were due to a unique cost–benefit tradeoff in the release of BlaM. When BlaM production is low, fast death is not advantageous as insufficient BlaM is released, and the remaining survivors do not benefit from its release. Conversely, fast death at high BlaM production rates serves to increase the time during which the survivors can benefit from the released BlaM, thus increasing the overall density of the population in the long term.

Interestingly, their model predicts that altruistic death can lead to a unique phenomenon called the Eagle effect, which is defined as increased bacterial growth at increasing antibiotic concentrations [37]. Guided by their mathematical model, the authors predicted that increasing the synthesis rate of E lysis gene would lead to a non-monotonic dependence of bacterial growth on 6-APA concentration. For a sufficiently high synthesis rate of the E lysis gene, bacterial growth was predicted to be highest at an intermediate concentration of 6-APA. Indeed, by increasing the rate of the E lysis gene expression through modulation of ribosomal binding sequences, the authors observed the Eagle effect using their engineered bacteria. The implications behind these findings could be of great importance in understanding the Eagle effect in the clinical setting [38] and have relevance in determining efficacious antibiotic treatments.

In many biological systems, cooperation is essential for survival. Often, cooperation may only be beneficial, and allow for survival, if the density of the population is above a critical density threshold. Often referred to as an Allee effect [39], this phenomenon is observed in invasive species [40], reintroduced species [41], the spread of infectious diseases [42] and in antibiotic resistant bacteria [43]. The Allee effect is often cited as a predominant factor that determines whether a population of cooperative organisms can spread and survive or goes extinct. Previous theoretical studies have indicated that dispersal, one of the primary drivers of spread, and the Allee effect may regulate the spread of species [44, 45]. However, direct experimental evidence of these predictions was lacking until Smith et al. created engineered bacteria to have an Allee effect and, using these bacteria, experimentally simulated spread in a synthetic ecosystem [46].

In their study, the authors created a synthetic circuit that couples survival to cooperation, which was meditated through the AHL 3OC6HSL [46]. Their circuit consists of a toxin module and a rescue module. In the toxin module, a P_{lac} promoter drives the expression of *ccdB*, which kills the cell. In the rescue module, a P_{lac} promoter drives the expression of *luxR* and *luxI*. Furthermore, the 3OC6HSL dependent P_{lux} promoter drives the expression of *ccdA*, which when expressed, inhibits the ability of CcdB to kill the cells. The circuit logic allowing for the Allee effect is as follows: at sufficiently low cell density, insufficient 3OC6HSL is synthesized, which allows CcdB to kill the cells. At sufficiently high cell density, sufficient 3OC6HSL is synthesized, which activates the expression of *ccdA* and allows the population to grow. To test the circuit logic, the authors grew the engineered bacteria with or without IPTG and varied their initial density. Without IPTG, the engineered bacteria grew at all initial cell densities. However, with IPTG, the engineered bacteria only grew if their initial cell density was above $\sim 10^4$ CFU/mL. Otherwise, the engineered bacteria died. As such, the authors successfully engineered bacteria that had the fundamental property of the Allee effect; a sufficiently high initial density of cells is required for growth and survival.

The authors then sought to determine how dispersal and the Allee effect dictate spread and survival of their engineered bacteria. They established a theoretical and experimental framework that included two types of patches: a source patch, which contains an initial amount of engineered bacteria, and a target patch, which does

not initially contain cells. Experimentally, these patches were realized by using two different wells of a 96-well plate. Dispersal was achieved by moving a fraction of the cells from the source patch to the target patch. Using this system, and guided by mathematical modeling, the authors moved cells from the source patch to the target patch at different dispersal rates (i.e., different fractions of bacteria) and quantified growth in both patches. When the engineered bacteria were grown in the absence of IPTG (circuit OFF), the engineered bacteria grew in both the source and target patches regardless of the dispersal rate. However, when the engineered bacteria where grown in the presence of IPTG (circuit ON), the authors observed that if dispersal was too slow, growth did not occur in the target patch. Here, insufficient cells were moved to the target patch (i.e., below the Allee threshold) and thus the engineered bacteria could not grow. If dispersal was too high, growth did not occur in the source patch. Here, dispersal removed too many cells from the source patch, causing its density to drop below the Allee effect threshold, which resulted in population extinction. Under both of these scenarios, spread did not occur as the engineered bacteria failed to grow in both patches. Spread only occurred when dispersal occurred at intermediate rates. Here, a sufficiently high density of cells (i.e., above the Allee threshold) existed in both the source and target patches, thus allowing the engineered bacteria to grow in both patches.

Interestingly, the authors observed that spread is also contingent upon the number of target patches in the system. In theory, increasing the number of patches that a population is dispersing to could make the spread of that species more prolific; the more colonized patches, the greater the overall population size. This was indeed the case for when the engineered bacteria were grown without IPTG; increasing the number of target patches increased the total population size. However, for a species with an Allee effect, this relationship between population size and the number of target patches was not straightforward. Specifically, as predicted by the authors' mathematical model, increasing the number of target patches contracts the range of intermediate dispersal rates that allow for successful spread. Furthermore, the mathematical model predicts a non-monotonic relationship between total population size and patch number where population size is maximized at intermediate numbers of target patches. Indeed, these mathematical predictions were confirmed experimentally using the authors' engineered bacteria. As such, this study served to reveal novel tradeoffs that govern the spread of cooperative species.

12.4 Conclusion

Herein, we have described several examples of where cell-to-cell communication, engineered through quorum sensing, has led to the discovery of novel tradeoffs and dynamics in ecological and evolutionary fields. As our ability to control and modulate such cell-to-cell communication increases and diversifies, synthetic

systems with increasing complexity are going to be created. These complex synthetic systems will serve to further our ability to understand increasingly complex ecological and evolutionary relationships, furthering our understanding of the mechanisms and forces that shape our environment.

References

1. Khalil AS, Collins JJ (2010) Synthetic biology: applications come of age. Nat Rev Genet 11:367–379
2. Weber W, Fussenegger M (2012) Emerging biomedical applications of synthetic biology. Nat Rev Genet 13:21–35
3. Smith R (2011) Design principles and applications of engineered microbial consortia. Acta Hortic 905:63–69
4. Brenner K, You L, Arnold FH (2008) Engineering microbial consortia: a new frontier in synthetic biology. Trends Biotechnol 26:483–489
5. Riccione KA, Smith RP, Lee AJ, You L (2012) A synthetic biology approach to understanding cellular information processing. ACS Synth Biol 1:389–402
6. Tanouchi Y, Smith R, You L (2012) Engineering microbial systems to explore ecological and evolutionary dynamics. Curr Opin Biotechnol 23:791–797
7. Payne S, Smith R, You L (2012) Quantitative analysis of the spatiotemporal dynamics of a synthetic predator-prey ecosystem. In: Weber W, Fussenegger M (eds) Synthetic gene networks. Humana Press, New York, pp 315–330
8. Gore J, Youk H, van Oudenaarden A (2009) Snowdrift game dynamics and facultative cheating in yeast. Nature 459:253–256
9. Kerr B, Neuhauser C, Bohannan BJM, Dean AM (2006) Local migration promotes competitive restraint in a host-pathogen 'tragedy of the commons'. Nature 442:75–78
10. Koschwanez J, Foster K, Murray A (2011) Sucrose utilization in budding yeast as a model for the origin of undifferentiated multicellularity. PLoS Biol 9:e1001122
11. Dunstan PK, Johnson CR (2005) Predicting global dynamics from local interactions: individual-based models predict complex features of marine epibenthic communities. Ecol Model 186:221–233
12. Miller MB, Bassler BL (2001) Quorum sensing in bacteria. Annu Rev Microbiol 55:165–199
13. You L, Cox RS, Weiss R, Arnold FH (2004) Programmed population control by cell–cell communication and regulated killing. Nature 428:868–871
14. Dwyer DJ, Kohanski MA, Hayete B, Collins JJ (2007) Gyrase inhibitors induce an oxidative damage cellular death pathway in *Escherichia coli*. Mol Syst Biol 3
15. Schaefer AL, Hanzelka BL, Parsek MR, Greenberg EP (2000) Detection, purification, and structural elucidation of the acylhomoserine lactone inducer of *Vibrio fischeri* luminescence and other related molecules. In: Methods in enzymology. Academic, New York, pp 288–301
16. Balagadde FK, You L, Hansen CL, Arnold FH, Quake SR (2005) Long-term monitoring of bacteria undergoing programmed population control in a microchemostat. Science 309:137–140
17. Balagadde FK, Song H, Ozaki J, Collins CH, Barnet M, Arnold FH, Quake SR, You L (2008) A synthetic *Escherichia coli* predator–prey ecosystem. Mol Syst Biol 4
18. Murray J (2002) Mathematical biology, 3rd edn. Springer, New York
19. Song H, Payne S, Gray M, You L (2009) Spatiotemporal modulation of biodiversity in a synthetic chemical-mediated ecosystem. Nat Chem Biol 5:929–935
20. Falkowski PG, Fenchel T, Delong EF (2008) The microbial engines that drive earth's biogeochemical cycles. Science 320:1034–1039
21. Reichenbach T, Mobilia M, Frey E (2007) Mobility promotes and jeopardizes biodiversity in rock-paper-scissors games. Nature 448:1046–1049

22. Hart BA, Zahler SA (1966) Lytic enzyme produced by *Myxococcus xanthus*. J Bacteriol 92:1632–1637
23. Kim HJ, Boedicker JQ, Choi JW, Ismagilov RF (2008) Defined spatial structure stabilizes a synthetic multispecies bacterial community. Proc Natl Acad Sci 105:18188–18193
24. Gonzalez JE, Marketon MM (2003) Quorum sensing in nitrogen-fixing rhizobia. Microbiol Mol Biol Rev 67:574–592
25. Diggle SP, Griffin AS, Campbell GS, West SA (2007) Cooperation and conflict in quorum-sensing bacterial populations. Nature 450:411–414
26. Darch SE, West SA, Winzer K, Diggle SP (2012) Density-dependent fitness benefits in quorum-sensing bacterial populations. Proc Natl Acad Sci U S A 109(21):8259–8263
27. Pai A, Tanouchi Y, You L (2012) Optimality and robustness in quorum sensing (QS)-mediated regulation of a costly public good enzyme. Proc Natl Acad Sci 109:19810–19815
28. Keller L, Surette MG (2006) Communication in bacteria: an ecological and evolutionary perspective. Nat Rev Microbiol 4:249–258
29. Pai A, You L (2009) Optimal tuning of bacterial sensing potential. Mol Syst Biol 5:286
30. Smith RS, Iglewski BH (2003) *P. aeruginosa* quorum-sensing systems and virulence. Curr Opin Microbiol 6:56–60
31. Zhu J, Miller MB, Vance RE, Dziejman M, Bassler BL, Mekalanos JJ (2002) Quorum-sensing regulators control virulence gene expression in Vibrio cholerae. Proc Natl Acad Sci 99:3129–3134
32. Hamilton W (1963) The evolution of altruistic behavior. Am Nat 97:354–356
33. Simpson EH (1951) The interpretation of interaction in contingency tables. J R Stat Soc Ser B (Stat Methodol) 13:238–241
34. Chuang JS, Rivoire O, Leibler S (2009) Simpson's paradox in a synthetic microbial system. Science 323:272–275
35. Chuang JS, Rivoire O, Leibler S (2010) Cooperation and Hamilton's rule in a simple synthetic microbial system. Mol Syst Biol 6
36. Tanouchi Y, Pai A, Buchler NE, You L (2012) Programming stress-induced altruistic death in engineered bacteria. Mol Syst Biol 8
37. Zimbelman JD, Palmer AL, Todd JK (1998) Failure of beta-lactam antibiotics (Eagle effect) and superiority of clindamycin in the treatment of invasive *Streptococcus pyogenes* infections. Pediatr Res 43:161
38. Stevens DL, Gibbons AE, Bergstrom R, Winn V (1988) The Eagle effect revisited: efficacy of clindamycin, erythromycin, and penicillin in the treatment of Streptococcal myositis. J Infect Dis 158:23–28
39. Allee W, Emerson A, Park O, Park T, Schmidt K (1949) Principles of animal ecology. W. B. Saunders, Pennsylvania
40. Tobin PC, Berec L, Liebhold AM (2011) Exploiting Allee effects for managing biological invasions. Ecol Lett 14:615–624
41. Deredec A, Courchamp F (2007) Importance of the Allee effect for reintroductions. Ecoscience 14:440–451
42. Gilligan CA, van den Bosch F (2008) Epidemiological models for invasion and persistence of pathogens. Annu Rev Phytopathol 46:385–418
43. Tan C, Smith R, Srimani J, Riccione K, Prasada S, Kuehn M, You L (2012) The inoculum effect and band-pass bacterial response to periodic antibiotic treatment. Mol Syst Biol 8:617
44. Fath G (1998) Propagation failure of traveling waves in a discrete bistable medium. Physica D 116:176–190
45. Jonsen ID, Bourchier RS, Roland J (2007) Influence of dispersal, stochasticity, and an Allee effect on the persistence of weed biocontrol introductions. Ecol Model 203:521–526
46. Smith R, Tan C, Srimani J, Pai A, Riccione K, Song H, You L (2014) Programmed Allee effect results in a tradeoff between population spread and survival. Proc Natl Acad Sci U S A 111:1969–1974

Index

S.J. Hagen (ed.), *The Physical Basis of Bacterial Quorum Communication*, Biological and Medical Physics, Biomedical Engineering, DOI 10.1007/978-1-4939-1402-9